Dissertation zur Erlangung des Doktorgrades
der Fakultät für Chemie und Pharmazie
der Ludwig-Maximilians-Universität München

Optimizing non-viral nucleic acid delivery: Sequence-defined, biodegradable, and receptor-targeted nanocarriers

Ricarda Carolin Durben, geb. Steffens

aus

Moers, Deutschland

2024

Erklärung

Diese Dissertation wurde im Sinne von §7 der Promotionsordnung vom 28. November 2011 von Herrn Prof. Dr. Ernst Wagner betreut.

Eidesstattliche Versicherung

Diese Dissertation wurde eigenständig und ohne unerlaubte Hilfe erarbeitet.

München, 26.09.2024

……

Ricarda Durben

Dissertation eingereicht am	26.09.2024
1. Gutachter:	Prof. Dr. Ernst Wagner
2. Gutachterin:	Prof. Dr. Olivia Merkel
Mündliche Prüfung am	13.11.2024

Meiner Familie

Science makes people reach selflessly for truth and objectivity;
it teaches people to accept reality, with wonder and admiration, not to mention the
deep awe and joy that the natural order of things brings to the true scientist.

Lise Meitner

Table of Contents

1 Introduction

This chapter provides a short introduction to basic principles and current developments in the field of nucleic acid delivery to create a framework for the topics addressed in this thesis. However, it is not intended to give a complete overview of this rapidly changing and expanding research field.

1.1 Nucleic acid therapeutics

The rapidly advancing field of nucleic acid therapeutics has been in the focus of many researchers. This innovative approach encompasses various strategies aimed at modulating or correcting genetic anomalies at their origin, with the potential to treat genetic disorders, cancer, and other diseases by altering gene expression.(1-6) A sustainable treatment on the genomic level can be achieved through the introduction of plasmid DNA or by gene editing techniques using the CRISPR/Cas9 system.(4, 7, 8) Additionally, RNA interference (RNAi) therapeutics are based on short interfering RNA (siRNA)(9, 10) or antisense oligonucleotide (ASO)(11) therapies that modulate gene expression at the mRNA level, preventing the production of specific proteins.(12, 13) Furthermore, mRNA therapeutics have emerged as a promising class of nucleic acid drug products that act on the cytosolic level of protein expression.(14, 15)

The American Society of Gene and Cell Therapy (ASGCT) has reported an increasing number of gene and mRNA therapies that are authorized for medical use or have entered the clinical development stage. Up to the second quarter of 2024, more than 60 therapies have been approved, and more than 2000 gene therapies are currently in clinical trials.(16)

A key factor to the success of nucleic acid-based therapies is the efficient delivery of the nucleic acid therapeutic into target cells. However, since this task is complicated by the inherent instability of nucleic acids and their poor cellular uptake, the development and implementation of suitable nucleic acid carrier systems is essential. In addition to providing protection and stabilization of the fragile nucleic acid cargo during the administration and delivery process, the carrier must ensure sufficient intracellular release of the drug to unfold its therapeutic capacity while enhancing the biocompatibility of the formulation.

To date, the majority of genetic medicines, whether approved or in clinical trials, are based on viral vectors thanks to their excellent gene delivery potency.(17) However, in recent years, also non-viral carrier systems have entered the field as strong contenders.(18). Over the last decade, lipid nanoparticle (LNP) formulations have gained significant attention as promising non-viral delivery platforms for nucleic acids, pioneered by the siRNA-LNP formulation Onpattro which has been approved for the market in 2018(19, 20) and, more recently, mRNA-based vaccines to contain the SARS-CoV-2 pandemic.(21-23) As research progresses, nucleic

acid therapeutics are expected to pave the way for personalized medicine and the treatment of previously incurable diseases.(24-26)

1.2 Nucleic acid delivery – Overcoming biological barriers

To ensure efficient delivery and to unfold therapeutic or prophylactic potential, nucleic acid therapeutics must overcome various challenges.(27) One challenge to address is protecting the nucleic acid against degradation by endogenous nucleases.(28) Furthermore, the formulation must allow for effective cellular uptake and subsequent release of the nucleic acid cargo at its site of action.(29-32) In addition to virus-based envelopes, which are inherently capable of delivering nucleic acids, non-viral carrier systems have emerged as a promising solution to the challenges encountered during the delivery process.

1.2.1 Non-viral delivery systems

Non-viral carrier systems are designed to complement viral vectors as they are considered to offer several benefits over traditional carriers.(33-35) In particular, non-viral carrier systems are used with the aim of minimizing the risks associated with viral vector drug products, such as immunogenicity or off-target mutagenesis. Thus, they provide a safe and adaptable alternative for various applications.(36)

Nanoparticles, especially particles prepared from biocompatible materials like lipids or polymers, have significant potential as vectors for nucleic acid delivery. They can be tailored in two primary ways: First, to meet the specific and individual requirements of each nucleic acid to ensure compaction and protection of the cargo(37-39) and second, to modulate the particle's size and surface properties in order to optimize cellular targeting, uptake, and toxicity profiles.(40-44) Moreover, the carrier design should enable efficient endosomal escape to release their cargo in response to specific intracellular conditions, thereby enhancing therapeutic efficiency.(45-47)

Polymeric as well as lipid-based carrier systems are being developed for these purposes. Polycations form nanoparticles with negatively charged nucleic acids, resulting in so-called 'polyplexes'(48, 49), which not only protect the cargo from degradation but also provide properties that support the delivery process.(50) For example, polyplexes composed of cationic polymers promote cellular uptake by interacting with the negatively charged outer layer of the cell membranes and support the endosomal escape by acidifying the endosomes.(51) Lipid-based carrier systems interact with both extracellular and intracellular membranes through their fusogenic properties(52, 53) and provide enhanced stabilization of the nucleic acid cargo.(54-57) Hybrid forms such as LNPs or lipopolyplexes contain both cationic and

lipidic domains, and combine the advantages of the formulations mentioned above to represent the most advanced approach to date.

Additionally, more complex formulations comprising additional structural motifs with tailored functionalities provide capabilities to respond to changes in the extracellular or intracellular environment. Understanding structure-activity relationships is critical for the improvement of the delivery process.(57) Consequently, the sequence-defined assembly of carrier molecules consisting of essential structural motifs allows to fulfill diverse requirements of the formulation.(58, 59) Sequence definition can be achieved by solid phase assisted synthesis(60) and is not limited to classic amino acids but allows the insertion of a wide range of structural motifs.(56, 61, 62) For example, cationic motifs are needed for nucleic acid compaction, and lipid domains enhance particle stability and facilitate cellular uptake, while pH- or redox-responsive functionalities facilitate cargo release(45, 58, 63-66). Fine-tuning of stability and release can be achieved through the incorporation of particle stabilizing motifs(67, 68) to enhance structural integrity as well as features to support endosomal escape to improve cargo release(67, 69-71), among other strategies.

1.2.2 Directed delivery of polyplexes – Shielding and targeting

1.2.2.1 Shielding of non-viral nucleic acid therapeutics

Non-viral nucleic acid formulations are often administered systemically, typically via intravenous (i.v.), intramuscular (i.m.) or subcutaneous (s.c.) injections.(1) Upon injection, these predominantly positively charged particles encounter the blood complement system, leading to the formation of a coat consisting of several serum proteins.(72) This ‘protein corona’ determines the subsequent fate of the carrier system by creating an individual biological identity (73-75) which may cause the activation of the immune system(76) or regulates and redirects the nanoparticle delivery.(77, 78)

Masking the positive surface charge can reduce these unwanted side effects. One strategy to achieve this is modifying the particle’s surface with ‘shielding agents’, which decreases the zeta potential, reduces interaction with serum proteins, and consequently prolongs blood circulation time.(79)

A commonly used shielding agent is polyethylene glycol (PEG), which is also utilized in the currently approved LNP formulation Patisiran as well as the COVID-19 mRNA vaccines.(80) Furthermore, numerous studies report the beneficial effect of PEGylated nanocarriers.(81, 82) PEG increases the solubility of the particles in hydrophilic environments and sustains carrier stability against particle aggregation.(83, 84) However, the ubiquitous use of PEG, not only in nucleic acid medicines but also as an excipient in other drug formulations or as an additive in cosmetics and food, has led to observed immunogenic reactions to PEG.(85-87) Research

efforts are put in finding alternatives to PEG. For example, polymer-based shielding agents, such as polysarcosine(88, 89), poly(*N*-(2-hydroxypropyl)-methacrylamide)(90) or poly(2-oxazoline) and its derivatives(91, 92), or polysaccharides such as hyaluronic acid (HA)(93, 94) or hydroxyethyl starch(95, 96) are subject to numerous studies and have shown encouraging shielding properties.

Another challenge associated with shielding is the potential reduction in the delivery system's efficiency due to decreased cellular uptake as a consequence of reduced interaction with cell membranes, also known as the PEG dilemma.(81, 97) This issue can be resolved, for example, by bio-stimuli triggered release or shedding of the shielding domain, as demonstrated by Patisiran or other labile PEG linkers(90, 98, 99) or by incorporation of targeting ligands.

1.2.2.2 Targeted nucleic acid delivery using carbohydrate-based ligands

Targeting strategies in nucleic acid delivery involve either ligands to bind specifically to cell surface receptors or chemical targeting based on surface characteristics leading to favored uptake by specific types of cells.(100, 101) Hence, selective uptake by target cells can be improved, accompanied by minimized off-target effects and toxicity, and is considered to enhance therapeutic efficacy by achieving increased intracellular nucleic acid concentrations.(102, 103) Recent advances have leveraged ligand-free targeting strategies by developing nanocarriers capable of organ-specific delivery based on their physicochemical surface properties by taking advantage of the natural tropism of certain materials or components of the carrier.(104-108)

In the landscape of receptor-based targeting strategies, carbohydrates represent prominent target ligands attached to nucleic acid carrier systems.(109-111) Glyco-ligands are essential for the cutting-edge development of nucleic acid-ligand conjugates, reaching marketable commodities. These advances have paved the way for the market authorization of multiple GalNAc-linked nucleic acid therapeutics during the last five years targeting diseases originating in the liver. (112, 113) The specific interaction between carbohydrate residues and their corresponding binding proteins, known as lectins, enables precise cellular targeting and enhances uptake efficacy. Lectins such as the asialoglycoprotein receptor (ASGPR) or mannose-specific receptors are frequently targeted due to their critical role in initiating receptor-mediated endocytosis of glycoconjugates from both endogenous and exogenous origin.(114-116)

The interaction between carbohydrates and lectins is mediated by reversible binding to the carbohydrate recognition domain (CRD).(117) A multivalent and spatially optimized presentation of the carbohydrate residues is crucial to achieve high binding affinity between receptors and ligands.(118-120) High affinities can also be obtained by the receptors presenting multiple binding sides, allowing for interaction in various binding modes.(121-124)

One notable example is *N*-acetyl-galactosamine (GalNAc), which is an ideal candidate for targeting ASGPR, a receptor almost exclusively expressed on the surface of hepatocytes.(116, 125) The synthesis of highly specific GalNAc ligands enhancing the binding affinity towards ASGPR has facilitated the development of efficient carrier systems for delivering therapeutic nucleic acids such as siRNA and antisense oligonucleotides.(126, 127)
Mannose, another prominent carbohydrate motif, is utilized as ligand for targeting antigen-presenting cells (APCs) such as dendritic cells and macrophages.(128-130) This specificity enables targeted delivery of nucleic acids to immune cells aiming to enhance immune responses or to modulate immune-related diseases.(131, 132) Ongoing innovations and improvements in carrier design have expanded the therapeutic potential of mannose-targeted delivery systems, opening new possibilities for treatments in cancer immunotherapy(133, 134), and for vaccine development.(135-137)

1.2.3 Intracellular fate of polyplexes – Endosomal escape

Polymer- and lipid-based nucleic acid carrier systems used for the delivery of nucleic acid therapeutics are internalized by the cells predominantly by endocytosis(138, 139). After cellular entry, the carriers are encapsulated into intracellular vesicles, the endosomes, and must release their cargo into the cytoplasm to unfold their therapeutic potential.(46) This process critically depends on endosomal escape, which many experts consider the major bottleneck in nucleic acid delivery.(31, 32, 140) In fact, it is reported that less than 5% of the nucleic acid load is released from the endosomes.(30, 141)
Endosomal escape is primarily achieved by mechanisms such as the proton-sponge effect(142), membrane destabilization(143), membrane fusion(144), or combinations of these, depending on the properties of the carrier system.(140, 145)
The proton-sponge effect, particularly prominent in polymer-based carriers, involves the buffer capacity of cationizable polymers, such as polyamidoamines (PAMAM) or polyethyleneimine (PEI)(146-148). These polymers act as weak bases, which leads to osmotic swelling due to acidification of the endosome and subsequent rupture of the endosomal membrane. In addition to that, buffering motifs such as histidines can be incorporated into the polymer to enhance the effect.(71, 149) In the case of cationic polymers lacking buffer capacities during endosomal maturation, endosomolytic reagents, such as chloroquine(150, 151), fusogenic or cell-penetrating peptides(152-157) can be added to facilitate endosomal release.
Lipid-based carriers, in contrast, often rely on membrane fusion or destabilization to facilitate escape, leveraging the lipid's affinity for endosomal membranes(158, 159). For example, the ionizable lipid component of LNPs induces a phase transition of the membranes, supporting the release of the cargo.(160, 161)

In recent work from our group, novel lipoamino fatty xenopeptide carriers have been developed, combining both lipidic and (reversibly) cationic characteristics. These hybrid carriers have demonstrated improved and accelerated nucleic acid release by synergistic endosomal release strategies.(107, 162)

Successful nucleic acid release into the cytoplasm is crucial for unfolding its therapeutic efficacy. However, the efficiency of endosomal escape can be variable, and incomplete escape may result in the degradation of the nucleic acid cargo within lysosomes, consequently leading to a loss of efficacy.(31)

Moreover, the fate of the carrier molecules subsequent to the cargo release must be considered in the development process with special regard to the development of safe and efficient formulations. Carrier molecules remaining in the cytoplasm potentially lead to cytotoxic effects if they are not readily degradable.(163, 164) Cytotoxicity can be intensified by several factors, such as the carrier's size, charge, and composition.(165) For instance, carriers promoting effective endosomal escape may exhibit the potential to disrupt both organelle membranes and plasma membranes, trigger the formation of reactive oxygen species (ROS) and induce apoptosis or necrosis.(166-170)

Thus, the carrier design requires a careful balance between enhancing endosomal escape and minimizing cytotoxicity to optimize the therapeutic potential and several strategies can be employed in carrier design to mitigate cytotoxicity. These include interrupting the polyethyleneimine to shorter amino ethylene building blocks, which display nucleic acid binding capacities and buffering properties promoting endosomal release accompanied by enhanced biocompatibility.(50, 171, 172) Incorporating degradable motifs into the carrier's backbone as defined breaking points to produce non-toxic, biodegradable byproducts or optimizing the carrier's size and surface charge to reduce membrane disruption also improves cellular tolerability.(163, 173) Therefore, modifying carriers by including pH-sensitive or redox-responsive elements can improve the controlled release and further reduce the potential for cytotoxicity.(45, 174)

1.3 Aims of the thesis

Non-viral carrier systems for the delivery of various genetic materials are becoming increasingly impactful in treating and preventing numerous diseases. By continuous optimization of the non-viral nucleic acid carriers, it may become possible to generate highly potent delivery systems. To achieve this, it is crucial to meet the individual requirements of each nucleic acid therapeutic. Several hurdles along the delivery process can be addressed in order to improve the activity of the nucleic acid drug formulations. This thesis contains the results of in two distinct projects dealing with different phases of the delivery process, both with the aim to optimize sequence-defined nanocarriers. Different cell types can be addressed by

integrating targeting ligands to facilitate specific uptake by targeted receptors. Furthermore, the incorporation of bio-responsive motifs or the modulation of the hydrophilic-lipophilic balance can be employed as a strategy to enhance endosomal escape or increase cell tolerance, enabling efficient and safe nucleic acid delivery.

The first aim of the thesis was to develop modular functionalized nanocarrier systems for targeted delivery of pDNA via receptor-mediated endocytosis. To achieve this, a small library of polycationic, succinoyl tetraethylene pentamine (Stp) based carriers with a dendrimer-like four-arm architecture had to be synthesized by solid phase assisted peptide synthesis (SPPS). These oligoaminoamides (OAAs) and equipped with azido-lysines allowing for modular and efficient functionalization with alkyne-bearing ligands, including PEG-agents as well as GalNAc- and mannose-ligands via strain-promoted alkyne-azide cycloaddition (SPAAC).
Initially, an extensive screening of the azido four-arm library was intended to identify suitable candidates for pDNA-transfection by both physicochemical (i.e., size, zeta potential, DNA compaction ability) and biological (gene expression, cytotoxicity) methods.
Subsequently, two different strategies for polyplex functionalization with shielding agents and/or carbohydrate-based targeting ligands were to be tested using the most promising candidates from the library. A pre-functionalization approach, whereby the OAAs are functionalized with the ligands prior to polyplex formation, was to be compared to a post-functionalization approach, in which the ligands are clicked to the OAAs after complexation with the nucleic acid.
For this purpose, a set of PEG-shielding agents with varying lengths of the shielding domain and suitable carbohydrate ligands with either GalNAc or mannose residues suitable for lectin-directed targeting to selected cells had to be synthesized. The PEG shielding agents and the carbohydrate ligands were planned to be equipped with a dibenzo cyclooctyne (DBCO) motif on the *N*-terminus for attachment to the OAAs. The resulting shielded and targeted polyplexes were then to be evaluated with regard to particle formation ability and transfection activity, including a comparison of the polyplex modification strategies. In addition to that, each OAA provides four azido-groups per molecule, which allows to compare varying degrees of functionalization from low to high by using different molar ratios for the click reaction. This versatility should enable the fine-tuning of polyplex properties to optimize ligand-receptor interaction and, hence, their efficacy. It was aimed to evaluate the sugar-functionalized polyplexes with particular regard to their ability to deliver pDNA to cells presenting highly specific carbohydrate receptors in suitable assays under the use of receptor-inhibiting substances.

The second aim of this thesis was to develop and evaluate effective, biocompatible sequence-defined nanocarriers that should derive from a novel class of double pH-responsive xenopeptide carriers. The design of these carriers was considered to be based on lipophilic, ionizable lipoamino fatty acids (LAFs) and the polar ionizable building block Stp, which have demonstrated transfection efficacies approaching those of viral vectors.

Structural variations were to be inserted in selected carriers of different topologies at strategically appropriate positions during the sequence assembly by solid phase synthesis with the aim to enhance biocompatibility and mitigate potential adverse effects on cell viability associated with the highly potent nanocarriers. These structural modifications should consist of either a bioreducible disulfide building block or a hydrophobic spacer. These features are considered to enhance hydrophobicity and, in the case of the ssbb-modified carriers, provide bioreducible cleavage sites to facilitate nucleic acid release after endosomal escape and to allow for fast cytosolic degradation of the carrier molecules.

After successful synthesis of the carriers, the examination of physicochemical and biophysical characteristics of polyplexes formed with either pDNA or mRNA and the novel modified LAF carriers was planned. Furthermore, the impact of the carrier modification on their ability to compact and release the nucleic acid cargo via suitable assays, as well as their lytic potential towards cell membranes, had to be assessed before and after the treatment with glutathione (GSH), a cytosolic reducing agent triggering the disassembly of the disulfide-modified carriers.

In the following, the carriers were to be screened on various tumor cell lines to evaluate transfection efficacy and cytotoxicity of both mRNA and pDNA polyplexes. Mechanistic studies involving the new carriers should be conducted to gain a deeper understanding of the underlying toxicity mechanisms of the novel lipoamino fatty acid carriers to facilitate further improvement regarding their efficiency and biocompatibility.

2 Directing the Way - Receptor and Chemical Targeting Strategies for Nucleic Acid Delivery

Ricarda C. Steffens[1,2] and Ernst Wagner[1,2,]*

[1]Pharmaceutical Biotechnology, Department of Pharmacy, Ludwig-Maximilians-Universität (LMU) Munich, 81377 Munich, Germany.

[2] Center for NanoScience (CeNS), LMU Munich, 80799 Munich, Germany.

* Corresponding Author: ernst.wagner@lmu.de

The following chapter was adapted from a review article which was published in Pharmaceutical Research (2023) 40(1), 47-76; https://doi.org/10.1007/s11095-022-03385-w. Published online: 15 September 2022. (100)

Author contributions

Both authors have contributed to this publication. Ricarda Steffens and Ernst Wagner: conceptualization of review topic, writing, editing, illustrations, review of the manuscript. Both authors have read and agreed to the published version of the review article.

2.1 Abstract

Nucleic acid therapeutics have shown great potential for the treatment of numerous diseases, such as genetic disorders, cancer and infections. Moreover, they have been successfully used as vaccines during the COVID-19 pandemic. In order to unfold full therapeutical potential, these nano agents have to overcome several barriers. Therefore, directed transport to specific tissues and cell types remains a central challenge to receive carrier systems with enhanced efficiency and desired biodistribution profiles. Active targeting strategies include receptor-targeting, mediating cellular uptake based on ligand-receptor interactions, and chemical targeting, enabling cell-specific delivery as a consequence of chemically and structurally modified carriers. With a focus on synthetic delivery systems including polyplexes, lipid-based systems such as lipoplexes and lipid nanoparticles, and direct conjugates optimized for various types of nucleic acids (DNA, mRNA, siRNA, miRNA, oligonucleotides), we highlight recent achievements, exemplified by several nucleic acid drugs on the market, and discuss challenges for targeted delivery to different organs such as brain, eye, liver, lung, spleen and muscle *in vivo*.

Keywords. Lipoplex; pDNA; polyplex; siRNA; targeting.

2.2 Introduction

Over the last three decades, vectors for the delivery of therapeutic genetic material were extensively evaluated and optimized. Currently, more than 3000 clinical trials on gene therapy have been conducted or are still ongoing. With about 2/3 of clinical trials on cancer diseases, gene delivery to tumors represents the primary target for nucleic acid therapy. However, other indications, such as monogenetic diseases, infections, inflammatory diseases, neurological and ocular disorders are also interesting targets for gene therapy.(3, 4, 175) For gene transfer, viral vectors are still the most advanced delivery systems in clinical gene therapy studies, attributed to their excellent transduction efficacies.(17, 176) Part of their efficacy is that they are naturally built to introduce nucleic acids into foreign cells, presenting natural receptor targeting agents and peptide sequences on their surface that enable cellular entry.

Synthetic delivery systems present a second class of transfer agents for nucleic acid therapeutics. They have the advantage that they can be designed to be non-immunogenic and have the potential to deliver a broad range of natural or synthetic and modified nucleic acids. Historically, transfections introduced functional genes by either using DNA transfer into the nucleus or RNA transfer into the cytosol.(177-179) In contrast to DNA, messenger RNA (mRNA) does not require nuclear entry since its site of action is located in the cytosol. Its great therapeutic potential (14, 180) was recently proven by the successful application of mRNA-based COVID-19 vaccines.(21, 22, 181) With the new millennium, RNA interference (RNAi) therapeutics were developed as another class of therapeutic nucleic acids, aiming for the down regulation of malignant gene expression by short interfering RNA (siRNA) (182) or micro-RNA (miRNA) (183). In addition, now for more than 30 years, antisense oligonucleotides have been therapeutically applied by blocking or modulating splicing of complementary mRNA.(11, 184) Most recently, the CRISPR/Cas technology has entered therapeutic application as a promising tool for genome editing (7, 185), either via Cas9 mRNA/single guide (sg) RNA or as Cas9 protein/sgRNA ribonucleoprotein complex.(8) These synthetic carriers range from organic, polycationic carriers to lipid structures and inorganic particles and were extensively optimized in order to enhance transfection efficacy and become more and more like artificial viruses.(186, 187) First of all, these synthetic carriers are designed to compact the genetic material for protection against degradation and shielding against undesired interactions. This can be achieved by polycations such as poly-L-lysine (PLL) (151, 188), polyethyleneimine (PEI) (28, 189), poly(amidoamines) (PAMAM) or dendrimers (190, 191) which interact with negatively charged nucleic acids and assemble in nano-sized particles, so-called “polyplexes”(48). Lipid-based structures including “lipoplexes”, in which the genetic material is packaged by positively charged lipidic carriers, and “LNPs”, containing the nucleic acid inside multi-component lipid nanoparticles, have also proven great potential as nucleic acid delivery systems (**Figure 2.1**).(48, 192)

In order to show comparable transfection efficacies to viral vectors, especially for *in vivo* studies, synthetic delivery systems need to fulfill further demands.

The particles should

a) show no interaction with blood components or aggregation tendency in physiological environment,
b) show prolonged blood circulation time to reach the target tissue
c) promote efficient cellular uptake and
d) release the genetic material into the cytoplasm, so it can reach its site of action.

Within this delivery process, one major challenge remains the transport and transfer of nucleic acids to the desired cell type or tissue. This requirement can be approached by modifying synthetic carriers with functional domains giving targeted delivery systems, which was first successfully implemented 35 years ago by Wu et al. using GalNAc-presenting ligands on PLL-polyplexes for directed delivery to hepatocytes.(188, 193)

In this review, we will give an overview about different active targeting strategies for synthetic delivery systems. We highlight recent advances in nucleic acid delivery to specific healthy tissues including the liver, lung, brain, immune cells, retina and muscle. Specific delivery to cell types can be mediated via defined ligand-receptor interactions (*receptor-targeting*) as well as modulating the physicochemical properties of the nucleic acid nanoparticles based on small structural variations of the synthetic carriers (*chemical targeting*). For tumor-specific targeting of nucleic acids we refer to other published work.(101, 194, 195)

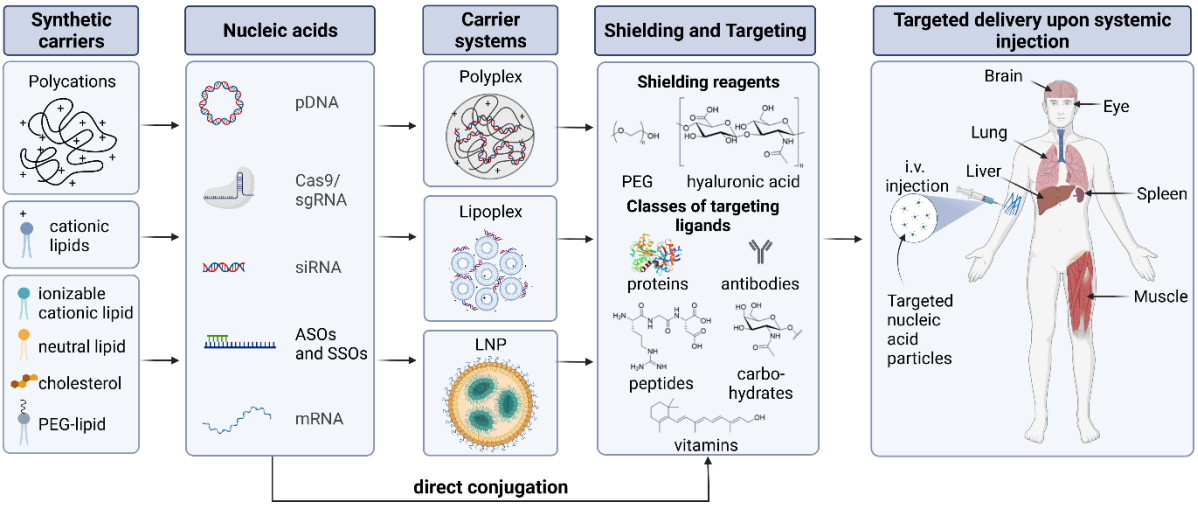

Figure 2.1. Nonviral carriers for the delivery of different nucleic acids, including their main components, particle types as well as shielding and targeting agents for organ- or cell-specific delivery upon systemic injection. Created with BioRender.com

2.3 Strategies for specific delivery

2.3.1 Shielding

Synthetic carriers have proven to be potent transfer vehicles for nucleic acid delivery for *in vitro* studies thanks to various optimizations. However, during the delivery process from injection to gene expression, several obstacles and cellular bottlenecks must be overcome to unfold the full therapeutic potential of the nucleic acid. Besides efficient encapsulation of the genetic material to protect against degradation, it must be ensured that the carriers circulate in the blood until reaching the target tissue.

Cellular uptake of positively charged polyplexes is enabled by non-specific endocytosis, in particular macropinocytosis from the extracellular fluid (196) (see **Figure 2.2 A**). The uptake can be further improved, even though not specified, by incorporation of cell-penetrating peptides in the formulation, such as octaarginine motifs.(155, 197) *In vivo* applied nanocarriers, however, are confronted with blood components like plasma proteins that adsorb on particle surface and hence sustainably affect circulation, transport to tissues and cellular uptake.(198-200) For instance, the formation of a protein corona comprised of opsonins will mediate phagocytosis removing particles from the circulation.

To this end, it is necessary to shield positively charged carriers against unspecific interactions with serum proteins that may result in phagocytosis of the particles. This can be achieved by incorporating shielding domains, for example polymers such as polyethylene glycol (PEG) (82), poly(N-(2- hydroxypropyl)methacrylamide) (pHPMA) (201), poly(2-oxazolines) (202) and poly-sarcosines (88) or polysaccharides such as hydroxyethyl starch (203) or hyaluronic acid (HA) (**Figure 2.1**) (94, 204, 205). Shielding the carrier's surface results in lowered surface charge and thus reduced interaction with serum proteins, which allows the particles to circumvent the reticuloendothelial system (RES) and increase circulation time in the blood.(82) However, poor targeting abilities resulting in off-target effects or low accumulation on the target site set limitations regarding the application of synthetic gene delivery systems *in vivo*. Consequently, to ensure tissue- or cell-selective delivery and to minimize accumulation in off-target sites, the particles can be surface-modified either by specific ligands that will interact with receptors on the targeted cell type for active targeting or by modification of their chemical composition leading to altered biodistribution for chemical targeting.

2.3.2 Active Targeting

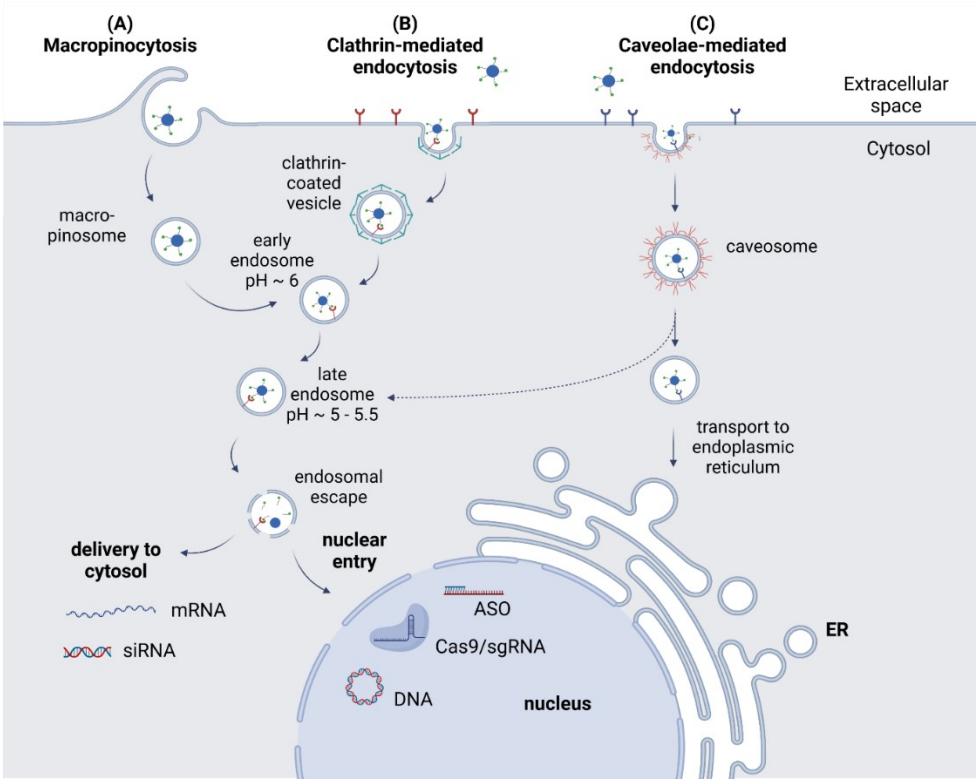

Figure 2.2. Internalization pathways of nucleic acid carriers by receptor-mediated endocytosis. Created with BioRender.com

Table 2.1. Characteristics of cellular uptake via clathrin- and caveolae-mediated endocytosis.

	Clathrin-mediated endocytosis	**Caveolae-mediated endocytosis**
Vesicles for transport	Clathrin-coated vesicle	Caveosome
Examples for receptors	TfR, ASGPR, LDLR	Folate receptor, VEGFR, Interleukin-2
Tolerated nanoparticle size	Up to 200 nm	200 to 500 nm
Intracellular fate of cargo	Formation of endosomes, maturation to late endosomes, lysosomal degradation or endosomal escape	Transport to endoplasmic reticulum, Golgi apparatus, facilitated delivery to nucleus

Receptor targeting. Decorating the carrier's surface with ligands can yield specific cellular uptake based on receptor-mediated endocytosis. Here, the fact that specific tissues differently express certain receptors is used to enhance cell-specific uptake of nucleic acid carriers (103). The types of ligands used for modification of delivery systems range from small chemical drug-derived compounds (206-209), peptides (210, 211) to large proteins (212, 213), antibodies

(214, 215), carbohydrates (216-218) and vitamins (219, 220) (**Figure 2.1**). Interaction with their specific receptors will lead to receptor-mediated endocytosis, a highly selective process of nanoparticle internalization.

In order to achieve receptor-mediated uptake, unspecific interactions of the carrier with blood-components have to be reduced by shielding. Cellular uptake is initiated by recognition of specific ligands by cell surface receptors. After cell binding, the receptor-ligand complex is internalized by the formation of vesicles from the cell membrane and delivered to the cytosol (**Figure 2.2 B, C**). The fate of nanocarrier transport through the cytosol is determined by the receptor type and the associated pathway of endocytosis, as summarized in **Table 2.1**. For example, prominent receptors used for targeted gene delivery such as transferrin receptor (TfR) (221), asialoglycoprotein receptor (ASGPR) (222) or low-density lipoprotein receptor (LDLR) (223) undergo clathrin-mediated endocytosis into early endosomes, followed by endosome maturation and fusion with lysosomes (224). Only small particles with a maximum size of 200 nm can be taken up by this route.(139) Other receptors, e.g., the folate receptor (225) or interleukin-2 receptor (226), are internalized via caveolae-mediated endocytosis.(227) This route tolerates uptake of particles up to 500 nm (139) and allows to bypass the fusion with lysosomes, leading to delivery to endoplasmic reticulum and facilitated nuclear transport.(228) Generally, the release of carriers from late endosomes is critical for efficient nucleic acid delivery to avoid either enzymatic degradation of the nucleic acid payload after fusion with lysosomes or exocytosis during receptor recycling. Conveniently, synthetic carriers have been designed to exhibit endosomolytic properties. For example, cationic carriers containing protonatable amines, e.g., PEI or histidine-containing constructs response to acidic pH in late endosomes promoting a proton-sponge effect, i.e. swelling and eventually disruption of the endosomes, leading to release of the nucleic acid to the cytosol.(71, 148) Lipid-based carriers are able to release their cargo by fusion with the negatively charged endosome membrane.(54)

Strategies to incorporate targeting ligands into the delivery system. Ligands for receptor-targeting as well as shielding domains can be integrated into the delivery system by both, pre-functionalization, and post-modification.(229) Multivalent ligand presentation on the carrier's surface may promote receptor recognition and increases binding affinity.(230, 231) The density of ligands required for efficient targeting strongly depends on both the chosen carrier system as well as the type and avidity of ligand. For polyplexes, the ligand to polycation ratio may range from 2.5% to >100% functionalization, depending on the type of ligand.(232-234) In LNPs, ligand-functionalized lipids may account for only 1-2 mol% per formulation, but still promote target-specific delivery.(235, 236) In direct conjugates such as trivalent GalNAc-siRNA, every nucleic acid is equipped with a targeting moiety. Accessibility of the targeting ligand is also important for receptor binding.(237) Pre-functionalization has been evaluated for

polymeric delivery systems which contain different domains for nucleic acid binding, shielding, and targeting.(218, 238, 239) An alternative functionalization strategy is based on the post-modification of pre-formed nanoparticles, mostly via covalent attachment of ligands to functional groups displayed on the surface. For example, copper-free (240, 241) or copper(I)-catalyzed (242) alkyne-azide click reactions were used for particle modification, as they are fast, selective and high-yielding. By means of this method, it can be ensured that the ligands are located on the surface of the particles. At the same time, the removal of excess ligands that may not have bound to the carrier may be required, as they could compete for the receptor and reduce cellular uptake. Non-covalent binding of ligands to the particle surface can also be considered. This modification method was successfully realized for targeting of synthetic carriers with insulin (243) and hyaluronic acid (205).

Dual targeting. Inspired by natural viruses, which have optimized cell association and cellular entry mechanisms by presenting several ligands on their surface, dual targeting represents an approach to further increase transfection efficacy. Here, cell entry properties of viral vectors are mimicked by using two (or more) ligands on a single carrier. For example, Nie et al. used dual-targeted PEGylated PEI-pDNA polyplexes, modified with the cell binding peptide B6 and the integrin targeting peptide RGD for increased transfection efficiency on DU145 and PC3 cells, showing increased transfection efficacy when both ligands were incorporated in the polyplex formulation. In addition, it was demonstrated how these ligands participate in both, cell association and internalization.(244) Additional studies of dual-targeted polyplexes with combinations of B6, GE11 (for EGFR targeting) and cyclic cRGDfk (for integrin targeting), respectively, revealed that the combination of B6 and GE11 was most promising for pDNA transfections to DU145 cells, which express all three receptors.(245) Dual-targeted LPEI-PEG polyplexes were also used for delivering the theranostic sodium iodide symporter gene to Huh7 cells, using a combination of GE11 and cMBP, which showed strong benefits compared to single-targeted polyplexes.(246)

Cascade targeting. Under certain circumstances, nucleic acid carriers have to overcome several barriers to reach their site of action, e.g., the blood-brain-barrier (BBB), followed by membranes of targeted cells. In order to generate cascade targeting delivery systems, nanoparticles can be designed to cross the BBB first and display targeting ligands selectively binding to receptors on specific cells behind the barrier. For example, Wang et al. developed such a gene delivery system by decorating the carrier with the I_6P_7 ligand, a heptapeptide derived from interleukin-6, which is able to promote both, BBB crossing and cell-specific delivery to interleukin-6 receptor presenting cells.(247) A cascade targeting concept was also used by Zhang et al. to deliver siRNA into neuronal cells after crossing the BBB for treatment

of Alzheimer's disease. In this study, BBB crossing was achieved via the ApoA-I ligand, which binds to the scavenger receptor B1, and selective uptake of the particles by neuronal PC12 cells could be demonstrated by incorporation of a peptide ligand, NL4 binding to tropomyosin receptor kinase A (TrkA). These findings were subsequently confirmed by in vivo studies resulting in downregulation of BACE1, an enzyme which is involved in pathogenesis of Alzheimer's disease.(248, 249)

Chemical targeting. In addition to actively targeted delivery supported by ligand-receptor specific interaction, chemical properties of the carrier system can also generate cell- or tissue-specific delivery. Unmodified polycationic carriers such as poly-L-lysine or PEI naturally interact with negatively charged heparan sulfate proteoglycans of the plasma membrane which leads to particle uptake.(51, 250) Lipoplexes and liposomes containing cationic lipids were found to destabilize the phospholipid bilayer of cell membranes and are subsequently internalized via receptor-independent endocytosis.(251) Recently, it was observed that liposomes and LNPs typically accumulate in the liver in their classical composition due to non-covalent attachment of serum proteins, especially apolipoprotein E (ApoE) resulting in transport to hepatocytes and uptake via low-density lipoprotein receptor (LDLR).(252-255) In fact, the composition of the carrier systems largely influences the interaction with blood proteins.(75) Therefore, together with active targeting for tissue- or cell-specific nucleic acid delivery by ligand-receptor specific interaction, chemical adjustment of the carrier system can be also utilized to generate organ-specific delivery. It could be observed that slight changes of the chemical or physicochemical properties of the formulation such as particle size and surface charge have a remarkable impact on the biodistribution and accumulation in certain tissues or cell types.

Chemical targeting has shown great potential for ligand-independent, but yet organ-specific delivery of nucleic acids. For example, Kowalski et al. observed organ-selective distribution of mRNA-LNPs with a library of amino-polyesters either in liver, spleen, or lung after i.v. injection.(256) Localization of structurally different LNPs after systemic administration was investigated by Dahlman et al. by developing a barcode tool in order to track biodistribution *in vivo*.(257) Furthermore, the group of Siegwart synthesized libraries of lipids for LNP formulations for delivery of mRNA as well as Cas9 with different properties by variation of charge, hydrophobicity and pKa, respectively, resulting in so-called "selective organ targeting" (SORT) lipids and studied the accumulation of these formulations in different tissues and cell types. For example, it was demonstrated that particles with higher amounts of positively charged dioleoyl-3-trimethylammonium propane (DOTAP) preferably accumulated in the lung, whereas the addition of negatively charged lipids led to selective delivery to the spleen.(258, 259) Recently, the mechanism behind SORT was studied, revealing both global and apparent pKa as well as the composition of the serum protein corona of the LNP formulation determining

the selective delivery. The study revealed first that particles with a pKa around 6-7 accumulated in the lung, while LNPs with lower pKa from 2 to 6 were preferably delivered to the spleen and second that different serum proteins bind to LNPs dependent on the component composition, therefore representing pioneering results for understanding LNP delivery beyond hepatocytes for future fields of applications.(104)

2.4 Liver as Target

The liver is a highly metabolic organ and source of numerous expressed genes and plasma proteins. Not surprisingly, this organ is also a main target for nucleic acid and gene therapy of a series of severe hereditary monogenetic diseases.(260-262) In addition, non-inherited hepatic diseases such as liver cirrhosis or hepatitis B and C or hepatocarcinoma are life-threatening.(263) Therefore, the liver presents a high-priority target for nucleic acid delivery. Targeting of hepatocytes can be approached either by active or indirect active targeting, dependent from the carrier system as summarized in **Table 2.2**.

Table 2.2. Targeted nucleic acid delivery to different liver cell types

Receptor	Delivery system	Ligand	Type of nucleic acid	Results	Ref.
Hepatocytes					
ASGPR	PLL polyplex	ASOR	pDNA	First report on targeted, hepatocyte-specific gene delivery	(188, 193)
	PLL polyplex	Artificial tetra-antennary GalNAc ligand	pDNA	Conjugation of artificial ligand to the polyplexes results in comparable gene transfer efficiency as with the natural ligand asialofetuin, monovalent ligand does not improve gene expression	(216)
	Polymer-nucleic acid conjugate	GalNAc	siRNA	*in vitro* and *in vivo* hepatocyte-specific delivery of siRNA	(264)
	Direct conjugate	Tri-GalNAc	siRNA	FDA and EMA approval of several products:	
	Direct conjugate	Tri-GalNAc	siRNA	- Givosiran for treatment of acute intermittent porphyria	(265)
	Direct conjugate	Tri-GalNAc	siRNA	- Lumarisan for treatment of primary hyperoxaluria type 1	(266, 267)
	Direct conjugate	Tri-GalNAc	siRNA	- Inclisiran for treatment of primary hypercholesterolemia	(268)
	LNP	Tri-GalNAc	siRNA	Exogenous ligand Tri-GalNAc mediates ASGPR-dependent uptake	(255)
	Direct conjugate	Tri-GalNAc	ASO	Enhanced uptake, improved delivery and activity duration of clinically relevant ASOs to hepatocytes *in vivo*	(127)
	Direct conjugate	Tri-GalNAc	ASO	Improved uptake and activity of targeted ASOs in human clinical trial	(269)

Receptor	Delivery system	Ligand	Type of nucleic acid	Results	Ref.
	Direct conjugate	Tri-GalNAc	ASO	Safety, pharmacokinetic and pharmacodynamic study of GalNAc-ASO for treatment of b-thalassemia in monkeys	(270)
	Direct conjugate	Tri-GalNAc	ASO	Enhanced uptake by hepatocytes, but not other liver cell types	(271)
	Direct conjugate	Tri-GalNAc	ASO	Increased delivery of anti-miRNA-ASOs to hepatocyte in presence of ligand	(272)
	Direct conjugate	Tri-GalNAc	Cas9 RNP	Disulfide linkage between Cas9 and GalNAc ligand led to receptor-dependent, selective uptake by hepatocytes and exhibited gene editing activity	(273)
LDLR	Direct conjugate	ApoB (endo-genous)	siRNA	Delivery of siRNA to hepatocytes generated gene silencing of apoB protein expression	(274)
	Direct conjugate	AopB (endo-genous)	ASO	Improved uptake of ASOs by hepatocytes after ligation of cholesterol	(271)
	LNP	ApoE (endo-genous)	siRNA	Uptake of LNPs is mediated by LDL-receptor determined by formation of ApoE-containing protein corona	(255)
	LNP	ApoE (endo-genous)	siRNA	Development of Patisiran for treatment of hereditary transthyretin amyloidosis, EMA and FDA approval in 2018	(20)
	LNP	ApoE	Cas9-mRNA/ sgRNA	Efficient TTR gene knockout *in vivo* in phase 1 clinical trial (57 % after infusion of 0.1 mg/kg and 87 % after 0.3 mg/kg); mild adverse effects	(185)
Hepatic stellate cells					
RBP receptor	Liposome	Vitamin A	siRNA	Down-regulation of collagen synthesis after RBP receptor mediated uptake led to resolution of liver cirrhosis and fibrosis in rats after repeated treatments	(220, 275)
PDGFR β	LNP	Cyclic peptide pPB	siRNA	Increased uptake of targeted SNALPs by HSCs; accumulation in liver after i.v. injection in mice, down regulation of gp46 mRNA expression, which is high in hepatic fibrosis	(235)
Liver sinusoidal endothelial cells and Kupffer cells					
n.a.	LNP	None (chemical targeting)	Barcode DNA, siRNA, sgRNA, mRNA	Alteration of cholesterol in LNP composition: Oxidized and esterified cholesterol mediated uptake by LSECs, cholesterol-oleate led to 3-fold enhanced gene editing activity in LSECs compared to hepatocytes	(276, 277)
n.a.	LNP	None (chemical targeting)	Barcode DNA, mRNA	Exchange of DLin-MC3 by cKK-E12 leads partly to LNP uptake by LSECs and KCs	(278)
n.a.	LNP	None (chemical targeting)	Barcrode DNA, mRNA	Adamantyl-phospholipids shifted distribution from hepatocytes to KCS and LSECs, but not to extrahepatic immune cells	(279)
n.a.	LNP	None (chemical targeting)	mRNA	Uptake by LSECs and KCs was achieved by replacing zwitterionic DSPC with anionic DSPG	(280)

Abbreviations: ASGPR, Asialoglycoprotein receptor; PLL, poly-L-lysine; ASOR, asialoorosomucoid; GalNAc, *N*-acetyl galactosamine; FDA, U.S. Food and Drug Administration; EMA, European medicines agency; LDLR, low-density lipoprotein receptor; ApoB, apolipoprotein B; ApoE, apolipoprotein E; RBP, retinol binding protein; PDGFR β, platelet-derived growth factor receptor β; pPB; SNALPs, stable nucleic acid lipid particle; HSC, hepatic stellate cell, LNP, lipid nanoparticle; LSECs, liver sinusoidal endothelial cells; DLin-MC3 4-(dimethylamino)-butanoic acid, (10*Z*,13*Z*)-1-(9*Z*,12*Z*)-9,12-octadecadien-1-yl-10,13-nonadecadien-1-yl ester.

2.4.1 Hepatocytes

2.4.1.1 Hepatocyte targeting via asialoglycoprotein receptor

Delivering nucleic acids into hepatocytes is mostly achieved by receptor-mediated endocytosis via the ASGPR, which is found almost exclusively and abundantly on hepatocytes.(125) ASGPR binds highly selective to terminal, multi-antennary galactose and *N*-acetyl galactosamine (GalNAc) residues of glycoproteins with defined spatial geometry in presence of calcium(II)-ions.(116, 281, 282)

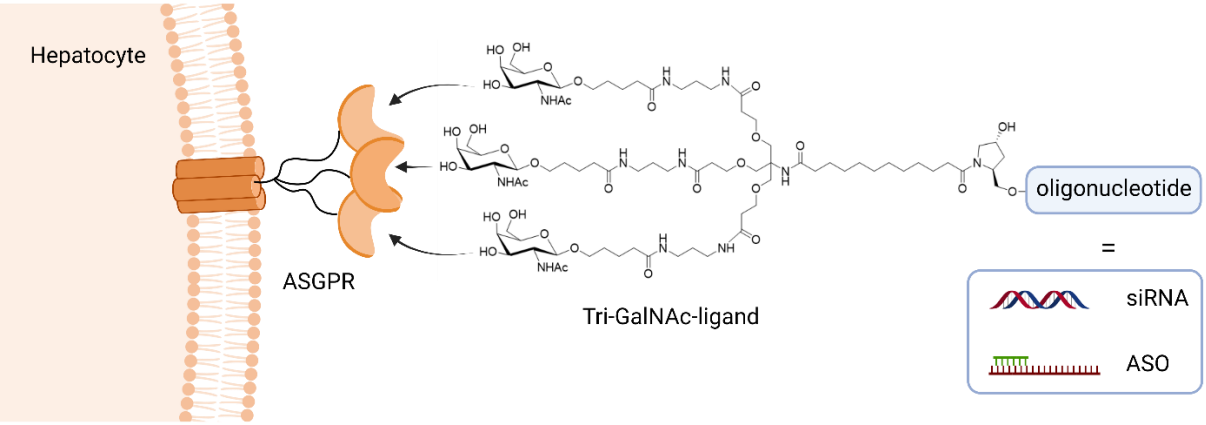

Figure 2.3. Optimized trivalent GalNAc-ligand for hepatocyte delivery of direct conjugates with siRNA and ASOs, respectively, via ASGPR-mediated endocytosis. Created with BioRender.com.

The first targeted delivery of DNA by a non-viral delivery system was reported by Wu et al. by using asialoorosomucoid-modified (ASOR) polylysine polyplexes mediating delivery to the liver via ASGPR *in vitro* and *in vivo* after intravenous (i.v.) injection.(188, 193) Later, Plank et al. used an artificial tetra-antennary galactose ligand for gene transfer of pDNA-poly(lysine) polyplexes to hepatocytes *in vitro*.(216) Artificial ligands for ASGPR targeting were extensively optimized, as spatial distance of the carbohydrate residues, a well-balanced equilibrium of hydrophilicity and hydrophobicity of the linker largely impact the binding affinity towards the receptor.(283)

Rozema et al. developed a dynamic polymer-nucleic acid conjugate, that fulfilled several tasks in one: The backbone itself provided endosomolytic properties, served as reaction site for the covalent attachment of siRNA and was grafted with GalNAc and PEG, giving a targeted and shielded vehicle. This formulation induced gene silencing activity in the liver after i.v. injection in mice.(264)

One milestone in both RNAi therapeutics and ASGPR mediated nucleic acid delivery is represented by the market release of Givosiran (Givlaari) in 2019 by the U.S. Food and Drug Administration (FDA) and European medicines agency (EMA). The nucleic acid, a chemically modified and stabilized siRNA, is directly conjugated to a tri-GalNAc ligand optimized towards ASGPR binding sites (**Figure 2.3**). When administered subcutaneously, the direct conjugate

enabled efficient gene silencing of aminolevulinic acid synthase 1 (ALAS1) aiming for reduced levels of ALA and PBG metabolites by RNAi for the treatment of acute hepatic porphyria.(115, 265, 284) Since then, two additional RNAi-therapeutics have been released to the market for treating rare, monogenetic hepatic diseases, using the same concept, i.e., the direct conjugation of trivalent GalNAc ligand to therapeutic siRNA, were released to the market for the treatment of rare, monogenetic hepatic diseases. Lumasiran (Oxlumo) gained FDA approval in 2020 and targets the silencing of the gene encoding glycolate oxidase for the treatment of primary hyperoxaluria type 1 (PH1).(266, 267) Inclisiran (Leqvio) also represents a direct siRNA-TriGalNAc conjugate targeting the inhibition of the translation of serum protease PCSK9 in order to regulate cholesterol blood level for the treatment of hypercholesteremia after subcutaneous injection.(268, 285, 286) Thanks to the success of GalNAc-siRNA direct conjugates, several further therapeutics based on the same concept are currently in phase 2/3 clinical trials.(287).

Additionally, the approach of direct conjugates has been further expanded to other cargos, e.g., antisense oligonucleotides (127, 269-272) or Cas9 RNP complexes.(273) For example, trivalent GalNAc ligands were conjugated to antisense oligonucleotides, which enabled hepatocyte-specific delivery and enhanced the activity of clinically relevant human ASOs in mouse models (127), monkeys (270) and humans.(269) In another study, ASOs were conjugated with trivalent GalNAc and cholesterol, respectively, reporting enhanced uptake by hepatocytes.(271) Recently, Yamamoto et al. demonstrated that the conjugation of GalNAc to anti-miRNA ASOs led to highly increased potency.(272) A novel, trivalent GalNAc ligand which showed high affinity towards ASGPR (K_D < 100 pM) mediated receptor-dependent, hepatocyte specific delivery and selective gene editing of CRISPR/Cas9 RNP complex.(273)

2.4.1.2 Hepatocyte targeting via LDL receptor

In addition to active targeting of hepatocytes via ASGPR by GalNAc-modified formulations, uptake of lipid formulations can be also achieved by LDLR-mediated endocytosis. For example, cholesterol-siRNA direct conjugates for apolipoprotein B (ApoB) silencing have been found to exhibit gene silencing activity in hepatocytes *in vivo*.(274) LDLR-mediated uptake was observed due to interactions of cholesterol with serum proteins. The same approach was used for ASO direct conjugates by Watanabe et al. to enhance uptake and ASO activity in hepatocytes.(271) Furthermore, it was found that neutral liposomes interact mostly with apolipoprotein E (ApoE) in the blood, which directs the transport to hepatocytes by LDLR-mediated endocytosis.(252-254) Based on this observation, it was concluded that LNPs, multicomponent mixtures of cholesterol, an ionizable, cationic lipid, neutral helper lipids and a PEG-lipid for nucleic acid compaction, which appear almost neutral in serum, interact in a similar way with ApoE.(255) Thus, ApoE was identified as an endogenous ligand mediating the hepatocytic uptake of LNPs via LDLR.(255) In particular, Patisiran (Onpattro), the first siRNA

product which was approved by FDA and EMA in 2018, is using LDLR interaction for the delivery of siRNA against transthyretin (TTR) mRNA to treat hereditary TTR mediated amyloidosis. By using a sheddable PEG-component, the formation of ApoE protein corona was observed, resulting in hepatocyte uptake via LDL receptor.(20, 288) In a recent phase I clinical study by Gilmore et al. the therapeutic effect of Cas9-mRNA/sgRNA targeting TTR, encapsulated by LNPs was evaluated. As a result of efficient TTR gene knockout, an average decrease of 87% of TTR protein levels was observed after one month in the patient group that received 0.3 mg/kg, accompanied with only mild side-effects.(185)

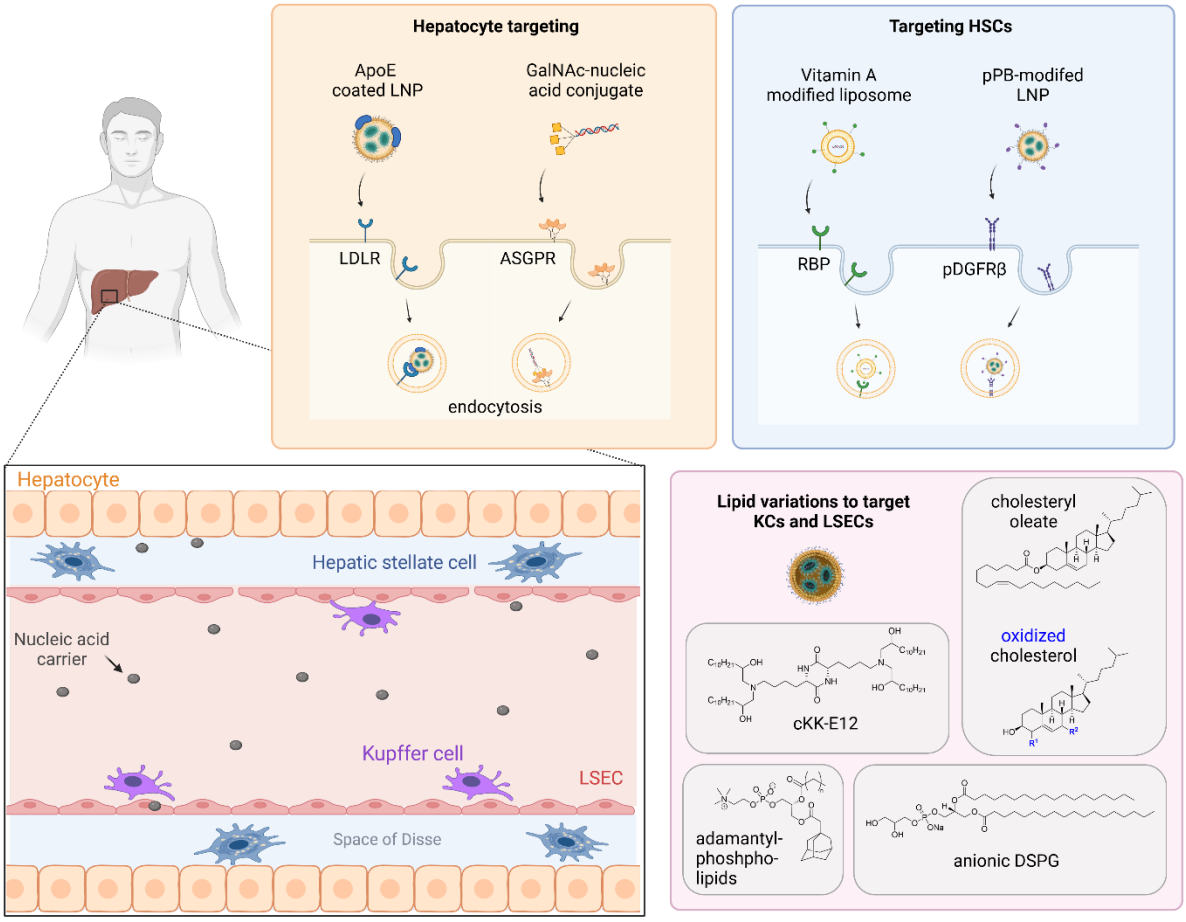

Figure 2.4. Strategies to target different liver cell types: Hepatocytes (orange), hepatic stellate cells (blue), Kupffer cells (purple) and liver sinusoidal endothelial cells (light red). Created with BioRender.com

2.4.2 Targeting liver cell types beyond hepatocytes

Approximately 80% of the liver is composed of hepatocytes. However, other cell types which are part of the hepatic reticuloendothelial system (RES), such as liver sinusoidal endothelial cells (LSECs), hepatic stellate cells (HSCs) and Kupffer cells (KCs) also represent interesting targets for nucleic acid therapeutics. Although KCs are very effective in removing and destroying nanosystems, they are much more difficult to be productively transfected with

commonly used nucleic acid carriers. Therefore, several attempts were made to enable nucleic acid delivery to these cell types, including receptor-targeting strategies as well as the development of novel lipids for LNPs aiming for chemical targeting (**Figure 2.4**).

2.4.2.1 Hepatic stellate cells

While hepatic stellate cells make up about 5-8% of the cells in a healthy liver, the fibrotic liver consists of 15% HSCs. Nucleic acid delivery to activated HSCs is believed to reduce fibrosis by regulating fibrogenic cytokines.(289, 290)

For example, Sato et al. accomplished HSC-targeted delivery of liposomes and LNPs by decorating the particle surface with vitamin A.(220, 275) As HSCs are a main storage for vitamin A, uptake of the liposomes was mediated by retinol binding receptor, which led to suppression of cirrhosis in a cirrhotic liver rat model by delivering therapeutic siRNA (220) and showed ability to promote regeneration of chronically injured liver.(275) Fibrotic HSCs were moreover targeted by modification of siRNA-LNPs with a cyclic peptide ligand (pPB) that interacts with the platelet-derived growth factor receptor β. It could be observed that pPB-targeted LNPs accumulated with high specificity in HSCs confirmed by biodistribution experiments after systemic injection.(235) Studies conducted by the Dahlmann group using the barcode technology described before for *in vivo* screening of lipid compositions aimed for delivery of chemically different LNP formulations beyond hepatocytes and the understanding of particle distribution in the liver microenvironment without the requirement for additional receptor-targeting ligands (278).

2.4.2.2 Liver sinusoidal endothelial cells and Kupffer cells

Targeted nucleic acid delivery to LSECs and KCs, which belong to the hepatic RES using chemical targeting has moved into the focus of attention. Dahlmann et al. used their barcode screening tool to tune the LNP biodistribution in mice based on alterations in the cholesterol component. As a consequence, the biodistribution shifted from hepatocytes to LSECs and KCs, respectively, using cholesterol-oleate or oxidized cholesterol.(276, 277) Additionally, the distribution of commercial LNP formulations with DLin-MC3 compared to the ionizable lipid cKK-E12 was assessed, revealing that both formulations were not only delivered to hepatocytes but partly to LSECs and KCs.(278) Furthermore, variations within the alkyl chains of the phospholipids giving “constrained” adamantyl-phospholipids which delivered the cargo specifically to KCs and LSECs, but not to immune cells outside the liver were evaluated.(279) Recently, Pattipeiluhu et al. developed LNPs for delivery of mRNA to hepatic RES resembling the Onpattro® formulation. By replacing the phospholipid within the LNP from the zwitterionic 1,2-distearoyl-sn-glycero-3-phosphocholine (DSPC) to the anionic 1,2-distearoyl-sn-glycero-3-phosphoglycerol (DSPG) a negative surface charge was created and specific uptake by LSECs under participation of Stabilin receptors in embryonic zebrafish and mice was achieved.(280)

2.5 Immune Cells as Targets

Immune cells represent an interesting target for nucleic acid delivery as they play an important role in a wide range of diseases, including cancer, inflammatory or autoimmune diseases, etc. Besides the hepatic RES, immune cells are ubiquitous in the organism, especially in the spleen. Delivery of nucleic acid therapeutics to leukocytes, which include macrophages and dendritic cells as well as lymphocytes, offers the way to introduce genetic material with anti-inflammatory potential or to provoke T-cell modulation as a mean of immune stimulation (291, 292) and are presented in **Table 2.3**.

2.5.1 Macrophages

Macrophages, including the aforementioned Kupffer cells, express membrane lectins which recognize certain carbohydrate patterns, such as the mannose receptor CD206, that mediate endocytosis as a central function of immune response.(293, 294) This mechanism was used for targeted delivery of nucleic acids to macrophages. For example, DNA transfection to macrophages was accomplished by Erbacher et al. using mannosylated PLL polyplexes by interaction with the mannose receptor.(295) Mannosylation of PEG-PLL polyplexes caused an increase in transfection efficacy by about 8 times compared to untargeted polyplexes in a recent study by Lopukhov. Within the same study, the transfection efficacy of polyAsp(DET)-DNA polyplexes was boosted about 500 times when mannose residues were incorporated in the formulation.(296) Moreover, mannose-functionalized nanohydrogels have shown to efficiently deliver siRNA to CD206+ primary macrophages both *in vitro* and *in vivo*, which offers the opportunity for targeted gene regulation in immunosuppressive macrophages.(297, 298) In addition, Uehara et al. demonstrated efficient, ligand dependent gene silencing activity of a direct conjugate between siRNA and a tetravalent, chemically modified mannose in macrophages, which represents the first report of systemic delivery of siRNA-ligand conjugates to leukocytes.(217)

2.5.2 Dendritic cells

DCs, serving as antigen presenting cells (APCs), play a crucial role in antigen recognition of antigens and activation of immune response after uptake of foreign particles. Particles are internalized via phagocytosis or receptor-mediated endocytosis, dependent on their size and surface modifications. However, for immunotherapy it can be desirable to target DCs specifically.

DNA delivery to DCs via mannose receptor was described by Diebold et al. by using mannose functionalized PEI polyplexes. Receptor-specific uptake was demonstrated in a competition assay with mannose albumin, which lowered gene expression of Man-polyplexes.(234) Gao

et al. designed mannose ligands optimized towards the carbohydrate recognition domains of mannose receptor and the DC-specific intercellular adhesion molecule-3-grabbing non-integrin (DC-SIGN, CD209), respectively. Liposome uptake by DC2.4 cells and DC-SIGN expressing HEK293 cells was observed in a ligand-dependent manner. These particles were not yet used to deliver nucleic acids to DCs but provided deeper insight in the understanding of ligand design to improve receptor interaction.(299) The impact of PEG spacer lengths on particle size, stability and transfection efficacy was also examined using Man-PEG-Cholesterol lipids in mRNA-LNP formulations. It could be shown that zeta potential and particle size remained unchanged by increasing PEG lengths, whereas PEG1000 showed highest transfection efficacy while maintaining serum stability.(300) Recently, the effect of mannan-coating of LNPs for the delivery of RNA vaccines was investigated by using mono- and multivalent mannose residues linked to cholesterol, resulting in an increased immunization arguing for the use of targeted, mannan-functionalized RNA vaccines.(137)

Targeting of dendritic cells was also achieved via DEC205, another receptor from the mannose receptor family (301, 302). Katakowski et al. formulated LNPs bearing a single-chain antibody to target DEC205 expressing murine DCs. Receptor-specific binding and uptake of the siRNA-LNPs were determined via flowcytometry, showing that uptake was 2-fold improved by targeted LNPs. DEC205-dependent internalization was further confirmed by reduced knock-down efficacy in DEC205 deficient mice.(303)

The spleen and more specifically DCs were chemically targeted by lipoplexes with an inversed lipid/RNA charge ratio giving negatively charged particles. After systemic administration, these particles successfully delivered mRNA encoding for antigens and promoted stimulation of APCs for cancer immunotherapy.(304)

2.5.3 T-lymphocytes

T-lymphocytes also play a crucial role in cellular immune response.(305) Therapy of immune related disorders, e.g., inflammation or cancer, can be achieved by RNAi in T-lymphocytes. As gene delivery in these cells has appeared to be challenging (291, 306), the carrier systems have been decorated with ligands, mostly monoclonal antibodies, to improve nucleic acid delivery. For example, Buschle et al. achieved gene transfer to human T-lymphocytes by decorating Tf-PLL polyplexes with antibodies against the CD3 T cell receptor.(214) Ramishetti et al. aspired to deliver siRNA-LNPs to CD4+ T-lymphocytes by attachment of anti-CD4-monoclonal antibody, whereby the specific delivery to CD4+ lymphocytes could be confirmed *ex vivo*. Additionally, i.v. injection in mice showed gene silencing activity in spleen, lymph nodes, bone marrow and blood.(215) Veiga et al. evaluated LNPs loaded with modified mRNA for delivery to Ly6c+ inflammatory leukocytes.(307) For this purpose, the targeting ligand was attached to the LNP via incorporation of lipoproteins interacting with antibodies.(308)

Decoration with targeting mAbs towards inflammatory leukocytes led to strongly increased interleukin-10 expression in spleen and intestine.(307)

Great advances regarding nucleic acid delivery to T-lymphocytes were made using the chemical targeting approach. Using the barcode screening technology, Lokugamage et al. studied the distribution of a library of 168 siRNA-LNP formulations with structural changes regarding the lipids in different cell types *in vivo* and showed that constrained LNPs preferably delivered the genetic material to splenic T lymphocytes instead of hepatocytes making these formulations interesting for immunotherapy.(309)

A screening of 14 structurally different ionizable lipids by variation of linker backbone, head group and alkyl chains for delivery of siRNA-LNPs into leukocytes was reported by Ramishetti et al. The biodistribution after i.v. injection in mice showed accumulation in spleen for piperazine head group and in liver for tertiary amine head group.(310) In the same study, specificity was further improved by combination of both, chemical and active targeting. Decoration of the LNPs with anti-integrin b-mAbs resulted in CD45 mRNA knockdown in CD4+ and CD8+ lymphocytes in spleen and lymph nodes. Nevertheless, only a limited gene silencing ability was detected overall (310).

Table 2.3. Active targeting of different immune cell types.

Receptor	Ligand	Delivery System	Type of nucleic acid	Key results	Ref.
Macrophages					
Mannose receptor	Mannose	PLL polyplexes	DNA	Transfection to monocyte-derived macrophages using Man-PLL polyplexes	(295)
	Mannose	PLL polyplexes and pAsp(DET) polyplexes	DNA	8x increased transfection efficacy for Man-PLL polyplexes, 500x increased transfection efficacy for Man-pAsp(DET) polyplexes in murine bone marrow derived macrophages	(296)
	CM Mannose	Direct conjugate	siRNA	Ligand-dependent gene silencing in monocyte-derived macrophages (*in vitro*) and in splenic and liver macrophages (*in vivo*)	(217)
	Mannose	Cationic nano-hydrogel	siRNA	Receptor-dependent delivery of siRNA to M2 macrophages and efficient gene knockdown in primary cells and in mice	(297, 298)
Dendritic cells					
Mannose receptor	Mannose	PEI polyplexes	pDNA	Increase of transfection efficacy by mannosylation of PEI polyplexes, uptake was reduced in presence of the inhibitor Mannose-BSA	(234)
	Mannose	PEGylated LNPs	mRNA	Variation of PEG-spacer length (PEG100, PEG1000 and PEG2000) was evaluated; LNPs with Man-PEG1000 showed highest transfection efficacy	(300)
	CMM	Direct conjugate	siRNA	Ligand-dependent gene silencing activity in monocyte derived DCs	(217)

Receptor	Ligand	Delivery System	Type of nucleic acid	Key results	Ref.
	Mannan	LNP	saRNA	Enhanced immunization was observed for LNPs decorated with multivalent mannose residues	(137)
DEC205	Anti-DEC205 scFv	LNP	siRNA	DEC205-dependency on uptake was demonstrated; targeted LNPs showed 2-fold increase in uptake compared to untargeted LNPs and LNPs with an isotype of scFv	(303)
T-lymphocytes					
CD3 T-cell receptor	Anti-CD3 antibodies	PLL polyplexes	pDNA	1000-fold enhanced gene expression compared to unmodified PLL and Tf-PLL in T-cells; successful transfection to primary human lymphocytes	(214)
CD4	Anti-CD4 mAb	LNP	siRNA	Specific delivery to CD4+ cells *ex vivo*; gene silencing activity was observed in blood, bone marrow, spleen and lymph nodes	(215)
Ly6c	Anti-Ly6-mAb	LNP	mmRNA	Targeted delivery to Ly6c positive cells *in vitro*; in vivo evaluation in IBD mouse model showed increased protein expression (20-fold in intestine, 10-fold in spleen); expression of anti-inflammatory IL-10 after delivery of IL-10 encoding mmRNA	(307, 308)
n.a.	None (chemical targeting)	LNP	Barcode siRNA, sgRNA	Screening of 168 different LNP formulations *in vivo* with variations of head group, lipid alkyl chains, phospholipid and molar composition; adamantyl-DSPC delivered siRNA and sgRNA to T cells (and Kupffer cells)	(309)
n.a.	None (chemical targeting)	LNP	siRNA	Variation of head group and alkyl chain; piperazine headgroup led to accumulation and gene silencing in the spleen	(310)
Integrin β_7	Anti-β_7-mAb	LNP	siRNA	CD45 mRNA silencing in CD4+ and CD8+ T cells in spleen and lymph nodes	(310)

Abbreviations: PLL, Poly-L-lysine; Man, Mannose; pAsp(DET) poly(N-[N-(2-aminoethyl)-2-aminoethyl] aspartamide); CM Mannose, chemically modified mannose; PEI, polyethylene imine; BSA, bovine serum albumin; DCs, dendritic cells; scFv, single chain antibody; CD, cluster of differentiation; Tf, Transferrin; mAb, monoclonal antibody; Ly6c, lymphocyte antigen 6 complex; mmRNA, modified messenger RNA; IBD, inflammatory bowel disease; mAb, monoclonal antibody

2.6 Lung as Target

Many severe, eventually lethal diseases are associated with the lung, for example cystic fibrosis, chronic obstructive pulmonary disease (COPD), asthma or pulmonary fibrosis amongst others. One advantage of nucleic acid delivery to the lung is certainly the accessibility of the lung via local and systemic administration routes. However, protective mechanisms and physiological barriers such as mucosal barrier or immune cells may impair the delivery of nucleic acids.(311). For selective, targeted nucleic acid transfer into the lung chemical as well as receptor-mediated targeting strategies have been evaluated with the key results summarized in **Table 2.4**.

Table 2.4. Receptor-mediated non-viral nucleic acid delivery to the lung.

Receptor	Ligand	Delivery System	Type of nucleic acid	Key results	Ref.
Insulin receptor	Insulin	PEI polyplex	pDNA	Selective delivery to alveolar epithelial cells	(243)
Lactoferrin receptor	Lactoferrin	PEI polyplex	pDNA	Selective delivery to bronchial epithelial cells	(233)
Integrin	RGD motif	Liposome	pDNA	High transfection efficacy in lung endothelial cells for targeted liposomes *in vivo*	(210)
	TAT-RGD motif	Direct conjugate	pDNA	Enhanced uptake of targeted particles by pulmonary cells	(312)
		Cationic liposome	pDNA	5-fold increased gene expression in A549 cells compared to lipofectamine	
	RGD motif	Lipoplex	pDNA	Significantly improved transfection efficacy for RGD-bearing polyplexes	(313)
Polymeric IgR	Antisecretory component antibody	PLL polyplex	pDNA	Proof of concept for transfection efficacy to human tracheal epithelial cells, competition assay blocked uptake of targeted polyplexes	(314)
PECAM	Anti-PECAM antibody	PEI polyplex	pDNA	Enhanced gene transfer efficacy and reduced toxicity	(315)
	Anti-PECAM antibody	LNP	mRNA	Enhanced protein expression in lung endothelial cells; reduced accumulation in hepatocytes	(236)
Transferrin receptor	Transferrin	PEI polyplex	siRNA	Enhanced uptake of Tf-PEI polyplexes by pulmonary ATCs *in vitro* and in asthma mouse model after intratracheal application; improved endosomal escape by addition of melittin, 40% more effective than lipofectamine	(316, 317)
β2-adreno-ceptor	Clenbuterol	PEI polyplex	pDNA	Enhanced gene expression in alveolar epithelial cells	(206)
	Salbutamol	Chitosan polyplex	siRNA	Delivery to bronchial epithelial cells	(207)
IP1	Iloprost and Treprostinil	PEI polyplex	pDNA	Enhanced transfection efficacy	(208)
Lectins	Galactose, Glucose, Lactose	PLL polyplex	pDNA	Improved, sugar-type dependent gene expression in cystic fibrosis airway epithelial cells	(318-321)
	Galactose	PEGylated PEI polyplex	pDNA	Increased transfection efficacy *in vitro* and *in vivo*	(322)

Abbreviations: PEI, polyethylene imine; RGD, arginine-glycine-aspartic acid; TAT, transactivated transcription peptide; Ig, immunoglobulin receptor; PLL, poly-L-lysine; PECAM, platelet endothelial cell adhesion molecule; IP1, prostacyclin receptor; PEI, polyethylene imine

Due to their positive surface charge, many polyplex (PEI) as well as cationic liposome formulations automatically accumulate in the lung when injected systemically.(323-326) In addition, efforts were made to generate lung targeted LNPs, which typically accumulate in

hepatocytes by modification of lipid composition and the type of ionizable lipid. In the course of the development of “SORT”-LNPs, it was reported that increasing amounts of the positively charged component DOTAP shifted accumulation from hepatocytes to lung endothelial cells.(258) Chemical targeted synthetic carriers for specific lung delivery of mRNA and pDNA were developed by Kaczmarek et al. The hybrid polymer-lipid formulations used in their studies, consisting of poly(β-amino esters) (PBAEs) and PEGylated lipids, generated protein expression in the lung after i.v. injection in mice, but not in other organs.(327-329)

Active targeting of lung epithelial cells resulting in receptor-mediated uptake of non-viral delivery systems was obtained by several classes of ligands, such as peptides, proteins, antibodies, carbohydrates and also small drugs. Elfinger et al. studied the selective delivery to different lung epithelial cell types. It was reported that pDNA/PEI polyplexes modified with lactoferrin delivered the nucleic acid selectively to bronchial epithelial cells via lactoferrin receptor, but not alveolar epithelial cells, whereas adsorption of insulin to pDNA/PEI polyplexes showed increased luciferase gene expression in alveolar epithelial cells, but not in bronchial epithelial cells.(233, 243)

Integrins are also abundantly found on lung cells and attempts were made to achieve receptor-mediated uptake via caveolae-dependent pathway by incorporation of arginine-glycine-aspartic acid (RGD) motifs into the delivery system.(210, 312, 313) More specific targeting of the lung was achieved using antibodies as ligands. In early studies, Ferkol et al. observed targeted delivery of pDNA-polylysine complexes conjugated with Fab fragments of immunoglobulins directed against the polymeric immunoglobulin receptor (IgR) which is involved in the transport of immunoglobulins A and M from cell surface into lung epithelial cells. A competition assay with excess of Fab ligand blocked delivery gives further evidence for receptor-mediated uptake.(314) Additionally, lung-specific nucleic acid transfer was accomplished using antibodies directed against the platelet endothelial cell adhesion molecule (PECAM). For example, Li et al. were able to generate higher gene expression after i.v. injection of anti-PECAM-mAb decorated pDNA-PEI polyplexes in mice, furthermore observing reduced cytotoxicity when using ligand-modified carriers.(315) More recently, mRNA-LNPs, which are known to accumulate in the liver, were modified with monoclonal antibodies directed against PECAM-1. Intravenous injection in mice avoided accumulation in hepatocytes but resulted in enhanced protein expression in lung endothelial cells.(236)

Transferrin (Tf) was used as targeting ligand to mediate the delivery of PEI-siRNA polyplexes to pulmonary activated T cells (ATCs). A study by Xie et al. has shown that transferrin modification led to enhanced cellular uptake and efficient, selective gene knockdown *in vitro* as well as in an asthma mouse model after intratracheal application (316). Further optimization of the Tf-PEI polyplexes by blending with PEI bearing the endosomolytic peptide melittin improved endosomal escape capability of the cargo resulting in enhanced cellular uptake

(317). In fact, optimization of endosomal escape properties for delivery of siRNA polyplexes to the lung has been subject of further studies. For example, Pun et al. developed a virus-inspired polymer for endosomal release (VIPER) (330), which was applied for efficient pulmonary delivery of siRNA both *in vitro* and *in vivo* (331). VIPER/siRNA polyplexes also showed antiviral effect by promoting suppression of viral replication of SARS-CoV-2 *ex vivo* in human lung tissues and in mouse models.(332)

Furthermore, small chemical compounds, which have already been used effectively as drugs for asthma treatment were used as targeting ligands coupled to synthetic nucleic acid carriers for targeted nucleic acid delivery to the lung. For example, agonists for the b2-adrenoceptor were successfully used for targeted and improved delivery of nucleic acids to lung epithelial cells. Elfinger et al. demonstrated enhanced gene expression in alveolar epithelial cells *in vitro* as well as *in vivo* after inhalation of Clenbuterol-functionalized polyplexes.(206) Specific delivery of siRNA to bronchial epithelial cells could be improved by coupling of Salbutamol to the formulation, as shown by Luo et al. using guanidinylated chitosan carriers.(207) In addition, PEI-polyplexes modified with Iloprost and Treprostinil, prostacyclin derivatives targeting the prostacyclin receptor IP1, also exhibited enhanced transfection efficacy of pDNA polyplexes in lung epithelial cells as well *in vivo* in the lungs of mice after aerosol administration.(208) For these chemical ligands, their possible dual role as drugs was not explored.

Additionally, lectins have been studied for lung-specific uptake of non-viral delivery systems. Several studies by Kollen et al. showed that gene expression of pDNA/polylysine polyplexes could be increased through functionalization with b-galactose, a-glucose as well as lactose compared to other monosaccharides and the non-targeted formulation after transfection to cystic fibrosis cells.(318-321) Transfection of galactosylated polyplexes also resulted in improved gene expression compared to non-targeted polyplexes in A549 cells as well as *in vivo* experiments after intratracheal administration.(322) In both studies, lectins were hypothesized to play a role in the specific uptake of the particles, although the particular uptake route was not further addressed.

2.7 Brain as Target

Many neurodegenerative disorders such as Alzheimer’s disease, Huntington’s disease, Parkinson’s disease or amyotrophic lateral sclerosis (ALS) originate in the central nervous system (CNS). Treatment of these diseases via systemic administration routes remains challenging due to poor accessibility of the brain through the blood-brain barrier (BBB). Therapeutic nucleic acids compacted into synthetic carrier systems are not able to cross the BBB via diffusion.(333) However, nucleic acid delivery to the brain via systemic administration

is highly desired, as topic routes like intracranial or intracerebroventricular injections as well as physical methods that enhance the permeability of the BBB are highly invasive. Thus, synthetic carriers must be decorated with ligands, which are recognized by receptors or carriers embedded in the BBB, becoming “trojan horses”, which are enabled to deliver nucleic acid to the brain through receptor-mediated transcytosis (RMT) or carrier-mediated transcytosis (CMT). Various synthetic carrier systems were modified with several ligands, ranging from proteins, peptides and aptamers to generate brain-targeted gene delivery (see **Table 2.5**).
A possible approach to facilitate nucleic acid transfer into the CNS is to use receptor-mediated transcytosis by transport proteins that enable the passage of essential nutrients, proteins or lipids across the BBB.

Table 2.5. Receptors and ligands for targeted delivery of nucleic acids to the brain.

Receptor	Ligand	Delivery System	Type of nucleic acid	Key findings	Ref.
Transferrin receptor	Transferrin	Lipoplex	siRNA	Efficient gene silencing in primary murine cortical neuronal cells and *in vivo* without cytotoxicity	(334)
	Transferrin	PEG-PAMAM dendrimer polyplex	pDNA	Enhanced gene expression in BCECs and in mice brain	(335)
	Transferrin	PPI polyplex	pDNA	Targeted polyplexes accumulated in mice brain	(336)
	Anti-TfR-mAb	Immuno-liposome	pDNA	TfR-mAb promoted both, crossing of BBB and delivery to TfR-expressing glioma cells	(337)
	re-TfR-peptide	Lipo-oligo-(amidoamine) polyplex	pDNA	Enhanced luciferase gene expression in N2a cells compared to non-targeted lipoplexes and scrambled peptide ligand	(211)
Lactoferrin receptor	Lactoferrin	PEG-PAMAM polyplex	pDNA	2.2-fold increased gene expression *in vivo,* selective gene transfer to the brain	(338)
	Lactoferrin	PPI Polyplex	pDNA	2.1-fold increased gene expression *in vitro*, significantly higher gene expression *in vivo*	(339)
LRP1	Angiopep-2	PEG-PAMAM dendrimer polyplex	pDNA	Selective uptake of polyplexes by BCECs, accumulation of targeted polyplexes in brain, untargeted in spleen	(340)
	Angiopep-2	LNP	siRNA	*In vitro* study of cellular uptake and gene silencing efficacy in U87MG and b.End3 cells	(341)
nAChR	RVG29	Oligoarginine polyplex	siRNA	Enhanced gene expression in brain after i.v. injection, but not in other organs	(342)
	RVG29	PEG-PAMAM dendrimer polyplex	pDNA	Brain accumulation after systemic administration, GABA receptor involved in uptake	(343)
	RVG29	PEI polyplex	miRNA	Reduced signal of reporter gene due to silencing activity, accumulation in brain	(344)
	RVG29	Trimethylated chitosan polyplex	siRNA	Efficient gene silencing of BACE1, accumulation in brain	(345)

Receptor	Ligand	Delivery System	Type of nucleic acid	Key findings	Ref.
	RVG29	Poly(mannitol-co-) PEI	siRNA	Efficient gene silencing of BACE1	(346)
	RVG29	Exosomes	siRNA	Gene knock-down of BACE1	(347)
	RVG-9r	SNALP	siRNA	Efficient silencing of Machado Joseph disease involved proteins *in vitro* and *in vivo*	(348)
Laminin receptor	EPRNEEK	Dendrigraft PLL polyplex	DNA	Improved uptake and gene expression by exogenous ligand compared to endogenous laminin ligand	(349)
Leptin receptor	Leptin-30 peptide	PEGylated PLL Polyplex	pDNA	Improved transfection efficacy in BV-2 cells; accumulation in brain after i.v. injection	(350)
VCAM1	Anti-VCAM-antibody	LNP	mRNA	Specific mRNA delivery to inflammatory brain, but not to leukocytes, expression of anti-inflammatory protein	(351)
GLUT1	Glucose	Polyplex	ASO	Accumulation in mice brain after i.v. injection depending on glucose-concentration	(352)

Abbreviations: PAMAM, poly(amidoamine); BCECs, brain capillary endothelial cells; PPI, polypropylene imine; TfR-mAb, transferrin receptor monoclonal antibody; re-TfR, retro-enantio transferrin receptor, N2a, neuro2a cell line; LRP-1, low-density lipoprotein receptor related protein 1; GLUT1, glucose transporter 1; nAChR, nicotinic acetylcholine receptor; RVG29, rabies virus derived 29-mer peptide; GABA, gamma-aminobutyric acid; BACE1, beta-secretase 1; SNALP, stable nucleic acid lipid particle; PLL, poly-L-lysine; VCAM1, vascular cell adhesion molecule 1

2.7.1 Receptor-mediated transcytosis

Receptors for iron transport proteins. Transport of iron across the BBB is mediated by several iron transport protein receptors, including transferrin, lactoferrin or melanotransferrin. Above all, transferrin receptor was widely studied for targeted uptake of synthetic carriers to the CNS. As known from previous studies, the transferrin protein itself holds great potential to mediate receptor-dependent polyplex uptake by TfR-expressing cells and therefore, was explored for mediating transcytosis across the BBB.(353, 354) For example, Cardoso et al. prepared Tf-modified siRNA-lipoplexes that showed superior uptake by neuronal cells as well as significant gene silencing in both, *in vitro* and *in vivo* compared to non-targeted particles.(334) Moreover, dendrimer-polyplexes based on PAMMA or PPI were functionalized with human transferrin, resulting in successful pDNA delivery across the BBB. Biodistribution studies further confirmed accumulation of TfR-targeted dendrimers in the brain.(335, 336) TfR was also targeted by immunoliposomes bearing monoclonal antibodies (mAb) directed against rat TfR for RNAi therapy via delivery of plasmids encoding for short hairpin RNA (shRNA). It could be demonstrated that TfR-targeted immunoliposomes provided a dual targeting effect, as they promoted BBB crossing and subsequent uptake of glioma cells, which are also overexpressing TfR.(337) Recently, TfR-mediated delivery to neuronal cells was successfully accomplished by our group using a retro-enantio peptide sequence that showed high affinity towards the transferrin receptor. The “retro-enantio” approach provides stability against peptide degradation by inversion of the peptide order and usage of D-configurated amino acids while

maintaining receptor binding affinity.(355) The retro-enantio ligand was conjugated to sequence-defined lipo-oligo(amidoamines) (lipo-OAAs) for the delivery of both, siRNA and pDNA, to N2a cells.(211)

Lactoferrin receptor. Besides TfR, the lactoferrin receptor (LfR) is also involved in cellular iron uptake and expressed on the BBB.(356) By using LfR, increased gene expression of dendrimer polyplex formulations bearing lactoferrin (Lf) could be observed. Lf-modification of PAMAM dendrimer polyplexes resulted in 2.2-fold increase of luciferase gene expression *in vivo* compared to untargeted particles. In addition, selective delivery to the brain was reported after systemic administration.(338) Additionally, lactoferrin-PPI-dendrimers showed improved transfection in b.End.3 cells and significantly increased accumulation in mice brain.(339)

Melanotransferrin. Furthermore, a short 12-amino acid peptide which has shown interaction with the iron transport protein melanotransferrin was able to mediate entry in the brain. Conjugation to siRNA enabled not only accumulation in the brain, but also *in vivo* gene silencing of NOX4, a gene that is upregulated during stroke.(357, 358)

LRP1. Nucleic acid transfer across the BBB was furthermore achieved by low-density lipoprotein receptor related protein (LRP1) mediated transcytosis. Demeule et al. developed Kunitz domain derived peptides from aprotinin, named Angiopep, that showed the ability to overcome BBB via LRP1-mediated transport.(359, 360) Angiopep-2 was attached to DNA/PAMAM-dendrimers showing selective uptake by BCECs *in vitro* and a shift of the biodistribution from spleen (for untargeted carriers) to brain (for targeted polyplexes) *in vivo.*(340) The same ligand was later included in siRNA-LNP formulations by Bruun et al. for *in vitro* studies on uptake and gene silencing activity in human glioblastoma U87MG and murine brain endothelial bEnd.3 cell line. In addition to an increased gene knock-down, it could be observed that uptake could be improved about 2.4-fold by Angiopep-2 modification.(341) Moreover, a novel artificial ligand named L57 was found to enable BBB crossing *in vivo* by interaction with LRP1.(361) Compared to Angiopep-7, L57 showed enhanced CNS uptake capability and low cytotoxicity.(362)

Leptin receptor. Moreover, the leptin receptor, which is responsible for recognition and transcytosis of the appetite regulating peptide leptin, was used for nucleic acid delivery to the brain.(363) It was shown that a leptin-derived 30-amino acid peptide attached to poly-L-lysine carrier was able to generate improved DNA transfection in BV-2 cells and accumulation in mice brain after i.v. injection.(350)

Pathogen-derived peptide ligands. In addition to ligands interacting with receptors which transport essential molecules across the BBB, another approach is to modify the carrier system with peptides deriving from viruses, bacteria or venoms that naturally show capabilities to enter the brain. For example, the peptide RVG29 was studied for nucleic acid transfer across the BBB. The ligand derived from rabies virus glycoprotein (RVG), which naturally shows the ability

to enter the brain as part of its pathology and targets mainly the nicotinic acetylcholine receptor (nAChR).(364) RVG29 was included in polyplex and LNP formulations yielding nucleic acid transfer across the BBB. For example, Kumar et al reported efficient gene silencing using RVG-bearing siRNA oligo(arginine) formulations.(342) A study by Liu et al., using RVG29-PEG-PAMAM/DNA polyplexes, revealed involvement of GABA receptor in uptake.(343) Efficient gene silencing of BACE1, a protein involved in Alzheimer's disease, could be achieved by several groups using polyplex as well as exosome formulations that were functionalized with RVG29.(345-347) Furthermore, a lipid-containing formulation bearing RVG-oligo(arginine) residues exhibited the ability to silence a mutant ataxin-3, involved in the pathology of Machado-Joseph disease, a hereditary ataxia disorder.(348) Furthermore, Liu et al. demonstrated the capability of a peptide sequence derived from meningitis-causing pathogen to mediate brain-specific delivery of surface-modified PLL/DNA-dendrimers via laminin receptor, resulting in enhanced cellular uptake by BCECs and U87MG cells compared to an endogenous laminin-targeting ligand.(349)

VCAM1. A recent study by Marcos-Contreras et al. explored the specific delivery of antibody-modified mRNA-LNPs using an anti-vascular cell adhesion molecule 1 (anti-VCAM1) antibody to the inflammatory brain. It was found that the particles were delivered to brain endothelial cells but not to leukocytes. Furthermore, as a consequence of successful mRNA delivery, expression of anti-inflammatory thrombomodulin could be observed in a mouse model.(351)

Direct conjugates for BBB-targeting. Some of the aforementioned ligands, such as Angiopep and RVG-29, as well as further peptide ligands were used for direct conjugation to phosphorodiamidate morpholino oligomers (PMOs), which function as splice-switching oligonucleotides. It was demonstrated that a truncated peptide-derivative of ApoE mediates PMO delivery in the CNS.(365)

2.7.2 Carrier-mediated transcytosis

Transcytosis via GLUT1. An additional pathway to overcome BBB is through transcytosis by glucose transporter 1 (GLUT1). As transport carrier for glucose, GLUT1 is abundantly expressed on brain capillary endothelial cell (BCEC) membrane, ensuring adequate glucose supply of the brain.(366) Researchers exploited this transport mechanism by using glucose modified nanoparticles as "trojan horses" to induce gene transfer into the brain and other GLUT1-rich cells. For example, Kataoka et al. developed glucose-decorated polymeric carriers, which facilitated nanoparticle delivery to GLUT1-rich cancer cells under glycemic control.(218, 367) These block-copolymers were applied for the delivery of ASOs to the brain via intravenous injection into mice, providing efficient gene knockdown.(352) Another glucose-ligand capable of crossing the BBB is an opioid-derived glyco-heptapeptide (g7). Even though the transport mechanism of g7-functionalized particles into the brain is not fully understood,

decoration of nanoparticles with g7 showed brain specific uptake after i.v. injection into rat and therefore presents a promising ligand for nucleic acid delivery to the CNS.(368-371)

2.8 Ocular targeting

2.8.1 Retina

Many genetic eye disorders, either inherited or environment-dependent, may lead to loss of vision eventually due to impaired functions of photoreceptors or retinal pigment endothelium (RPE). Therapeutic approaches mostly use classic gene therapy with DNA for gene replacement or gene-editing methods. Formulations are usually injected subretinal or intravitreal due to the blood ocular barrier and in order to reduce off-target effects or elimination by immune system. Furthermore, persistent high levels of gene expression after single injections are highly desired for retinal gene therapy. Sustainable gene expression was achieved by using PEG-PLL/DNA polyplexes, which were locally injected in mouse models.(372-374) Delivery of nucleic acid therapeutics to the retina resulting in long-term gene expression was also reported by the group of Zheng-Rong Lu.(375) Lu and co-workers have developed a multifunctional ionizable lipid, called “ECO”, which served as efficient gene carrier system in several applications.(376-378) A hybrid ECO/G4-dendrimer formulation was applied successfully as carrier system for GFP reporter gene to human ARPE-19 cells and in animal experiments.(379) Moreover, ECO served as carrier for the therapeutic ABCA4 plasmid, supported by a rhodopsin promoter, for the treatment of Stargardt disease. These formulations provided up to 8 months of gene expression and disease progression delay for 6 months in ABCA4 deficient mice.(380) ECO/DNA formulations were also functionalized with $PEG_{3.4kDa}$-all-*trans*-retinylamine to target the interphotoreceptor retinoid binding protein (IRBP), a key protein in the retinoid cycle.(381) In this study, high transfection efficacy of the reporter gene GFP could be demonstrated in ARPE-19 cells and mouse models of Leber’s congenital amaurosis (LCA) type 2 after subretinal injection with high expression levels up to 120 days.(382) Additionally, a chemically stable retinoid analogue ACU4429, linked to the carrier system via pH-sensitive hydrazone-$PEG_{3.4kDa}$-spacer, was used for IRBP-mediated delivery of ECO/DNA particles and gene expression of ABCA4 in ARPE-19 cells as well as in *abca4*$^{-/-}$ mice.(383)

Furthermore, liposome-protamine complexes have shown potential to promote long term gene expression or gene knock-down, respectively.(384-386) More recently, LNP formulations encapsulating either mRNA (387) or siRNA (388) were screened to investigate cell-specific retinal nucleic acid transfer depending on surface charge and LNP composition. It was observed that mRNA-LNPs containing ionizable lipid are preferably internalized by RPE cells, suggesting ApoE-mediated uptake, whereas formulations with permanently cationic lipids

showed only low transfection efficacies in the retina.(387) Another study using siRNA-LNPs demonstrated that LNPs with positive zeta potential around +35 mV distributed preferably in the vitreous and retina after local injection.(388)

2.8.2 Cornea

In order to address corneal gene delivery, researchers used hyaluronic acid as a targeting ligand for the CD44-receptor, which is expressed by human corneal epithelial cells and is responsible for turnover of HA.(389-391) For instance, de la Fuente et al. developed HA-chitosan nanoparticles loaded with reporter DNA which successfully transfected human corneal epithelial (HCE) cells and conjunctiva cells via the CD44-receptor.(392, 393) Further investigations of the internalization pathway revealed that the particles were endocytosed by caveolae-mediated endocytosis.(103, 394) CD44-receptor mediated intracorneal uptake was also assessed by Hornof et al. using HA-coated PEI/DNA polyplexes demonstrating that nanoparticles coated with low-molecular weight HA generated well shielded, stable particles while maintaining efficient transfection activity.(205)

2.9 Muscle as Target

The delivery of nucleic acids to skeletal and cardiac muscles allows the treatment of muscle-related disorders such as muscular dystrophy. Efforts were made to develop lipid-siRNA conjugates that enable muscle-targeted delivery upon systemic injection. Therefore, a library of lipid-ASO conjugates was screened regarding their ability to deliver functional ASOs to muscle cells after i.v. injection in mice. It was demonstrated that delivery to muscle cells depended on the length of the fatty acid, with C16 to C22 showing highest accumulation based on their affinity to albumin which mediated transport to muscle cells.(395) The palmitic-ASO conjugate was further evaluated revealing a slight increase in ASO activity, but relatively rapid clearance.(396) A following study evaluated ASO potency and association with human, rodent and monkey plasma proteins, showing a preferred binding of palmitate-ASOs to human and rodent albumin as well as histidine-rich glycoprotein possibly explaining enhanced ASO activity in the muscle. Additionally, an enhanced *in vivo* ASO potency was observed in rodents, but only a modest improvement in monkeys.(397) Moreover, different lipids were conjugated to chemically stabilized siRNA for a distribution study in mice. Most formulations accumulated in clearance organs such as liver or kidney, while docosanoic acid-siRNA conjugate (DCA) delivered siRNA partly to other tissues.(398) Compared to cholesterol-siRNA, delivery of DCA-conjugates to skeletal and cardiac muscles was enhanced about 3-fold and 2.5-fold, respectively. Using DCA conjugates, sustained silencing of myostatin mRNA in muscles was obtained leading to reduced myostatin protein levels and promotion of muscle growth after systemic injection.(399)

2.10 Active targeting: *in vitro* versus *in vivo*

It is noticeable that delivery systems using targeting ligands are rather rare on the medical market. Only a few products such as GalNAc direct siRNA conjugates and ApoE endogenously targeted Patisiran were approved by FDA. In fact, the majority of targeting ligands was evaluated in cell culture studies, demonstrating improved *in vitro* performance. However, most formulations have not taken the step to product development for *in vivo* applications.

Potential reasons for this observation must be considered and evaluated in order to find explanations for this translational bottleneck. There is a great discrepancy between the results obtained from *in vitro* studies and *in vivo* performance, making predictions for (pre-)clinical studies questionable when drawn from cell culture evaluation.(198-200)

In vivo nucleic acid delivery appears to be affected by several barriers. In contrast to small molecule drugs, nucleic acids exhibit unfavored pharmacokinetic and pharmacodynamic profiles due to their high molecular weight and charge, excluding membrane diffusion as internalization route. The demand for endocytic internalization pathways, membrane barriers become more difficult to overcome, and formulation properties have to be carefully tailored, resulting in complex, multi-component nanoparticle formulations. Furthermore, different types of nucleic acid therapeutics have different requirements on the formulation. Therefore, addressing new obstacles, i.e., cellular barriers such as nanoparticle uptake and endosomal escape represent major bottlenecks for clinical translation, as discussed in detail by several researchers.(18, 400-402) Prior to cellular uptake and endosomal escape, interaction of carriers with blood components determine not only transport but eventually also efficiency. Thus, the behavior in plasma represents a critical obstacle for the delivery system. Depending on their physicochemical properties, including size, zeta potential and surface modification, certain proteins will adsorb on their surface to form a “protein corona”. This protein corona largely determines the characteristics of the particles in the organism, i.e., biodistribution, pharmacokinetics and immunogenicity. It was observed that the adsorption of plasma proteins leads to reduced accessibility or interaction between exogenously incorporated ligands and their targeted receptors (**Figure 2.5**). For example, several studies reported that transferrin-coated nanoparticles showed reduced or lacking specificity towards TfR in presence of the protein corona as a result of ligand blockade.(403-405) The resulting “biological identity” was highly dependent on the composition of the protein corona. In particular, *in vitro* protein corona depleted targeting capability, whereas a protein corona resembling *in vivo* conditions caused only a reduction in specific receptor-mediated uptake.(404)

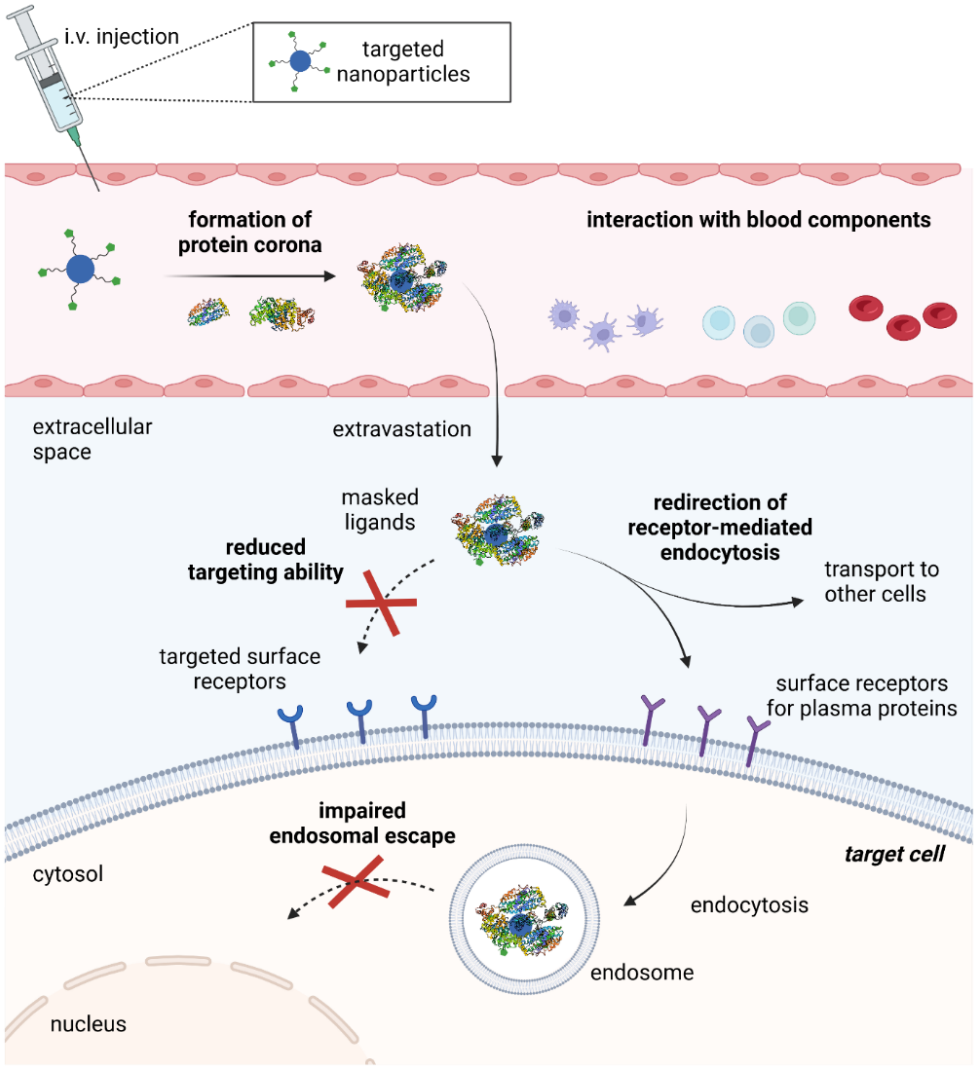

Figure 2.5. Interaction of i.v. injected targeted nanoparticles with blood components and consequences for the delivery process. Formation of protein corona leads to reduced intended targeting ability due to masked ligands. Protein corona may lead to transport to other cells or uptake via receptors recognizing plasma proteins. Additionally, endosomal escape can be hampered by protein layer. Created with BioRender.com

Interestingly, two studies could prove that the *in vivo* protein corona even enhanced the overall uptake of the nanoparticles, hypothesizing redirection of cellular uptake by the protein layer and opening new paths for particle internalization.(405, 406) As a consequence, plasma protein adsorption could also lead to redirected transport to off-target cells such as the RES, which hampers selective nucleic acid delivery and efficacy. In addition, Tonigold et al. observed that antibodies covalently bound to nanoparticles lose their targeting ability almost completely in presence of serum. Particles with physically adsorbed antibodies, however, maintained their targeting ability, probably due to the fact that these antibodies were not completely exchanged or masked by serum proteins.(237)

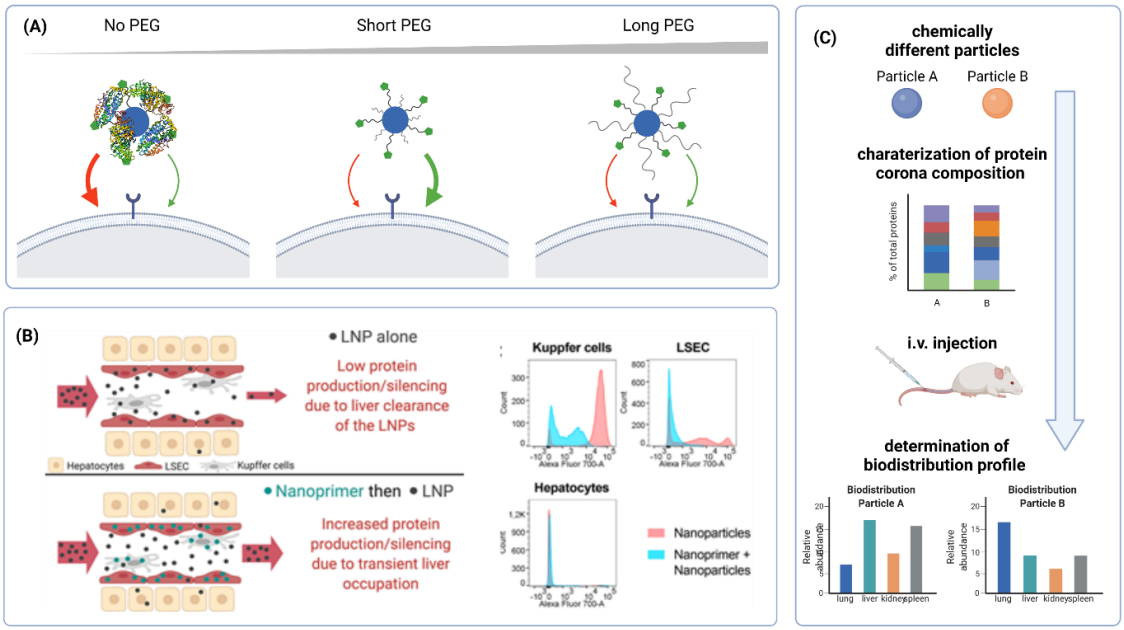

Figure 2.6. Strategies to improve or maintain targeting ability in vivo. (A) PEG-Backfilling avoids formation of protein corona, which would mask targeting ligands. Short PEG chains are necessary to maintain accessibility of the ligands (407). (B) Application of a nanoprimer is reducing off-target LNP uptake by Kupffer cells and LSECs and enhances delivery to hepatocytes. Reproduced with permission from reference(408) with Copyright © 2020, American Chemical Society. (C) Adjustment of surface chemistry leads to modified protein corona composition and can be used for targeted delivery by altered biodistribution profile. Created with BioRender.com

Traditionally, masking the surface properties causing plasma protein adsorption is a key strategy to overcome this issue and to maintain targeting ability. PEGylation has proven to reduce undesired interactions and consequently retain ligand-accessibility which is essential for targeted delivery *in vivo*.(82) One approach to further attenuate particle interaction with plasma proteins is PEG "backfilling" (**Figure 2.6 A**). Therefore, the surface of gold nanoparticles (Au-NPs), functionalized with targeting transferrin-PEG(5kDa) was further modified at free reaction sites with PEG spacers of varying lengths, preventing the particles from protein corona formation. In order to enable receptor-recognition, PEG chains for shielding had to be shorter than the spacer between particle and targeting ligand.(407) Despite these difficulties, there are promising examples which have already demonstrated efficient, cell- or tissue-specific delivery of nucleic acids. Additionally, scientists have started to exploit the protein corona to tune particle distribution *in vivo*. It is commonly known that plasma proteins adsorption depends on particle surface characteristics. Hence, slight structural changes of the particle surface have shown to affect the protein corona composition. As a consequence of protein corona modification, transport to target cells by coating with certain plasma proteins which serve as endogenous ligands can be obtained *in vivo*. For example, DOTAP/DNA lipoplexes have shown to adsorb vitronectin which mediated receptor-dependent uptake by tumor cells expressing a_Vb_3 integrins.(409) Patisiran is another prominent example for targeted transport to hepatocytes, mediated by coating with endogenous ApoE.(20, 255) Manipulation of the interaction with receptors *in vivo* and therefore targeted delivery to other

cell types could be achieved by an altered protein corona as a consequence of exchanging certain lipid components of the Patisiran formulation.(280) Additionally, Saunders et al. used “nanoprimers” administered shortly before injection of therapeutic LNPs that were taken up by cells of the hepatic RES (**Figure 2.6 B**). By inhibiting KCs and LSECs, LNPs could be preferentially delivered to hepatocytes, the desired target site.(408)

Based on these observations, methods which enable fast screening of broad libraries of nucleic acid carriers *in vivo* were developed.(256-259) By means of that, evaluation and characterization of predominant plasma proteins in the corona and tuning the biodistribution profile based on facile structural variations becomes feasible, pathing the way for improved targeted, cell-specific nucleic acid delivery *in vivo* (see **Figure 2.6 C**) (104, 276-279).

2.11 Conclusion

Cell-specific delivery, especially for *in vivo* applications, remains a central challenge for the development of new nucleic acid therapeutics. Tremendous efforts were put into the optimization of existing delivery systems as well as in the development of new carriers due to numerous barriers that have to be overcome for efficient delivery and activity of the nucleic acid therapeutic. Receptor-mediated and chemical targeting strategies represent key approaches for targeted delivery and improved performance of synthetic carriers and have proven their ability for enhanced transfection efficacy in the desired cell type. Receptor-mediated nucleic acid delivery can be highly specific towards certain cell types (e.g., ASGPR) and even allows receptor-mediated transport across internal barriers (e.g., BBB). New, high-affinity ligands for specific delivery are discovered continuously and can be conjugated to synthetic carriers in numerous ways. Chemical targeting achieved by structural alterations of the particle components has also shown great potential for promoting cell-specific nucleic acid delivery. As a result, shifted biodistribution profiles were observed which enabled delivery to desired cells. In addition, new technologies as the barcoding method combined with high throughput processes could path the way for future applications, readily adjustable formulations and a deeper understanding of *in vivo* performance.

Declarations

Acknowledgement and Funding

The authors are greatly thankful for the support of their work by the German Research Foundation (DFG) via the Collaborative Research Centre SFB 1032 sub-project B4.

Conflict of Interest

The authors have no conflicts of interest to declare.

3 GalNAc- or Mannose-PEG Functionalized Polyplexes Enable Effective Lectin-mediated DNA delivery

*Ricarda C. Steffens[1,6], Paul Folda[1], Nikole L. Fendler[2], Miriam Höhn[1], Katharina Bücher-Schossau[3], Susanne Kempter[4,6], Nicole L. Snyder[2], Laura Hartmann[3,5], Ernst Wagner[1,6], Simone Berger[1,6,]**

[1]Pharmaceutical Biotechnology, Department of Pharmacy, Ludwig-Maximilians-Universität (LMU) Munich, 81377 Munich, Germany.

[2] Department of Chemistry, Davidson College, Davidson, North Carolina 28035, USA.

[3] Institute of Organic Chemistry and Macromolecular Chemistry, Heinrich-Heine-University Düsseldorf, Universitätsstr. 1, 40225 Düsseldorf, Germany.

[4] Faculty of Physics, LMU Munich, 80539 Munich, Germany.

[5] Institute for Macromolecular Chemistry, University Freiburg, Stefan-Meier-Str. 31, 79104 Freiburg im Breisgau, Germany.

[6] Center for NanoScience (CeNS), LMU Munich, 80799 Munich, Germany.

* Correspondence: simone.berger@cup.uni-muenchen.de

This chapter is adapted from a research paper published in Bioconjugate Chemistry, 2024 March 05, Volume 35, page 351-370. DOI: 10.1021/acs.bioconjchem.3c00546. (410)

Author contributions

The manuscript was prepared with collective contributions of all authors listed. Ricarda C. Steffens: conceptualization, writing, illustrations, review, editing, synthesis of GalNAc-ligand, PEG-agents and mannose-ligand, polyplex formulations, physico-chemical characterization, transfections; Paul Folda: synthesis, analytical and physico-chemical characterization of azido-4-arm library, writing and editing; Nikole L. Fendler and Katharina Bücher-Schossau: synthesis and characterization of the GalNAc ligand precursor, reviewing, editing; Miriam Höhn: receptor-staining experiments; Susanne Kempter: TEM experiments, reviewing; Nicole L. Snyder and Laura Hartmann: conceptualization and super vision of the synthesis of the GalNAc ligand, writing, reviewing, editing, funding acquisition; Ernst Wagner: supervision, conceptualization, writing, reviewing, editing, funding acquisition; Simone Berger: supervision, conceptualization, formulations, physicochemical and *in vitro* evaluation of mannose-functionalized polyplexes, illustrations, writing, reviewing, editing. All authors have read and agreed to published version of this manuscript.

3.1 Abstract

A cationic, dendrimer-like oligo(aminoamide) carrier with 4-arm topology based on succinoyl tetraethylene pentamine and histidines, cysteines, and N-terminal azido-lysines was screened for plasmid DNA delivery on various cell lines. The incorporated azides allow modification with various shielding agents of different polyethylene glycol (PEG) lengths and/or different ligands by copper-free click reaction, either before or after polyplex formation. Pre-functionalization was found to be advantageous over post-functionalization in terms of nanoparticle formation, stability, and efficacy. A length of 24 ethylene oxide repetition units and pre-functionalization of ≥ 50% of azides per carrier promoted optimal polyplex shielding. PEG shielding resulted in drastically reduced DNA transfer, which could be successfully restored by active lectin targeting via novel GalNAc or mannose ligands, enabling enhanced receptor-mediated endocytosis of the carrier system. The involvement of asialoglycoprotein receptor (ASGPR) in the uptake of GalNAc-functionalized polyplexes was confirmed in the ASGPR-positive hepatocarcinoma cell lines HepG2 and Huh7. Mannose-modified polyplexes showed superior cellular uptake and transfection efficacy compared to unmodified and shielded polyplexes in mannose-receptor expressing dendritic cell-like DC2.4 cells.

Graphical Abstract

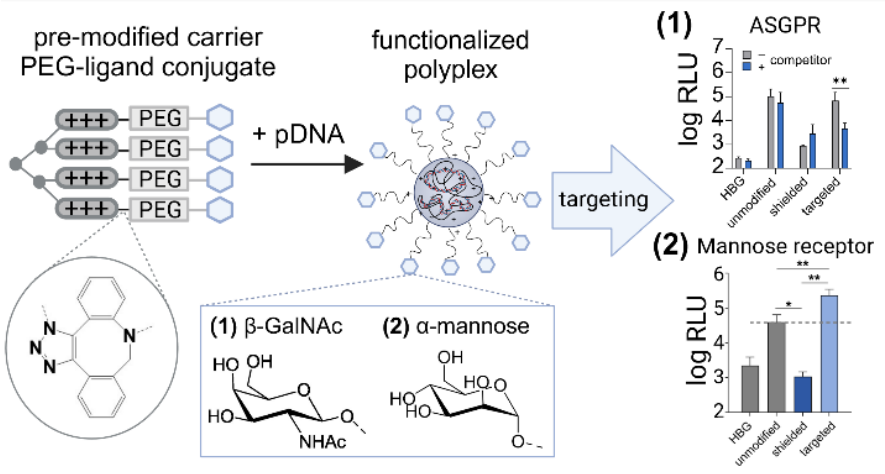

Figure 3.1. Graphical abstract.

Keywords. plasmid DNA, polyplex, mannose, GalNAc, polyethylene glycol, targeting.

3.2 Introduction

Therapeutic intervention at the genomic level offers various options for the preventive or causal treatment of severe diseases such as viral infections, cancer, or genetic disorders. Currently, a steadily increasing number of such therapeutic approaches is evaluated in clinical trials or has already achieved market authorization.(2, 411) An advantage of DNA-based therapies is that they provide long-term protein expression, ideally facilitating curative treatment of chronic and genetic diseases by single application. In view of translation into the clinical setting, the nucleic acid drug product requires a suitable delivery system with sufficient stability, high transfection efficiency, and good biocompatibility. So far, the majority of clinical gene therapy trials utilizes viral vectors,(2, 412) but these entail several limitations such as immunogenicity, limited cargo capacity, rather sophisticated production, difficult production upscale, and high production costs.(171, 413) Non-viral delivery systems, including polyplexes and lipoplexes,(48) may be adequate alternatives. However, many synthetic nanocarriers still suffer from low transfection efficiency, especially in comparison with viral vectors, and toxicity issues.(166, 167, 414, 415) Thus, a more bio-inspired approach (so-called “molecular and chemical evolution”) that relies on knowledge of highly effective viral transfection processes has been applied to continuously improve non-viral delivery systems.(50, 58, 413) For successful gene delivery *in vivo,* extracellular stability and intracellular release of the cargo in its active form at the site of action is of great importance (“polyplex dilemma”). Incorporation of bio-responsive elements allows for dynamic, spatially and timely controlled delivery.(45) Nanoparticle shielding with *e.g.*, polyethylene glycol (PEG), which reduces the adsorption of blood proteins on the nanoparticle surface and creates a “stealth” character, can enhance nanoparticle stability in the blood stream, and by this increase the blood circulation time.(79, 82, 416, 417) However, shielding is also associated with reduced cell membrane interaction and cellular uptake, and consequently decreased transfection efficiency (so-called “PEG dilemma”). Active targeting strategies (*e.g.*, chemical targeting by nanoparticle surface modification, or receptor targeting with specific ligands) can be remedies hereto.(100, 101) Noteworthy, PEGylation may also interfere with plasmid DNA (pDNA) compaction as a result of increased hydrophilicity and carrier solubility, leading to less condensed polyplexes with larger sizes.(211, 418, 419) Careful choice of PEG agents (in terms of length, branching etc.) and incorporation strategies is therefore of great importance.

In the current study, pDNA polyplexes should be functionalized with different shielding and targeting agents. There exist two different ways to incorporate PEG/ligand units into the nanoparticles, either before (pre-functionalization) or after (post-functionalization) polyplex formation. The most suitable functionalization strategy was to be identified in the present work. In previous studies, lipid-free sequence-defined oligo(aminoamides) (OAAs) with a dendrimer-resembling 4-arm topology were used as such nanocarriers and were particularly efficient in

gene transfer in cell culture and *in vivo* in tumor mouse models.(71, 90, 245, 418, 420, 421) Incorporation of shielding and targeting moieties was accomplished by synthesizing PEG/ligand-OAA conjugates and mixing them with PEG/ligand-free OAAs in different ratios. Despite encouraging results, the system used in these studies suffered from limitation of ligand variation and required careful consideration of the OAA-PEG/ligand sequence. In addition, this strategy is limited to rather simple, linear peptide ligands.

In order to gain more flexibility for variable modifications and to enable access to more complex ligands, such as proteins or carbohydrates, PEG/ligand attachment was achieved by post-functionalization of polyplexes via thiol-active linkers,(422-424) or strain-promoted alkyne-azide cycloaddition (SPAAC)(240, 241). Previously, Loy et al. introduced modularity into the formulation process of targeted and shielded siRNA polyplexes by using SPAAC to pre-click diverse PEG-ligand conjugates to “lipid anchors”, followed by co-formulation with lipid-containing T-shaped OAAs and small interfering RNA (siRNA).(425) This approach, however, could not be translated to DNA polyplex systems, where lipid-free, highly cationic 4-arm OAAs were superior over lipo-OAAs.(37, 50, 58)

Consequently, in this study, the rationale of the modularity of the “lipid anchor” strategy was combined with the former co-mixing approach of lipid-free OAAs with and without PEG/ligand. For this purpose, azido-functionalized 4-arm carriers were applied as “cationic anchors” allowing for modular pre-functionalization and compacting pDNA into polyplexes by electrostatic interactions. Based on the 4-arm carrier sequence ***573***,(71) A-K-[H-K-(H-Stp)$_3$-C)$_2$]$_2$, a small library of six OAAs was generated by solid phase-assisted peptide synthesis (SPPS). All structures contain *i)* lysines as branching points to create the distinct 4-arm topology, *ii)* cationizable artificial amino acid succinoyl tetraethylene pentamine (Stp)(61) for pDNA compaction and together with histidines(71, 426-428) in alternating sequence (H-Stp) promoting endosomal escape, *iii)* cysteines for stabilization via disulfide cross-linkage,(61, 174, 429) as well as *iv)* four *N*-terminal azido-lysines (one per arm), allowing for functionalization via SPAAC. Amino acid variations comprised additional *i)* tyrosine-tripeptides (Y_3), *ii)* tryptophans, or *iii)* arginines, both either in alternating sequence with Stp and histidines (Stp-H-W, Stp-H-R), or as tripeptides (W_3, R_3). These amino acid motifs have previously been reported for diverse nanocarrier structures for gene delivery, including poly/oligo-ethylenimine,(430-432) poly(amidoamine) dendrimers,(433) polyacrylamides,(434) and (xeno)peptides.(68, 435) Since the effect of amino acid modifications was strongly dependent on the underlying carrier sequence, the influence was to be explored for the 4-arm OAAs. Notably, tyrosine-tripeptides are considered to promote stabilization by hydrophobic, aromatic interactions (π-π stacking effect)(68, 435-437) and increased insolubility,(432) whereas, incorporation of arginines has the potential to stabilize pDNA polyplexes by stronger electrostatic interactions due to the permanently cationic guanidine units (pKa 12.5).(430, 433,

434, 436, 438, 439) Additionally, cellular internalization might be enhanced as a result of increased interaction with negatively charged cell membranes and induced membrane permeabilization. Tryptophan as cationizable, aromatic amino acid (indole unit) might help also in endosomal buffering as well as hydrophobic stabilization(431-433) but could negatively affect pDNA condensation and transfection efficiency.(436)

Most suitable azido 4-arm carriers should then be functionalized in both a pre- and post-functionalization approach with diverse dibenzocyclooctyne (DBCO)-bearing PEG agents of different lengths (PEG_n, n = ethylene oxide (EO) units 12, 24, 48, 96) in order to identify the best functionalization method and the ideal PEG length for effective shielding.

For active targeting, lectins (*i.e.*, carbohydrate-binding proteins) such as the asialoglycoprotein receptor (ASGPR), or mannose receptors represent interesting targets due to their high degree of specificity.(100) Targeting of ASGPR expressed on hepatocytes has already been subject of many studies.(115, 216, 438, 440-445) ASGPR shows high affinity and specificity towards multi-antennary galactose and *N*-acetyl galactosamine (GalNAc) and induces receptor-mediated endocytosis.(116, 125) Whereas the first reported targeted gene delivery focused on natural ligands for targeting ASGPR,(188, 193) artificial GalNAc-ligands became extensively studied and were continuously optimized for improved nucleic acid transfer to hepatocytes.(216, 283) This optimization resulted in the market approval of several direct ligand-siRNA conjugates for the treatment of rare diseases.(260, 261, 446) Mannose receptors, i.e., C-type lectins known for the recognition of mannose, fucose, and *N*-acetylglucosamine residues, have also been addressed by researchers for directed nucleic acid delivery to immune cells such as dendritic cells and macrophages,(128, 234, 293-296, 299, 447-453) which is particularly interesting for vaccination approaches and cancer immunotherapy.(454, 455)

In summary, the present study aimed at finding an efficient delivery system for pDNA, including identification of *i)* an effective polyplex carrier, *ii)* the ideal PEG chain length and ligand density, and *iii)* the most suitable functionalization method. In this regard, two novel DBCO-bearing carbohydrate ligands targeting ASPGR, or mannose receptors were designed and evaluated *in vitro* for their ability to target these receptors .

3.3 Materials and Methods

3.3.1 Materials

Acetic anhydride, boron trifluoride diethyl etherate (for synthesis), copper sulfate ($CuSO_4$), 4-(dimethyl amino)pyridine (DMAP), D-galactosamine hydrochloride, D-mannose, pyridine, sodium azide, sodium bicarbonate, sodium diethyl dithiocarbamate, and super-DHB were purchased from Sigma Aldrich (Munich, Germany). 2-Bromoethanol and sodium methoxide

were purchased from Thermo Scientific (Schwerte, Germany). Sodium ascorbate was purchased from Panreac AppliChem (Darmstadt, Germany), DBCO (dibenzoazacyclooctyne)-PEG_{24}-TFP (2,3,5,6-tetrafluorophenol) ester was obtained from Quanta BioDesign (Plain City, Ohio, USA), and sodium sulfate (dry, 99%) was purchased from ORG Laborchemie (Bunde, Germany). Luer stopper and polypropylene (PP) reactors with polyethylene (PE) frit were purchased from Multi-SynTech GmbH (Witten, Germany). Tentagel S HMBA (4-(hydroxymethyl)benzoic acid) and Tentagel S Rink Amide resins were purchased from Rapp Polymere (Tübingen, Germany), and 2-chlorotrityl chloride resin was obtained from Iris Biotech GmbH (Marktredwitz, Germany). Benzotriazole-1-yl-oxy-tris-pyrrolidino-phosphonium hexafluoro-phosphate (PyBOP), 1,8-diazabicyclo[5.4.0]undec-7-ene (DBU), DBCO-acid, *N,N′*-diisopropyl carbodiimide (DIC), *N,N*-diisopropylethylamine (DIPEA), diethyl ether, 1-hydroxybenzotriazole hydrate (HOBt), phenol triisopropyl silane (TIPS), tris(hydroxymethyl)aminoethane, and triton X-100 were purchased from Sigma Aldrich (Munich, Germany). Dimethylformamide (DMF, for peptide synthesis), Fmoc-protected amino acids, and piperidine (peptide grade) were purchased from Iris Biotech GmbH (Marktredwitz, Germany). Fmoc-NH-$dPEG_n$-COOH (n= ethylene oxide (EO) units = 12, 24) were obtained from Quanta BioDesign (Plain City, Ohio, USA). Ninhydrin was purchased from AppliChem (Darmstadt, Germany). Trifluoroacetic acid (TFA) (99%, extra pure) was obtained from Thermo Scientific (Schwerte, Germany). Acetonitrile (ACN), dichloromethane (DCM), and methanol (MeOH) (all HPLC reagent grade) were purchased from Fisher Scientific (Schwerte, Germany), anhydrous DCM and dry dimethyl sulfoxide (DMSO) from Thermo Scientific (Schwerte, Germany). Deuterated solvents were obtained from Eurisotop (Fluorochem, Hadfield, UK). Hydrochloric acid and GelRed (10,000x) was purchased from VWR (Darmstadt, Germany), sodium hydroxide (1 M) from Fisher Scientific (Schwerte, Germany), ethylene diamine tetra acetic acid (EDTA) from Merck (Darmstadt, Germany), and *N*-(2-hydroxyethyl)piperazine-*N′*-(2-ethanesulfonic acid) (HEPES) from Biomol (Hamburg, Germany). Agarose BioReagent (low EEO) and ethidium bromide (EtBr) were purchased from Sigma Aldrich (Munich, Germany). Cell culture consumables were purchased from Faust Lab Sciences (Klettgau, Germany); Dulbecco's Modified Eagle Medium (DMEM) Ham's F12 was purchased from Capricorn Scientifics (Ebsdorfergrund, Germany); adenosine 5′-triphosphate (ATP) disodium salt trihydrate, asialofetuin, coenzyme A trilithium salt, 3-(4,5-dimethylthiazol-2-yl)-2,5-diphenyiltetrazolium bromide (MTT), DMEM low glucose, fetal bovine serum (FBS), L-glutamine, Iscove's Modified Dulbecco's Medium (IMDM), mannan (from *Saccharomyces cerevisiae*), antibiotics (penicillin, streptomycin), and trypsin/EDTA were purchased from Sigma Aldrich (Munich, Germany) and PAN-Biotech (Aidenbach, Germany). CellTiter-Glo Kit, D-luciferin sodium salt, and luciferase cell culture lysis reagent (5x) were purchased from Promega (Mannheim, Germany). Plasmid pCMVLuc (encoding *Photinus pyralis* firefly

luciferase under the control of a cytomegalovirus promoter and enhancer)(216) was obtained from Plasmid Factory GmbH (Bielefeld, Germany). Plasmid pFscnLuc (encoding *Photinus* pyralis firefly lucierfase under the control of an optimized human *fascin1* gene promoter)(456) was obtained from Plasmid Factory GmbH (Bielefeld, Germany). Mirus Label-IT Cy5 Kit for labeling of pDNA (flow cytometric studies) was obtained from VWR (Darmstadt, Germany). Further solvents and reagents were purchased from Sigma-Aldrich (Munich, Germany), Iris Biotech (Marktredwitz, Germany), Merck (Darmstadt, Germany), or AppliChem (Darmstadt, Germany).

LPEI 22 kDa was synthesized and analyzed as described before.(457, 458) The starting product poly(2-ethyl-2-oxazoline) was purchased from Sigma-Aldrich (Munich, Germany).

3.3.2 Analytical methods

3.3.2.1 ^{1}H-NMR spectroscopy

^{1}H-NMR (nuclear magnetic resonance) spectra were recorded by using a Bruker Avance III HD 400 (400 MHz). Signals were calibrated to the residual, non-deuterated signals of the used solvent as an internal standard (acetone-d_6 2.05 ppm; D_2O 4.79 ppm; $CDCl_3$ 7.26 ppm). Chemical shifts (δ) were reported in parts per million (ppm). The spectra were analyzed by MestreNova (MestReLab Research x64). Integration was performed manually. Multiplicities were abbreviated as follows: s, singlet; d, doublet; t, triplet; m, multiplet.

3.3.2.2 Analytical reversed-phase HPLC

Reversed-phase high performance liquid chromatography (RP-HPLC) analysis was performed with a VWR-Hitachi Chromaster 5160 Pump System (VWR, Darmstadt, Germany), VWR-Hitachi Chromaster 5260 Autosampler (VWR, Darmstadt, Germany), and a Diode Array Detector (DAD) (VWR-Hitachi Chromaster 5430; VWR, Darmstadt, Germany) at 214 and 280 nm using a Hydrosphere C18 column (5 µm, 150 x 4.6 mm I.D., YMC Europe GmbH, Dinslaken, Germany). As solvent system, ACN/H_2O with 0.1% TFA was used with a gradient from 95/5 (v/v) – 0/100 (v/v) in 20 min.

3.3.2.3 Preparative HPLC

Preparative HPLC was performed on Büchi Pure C-830 Prep (BÜCHI Labortechnik GmbH, Essen, Germany) using a SymmetryPrep^{TM} C18 column (7 µm, 19 x 150 mm column, Waters, Milford, Massachusetts, USA). HPLC runs were performed with solvent A (100% ACN supplemented with 0.1% TFA) and solvent B (100% H_2O supplemented 0.1% TFA). A gradient from 95% B to 5% B was chosen with a run time of 20 min at a flow rate of 20 mL/min. Absorption of eluents was detected using a UV/Vis detector at 214, 254, 280, and 308 nm.

3.3.2.4 Liquid chromatography-mass spectrometry (LCMS)

LCMS analyses were recorded on a Bruker microTOF II in positive ionization mode. As column, an Ultra-Fast LC Column YMC-UltraHT Pro C18 (pore size 120 Å, 2.9 x 75 mm; YMC Europe GmbH, Dinslaken, Germany) installed in an Ultimate 3000 RP-HPLC system (ThermoFisher Scientific) was used. UPLC (ultra performance liquid chromatography) runs were performed at 25°C using the following mobile phases H_2O (A) and ACN (B), both supplemented with 0.1% formic acid, following a gradient from 5% solvent B to 95% solvent B over 8 minutes. Injection volume ranged between 10-20 µL with a sample concentration of 1 mg/mL. Elution of products was monitored by UV/Vis detection at 214, 254, 280, and 308 nm with a diode array detector.

3.3.2.5 MALDI-TOF mass spectrometry (MS)

MALDI-TOF (matrix assisted laser desorption ionization – time of flight) MS was conducted using an Autoflex II mass spectrometer (Bruker Daltonics, Germany). As matrix, a solution of 10 mg/mL super-DHB (9/1 (w/w) mixture of 2,5-dihydroxybenzoic acid and 2-hydroxy-5-methoxybenzoic acid) in 69.93/30/0.07 (v/v/v) H_2O/ACN/TFA was used. 1 µL of matrix solution was spotted on a MTP AnchorChip (Bruker Daltonics, Germany). Subsequently, 1 µL of sample solution, dissolved in H_2O or ACN at a concentration of 1 mg/mL, was added onto the matrix, co-crystallized and analyzed. Spectra were recorded in positive or negative ion mode.

3.3.2.6 ESI mass spectrometry

ESI (electrospray ionization)-MS of samples dissolved in a suitable solvent at a concentration of 0.1-1 mg/mL was performed using a Thermo Scientific LTQ FT Ultra Fourier transform ion cyclotron and an IonMax source. Data is either shown as $[M+X]^z$ after positive ionization or $[M-X]^{-z}$ after negative ionization.

3.3.2.7 Lyophilization

Lyophilization of the final synthesis products was achieved using Freeze-dryer ALPHA 3-4 LSCbasic (Martin Christ Gefriertrocknungsanlagen GmbH, Osterode am Harz, Germany). The condenser temperature was set to -105 °C at 0.050 mbar.

3.3.2.8 UV/Vis spectroscopy

UV/Vis spectra were recorded on an Agilent Cary 3500 UV-Vis Multicell Peltier spectrophotometer using micro UV-cuvettes (Brand GmbH & Co. KG, Wertheim, Germany). Absorption was recorded either as scan from 200 to 800 nm or at distinct wavelengths (i.e., 301 nm for determination of resin loading via Fmoc detection or 308 nm for detection of the DBCO unit).

For click reaction monitoring, both pre-functionalization and post-functionalization were assessed. In the case of post-functionalization, the polyplex was formed as described in section 4.2 of the main manuscript at a total volume of 300 µL in a cuvette. After 40 min of

incubation, 100 µL of the diluted PEG_{24}-DBCO ligand (1 eq, FD 25%) was added and the absorbance (λ = 308 nm) was measured in intervals of 15 min for a total duration of 12 h. In the case of pre-functionalization, the azido-carrier and 1 eq of the PEG_{24}-DBCO ligand (aiming for FD 25%) were mixed by rapid pipetting and diluted to a total sample volume of 400 µL to resemble the volume of the post-click conditions. The solution was transferred into a cuvette, and the absorbance (λ = 308 nm) was measured in intervals of 15 min for a total duration of 12 h.

3.3.3 Syntheses

3.3.3.1 Synthesis of azido 4-arm oligoaminoamides

The oligoaminoamide (OAA) library was synthesized via solid phase-assisted peptide synthesis (SPPS) according to the protocol of Lächelt et al.(71) with some minor improvements. In particular, 1% (v/v) triton X-100 was added to all solvents and used in every synthesis step to enhance conversion of the coupling reaction. Regarding the Fmoc deprotection, a solution of 20% (v/v) piperidine, 2% (v/v) DBU, and 1% (v/v) triton X-100 in DMF was used instead of commonly used 20% (v/v) piperidine in DMF. DBU was added to achieve more efficient deprotection, whereas triton was used to prevent the long peptide sequences from aggregating. Another measure to avoid aggregation and reduce sterical hindrance during sequence elongation was a low resin loading of 0.05 mmol/g. All 4-arms were purified by size exclusion chromatography using an Äkta system (GE Healthcare Bio-Sciences AB, Uppsala, Sweden) based on a P-900 solvent pump module, a UV-900 spectrophotometric detector, a pH/C-900 conductivity module, a Frac-950 automated fractionator, a Sephadex G-10 column, and a solution of 10 mM hydrochloric acid in H_2O/ACN 7:3 (v/v) as solvent. Subsequently, the OAAs were lyophilized and stored at -20 °C. Identity and purity were determined via ^{1}H-NMR spectroscopy (see 3.3.2.1) and analytical RP-HPLC (see 3.3.2.2). For experiments, stock solutions of 10 mg/mL OAA in H_2O were used. The NMR spectra and chromatograms are presented in the appendix, chapter 6.1.1.

3.3.3.2 Synthesis of PEG_n-DBCO agents – General procedure for the synthesis

PEG_n-DBCO shielding agents were prepared on solid phase using an acid-labile 2-chlorotrityl chloride resin (loading: 1.55 mmol/g). Firstly, the resin was loaded into a polypropylene reaction syringe and swelled in 2 mL of dry DCM for 20 min under shaking. The solvent was ejected and Fmoc-dPEG_n-OH (0.3 eq) with n = 12 (for PEG_{12}-DBCO) or n = 24 (for all other PEG-DBCO agents) and DIPEA (0.9 eq) were dissolved in 2 mL of dry DCM and added to the syringe reactor for 2 h and placed on a mechanical shaker. Afterwards, the coupling solution was discarded, and the resin was treated with a mixture of DCM/MeOH/DIPEA (1 mL/0.75 mL/0.125 mL) for 30 min for capping unreacted coupling sites. Then, the capping

solution was ejected, and the resin was washed with DMF and DCM (each 5x 3 mL). For Fmoc deprotection, 3 mL of a solution of 20% piperidine in DMF was added to the resin and incubated for 10 min under shaking, then discarded. The procedure was repeated 3 times. Afterwards, the resin was washed with DMF (5x 3 mL) and DCM (5x 3 mL). For PEG_{48} and PEG_{96}, coupling of the Fmoc-$dPEG_{24}$-OH building block (with prolonged reaction times of 16 h) and subsequent Fmoc deprotection were repeated until the desired sequence was obtained. Once the desired sequence was assembled, the terminal Fmoc protecting group was removed according to the protocol described above.

For introducing the DBCO-functionality, DBCO-acid (4 eq), PyBOP (4 eq) and HOBt (4 eq) were dissolved in 2 mL of DMF. DIPEA (8 eq) was added to the solution and the reaction mixture was added to the syringe and allowed to incubate for 90 min while shaking. Afterwards, the solution was ejected, and the resin was washed with DMF (5 x 3 mL) and DCM (5x 3 mL). The PEG_n-DBCO agent was then cleaved from the resin by treatment with 3 mL of a cleavage cocktail containing 5% TFA, 2.5% TIPS, and 92.5% DCM. After 45-60 min, the cleavage solution was precipitated into 40 mL of ice-cold MTBE/n-hexane (1:4 v/v) and centrifuged for 15 min at 4000 rpm at 4 °C. The supernatant was discarded, and the pellet was dried under nitrogen flow. The dry pellet was then dissolved in 1 mL of 0.05 M $NaOH_{aq}$ solution, and the pH was adjusted to 7. Purification was accomplished by dialysis against de-ionized H_2O for 24 h at 4 °C. The resulting dialysate was lyophilized. The PEG_n-DBCO agents were analyzed for identity and purity via MALDI-TOF MS (3.3.2.5) and LCMS (3.3.2.4). The mass spectra and chromatograms are presented in the appendix, see chapter 6.1.2.

Yields (for 0.1 mmol resin):

PEG_{12}-DBCO	7.6 mg, (7.9 µmol, 78%)
PEG_{24}-DBCO	22.7 mg (15.3 µmol, 78%)
PEG_{48}-DBCO	19.0 mg (7.3 µmol, 45%)
PEG_{96}-DBCO	37.8 mg (7.8 µmol, 58%)

3.3.3.3 Synthesis of trivalent GalNAc-ligand $(GalNAc)_3$-PEG_{24}-DBCO

Syntheses of building blocks

TDS (triple bond diethylenetriamine succinyl) building block.

1-(fluorenyl)-3,11-dioxo-7-(pent-4-ynoyl)2-oxa-4,7,10,-triazatetra-decan-14-oic acid) was synthesized as reported previously by Ponader et al.(459)

2,3,4,6-tetra-O-acetyl-β-(2-azidoethanol)-D-galactosamine.

The synthesis protocol was adapted and adjusted from a protocol reported by Soria-Martinez et al.(460)

1,2,3,4,6-penta-O-acetyl-D-galactosamine. The synthesis for the preparation of per-acetylated GalNAc followed a protocol by Bernardes et al.(461) To a cooled solution of β-D-galactosamine hydrochloride (5.07 g, 23.5 mmol, 1 eq) in pyridine (28 mL, 352.7 mmol, 15 eq), acetic anhydride (16.7 mL, 176 mmol, 7.5 eq) was added dropwise over 30 min under nitrogen atmosphere while stirring. The reaction mixture was allowed to come up to room temperature (RT) and stirred overnight for 16 h. Then, the reaction mixture was poured into ice water (500 mL) to precipitate the product was white crystals. The precipitate was filtered, washed with H_2O and dried under high vacuum to give the product (quantitative yield).

2,3,4,6-tetra-O-acetyl-β-(2-bromoethanol)-D-galactosamine. Synthesis of bromoethyl-GalNAc was performed following a protocol by Soria-Martinez.(460) Peracetylated GalNAc (7.2 g, 18.5 mmol) was dissolved in 35 mL of dry DCM. Under inert atmosphere, 2-bromoethanol (1.6 mL, 22.2 mmol, 1.2 eq) was added and the reaction mixture was cooled to 0 °C. Boron trifluoride diethyl etherate (11.7 mL, 39.2 mmol, 5 eq) was added dropwise over 15 min and the reaction solution was allowed to come up to RT and agitated for 20 h. Subsequently, the reaction was quenched by pouring the solution into 200 mL of an ice-cold, saturated aqueous solution of sodium bicarbonate. After stirring for additional 2 h, the organic layer was separated, washed with saturated sodium bicarbonate solution (2x 50 mL), dried over sodium sulfate and filtered. The solvent was then removed under reduced pressure to give a yellow oil (4.25 g, 9.44 mmol, 51%). The crude product (termed as bromoethyl-GalNAc) was used in the next step without further purification.

2,3,4,6-tetra-O-acetyl-β-(2-azidoethanol)-D-galactosamine. Introduction of the azido group was achieved adapting a protocol by Lindhorst et al. and Soria-Martinez et al.(460, 462) Bromoethyl-GalNAc (4.25 g, 9.4 mmol, 1 eq) was dissolved in DMF (10 mL/g), and sodium azide (3.04 g, 46.8 mmol, 5 eq) was added while stirring. The solution was heated with an oil bath to a constant temperature of 60 °C and stirred for 72 h. Afterwards, the reaction mixture was diluted with 200 mL of H_2O and extracted with ethyl acetate. The organic layer was separated, washed three times with H_2O, dried over sodium sulfate and concentrated under reduced pressure. The product was obtained after purification by silica column chromatography using 100% ethyl acetate as solvent (300 mg, 0.75 mmol, 8%). ^{1}H-NMR spectroscopy analysis is in accordance with literature,(463) see appendix, section 6.1.3.1.

Solid phase synthesis of ligand backbone

The ligand backbone was assembled by SPPS using Tentagel® S Rink amide modified resin on a 0.1 mmol scale (loading 0.23 mmol/g).

Preparation of resin. The resin was swollen in DCM (1 mL solvent per 100 mg resin) for 30 min in a reaction syringe and afterwards washed ten times with DMF.

Fmoc deprotection. The resin was treated with a solution of 20% (v/v) piperidine in DMF for 2x 15 min. Afterwards, the resin was washed ten times with DMF.

Standard coupling protocol. 5 eq of the relevant building block and 4.9 eq of PyBOP were dissolved in DMF (approx. 3-5 mL). Immediately before adding the solution to the resin, 10 eq of DIPEA are added to the coupling solution for activation. The coupling solution was added to the resin and allowed to react for 60-90 min under constant shaking. Afterwards, the solution was discarded, followed by washing the resin with DMF and DCM (10x 5 mL each).

Assembly of ligand backbone. For the assembly of the ligand backbone, three units of the TDS building block were coupled successively to the resin by alternating Fmoc deprotection and coupling steps. After the third TDS coupling, the terminal Fmoc protecting group was removed.

Kaiser test. The success of coupling and deprotection of N-terminal protecting groups was determined qualitatively by a Kaiser test. For this, a small amount of resin was transferred into an Eppendorf tube and one drop of each of the following solutions were added: 5% (w/v) ninhydrin in ethanol, 80% (w/v) phenol in ethanol, and 20 µM potassium cyanide in pyridine. The tube was incubated for 5 min at 99 °C under shaking at 600 rpm. The presence of free amino groups was indicated by a dark blue color, the absence by no change of color, respectively.

Glycosylation by copper(I)-catalyzed click reaction

GalNAc-OCH_2CH_2-N_3 (2.5 eq per alkyne moiety) was dissolved in DMF. $CuSO_4$ (2.5 eq per alkyne) and sodium ascorbate (2 eq) were dissolved separately in H_2O with a concentration of 100 mg/mL. The carbohydrate solution was then added to the syringe reactor, followed by aqueous $CuSO_4$ and sodium ascorbate solutions. The color of the reaction solution turned from light yellow to turbid orange. The glycosylation was allowed to proceed overnight at RT under exclusion of light (covered by aluminum foil). Once the reaction was complete, the solution was discarded, and the resin was washed with the following procedure to eliminate copper ions: i) 23 mM solution of sodium diethyl dithiocarbamate (SDTC) in DMF/ H_2O 1:1 (v/v); ii) DMF; iii) H_2O; and iv) DCM (5x 5 mL each). The washing procedure is repeated until the resin retained its light-yellow color, and the washing solutions remain colorless.(464)

Removal of acetyl protecting groups on GalNAc residues

After glycosylation, carbohydrate acetyl protecting groups were removed through addition of a solution of 0.2 M sodium methoxide in MeOH for 2x 45 min. Afterwards, the resin was washed with DCM, MeOH and DCM (5x 5 mL each).

Cleavage from the resin

Peptide cleavage was obtained by treatment of the resin with a cleavage solution containing 95% TFA, 2.5% DCM, and 2.5% TIPS. The resin was incubated with 3 mL of the cleavage solution for 60 min. Afterwards, the solution was dispensed into ice-cold diethyl ether (40 mL). The cleaved ligand precipitated and was centrifuged for 8 min at 4400 rpm and at 4 °C. The supernatant was removed, and the precipitate was resuspended in diethyl ether and centrifuged again. The pellet was dried and dissolved in H_2O for lyophilization. The intermediate product $(GalNAc)_3$-amine was analyzed by ^{1}H-NMR spectroscopy (3.3.2.1), MALDI-TOF-MS (3.3.2.5) and analytical HPLC (3.3.2.2) to confirm purity and identity. The spectra and chromatograms are presented in the appendix, see 6.1.3.

Functionalization with PEG_{24}-DBCO

Introduction of a PEG_{24} shielding domain and DBCO functionality for subsequent polyplex modification was conducted at the N-terminus of the ligand using an active ester reagent. The ligand (10 mg, 5.9 µmol, 1 eq) bearing a terminal amino group was dissolved in 200 µL of sodium bicarbonate buffer, and pH was adjusted to 8.4 by addition of aqueous sodium hydroxide solution (0.05 M). DBCO-PEG_{24}-TFP ester (10 mg, 6.5 µmol, 1.1 eq) was dissolved in water-free DMSO. The solutions were combined, and the reaction was allowed to proceed overnight at RT while gently shaking. Afterwards, the reaction solution was applied to a preparative HPLC column for purification (3.3.2.3). Fractions were collected and organic solvents were removed under reduced pressure. The residue was diluted with water and lyophilized to give the product (yield: 5.5 mg, 1.8 µmol, 30%). Characterization of the product was done by LCMS (3.3.2.4) and MALDI-TOF MS (3.3.2.5). Mass spectrum and chromatogram are presented in the appendix, see 6.1.3.1.

3.3.3.4 Synthesis of mannose-ligand Gly-Ser(Man)-PEG_{24}-DBCO

Synthesis of mannosylated serine building block

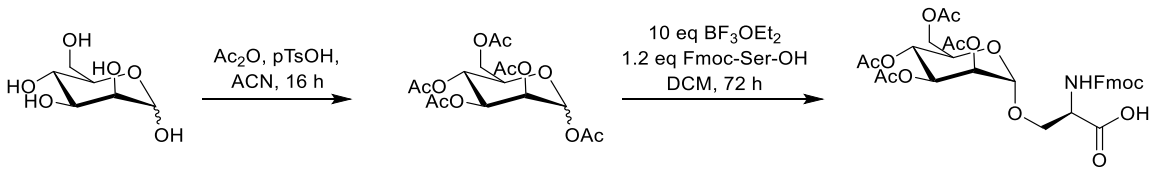

1,2,3,4,6-penta-O-acetyl-D-mannose. The synthesis was adapted from a method published by Ponader et al. and Soria-Martinez et al.(459, 460) Briefly, α-D-mannose (5 g, 27.8 mmol, 1 eq) and p-toluene sulfonic acid (475 mg, 2.78 mmol, 0.1 eq) were suspended in 65 mL of ACN and stirred for 60 min under nitrogen atmosphere. Acetic anhydride (15.6 mL, 16.7 mmol, 6 eq) was added dropwise and the solution was stirred overnight at RT. After 18 h, the solvent was removed under reduced pressure. The residue was re-dissolved in 200 mL of ethyl acetate

and the organic phase was washed five times with saturated sodium bicarbonate solution and once with H_2O (200 mL each). Subsequently, the organic phase was dried over sodium sulfate and the solvent was removed under reduced pressure to give a colorless oil (yield: 26.7 mmol, 96%). Acetylated mannose was characterized via ^{1}H-NMR spectroscopy. The spectrum is presented in the appendix, see 6.1.3.2.

***N*'-(9-Fluorenylmethoxycarbonyl)3-O-(2,3,4,6-tetra-O-acetyl-α-D-mannopranosyl)serine.** The synthesis was adapted and optimized according to previously published protocols.(465, 466) Fmoc-serine-OH (1 g, 3.06 mmol, 1 eq) and mannose-pentaacetate (1.49 g, 3.82 mmol, 1.25 eq) were dissolved in dry ACN (50 mL) under inert atmosphere. Boron trifluoride diethyl etherate (3.8 mL, 30.55 mmol, 10 eq) was added dropwise. The reaction solution was stirred in the dark at RT under inert gas atmosphere for 20 h. Afterwards, the reaction solution was diluted with 100 mL of DCM, cooled to 0 °C and subsequently poured in 500 mL of ice water. The layers were separated, and the organic phase was washed successively with ice water and saturated sodium bicarbonate solution (200 mL each). The organic phase was dried over Na_2SO_4, filtered and the solvent was removed under reduced pressure. The crude product was purified by silica gel column chromatography with 5:95 (v/v) MeOH/DCM to give the product as a light-yellow foam (yield: 624 mg, 0.95 mmol, 31%). Analysis was done by ESI-MS (3.3.2.6) and ^{1}H-NMR spectroscopy (3.3.2.1). The analytical data are presented in the appendix, see 6.1.3.2.

Synthesis of Gly-Ser(Man)-PEG$_{24}$-DBCO

Preparation of the resin. The synthesis of the mannose-ligand was conducted on a base-labile Tentagel® S HMBA resin. 50 mg of the resin (12.5 µmol) was loaded into a polypropylene reaction syringe and swelled in 2 mL of dry DCM for 20 min before subsequent loading with Fmoc-Gly-OH. Therefore, 5 eq of the amino acid, 0.1 eq of DMAP, and 5 eq of DIC were dissolved in 1 mL of DMF and pre-activated for 5 min under shaking. The solution was then added to the resin and incubated for 2 h on a mechanical shaker. Afterwards, the resin was washed with DMF and DCM (5x 2 mL each) and a Kaiser test was performed to ensure complete loading.

Fmoc deprotection. Removal of Fmoc protecting group was achieved by treating the resin with a solution of 20% piperidine in DMF (v/v) for 3x 15 min (2 mL each). Afterwards, the resin was washed with DMF and DCM (5x 2 mL each).

Couplings on solid support. After removing the Fmoc protecting group, Fmoc-Ser(Man(Ac)$_4$)-OH was coupled. Therefore, the building block (5 eq), PyBOP (5 eq) and HOBt (5eq) were dissolved in a total volume of 2 mL of DMF and DCM (1:1, v/v). After complete dissolvement of the reagents, DIPEA (10 eq) was added to the solution. The solution was then

added immediately to the resin and allowed to react for 2 h. Afterwards, the coupling solution was discarded, and the resin was washed DMF and DCM (5x 2 mL each), followed by a Kaiser test to confirm completion of the coupling. Next, Fmoc protection group was removed and Fmoc-dPEG$_{24}$-OH was coupled to the resin as described above (3.3.3.2) with a prolonged reaction time of 16 h. Afterwards, the resin was washed with DMF and DCM, and the *N*-terminal Fmoc protecting group was removed following the protocol described above.

Cleavage and saponification of acetyl groups. The resin was treated with a cleavage cocktail (10 mL/g resin) containing 0.5 M NaOH$_{aq}$/ACN (1:1, v/v) for 30 min while placed on a mechanical shaker. Afterwards, H_2O (2 mL/g) were added to the mixture and the syringe reactor was shaken with a mechanical shaker at RT for another 30 min. The resin was then filtered, washed twice with 2 mL of ACN and the collected solutions were neutralized by addition of aqueous hydrochloric acid (0.5 M). The solution was diluted with H_2O and dialyzed overnight against H_2O and lyophilized to give the peptide acid (yield for 12.5 µmol resin: 16.2 mg, 10.8 µmol, 87%). By using this method, saponification of the acetyl protecting groups was achieved *in situ*. The ligand was used in the next step without further purification.

DBCO-functionalization. The ligand (16.2 mg, 10.8 µmol) containing a free amino on the *N*-terminus was dissolved in 250 µL of HEPES, the pH was adjusted to 8, and the solution was cooled to 0 °C. DBCO-NHS (5.5 mg, 13 µmol, 1.1 eq) was dissolved in 250 µL of DMF and cooled to 0 °C. When the ligand solution was added to the DBCO-NHS solution, a precipitate occurred which was redissolved by addition of a few drops of DMF. The reaction was then allowed to proceed overnight at RT. Afterwards, the crude reaction solution was diluted with H_2O and ACN and applied to preparative HPLC for purification using the protocol described above (3.3.2.3). The desired fractions were lyophilized to give the final ligand (yield: 13.5 mg, 7.8 µmol, 70%) and characterized via MALDI-TOF MS (3.3.2.5). The mass spectra is presented in the appendix, see 6.1.3.2.

3.3.4 Polyplex formation and functionalization

3.3.4.1 Polyplex formation

pCMVLuc DNA and the calculated amount of OAA (based on the indicated N/P (nitrogen of protonable amine to phosphate) ratio) were diluted separately in equal volumes of HBG buffer (20 mM HEPES, 5% glucose (w/v), pH 7.4). For the calculation of N/P ratio, *N*-terminal and secondary amines of the Stp building block were taken into consideration. Polyplexes were formed by addition of the DNA solution to the OAA solution, followed by rapid pipetting and incubation for 40 min at RT.

3.3.4.2 Polyplex functionalization

Post-functionalization. For post-functionalization, polyplexes were prepared as described above (3.3.4.1). After 40 min of incubation time, the indicated amount of DBCO-agent was diluted in HBG to 25% of the total polyplex solution, added to the polyplex solution and mixed by pipetting a few times. Then, the click reaction was allowed to proceed for 4 h at RT. Different ligand densities were achieved by addition of either 1 eq, 2 eq, or 4 eq of DBCO-click reagent related to the OAA, resulting in functionalization degrees of 25%, 50%, or 100%, respectively.

Pre-functionalization. The calculated molar amount of DBCO-ligand was added to the azido-OAA solution and mixed. The click reaction was allowed to proceed overnight at RT while placed on a mechanical shaker. The pre-clicked ligand/PEG-OAA conjugate was used for polyplex formation as described above (3.3.4.1), either alone or in combination with unmodified OAA at indicated ratios.

3.3.5 Physicochemical characterization

3.3.5.1 Zetasizer measurements

Measurements were performed using a Zetasizer Nano ZS (Malvern Instruments, Malvern, Worcestershire, United Kingdom) using a folded capillary cell (DTS1070) by dynamic and electrophoretic laser light scattering (DLS, ELS). For determination of particle size and polydispersity index (PDI), 100 µL of polyplex solutions were formed as described above (3.3.4) at pDNA concentration of 10 or 25 µg/mL, respectively, and measured with the settings as follows: 30 sec of equilibration time, temperature 25 °C, refractive index 1.330, viscosity 0.8872 mPa*s. Each sample was measured three times with six sub-runs per measurement. For determination of zeta potential, the polyplex solution was diluted with 700 µL of HBG and mixed by pipetting immediately prior to measurement. Measurement parameters were identical to size determination, with an increase of equilibration time to 60 sec. Each sample was measured with 15 sub-runs (10 sec each) and zeta potential were calculated by Smoluchowski equation. All values (size, PDI, and zeta potential) were displayed as mean ± SD out of these measurements.

3.3.5.2 Ethidium bromide (EtBr) exclusion assay

The pDNA compaction ability of the distinct carriers was evaluated via an EtBr exclusion assay. The EtBr fluorescence intensity correlates with the amount of less compacted or free pDNA, as only these states are accessible for EtBr intercalation. In less stable, dissociating nanoparticles, pDNA is less compacted, resulting in stronger EtBr fluorescence. On the opposite, pDNA might be less accessible in destabilized, aggregated nanoparticles. Quantification of EtBr fluorescence was carried out using a microplate reader (Spectrafluor Plus, Tecan, Switzerland) with an excitation wavelength λ_{ex} = 535 nm and an emission

wavelength λ_{em} = 590 nm. Polyplexes were prepared as described in section 3.3.4 with a total volume of 50 µL at a final pDNA concentration of 10 µg/mL. After the indicated incubation time (40 min for unmodified and pre-functionalized polyplexes, respectively and additional 4 h for post-functionalized formulations) 250 µL of aqueous EtBr solution (c = 0.5 µg/mL) was added to the polyplexes. After additional incubation for 10 min at RT, 260 µL of each sample was transferred into a TPP-ft 96-well-plate and fluorescence intensity was measured. A calibration curve with free pDNA (linear concentration range from 0 to 10 µg/mL) diluted in HBG was used for quantification. The amount of less compacted pDNA was calculated based on the calibration of free pDNA and displayed as percentage of EtBr fluorescence in relation to 100% of free pDNA.

3.3.5.3 Agarose gel shift assay

The presence of free pDNA within the polyplex samples was assessed via an agarose gel shift assay. Free pDNA moves to the anode and can be detected as bands in the gel. Smearing bands may be an indicator for less stable, dissociating nanoparticles but might also occur in the case of negatively charged nanoparticles, which shift towards the anode, as it was already observed previously.(241) In contrast, in the case of aggregates, pDNA might be still compacted and retained within the aggregated particles. 1% (w/v) agarose gel was prepared by microwave assisted heating of agarose in TBE buffer (18.0 g of tris(hydroxymethyl)-aminomethane, 5.5 g of boric acid, 2 mM EDTA at pH 8 in 1 L of H_2O). After cooling to ~ 50 °C, 1x GelRed was added to the solution (i.e., 1:1000-dilution of 1000x GelRed stock solution). Afterwards, the solution was casted into an electrophoresis unit and cooled to allow for gelation. Polyplexes were formed as described as described in section 3.3.4 with a total volume of 20 µL at a pDNA concentration of 10 µg/mL. After 40 min of incubation, 4 µL of loading buffer (6x; prepared from 6 mL of glycerol, 1.2 mL of 0.5 M EDTA, 2.8 mL of H_2O, 0.02 g of bromophenol blue) were added to the polyplex solution. 20 µL of the samples were loaded to the gel. Electrophoresis was performed at 120 mV for 70 min in 1x TBE buffer and analyzed with Dark Hood DH-40 (biostep, Burkhardtsdorf, Germany) and the biostep argusX1 software. Free pDNA diluted in HBG to a concentration of 10 µg/mL was used as control.

3.3.5.4 Transmission electron microscopy (TEM)

Unmodified, pre- and post-functionalized polyplexes containing 10 µg/mL pDNA in H_2O were formed at an N/P ratio of 12 and a functionalization degree of 50% as described in section 3.3.4. Mild plasma cleaning under argon atmosphere (420 V, 1 min) was used to activate and hydrophilize the formvar/carbon-coated 300 mesh copper grids (Ted Pella Inc., Redding, CA, USA). Thereafter, 10 µL of the polyplex solution was placed on the grids. After an incubation for 1.5 min, excess liquid was removed using a filter paper. Then, the grids were washed with 5 µL of staining solution (1% (w/v) aqueous uranylformate solution), followed by incubation with 5 µL of staining solution for 0.5 min. Excess liquid was again blotted off, followed by air-

drying for 30 min at RT. Samples were then imaged at 80 kV using a JEM-1011 electron microscope (Jeol, Freising, Germany).

3.3.6 *In vitro* evaluation

3.3.6.1 Cell culture

The human adherent hepatic carcinoma cell lines Huh7 wild-type (wt) (Japanese Collection of Research Bioresources Cell Bank, Osaka, Japan) and HepG2 wt (ATCC, American Type Culture Collection, Manassas, VA, USA) were cultured in DMEM Ham's F12 medium. The human adherent cervix carcinoma cell line HeLa wt (DSMZ, German Collection of Microorganisms and Cell Cultures GmbH, Braunschweig, Germany) and the murine adherent neuroblastoma cell line Neuro2a (N2a) wt (ATCC, Manassas, VA, USA) were cultured in DMEM low glucose (1 g/L glucose). Cell culture media were supplemented with 10% fetal bovine serum (FBS), 4 mM of stable glutamine, 100 U/mL penicillin, and 100 µg/mL streptomycin. The murine dendritic cell (DC)-like cell line DC2.4 (Merck Millipore, Darmstadt, Germany) was grown in IMDM, supplemented with 10% (v/v) FBS, 4 mM of stable L-glutamine, 100 U/mL of penicillin, 100 µg/mL of streptomycin, and 50 µM of β-mercapto ethanol. Cells were cultured at 37 °C with 5% CO_2 and a relative humidity of 95% in an incubator.

3.3.6.2 Transfections

All transfections were performed in the presence of 10% (v/v) fetal bovine serum (FBS). The polyplexes were prepared as described above (3.3.4). Cells were seeded 24 h prior to the treatment. For Huh7 and HeLa cells, 8000 cells/well, for N2a and HepG2 cells, 10,000 cells/well, and for DC2.4, 5000 cells/well were seeded in a 96-well plate. Prior to the treatment, the medium was renewed by 80 µL/well of fresh medium supplemented with 10% (v/v) FBS. Afterwards, 20 µL of polyplex solution were added to each well, containing 200 ng (in case of tumor cells) or 500 ng pCMVLuc (in case of DCs), respectively. HBG was used as negative control; LPEI (N/P 6) was used as positive control.(67, 71, 467) Transfections were performed in triplicate.

For dose titration experiments, different volumes of the polyplex solution were applied to the wells at a pDNA concentration of 10 µg/mL (for tumor cells), or 25 µg/mL (for DCs).

For competition experiments, cells were pre-incubated with competitor for 15 min (in case of asialofetuin) or 30 min (in case of mannan) prior to transfection. Hereto, medium was replaced with 80 µL of fresh medium, containing asialofetuin (with a final concentration of 5 mg/mL) or mannan (final concentration in the well of 2 mg/mL(468)). Afterwards, cells were treated with polyplexes in presence of the competitor.

3.3.6.3 Luciferase gene expression assay

Transfections of polyplexes were performed as described above (3.3.6.2). After the indicated incubation time (48 h for hepatocarcinoma cell lines, 24 h for all other cell lines), the medium was removed. 100 µL of 0.5x lysis buffer were added to each well and the cells were stored at -80 °C overnight. Before the determination of luciferase expression, plates were allowed to come up to RT and incubated for 1 h. For measurement, 35 µL of cell lysate were transferred into an opaque 96-well plate. Luciferase activity was measured for 10 sec in a Centro LB 960 plate reader luminometer (Berthold Technologies, Bad Wildbad, Germany) after addition of 100 µL of LAR buffer (20 mM glycylglycine; 1 mM $MgCl_2$; 0.1 mM ethylenediaminetetraacetic acid; 3.3 mM dithiothreitol; 0.55 mM adenosine 5′-triphosphate; 0.27 mM coenzyme A; pH 8-8.5) supplemented with 5% (v/v) of a mixture of 10 mM luciferin and 29 mM glycylglycine. Transfection efficiency was calculated for the seeded number of cells and presented as relative light units (RLU) per well.

3.3.6.4 MTT assay to assess cell viability

Transfections of polyplexes were performed as described in section 3.3.6.2. At 24 or 48 h post transfection, 10 µL of MTT (5 mg/mL) were added to each well and the wells were incubated for 2 h at 37 °C. Afterwards, the supernatant was removed, and the plates were stored at least for 1 h at -80 °C for complete cell lysis. Then, the purple formazan product was dissolved in 100 µL of DMSO and incubated in the wells for 30 min at 37 °C under slow constant shaking. Photometric analysis was carried out using a Tecan microplate reader (Spectrafluor Plus, Tecan, Männedorf, Switzerland). Absorbance was measured at wavelength λ = 590 nm with a background correction at λ = 630 nm. Relative metabolic activity was related to control wells treated with HBG and calculated by $[A]_{sample}/[A]_{control}$.

3.3.6.5 CellTiter-Glo assay to assess cell viability

Transfections were performed as described in section 3.3.6.2. The supernatant was removed at 24 h after transfection, and 25 µL of medium as well as 25 µL of CellTiter-Glo Reagent were added to each well. After incubation on an orbital shaker for 30 min at RT, luminescence was recorded using a Centro LB 960 plate reader luminometer (Berthold Technologies, Bad Wildbad, Germany). The luminescent signals (in relative light units, RLU) of the samples were set in relation to the luminescent signal of the negative control (HBG buffer-treated control cells). Results are presented as relative metabolic activity normalized to the negative control. Experiments were performed in triplicate.

3.3.6.6 Receptor expression in different cell lines – Flow cytometric analysis

Receptor staining of tumor cells. HepG2, Huh7, and HeLa cells (10^6 cells each), suspended in FACS buffer, were incubated with 20% (v/v) primary antibody solutions for 1 h on ice, followed by staining with a secondary antibody, 1:100-diluted, for 1 h on ice. For staining of the

asialoglycoprotein receptor (ASGPR), mouse anti-human ASGPR1 (8D7) monoclonal antibody (100 µg/mL; Novus Biologicals, Centennial, CO, USA) was used. Negative control mouse IgG1 (100 µg/mL; Agilent Technologies. Santa Clara, CA, USA) served as control. Alexa Fluor 488 (AF 488) goat anti-mouse IgG1 (H+L) (2 mg/mL; Invitrogen, ThermoFisher Scientific, Waltham, MA, USA) was used as secondary antibody.

Receptor staining of DC2.4 cells. 10^6 DC2.4 cells, suspended in FACS buffer (10% (v/v) FBS in phosphate-buffered saline, PBS), were stained with 10% (v/v) of antibody solution for 1 h on ice. PE anti-mouse CD206 (25 µg/mL) was used for staining of the macrophage mannose receptor and PE anti-mouse CD209a (25 µg/mL) for staining of the DC-SIGN receptor (both from BioLegend, Koblenz, Germany). Untreated cells as well as cells treated with antibody FITC mouse IgG1 K isotype Ctrl (50 µg/mL; BioLegend) served as controls.

Afterwards, cells were centrifuged (1000 rpm, 5 min, 4 °C), washed with FACS buffer, and subjected to analysis in a CytoFLEX S flow cytometer (Beckman Coulter, Brea, CA, USA). Measurements were carried out at λ_{ex} = 488 (FITC, AF 488) or 561 nm (PE), respectively, and λ_{em} = 525 (FITC, AF 488) or 585 nm (PE), respectively. Dead cells were detected via DAPI; λ_{ex} = 405 nm, λ_{em} = 450 nm. At least 20,000 events per sample were recorded and analyzed by FlowJo 7.6.5 flow cytometric analysis software (FlowJo, Ashland, OR, USA).

3.3.6.7 Cellular uptake study – Flow cytometry

At 24 h prior to the experiment, DC2.4 cells were seeded in 96-well plates at a cell density of 5000 cells/well. Prior to transfection, medium was replaced by fresh medium (occasionally supplemented with competitor mannan). Then, transfection was performed by applying different volumes of polyplexes prepared at a pDNA concentration of 10 µg/mL (20% Cyanine5 (Cy5)-labeled; pDNA labeling via Mirus Label-IT Cy5 Kit according to the manufacturer's protocol) as described in section 3.3.4. After 24 h, cells were washed with phosphate-buffered saline (PBS), followed by treatment with 100 µL of heparin (1000 IU/mL) for 10-15 min on ice in order to remove polyplexes non-specifically bound to the cell surface. Afterwards, cells were washed with PBS, detached with trypsin/EDTA, and centrifuged (1000 rpm, 5 min, 4 °C). The cell pellets were re-suspended in FACS buffer (10% (v/v) FBS in PBS), supplemented with 0.1% (v/v) of DAPI (1 mg/mL) to discriminate dead cells. Cellular uptake was assessed via a CytoFLEX S flow cytometer (Beckman Coulter, Brea, CA, USA) through excitation of Cy5 at 635 nm and detection of emission at 665 nm. Cells were gated based on the forward- and side-scatter profile. Data were recorded by collection of 2500 events per sample and analyzed by FlowJo 7.6.5 flow cytometric analysis software (FlowJo, Ashland, OR, USA). Results are displayed as mean fluorescence intensity (MFI; *n*=6; mean + SD) in Cy5-positive cells (Cy5-A) after background subtraction (HBG-treated control cells) normalized to MFI values of unmodified polyplexes.

3.3.7 Statistical analysis

Results are presented as mean values (arithmetic mean) of at least triplicates. Error bars display the standard deviation (SD). Statistical analysis of the results (mean ± SD) was evaluated by unpaired Student's two-tailed *t*-test with Welch's correction. Calculations and graphical presentation were performed with Prism 9.5.1 (GraphPad Software Inc.).
ns (statistically not significant) $p > 0.05$; * $p \leq 0.05$; ** $p \leq 0.01$; *** $p \leq 0.001$; **** $p \leq 0.0001$.

3.4 Results and Discussion

3.4.1 Azido-4-arm library

3.4.1.1 Design of the azido 4-arm library

In order to achieve efficient gene delivery, nanocarriers need to fulfill certain requirements, including the formation of stable particles with well-compacted pDNA in the extracellular space and the release of the cargo in effective form after efficient cellular uptake and endosomal escape. To meet these demands, six nucleic acid binding carriers with a precise 4-arm topology were synthesized by solid phase-assisted synthesis (**Table 3.1**; for the method, see 3.3.3.1), based on the sequence of OAA ***573*** developed by Lächelt et al.(71) **Scheme 3.1 A**). All carriers contain

i) lysines as branching points for creating the distinct 4-arm topology,
ii) the cationizable artificial amino acid Stp(61) for pDNA compaction and in combination with histidines in an alternating pattern (Stp-H) promoting endosomal escape, as well as
iii) cysteines for stabilization via disulfide cross-links. Furthermore, different structural variations were incorporated, namely, tyrosines, tryptophans and arginines either as block-wise tripeptides (Y_3, W_3, R_3), or in alternating sequence with Stp and histidines (Stp-H-W, Stp-H-R) (**Scheme 3.1 B**).

These modifications were chosen to enhance polyplex stability either via π-π stacking(437) in the case of amino acids tyrosine and tryptophan, or by enhanced electrostatic interactions with negatively charged pDNA mediated by the basic amino acid arginine (pK_a 12.5).(430, 433, 434, 436, 438, 439) Arginine is further known to promote polyplex uptake due to ionic interactions with the negatively charged membrane lipids,(433, 434) and subsequently improve transfection.
Additionally, *N*–terminal azido-lysines were introduced in the carriers, which serve as anchor-points for optional incorporation of shielding agents or targeting ligands via SPAAC. Azido-DBCO click chemistry is site-specific, orthogonal, and works in aqueous solutions.(240, 469,

470) Moreover, it provides great flexibility in modifications of the delivery system. In contrast to previous work by e.g., Kos et al.,(245, 418) SPAAC enables the quick equipment of the carriers with a broad variety of targeting and shielding moieties in a modular design. All carriers were purified via size exclusion chromatography and analyzed by ^{1}H-NMR spectroscopy and analytical RP-HPLC to confirm identity and purity (see Appendix, 6.1.1 Analytical data of the azido 4-arm library).

Scheme 3.1. Design of an azido-4-arm oligoaminoamide (OAA) library.

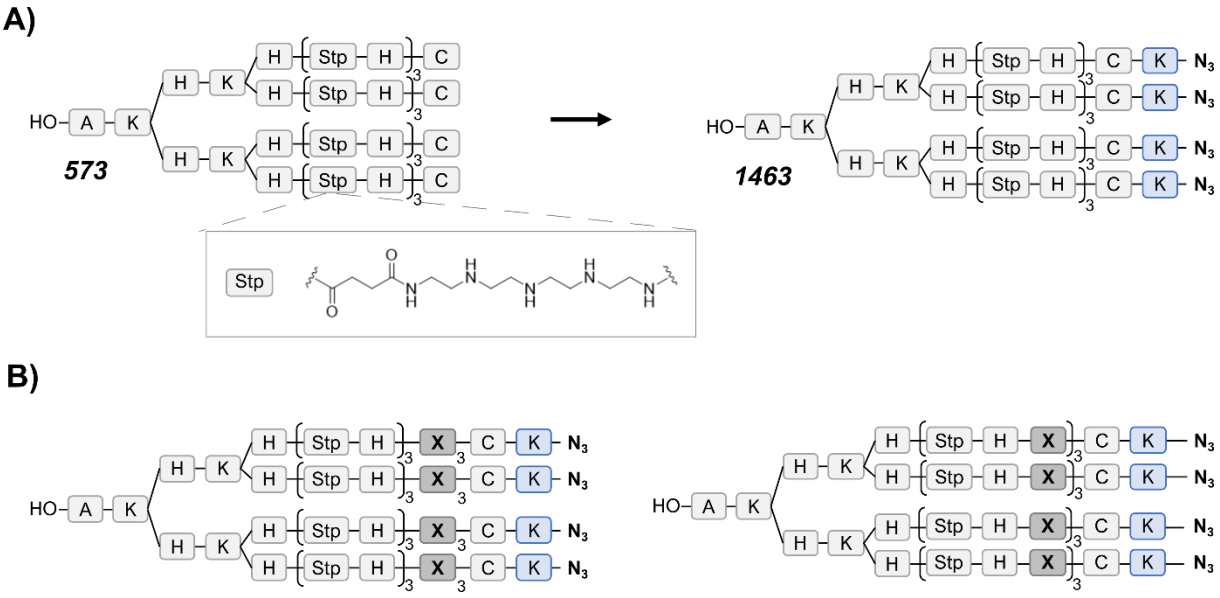

A) Evolution from original 4-arm OAA ***573*** to azido-OAA by introduction of N-terminal azido-lysines for subsequent modification via SPAAC. **B**) Modifications of azido 4-arm OAA with amino acid X either as block-tripeptide (X_3, left) or in an alternating pattern within the Stp-H motif (Stp-H-X, right). X represents either arginine, tryptophan or tyrosine.
A, alanine; C, cysteine; H, histidine; K, lysine; K(N_3), azido-lysine; R, arginine; Stp, succinoyl tetraethylene pentamine; W, tryptophan; Y, tyrosine.

Table 3.1. Library of azido 4-arm OAAs.

Abbreviation	ID	Sequence (C → N)
Original	***573***	A-K-[H-K-(H-Stp)$_3$-C)$_2$]$_2$
Stp-H	***1463***	A-K-[H-K-(H-Stp)$_3$-C-K(N_3)]$_2$]$_2$
Stp-H-Y_3	***1479***	A-K-[H-K-(H-Stp)$_3$-Y_3-C-K(N_3)]$_2$]$_2$
Stp-H-W_3	***1482***	A-K-[H-K-(H-Stp)$_3$-W_3-C-K(N_3))$_2$]$_2$
Stp-H-R	***1493***	A-K-[H-K-(H-Stp-R)$_3$-C-K(N_3))$_2$]$_2$
Stp-H-W	***1494***	A-K-[H-K-(H-Stp-W)$_3$-C-K(N_3))$_2$]$_2$
Stp-H-R_3	***1495***	A-K-[H-K-(H-Stp)$_3$-R_3-C-K(N_3))$_2$]$_2$

A, alanine; C, cysteine; H, histidine; K, lysine; K(N_3), azido-lysine; R, arginine; Stp, succinoyl tetraethylene pentamine; W, tryptophan; Y, tyrosine.

3.4.1.2 Formation and physicochemical characterization of 4-arm pDNA polyplexes

Prior to nanoparticle formation, pDNA and 4-arm OAAs were diluted in HBG buffer (20 mM HEPES (hydroxyethyl piperazinoethane sulfonic acid), 5% (w/v) glucose; pH 7.4) to equal volumes. Nanoparticles were formed by adding pDNA encoding the luciferase reporter gene (pCMVLuc) to the corresponding carrier at the indicated N/P (nitrogen-to-phosphate) ratios, followed by rapid mixing and incubation for 40 min at RT. The N/P ratio is hereby defined as the molar ratio of protonatable nitrogens of the carrier (secondary nitrogens of Stp, *N*-terminal amines, and the guanidinium of arginines) to the negatively charged phosphate groups of the pDNA backbone. As the optimum N/P ratio is carrier- and also cell line-dependent, different N/P ratios were evaluated for the new library.

The impact of the different modifications on the pDNA binding ability was assessed by an ethidium bromide (EtBr) exclusion assay (**Figure 3.2A**). In this assay, only less compacted pDNA is accessible for EtBr intercalation. Each carrier was tested at the N/P ratios of 6, 12, and 20. All carriers showed effective pDNA compaction (≤ 20% free pDNA); higher N/P ratios led to better compaction. Comparing ***573*** and ***1463***, the *N*-terminal azido-lysine within ***1463*** seems to slightly interfere with pDNA compaction (approx. 1.5-fold less pDNA compaction). Incorporation of additional tryptophans either in an alternating (***1494***) or block-wise motif (***1482***) further lowered pDNA binding ability, especially at lower N/P ratio (N/P 6, approx. 20% free pDNA). In contrast, the presence of tyrosine tripeptides had a positive effect on pDNA compaction due to hydrophobic stabilization via π-π stacking, which is in line with previous findings for T-shaped lipo-OAAs.(68) The best binding ability amongst all carriers was achieved for ***1493*** and ***1495***, both containing arginine either as an alternating motif (***1493***) or tripeptide (***1495***). Arginine (guanidine, pKa 12.5)(471) increases the positive charge density within the carriers, by this promoting improved pDNA binding ability.

All carriers were able to form defined homogeneous nanoparticles with sizes mostly between 100-200 nm (exceptions, ***573*** and ***1494*** at N/P 6) and positive zeta potentials around +5 to +25 mV, as determined via dynamic and electrophoretic light scattering (DLS, ELS; **Figure 3.2 B, C**). As expected, higher N/P ratios led to smaller particles with higher zeta potential. Again, incorporated tryptophans (carriers ***1494***, ***1482***) had a negative effect on particle formation, resulting in larger particles, especially at lower N/P ratios (z-average up to 500 nm). This was also supported by an increased polydispersity index (PDI) of 0.4 for ***1494***. These observations further confirmed the findings of the EtBr exclusion assay (**Figure 3.2 A**).

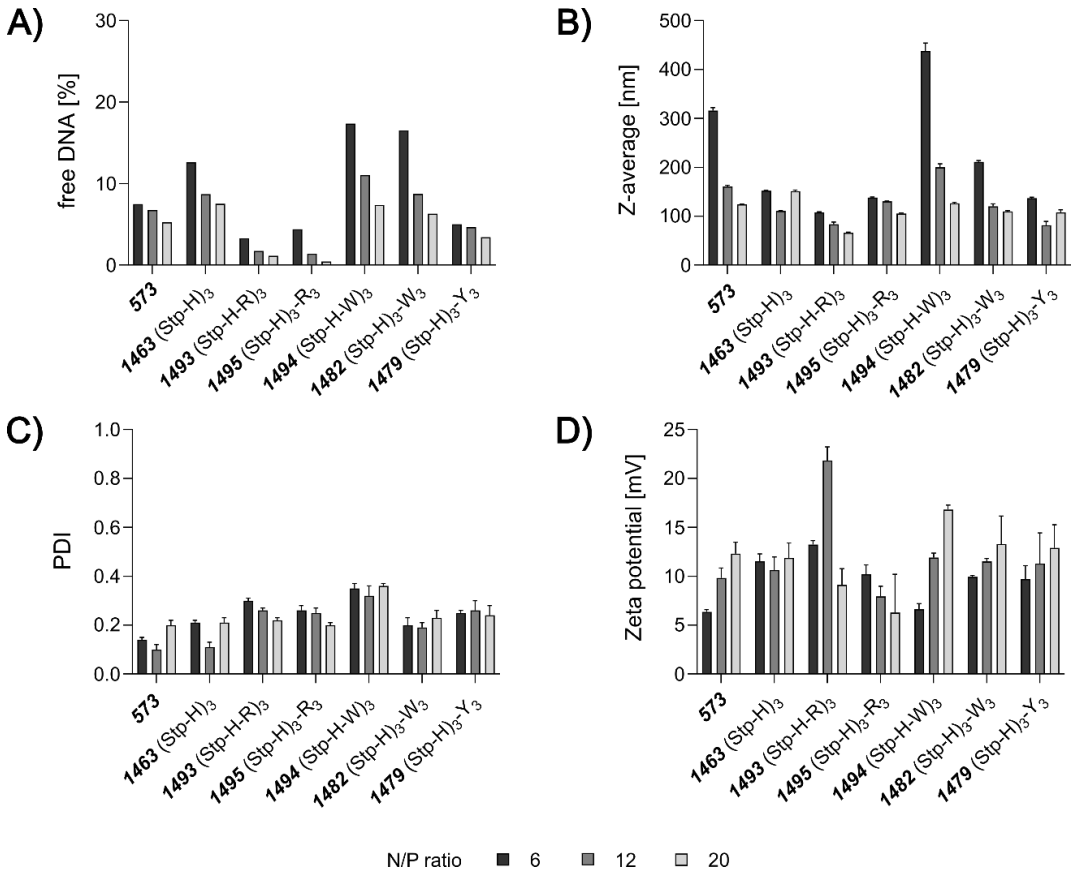

Figure 3.2. Physicochemical characterization of azido 4-arm OAA pDNA polyplexes at N/P ratios of 6, 12, and 20. A) Ethidium bromide (EtBr) exclusion assay. EtBr fluorescence correlates with the amount of free and non-compacted pDNA, as pDNA is only in this state accessible for EtBr intercalation. 100% EtBr fluorescence refers to the fluorescence of free pDNA without carrier in the same concentration as used for polyplex formation. B) Polyplex sizes (z-average by intensity) determined by DLS (n=3, mean + SD); C) polydispersity index (PDI); D) zeta potential determined by ELS (n=3, mean + SD). The experiments were performed by Paul Folda (Pharmaceutical Biotechnology, LMU Munich).

3.4.1.3 *In vitro* evaluation of the azido 4-arm library

The new 4-arm carriers were tested regarding their transfection efficiency (luciferase reporter gene assay) and cytotoxicity (MTT assay) in cell culture (**Figure 3.3**). Hereto, pDNA polyplexes at three different N/P ratios (6, 12, and 20) were applied for 24 h to three different tumor cell lines, namely, neuroblastoma cells (N2a), and two hepatocarcinoma cell lines (Huh7, HepG2). Linear polyethyleneimine (LPEI), which is the gold standard for pDNA delivery,(28, 71, 467) was used as positive control at its optimum N/P ratio of 6, which represents a compromise between efficacy and toxicity.(67, 71, 467) Cell line- and carrier-dependent differences were found. All carriers were well tolerated in all three cell lines (**Figure 3.3 B**). The only exception was ***1479***, containing tyrosine tripeptides that were already known to be toxic from previous studies.(435)

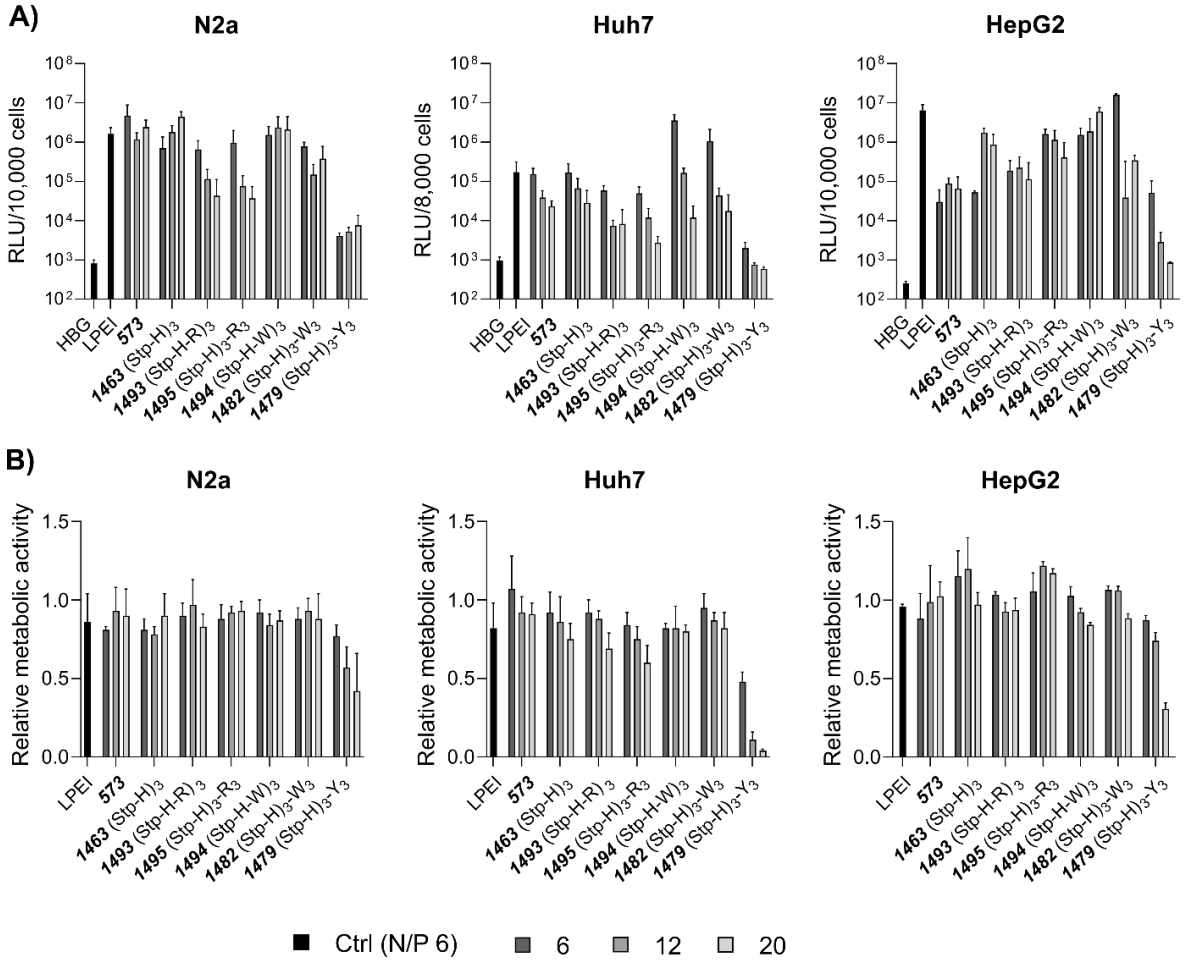

Figure 3.3. *In vitro* evaluation of the azido 4-arm library. Polyplexes were formed either at N/P 6, 12, or 20, and at a pCMVLuc concentration of 200 ng/well. A) Gene transfer activity determined at 24 h after transfection by a luciferase gene expression assay (n=6, mean + SD), and B) metabolic activity of cells at 24 h after transfection with 4-arm pDNA polyplexes in relation to HBG-treated control cells determined by an MTT assay (n=6, mean + SD). LPEI polyplexes (N/P 6) served as positive control.

For N2a and Huh7 cells, similar transfection patterns were obtained. Here, incorporation of azido-lysines (compare ***573*** and ***1463***) had no considerable impact. Both carriers showed good efficiency comparable to LPEI. Also, the tryptophan-containing carriers (***1494***, ***1482***) mediated high gene expression, especially at lower N/P ratios in Huh7 cells, outperforming LPEI by 6-fold (***1482***), and 20-fold (***1494***). Physicochemical characterization (**Figure 3.3**) demonstrated that tryptophan incorporation led to less compacted, larger pDNA polyplexes, which might be beneficial for *in vitro* transfections. In contrast, arginine modification both in alternating (***1493***) or block-wise sequence (***1495***) led to reduced transfection efficiency compared to ***573/1463***, particularly for higher N/P ratios and in N2a cells. In Huh7 cells, this might be partially explained by the observed slightly increased cytotoxicity at higher N/P ratios (N/P 20, metabolic activity of ~70% (***1493***) and ~60% (***1495***)), but this does not apply for N2a cells. Thus, the most reasonable explanation is that the improved pDNA compaction (as observed in the EtBr assay, **Figure 3.3 A**) hampered efficient pDNA delivery. Already in previous work, it was found that polyplex stability and sufficient cargo release have to be well-balanced for good transfection

activity.(67, 472) Furthermore, additional tyrosine tripeptides, which promote enhanced hydrophobic polyplex stabilization, were disadvantageous for transfection efficiency. Drastically reduced (N2a, two to three log units lower RLU (relative light units) values compared to ***1463***) or absent (Huh7, HBG level) gene expression was observed. Both the improved polyplex stability and the increased cytotoxicity of ***1479*** may be possible explanations. In HepG2 cells, however, any modification apart from tyrosine tripeptides could improve transfection efficiency compared to ***573***. Azido-lysine was beneficial at higher N/P ratios (***1463***, 10^6 RLU; ***573***, 10^5 RLU). Again, tryptophan incorporation was advantageous, leading to comparable gene transfer activity than LPEI in the case of ***1494*** (all N/P ratios) and ***1482*** (N/P 6). In contrast to the other two cell lines, arginine incorporation led to enhanced gene transfer performance in HepG2 cells (approx. two log units higher RLU values than ***573***).

Altogether, compiling transfection data of the three cell lines, the best performers were ***1463*** (Stp-H) and ***1494*** (Stp-H-W), showing high efficiency and biocompatibility. Therefore, these two carriers were chosen for subsequent experiments.

3.4.2 Shielding of selected azido 4-arm carriers

Many studies have emphasized the importance of shielded and targeted delivery systems to generate biocompatible, cell specific and site-directed nucleic acid vehicles.(100, 101) Besides numerous benefits achieved by PEGylation, foremost prolonged blood circulation time, some negative effects could occur, including poor nucleic acid compaction and polyplex stability, reduced cellular uptake (as a result of decreased interaction with negatively charged cell membranes), and hampered endosomal release (due to decreased cationic membrane destabilization). Such limitations can lead to decreased transfection potency and ask for careful consideration and development of polyplex modification strategies to obtain optimum shielding while maintaining polyplex stability and transfection efficiency.(189, 419) In the present study, the aim was to create well-shielded, stable nanoparticles with strongly reduced surface charge and consequently decreased membrane interactions. The resulting decreased gene transfer ability should then be reconstituted by active targeting via carbohydrate ligands. To identify best shielding conditions, two functionalization strategies, pre- and post-modification (**Figure 3.4**), as well as different PEG-shielding agents (different PEG lengths) and PEG densities on the polyplex surface were evaluated.

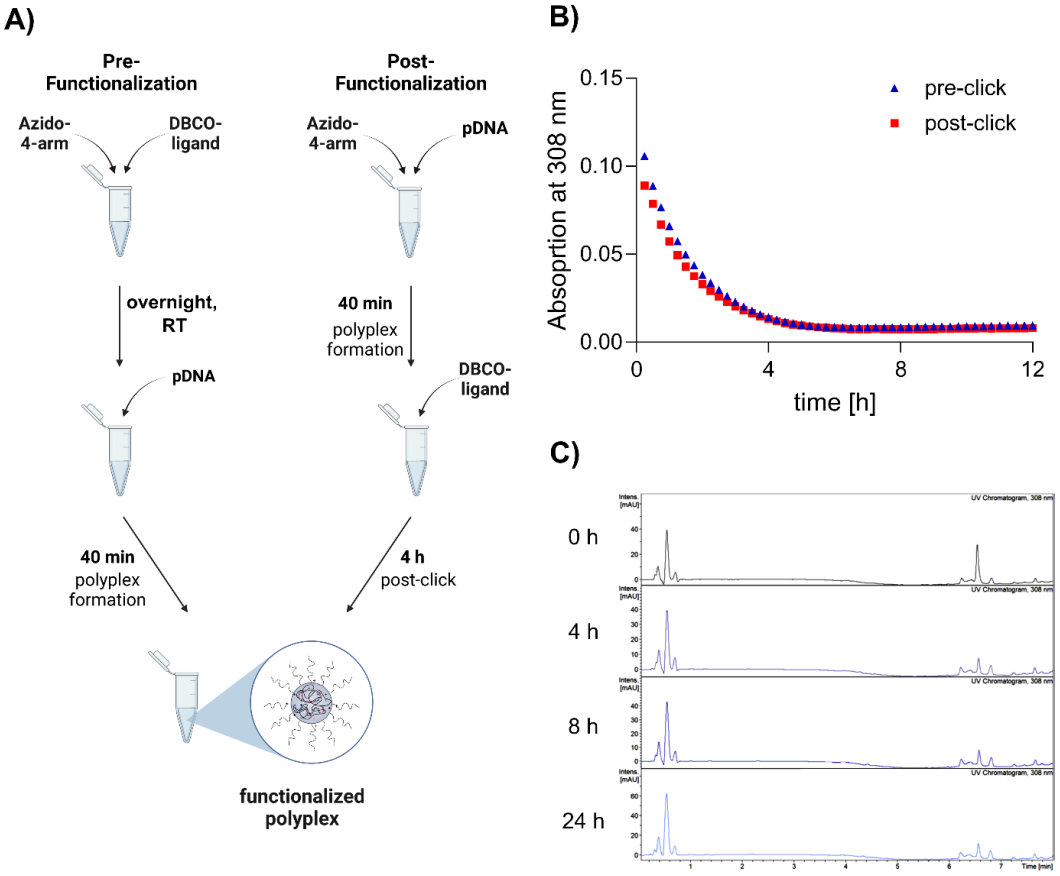

Figure 3.4. OAA modification by SPAAC. A) Mixing schemes and incubation times for polyplex formulations modified by either pre- (left) or post-functionalization (right). Evaluation of incubation times for successful SPAAC reaction between the azido-OAA ***1463*** and PEG_{24}-DBCO aiming for 25% functionalization by detection of the DBCO signal at 308 nm via B) UV/Vis spectroscopy for pre-functionalization (blue) and post-functionalization (red), and C) HPLC for pre-functionalization only.

3.4.2.1 Synthesis of sequence-defined, monodisperse PEG-DBCO agents

Sequence-defined PEG-DBCO agents of different lengths (PEG_n with n = ethylene oxide (EO) units = 12, 24, 48, 96) were synthesized using SPPS (see method 3.3.3.2). Longer PEG-DBCO agents (n = 48, 96) were assembled by either two or four successive couplings of the commercially available Fmoc-NH-dPEG_{24}-COOH building block on solid support. Due to increased steric hindrance by successive elongation of the PEG chain under standard coupling conditions, the reaction molar equivalents (eq) and coupling time were increased to 5 eq of the PEG_{24} building block and 16 h to ensure complete coupling. Afterwards, the DBCO motif was also coupled to the PEG-chain on solid support and the final product was cleaved from the resin under mild cleavage conditions (5% TFA) to avoid acid-triggered DBCO rearrangement,(241, 473) neutralized by addition of 0.1 M $NaOH_{aq}$, and stored in HEPES buffer (20 mM, pH 7.4) to avoid degradation of the DBCO group (via acid-mediated 5-endo-dig cyclo-isomerization(474)). All PEG_n-DBCO compounds were analyzed by LCMS and MALDI-TOF MS to confirm purity and identity (analytical data see Appendix, section 6.1.2).

3.4.2.2 PEGylation of 4-arm pDNA polyplexes

For PEGylation studies, the best performers of the 4-arm library screening (see chapters 3.4.1.2 and 3.4.1.3), namely, ***1463*** (i.e., azido derivative of ***573***) and ***1494*** (containing an alternating Stp-H-W motif), were selected.

Physico-chemical evaluation – comparison of pre- vs. post-PEGylation

PEGylated pDNA polyplexes were formed in HBG (pH 7.4) at two different N/P ratios (i.e., 6 and 12) and characterized regarding their size and zeta potential (DLS and ELS measurements), as well as their pDNA compaction ability (agarose gel shift assay, EtBr exclusion assay). In this regard, two different PEGylation approaches were compared (pre- vs. post-modification). The distinct PEG-DBCO agents were introduced via SPAAC either before (pre-PEGylation) or after polyplex formation (post-PEGylation) (**Figure 3.4 A**). The SPAAC reaction time was monitored by the decrease of the DBCO-signal at 308 nm over time via UV/Vis spectroscopy for the pre- and post-functionalization approach at polyplex mixing conditions (**Figure 3.4**), and by HPLC with UV/Vis detection (**Figure 3.4 C**, for pre-functionalization only). After around 4-6 h, most of the DBCO-agent was clicked to the azido-OAA, as observed by a fast decrease of the absorbance at 308 nm, which also supports the chosen incubation time of 4 h for post-functionalization. Post-functionalization was achieved by formation of core-polyplexes by mixing OAA and DNA for 40 min, followed by subsequent addition of the DBCO-ligand for 4 h (**Figure 3.4 A**, *right*). For the pre-functionalization approach, the OAA was functionalized with the desired molar amount of ligand in regard to the azido groups in an overnight reaction at constant slight shaking (**Figure 3.4 A**, *left*). Afterwards, pDNA was added to the PEGylated OAA by rapid pipetting for polyplex formation. As the azido 4-arm structures provide four azido groups per OAA, different functionalization degrees (FDs), from 25% (statistically one azido group per OAA molecule clicked with PEG-DBCO agent) up to 100% (all four azido groups clicked with PEG-DBCO agent) were included in the evaluation. Thus, for achieving different FDs, either 1, 2, or 4 equivalents of PEG_n-DBCO agent in relation to the molar amount of the OAA carrier were clicked.

As a result of effective shielding, it was expected that PEGylation would lead to a decreased zeta potential by shielding the positive surface charge of the carriers and by providing terminal, outward oriented carboxyl groups. At the same time, it was highly desired that a high compaction efficiency and the ability to form nanosized particles was maintained.

DLS and ELS measurements (**Figure 3.5** and **Figure 3.6**)**.** The unmodified ***1463*** polyplexes formed small, homogeneous particles with sizes around 100 nm and a positive zeta potential between 10-15 mV.

Pre-PEGylation had almost no influence on the polyplex size, except for the shorter PEG_n-DBCO agents, where aggregation was observed for FD 100% with PEG_{12} at both N/P 6 and 12, as well as for FD 25% with PEG_{24} at N/P 6. By modification with longer PEG-agents (n = 48, 96) aggregation could be avoided at all FDs, which might be a result of steric shielding between the particles. For PEG_{12}, no significant decrease of the zeta potential was observed, leading to the assumption that PEG_{12} had no shielding effect on the polyplexes. For polyplexes pre-functionalized with $PEG_{\geq 24}$, the shielding effect was confirmed by a decrease of zeta potential from 10-15 mV of the unmodified control polyplex to almost neutral while maintaining nanosized dimensions.

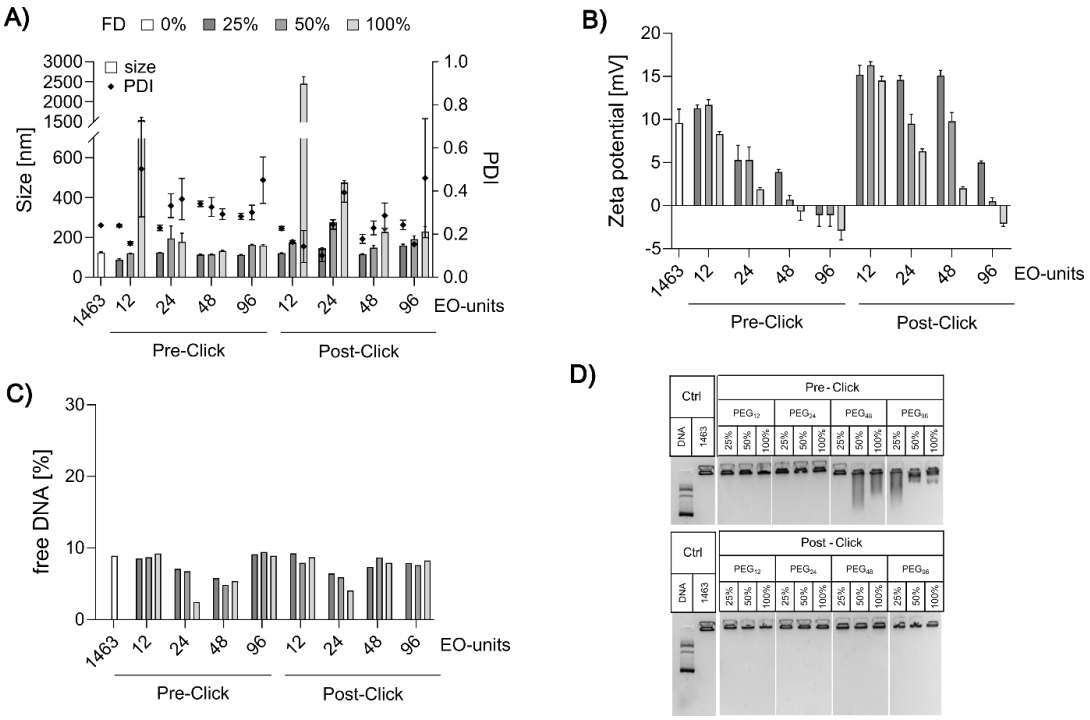

Figure 3.5. Physicochemical evaluation of PEGylated ***1463*** pDNA polyplexes at N/P 12. A) Polyplex sizes (z-average by intensity) and polydispersity index (PDI) values determined via DLS (n=3, mean ± SD), as well as B) zeta potential results obtained by ELS (n=3, mean + SD) of polyplexes pre- or post-functionalized with PEG_n-DBCO agents (n = ethylene oxide (EO) units = 12, 24, 48, 96) at different functionalization degrees (FDs, 25%, 50%, and 100%) in comparison to unmodified polyplexes (FD 0%). Compaction ability was determined by C) ethidium bromide (EtBr) exclusion assay, and D) agarose gel shift assay in comparison to unmodified polyplexes. EtBr fluorescence correlates with the amount of less compacted pDNA, as pDNA is only in this state accessible for EtBr intercalation. 100% EtBr fluorescence refers to the fluorescence of free pDNA without carrier in the same concentration as used for polyplex formation.

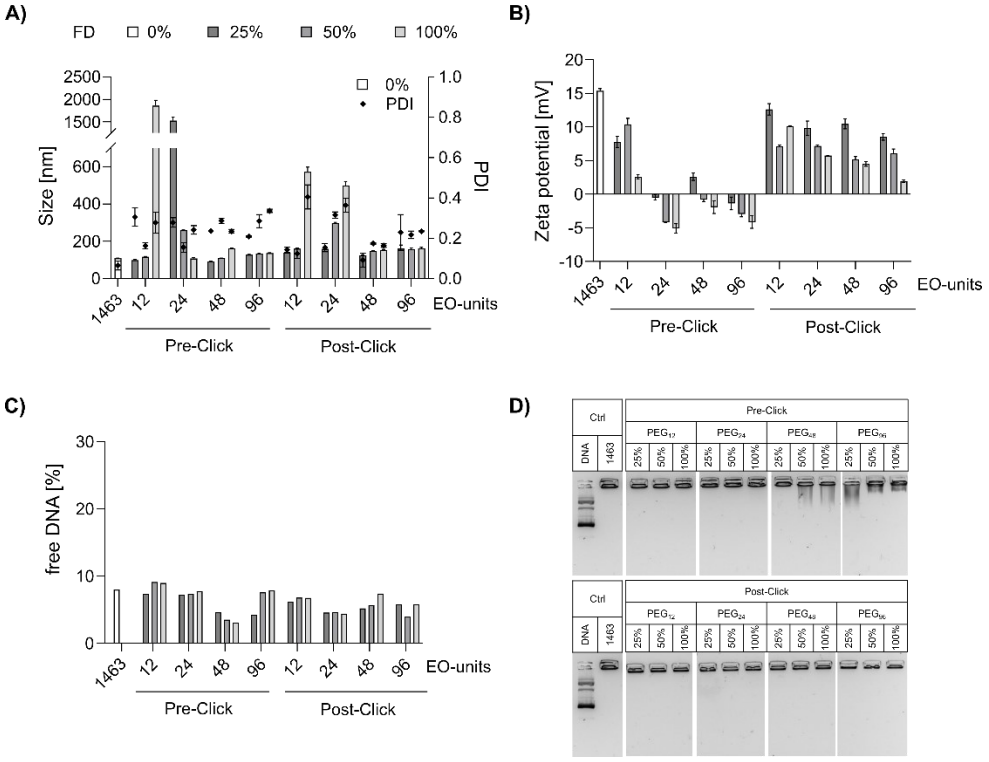

Figure 3.6. Physicochemical analysis of shielded ***1463*** pDNA polyplexes at N/P 6. The polyplexes were formed at N/P 6. PEGylation was achieved either by pre- or post-functionalized with different PEG_n-DBCO agents (n = ethylene oxide (EO) units = 12, 24, 48, 96) at different functionalization degrees (25%, 50%, and 100%). The shielded polyplexes were physicochemically characterized in comparison to unmodified polyplexes by DLS and ELS measurements (n=3, mean ± SD), determining A) size (z-average by intensity) and polydispersity index (PDI), and B) zeta potential of the polyplexes. Compaction ability was determined by C) ethidium bromide (EtBr) exclusion assay, and D) agarose gel shift assay. EtBr fluorescence correlates with the amount of less compacted pDNA, as pDNA is only in this state accessible for EtBr intercalation. 100% EtBr fluorescence refers to the fluorescence of free pDNA without carrier in the same concentration as used for polyplex formation.

For post-functionalization, significant differences were observed compared to pre-functionalization. A slight increase in the z-average was detected that correlated with increased FDs for the evaluated N/P ratios, ranging e.g., from 140-160 nm for FD 25%, up to 500 nm for FD 100% in the case of PEG_{24}. In accordance, the PDI values increased. This indicates destabilization by post-functionalization with PEG, as already observed in previous studies.(211, 418, 419) Longer PEG reagents led to less changes in the z-average most likely due to steric stabilization. The effects on zeta potential upon post-PEGylation were less pronounced than for pre-PEGylation. Besides a clear effect of both, the PEG length and the FD, sufficient shielding was only generated with PEG_{48} and PEG_{96} at a FD of 100%.

Overall, the length of the PEG-DBCO agent and functionalization method had a noteworthy effect on the surface charge of the resulting polyplexes. The effects were stronger for N/P 6 than for N/P 12. Additionally, the use of longer PEG and higher FDs led to a strong decrease of zeta potential, as a result of masking the positive surface charge of the polyplex. PEG_{12} had only a slight influence on the zeta potential and a significant decrease was only obtained for PEG_n with $n \geq 24$, suggesting that a minimum PEG length of 24 repetition units is required for

efficient shielding of ***1463*** pDNA polyplexes. While post-PEGylation in general led to polyplex destabilization and only a minor decrease of surface charge, pre-PEGylation seemed to be the more suitable functionalization approach for the 4-arm carrier.

Transmission electron microscopy (TEM, **Figure 3.7**). Morphologic characteristics of the PEGylated nanoparticles (N/P 12, FD 50%) were investigated via TEM. The findings were in line with the DLS data. However, the nanoparticle sizes of TEM samples were overall smaller than those obtained via DLS. This discrepancy can be explained by the fact that TEM samples were dried on the grid, leading to dehydrated particles, whereas the native hydrodynamic diameter is determined in the case of DLS.(67, 423). Again, pre-click seemed to be more favorable than post-click, leading to homogeneous, small-sized nanoparticles with narrow size distribution. Moreover, pre-click with both PEG_{24} and PEG_{96} resulted in polyplexes in the same size range than the unmodified particles. In the case of post-click, TEM images revealed a more heterogeneous mixture of larger and smaller particles, mostly appearing in clusters. In general, introduction of PEG slightly changed the shape of the nanoparticles from spheres (unmodified polyplexes) to rod-like structures, especially in the case of PEG_{96} and pre-functionalization.

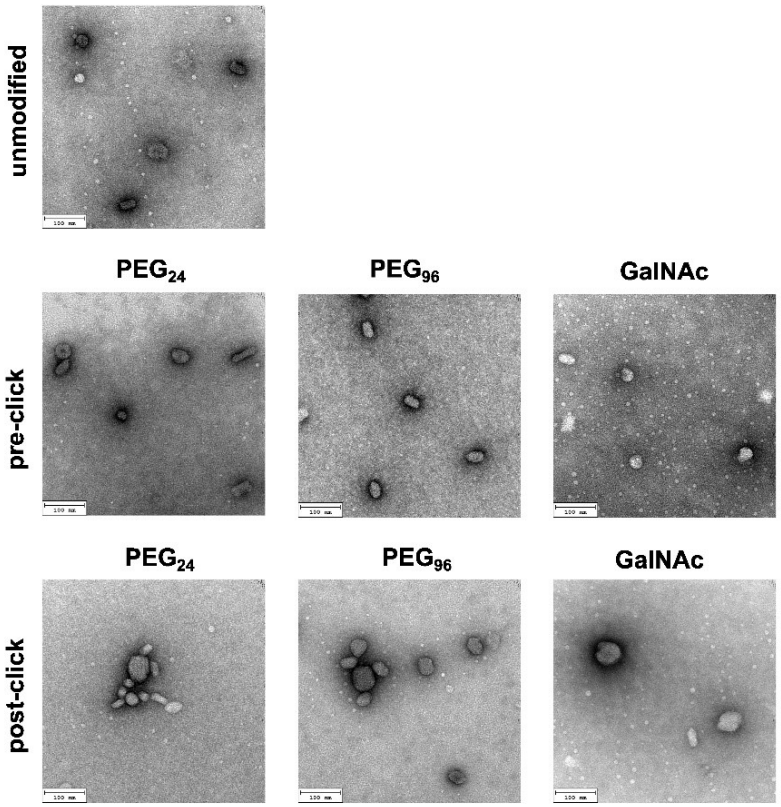

Figure 3.7. Representative TEM images of unmodified, shielded, and targeted ***1463*** pDNA polyplexes. The polyplexes were formed in H_2O at N/P 12, modified either by pre- (middle row) or post-functionalization (lower row) with PEG_{24}-DBCO (left column), PEG_{96}-DBCO (middle column), or $(GalNAc)_3$-PEG_{24}-DBCO (right column) at a functionalization degree (FD) of 50% and compared to unmodified polyplexes (upper left). Scale bar: 100 nm. The preparation of polyplexes was carried out by Simone Berger (Pharmaceutical Biotechnology, LMU Munich), TEM experiments were performed by Susanne Kempter (Soft Matter Physics, LMU Munich).

Agarose gel shift and EtBr exclusion assay (**Figure 3.6** and **Figure 3.7**). The compaction ability of shielded ***1463*** polyplexes at N/P 6 and 12 was further examined in an agarose gel shift and EtBr exclusion assay. In the agarose gel shift assay, no considerable amount of free DNA was detected in any formulation. For polyplexes pre-functionalized with PEG_{48} or PEG_{96}, smearing bands were detected at both N/P ratios, indicating slightly reduced pDNA compaction, which could be also seen in the EtBr exclusion assay. Apparently, high PEG content led to destabilization, as also indicated by the elevated PDI values (**Figure 3.5 A** and **Figure 3.6 A**). Overall, the EtBr assay showed effective compaction ability for all tested formulations with less than 20% free DNA.

To conclude, the pre-PEGylation approach exhibited remarkable benefits over the post-functionalization approach. Nonetheless both functionalization strategies demonstrated high effectivity of the click reaction and nearly full conversion of the DBCO motif (**Figure 3.4 B, C**). Pre-functionalization resulted in more homogeneous and defined particles, with strongly decreased zeta potential, as evidenced by the physicochemical characterization data. In the case of pre-functionalization, it can be assumed that all used DBCO agent clicked completely to the azido-OAAs (overnight click reaction). This in turn means that in the subsequent polyplex formation process a defined amount of conjugated OAAs is used, resulting in well-formed, defined nanoparticles. In the case of post-functionalization, SPAAC reaction is exerted after polyplex formation, suggesting that click reaction proceeds at accessible azido groups at the polyplex surface and of free excess OAAs, which are present due to the N/P ratio of 6 and 12. Although monitoring of this click reaction revealed comparable conjugation effectivity as for the pre-click approach (**Figure 3.4 B**), this post-functionalization process might interfere with the already formed polyplexes, leading to destabilization and less compacted nanoparticles, as it was already observed previously.(211)

Analogous PEGylation experiments with ***1494*** polyplexes resulted in less favorable nanoparticle properties such as aggregation tendency (especially at lower N/P ratio and in case of post-PEGylation) as observed by DLS and ELS measurements (**Figure 3.8**). Therefore, further evaluation was continued with ***1463*** polyplexes only.

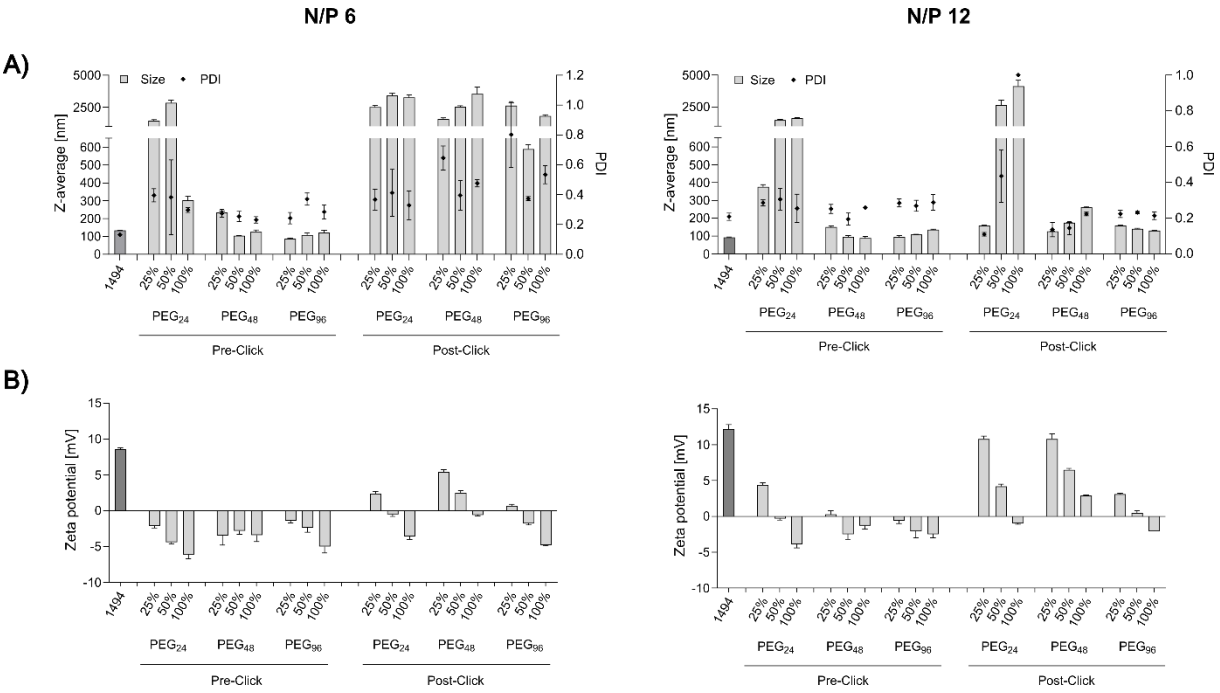

Figure 3.8. Physicochemical characterization of PEGylated ***1494*** pDNA polyplexes. The polyplexes were formed in HBG at N/P 6 (left) or N/P 12 (right) and were PEGylated either by pre- or post-functionalized with different PEG_n-DBCO agents (n = 12, 24, 48, 96) at different functionalization degrees (25%, 50% and 100%). A) Z-average (by intensity) and polydispersity index (PDI) determined via DLS (n=3; mean ± SD). B) Zeta potential determined via ELS (n=3; mean + SD).

3.4.2.3 *In vitro* evaluation of pre- vs. post-PEGylated 4-arm pDNA polyplexes on hepatocyte cell lines

Transfection efficacy of PEGylated ***1463*** pDNA polyplexes was determined by a luciferase gene expression assay in two hepatoma cell lines (Huh7 and HepG2). For each cell line the best working N/P ratio was selected based on the initial library screening (see chapter 3.4.1.3; **Figure 3.3**), which was N/P 6 for Huh7 and N/P 12 for HepG2 cells. Again, LPEI polyplexes at their optimum N/P ratio of 6 were used as positive control.(67, 71, 467)

Pre- and post-PEGylated ***1463*** polyplexes showed remarkable differences in transfection efficacies and a minimum PEG-length for shielding could be identified (**Figure 3.9 A, B**). In the case of PEG_{12}-DBCO, no decrease in transfection efficacy was observed. High PEG_{12} densities even led to enhanced luciferase expression, which may be due to lower polyplex stability and decreased DNA compaction as indicated by the increased polyplex sizes (**Figure 3.5 A** and **Figure 3.6 A**). For longer PEG agents, pre-PEGylation caused a strong reduction in transfection efficacy by two log units compared to unmodified polyplexes, independent of the cell line. These observations were consistent with the results of the ELS measurements (**Figure 3.5 B** Figure **3.6 B**), where pre-PEGylation led to a stronger reduction of particle surface charge, which consequently reduces the adhesion of the polyplexes to cell membrane surfaces, by this decreasing cellular uptake and transfection efficacy.

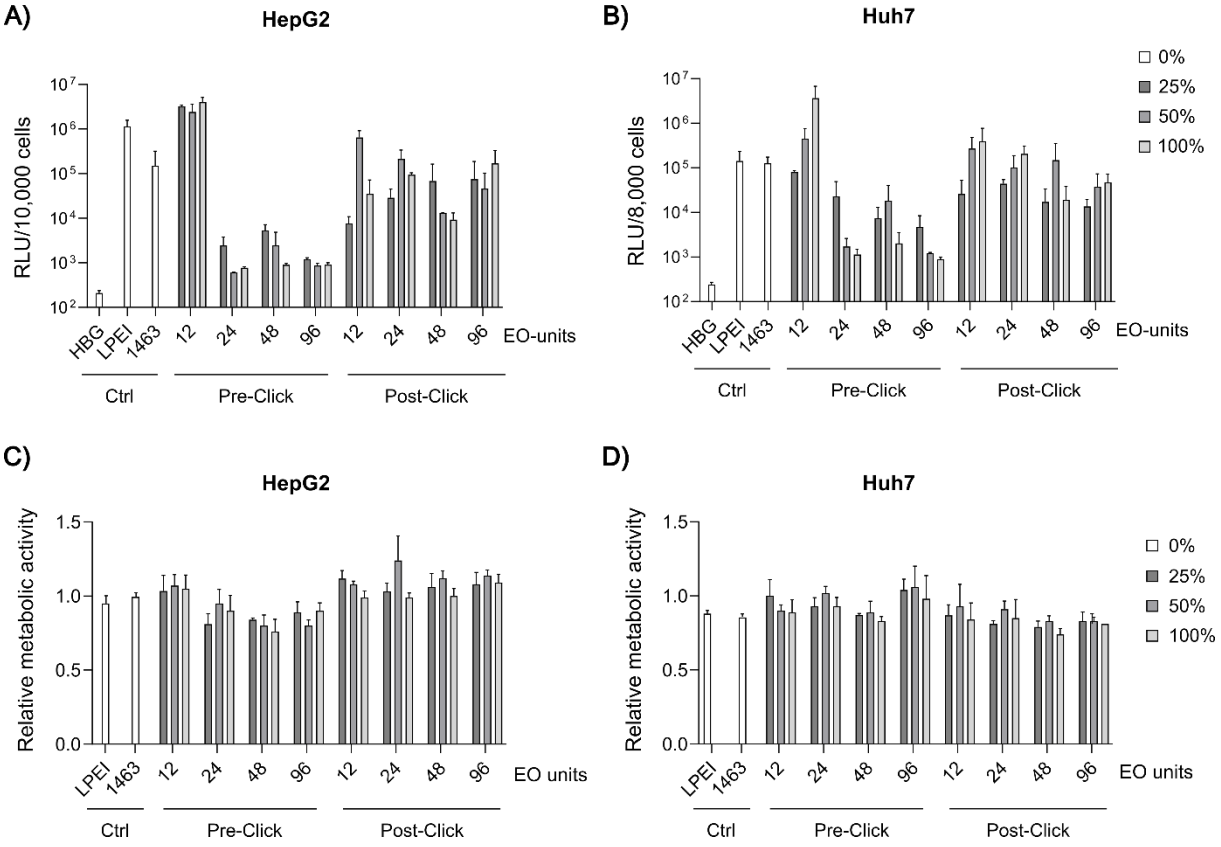

Figure 3.9. *In vitro* evaluation of PEGylated ***1463*** pDNA polyplexes on hepatocarcinoma cells. Gene transfer activity of shielded polyplexes in HepG2 (A) and Huh7 cells (B) at 48 h after transfection and metabolic activity of hepatoma cells (HepG2 cells, C and Huh7 cells, D) transfected with pre- and post-PEGylated ***1463*** pDNA polyplexes. Comparison of unmodified with functionalized polyplexes; LPEI polyplexes (N/P 6) served as positive control. Polyplexes were formed at a pCMVLuc concentration of 200 ng/well at N/P 12 for transfections in HepG2 and at N/P 6 for Huh7, respectively. Polyplexes were either pre- or post-functionalized with PEG-DBCO agents of different lengths (12, 24, 48 or 96 ethylene oxide units) at different functionalization degrees (FDs, 0%, 25%, 50%, and 100%). Transfection efficacy was determined by luciferase gene expression assay (n=3, mean + SD). Metabolic activity was determined via an MTT assay (n=3; mean + SD). Relative metabolic activity was normalized to HBG-treated control cells.

In addition, a PEG ratio-dependent effect was observed. High FDs caused a stronger decrease of surface charge and hence showed reduced gene transfer activity. In contrast, post-PEGylation had no significant impact on the transfection efficacy, showing RLU values comparable to the unmodified control at all tested FDs and PEG lengths, indicating once more that post-modification was less favorable for effective shielding than the pre-click approach. Determination of the relative metabolic activity of both, Huh7 and HepG2 cells via an MTT assay showed no negative influence of PEGylation on cell viability (**Figure 3.9 C, D**).

To sum up, the optimal PEG length for efficient shielding depends on the carrier. The intention was to reduce transfection efficiency to a minimum by PEGylation as a means of shielding and restore it by active ligand targeting. Therefore, the criteria for efficient shielding were well-compacted nanoparticles with strongly reduced surface charge and consequently drastically decreased transfection efficiency. For ***1463***, these conditions were fulfilled best for PEG_{24} at a

FD of 50% and higher. The pre-PEGylation approach was found to be beneficial for this class of polycationic carriers in terms of shielding efficiency, and thus was selected for subsequent targeting experiments with azido-OAA ***1463.*** PEG_{24} was used as shielding unit.

3.4.3 Targeting of 4-arm polyplexes

Finally, the ***1463*** polyplexes were equipped with targeting ligands to evaluate their targeting ability. Since PEGylation led to reduced transfection efficacy because of decreased interaction with cell membranes caused by neutral or slightly negative zeta potential, targeting ligands were introduced to restore transfection potency and to provide cell- or organ-specific delivery.

Therefore, in this work carbohydrate-functionalized polyplexes were created, which were capable of delivering DNA to specific cell types by receptor-mediated endocytosis via lectins. For this purpose, the well-known ASGPR present on hepatocytes, as well as mannose receptors present on dendritic cells were addressed by either GalNAc- or mannose-functionalized 4-arm pDNA polyplexes. ASGPR targeting has already been applied in many studies with direct conjugates of a GalNAc-trimer linked to chemically stabilized siRNA,(115, 440, 441, 446) or Cas9 protein,(273) GalNAc- or galactose-modified polymeric carriers,(216, 438, 444, 445, 475) as well as GalNAc-equipped LNPs.(442, 443) Consequently, GalNAc-functionalized polyplexes represent a great delivery system for a first proof-of-concept study, which was then extended towards targeting of dendritic cells by functionalization of ***1463*** pDNA polyplexes with mannose ligands.

3.4.3.1 ASGPR-targeted polyplexes

For targeting of ASGPR on hepatocytes, a novel ligand was designed with trivalent GalNAc moieties on a biocompatible, flexible backbone. Notably, this ligand included an *N*-terminal amino group for subsequent incorporation of a PEG_{24}-spacer and DBCO for click reactions.

Synthesis of trivalent GalNAc-ligand $(GalNAc)_3$-PEG_{24}-DBCO

The synthesis of $(GalNAc)_3$-PEG_{24}-DBCO is described in section 3.3.3.3. The ligand backbone, consisting of a trimer of the functional building block TDS (triple bond diethylene triamine succinic acid) was assembled on solid phase.(459) TDS, bearing an alkyne side chain, was used for the introduction of azido-functionalized GalNAc moieties via copper(I)-catalyzed alkyne-azide cycloaddition (CuAAC) on resin. Extensive washing of the resin with a solution of the chelator agent sodium diethyl dithiocarbamate (SDTC) was performed to ensure complete removal of copper traces.(464) After deprotection of the *N*-terminal Fmoc-protecting group, saponification of carbohydrate protecting groups, and cleavage of the ligand precursor from the resin, the DBCO motif for subsequent click reaction to azido-OAAs was introduced by coupling DBCO-PEG_{24}-TFP (2,3,5,6-tetrafluorophenol) ester in solution, followed by

purification using preparative RP-HPLC. Trivalent GalNAc moieties were introduced following a rational design to provide suitable spatial arrangement and intramolecular flexibility enabling high affinity towards the binding sites of the targeted receptor.(283) In addition, PEG_{24} was incorporated, serving not only as spacer between ligand and carrier, but also for comparability with the shielded polyplexes. The intermediate oligomer $(GalNAc)_3$-amine was characterized via ^{1}H-NMR spectroscopy, MALDI-TOF MS, and analytical RP-HPLC. Identity and purity of the final ligand $(GalNAc)_3$-PEG_{24}-DBCO were confirmed by MALDI-TOF MS and LCMS (for analytical data, see appendix chapter 6.1.3.1).

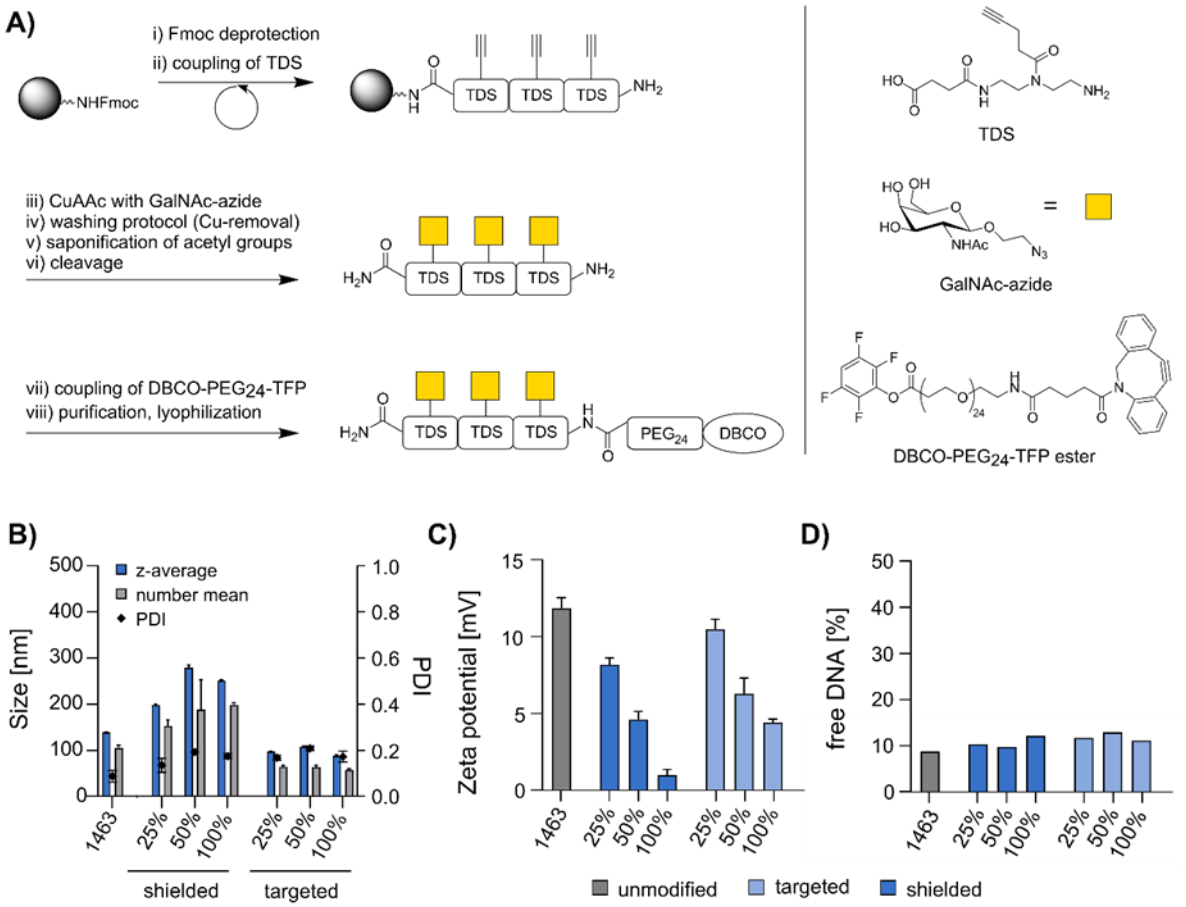

Figure 3.10. Synthesis of trivalent GalNAc-ligand and physicochemical evaluation of GalNAc-functionalized ***1463*** pDNA polyplexes. A) Synthesis scheme for successive assembly of the trivalent GalNAc-ligand for click reaction to azido 4-arm carrier ***1463***. The synthesis of $(GalNAc)_3$-PEG_{24}-DBCO is described in section 3.3.3.3. The ligand was used for modification of polyplexes formed at N/P 12 in HBG with 1 µg DNA per 100 µL polyplex solution by pre -functionalization at different molar amounts leading to different functionalization degrees (FDs; 25%, 50%, and 100%). Targeted polyplexes were evaluated in direct comparison with unmodified and PEG_{24}-shielded polyplexes by determination of B) polyplex size (z-average by intensity and number mean) and polydispersity index (PDI), and C) zeta potential via DLS and ELS measurements (n=3, mean + SD), as well as D) regarding their DNA compaction ability in an ethidium bromide (EtBr) exclusion assay. EtBr fluorescence correlates with the amount of free and non-compacted pDNA, as pDNA is only in this state accessible for EtBr intercalation. 100% EtBr fluorescence refers to the fluorescence of free pDNA without carrier in the same concentration as used for polyplex formation. The synthesis of the ligand precursor, up to the intermediate of the free amine was performed by Nikole L. Fendler (Chemistry, Davidson College) and Katharina Bücher-Schossau (Organic and macromolecular chemistry, HHU Duesseldorf).

Physicochemical characterization of GalNAc-functionalized polyplexes

The successfully synthesized GalNAc-ligand was used for functionalization of azido 4-arm pDNA polyplexes. Since the pre-modification strategy turned out to be beneficial for particle formation with PEG agents (section 3.4.2.2), this approach was selected for subsequent experiments. ***1463*** pDNA polyplexes were formed at N/P 6 and 12 and subsequently evaluated for their physicochemical properties.

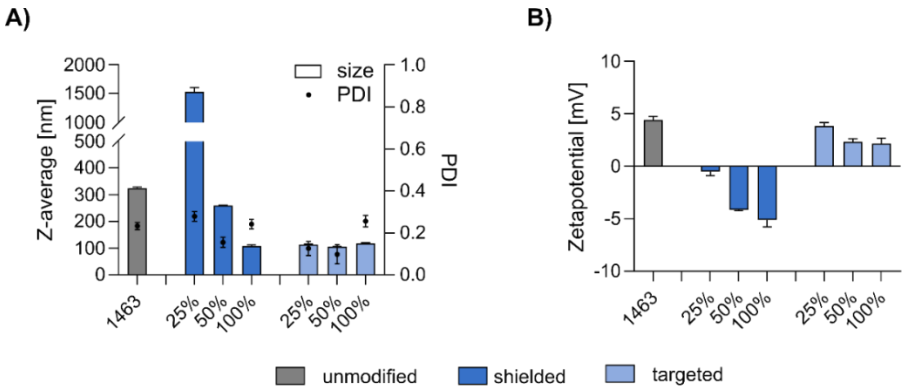

Figure 3.11. Physicochemical characterization of pre-targeted vs. pre-shielded ***1463*** pDNA polyplexes at N/P 6. The polyplexes were formed in HBG at N/P 6 and pre-functionalized either with $(GalNAc)_3$-PEG_{24}-DBCO (targeted, light blue) or PEG_{24}-DBCO (shielded, dark blue) at different functionalization degrees (25%, 50%, and 100%). A) Z-average (by intensity) and polydispersity index (PDI) determined via DLS (n=3; mean ± SD). B) Zeta potential determined via ELS (n=3; mean + SD).

DLS and ELS results of PEGylated polyplexes were already discussed in chapter 3.4.2. Polyplex functionalization with the GalNAc-ligand led to homogeneous particles (PDI <0.3 for all formulations, independent of the evaluated N/P ratios) (**Figure 3.10** and **Figure 3.11**). Small sizes of 55-65 nm (number mean) and 90-100 nm (z-average by intensity), respectively, were obtained for GalNAc polyplexes formed at N/P 12 which is considered to be favorable for hepatocyte delivery.(476, 477) TEM images confirmed the formation of homogeneous, small-sized nanoparticles in the case of pre-functionalization (**Figure 3.7**). Worth to mention, post-click with the GalNAc ligand led to a size increase as compared to unmodified and pre-clicked polyplexes. Opposed to N/P 12, polyplex diameters increased by up to 25% for polyplexes at N/P 6. Furthermore, introduction of the GalNAc ligand mediated a zeta potential reduction, which was dependent on the FD; increasing ligand density (and thus increased PEG content) led to a decreased zeta potential (unmodified: +11.8 mV; targeted: 25%, +10.5 mV; 100%, +4.4 mV at N/P 12). Both the agarose gel-shift assay and EtBr exclusion assay confirmed effective compaction ability of the targeted polyplexes with less than 15% of free DNA (**Figure 3.12**). Surprisingly, for shielded polyplexes, especially at higher FDs and the lower N/P ratio of 6, smearing bands occurred (**Figure 3.12 B**), which were not observed in former experiments (**Figure 3.5 D** and **Figure 3.6 D**). Obviously, functionalization with PEG_{24}, especially at a higher FD of 100%, might yield particles with meta-stability and somewhat aggregation tendency, as also supported by the increased PDI value. However, DLS and ELS measurements (**Figure**

3.10, Figure 3.12 B, C and **Figure 3.11**) as well as the EtBr exclusion assay (**Figure 3.12**) showed that still defined nanoparticles were generated. This emphasizes once more that the higher the PEG content within the formulation is (longer PEG chain lengths, higher FDs), the higher is the destabilizing effect, leading to less compacted nanoparticles. In the case of targeted polyplexes, $(GalNAc)_3$ units might mediate sterical hindrance, leading to reduced aggregation tendency and more stable particle formation.

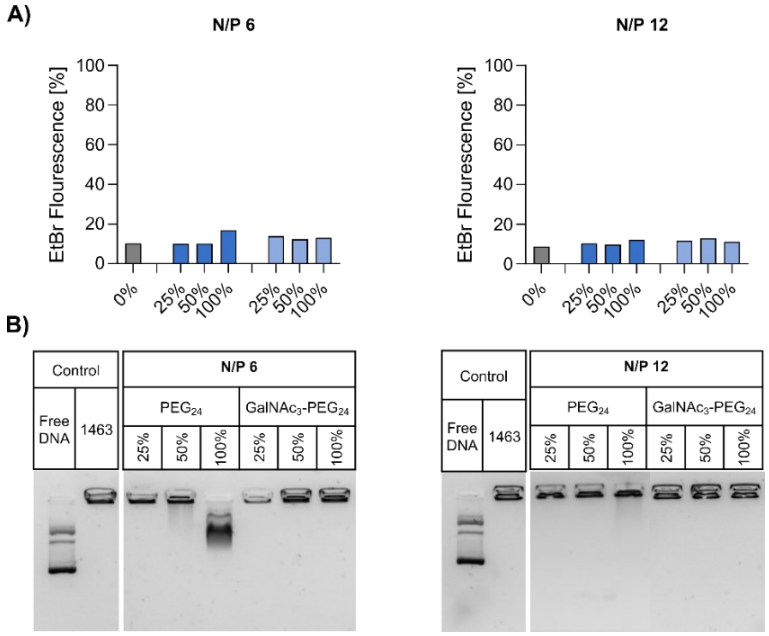

Figure 3.12. Compaction ability of pre-targeted vs. pre-shielded ***1463*** pDNA polyplexes. The polyplexes were formed in HBG at N/P 6 (left) and N/P 12 (right) and were pre-functionalized either with $(GalNAc)_3$-PEG_{24}-DBCO (targeted, light blue) or PEG_{24}-DBCO (shielded, dark blue) at different functionalization degrees (25%, 50%, and 100%). A) Ethidium bromide exclusion assay for detection of non-compacted DNA. EtBr fluorescence correlates with the amount of less compacted pDNA, as pDNA is only in this state accessible for EtBr intercalation. 100% EtBr fluorescence refers to the fluorescence of free pDNA without carrier in the same concentration as used for polyplex formation. B) Agarose-gel shift assay.

In vitro evaluation of GalNAc-functionalized polyplexes

The evaluation of shielded 4-arm polyplexes has shown that the pre-PEGylation approach not only helped to avoid particle aggregation, but also leads to better shielded polyplexes yet with a remarkable negative effect on transfection efficiency. The physicochemical evaluation of polyplexes pre-functionalized with the GalNAc ligand revealed well-defined, homogeneous small-sized particles, making them particularly promising for ASGPR-targeted DNA delivery.

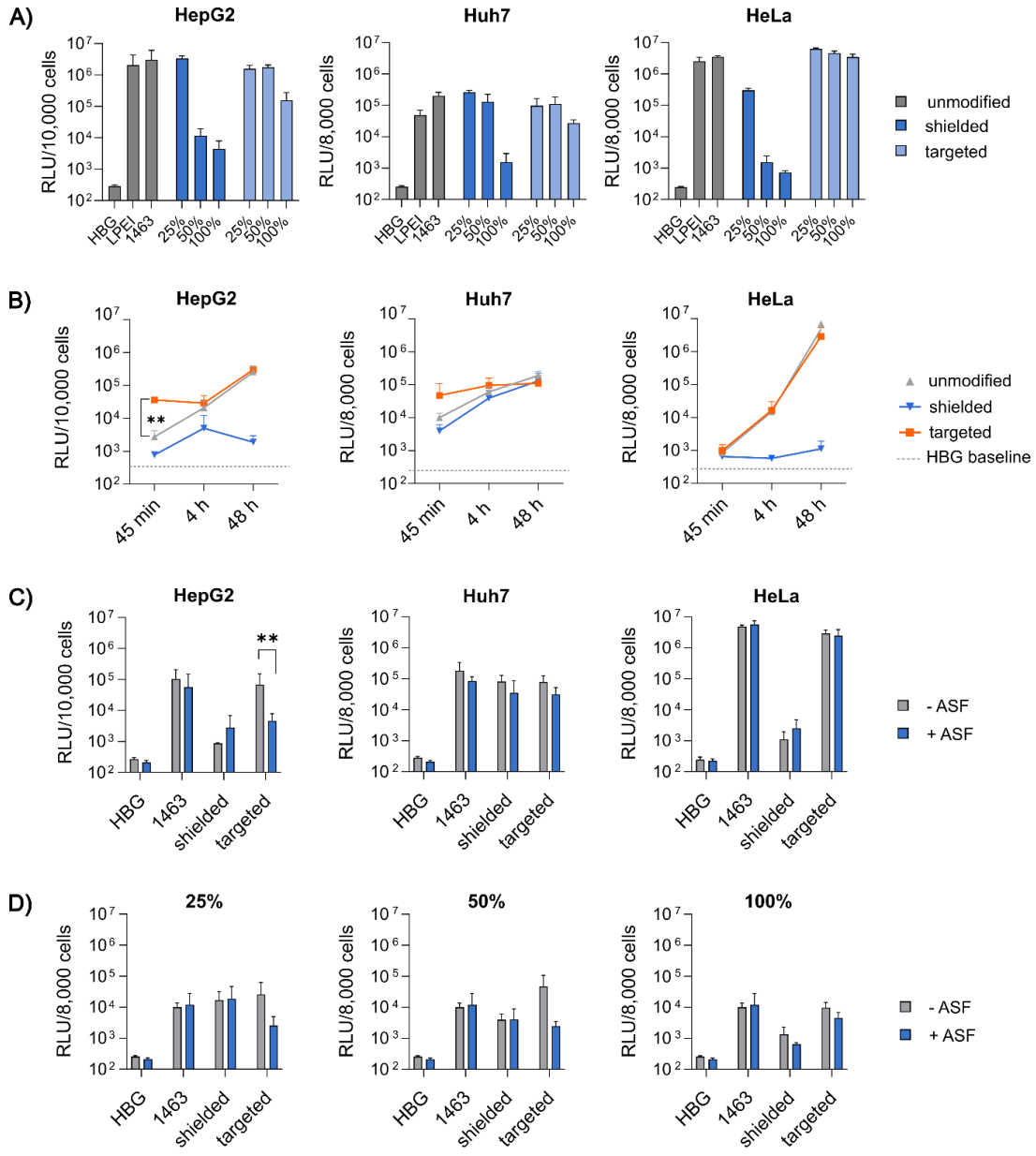

Figure 3.13. *In vitro* evaluation of GalNAc-functionalized 1463 pDNA polyplexes and evaluation of gene transfer activity under various conditions**.** OAA **1463** was pre-functionalized either with PEG_{24}-DBCO (shielded) or $(GalNAc)_3$-PEG_{24}-DBCO (targeted), and polyplexes were formed with 200 ng pCMVLuc-DNA per 20 µL polyplex solution either at N/P 6 (Huh7) or N/P 12 (HepG2, HeLa). Luciferase gene expression was determined after a total incubation time of 48 h (n=3; mean +SD). **A)** Ligand titration. Comparison of luciferase gene expression of unmodified polyplexes (**1463**, grey), with pre-functionalized polyplexes with PEG_{24}-DBCO (shielded, dark blue) or $(GalNAc)_3$-PEG_{24}-DBCO (targeted, light blue) at different functionalization degrees (FDs; 25%, 50%, and 100%). LPEI polyplexes (N/P 6) served as positive control. **B)** Kinetics of transfection. Unmodified polyplexes (grey), shielded (blue) or targeted (orange) polyplexes, generated by pre-functionalization with either PEG_{24}-DBCO or $(GalNAc)_3$-PEG_{24}-DBCO aiming for 50% FD, were transfected to HepG2 (10,000 cells per well), Huh7 and HeLa cells (each 8,000 cells per well). Cells were incubated with polyplexes for 45 min, 4 h, or 48 h before renewal of medium. Luciferase gene expression was determined after a total incubation time of 48 h. **C)** Competition assay with asialofetuin (ASF). Polyplexes were pre-functionalized to 50% FD and transfected to HepG2, Huh7, and HeLa cells in presence of 5 mg/mL ASF. Luciferase gene expression was determined 48 h after transfection. **D)** Competition assay combined with short time incubation. Transfection of polyplexes (pre-shielded or pre-targeted, both 50% FD) compared to unmodified polyplexes in Huh7 cells in presence of ASF. Renewal of medium at 45 min after transfection and total incubation time of 48 h before the read-out.

Significant differences: * $p \leq 0.05$; ** $p \leq 0.01$ (unpaired Student's two-tailed t-test with Welch's correction; GraphPad Prism™ 9.5.1).

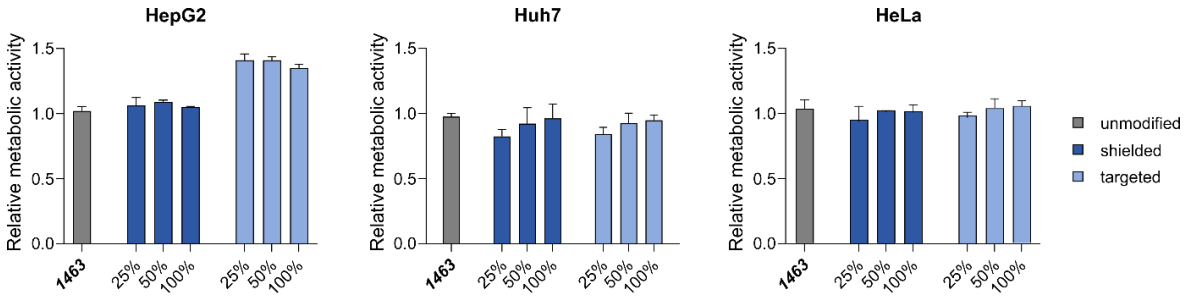

Figure 3.14. Metabolic activity of cells transfected with ASGPR-targeted polyplexes compared to shielded and unmodified ***1463*** pDNA polyplexes. The polyplexes were formed at a pCMVLuc concentration of 200 ng/well. N/P 12 was used for transfections in HepG2 and HeLa cells, and N/P 6 for Huh7 cells (n=3, mean + SD). OAAs were pre-modified with $(GalNAc)_3$-PEG_{24}-DBCO (targeted, light blue) or PEG_{24}-DBCO (shielded, dark blue) at different functionalization degrees (25%, 50%, and 100%). Relative metabolic activity was measured 48 h after transfection via an MTT assay and normalized to HBG-treated control cells.

Ligand titration. In a first screening, the transfection efficacy (**Figure 3.13 A**) and cytotoxicity (**Figure 3.14**) of unmodified, shielded and GalNAc-targeted polyplexes with different ligand densities (FDs of 25, 50, and 100%) were evaluated on two ASGPR-expressing cell lines (HepG2(478-480) and Huh7(480)) as well as on HeLa cells, which lack the receptor.(481) The ASGPR receptor status of HepG2, Huh7, and HeLa cells was examined and verified via flow cytometric analysis after receptor staining (**Figure 3.15**). None of the formulations had a negative influence on the metabolic activity of the cells. As observed before, PEGylation led to decreased transfection efficacy at higher FDs (50%, 100%). In contrast, the targeted polyplexes showed transfection efficacies on the same level as the unmodified control, with a slight reduction for highly functionalized GalNAc polyplexes (FD of 100%). This might be due to the higher PEG content, which in turn means better surface shielding, as indicated by the almost neutral zeta potential (**Figure 3.10 C**), resulting in less interaction with cell membranes and less cellular internalization. Since relatively high RLU values (in the same range as unmodified polyplexes) were observed for both ASGPR-positive (HepG2, Huh7) and -negative cells (HeLa), the high transfection efficacy of the targeted polyplexes might not only be a result of ligand-receptor interaction. The positive surface charge of the polyplexes and free cationic carriers might promote unspecific endocytosis due to enhanced interaction with negatively charged cell membranes, especially at longer incubation times such as the applied 48 h. Similar observations were also made by Reineke and colleagues with their GalNAc-based diblock polymers.(444) Further experiments investigating shorter incubation times and receptor competition were performed (**Figure 3.13 B-D**) to explore the involvement of ASGPR in polyplex delivery of GalNAc-targeted polyplexes in more detail.

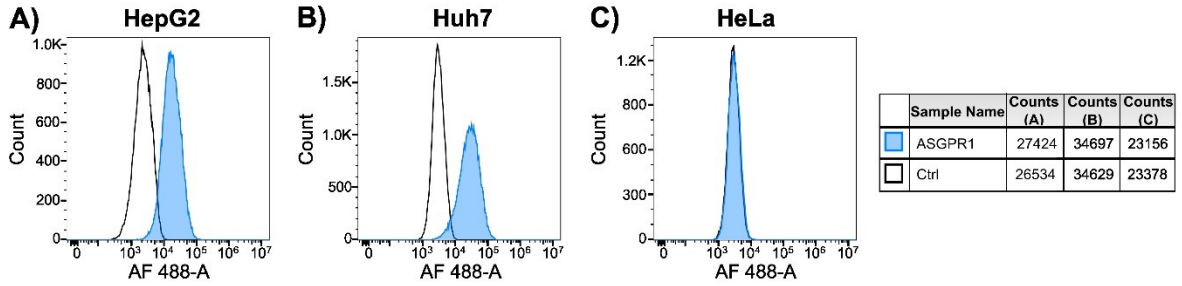

Figure 3.15. Receptor staining of tumor cells. ASGPR expression levels determined via flow cytometry after staining of HepG2 (A), Huh7 (B), and HeLa cells (C) with primary antibody (mouse anti-human ASGPR1 (8D7) monoclonal antibody, blue) in comparison to control (Ctrl, negative control mouse IgG1, white) and detection via secondary antibody [Alexa Fluor 488 (AF 488) goat anti-mouse IgG1 (H+L)]. This experiment was kindly performed by Dr. Simone Berger and Miriam Höhn (Pharmaceutical Biotechnology, LMU Munich)

Kinetics of transfection (**Figure 3.13 B**)**.** Targeting is assumed to mediate enhanced and faster cellular uptake through ligand-receptor interactions and receptor-mediated endocytosis. Thus, gene transfer activity can be achieved even after shorter incubation on the cells. Therefore, targeted vs. shielded polyplexes, both at a FD of 50%, as well as unmodified polyplexes were used for transfection and incubated with the cells for 45 min, 4 h, and 48 h, respectively. As the process of luciferase gene expression by the cells demands more time, the total incubation time was kept at 48 h in all cases. On ASGPR-expressing cell lines (HepG2, Huh7), a significantly higher transfection efficacy of the targeted polyplexes compared to PEGylated polyplexes and unmodified control was observed for short polyplex incubation (45 min), as the GalNAc-functionalized polyplexes benefit from receptor-mediated endocytosis, showing significantly increased RLU values compared to unmodified (**, $p = 0.0082$) and shielded polyplexes (**, $p = 0.0099$). At the incubation time of 4 h, transfection of unmodified and targeted polyplexes reached the same level, which was maintained also for the incubation time of 48 h. The gene transfer activity of the PEGylated particles remained low in HepG2 cells over all tested time points but increased from 45 min to 48 h in Huh7 cells, reaching comparable levels as unmodified and targeted polyplexes. On ASGPR-negative HeLa cells, however, the transfection efficacy of all three formulations was low after 45 min, and steadily increased over time for unmodified and targeted polyplexes to the same extent yet remained low for PEGylated polyplexes over all tested time points. Altogether, the kinetic studies suggest an advantage of the targeting ligand on enhanced cellular internalization and improved transfection efficiency already after short incubation times.

Competition assay. In order to confirm the participation of ASGPR in the internalization process of GalNAc-functionalized polyplexes, a competition assay (**Figure 3.13 C**) was performed using asialofetuin (ASF), a natural ligand of ASGPR, as competitor.(475) The cells were treated with ASF-containing medium (5 mg/mL) 15 min prior to transfection to block the receptor. Afterwards, cells were transfected with polyplexes formed at N/P 12 for HepG2 and HeLa cells, and N/P 6 for Huh7 cells, with 50% FD for shielded and targeted polyplexes and

incubated in the presence of ASF for a total incubation time of 48 h. For ASGPR-expressing HepG2 cells, the transfection efficacy of the targeted polyplexes was significantly reduced in presence of ASF (**, p = 0.0023), whereas for control polyplexes (unmodified and PEGylated) no considerable change in gene expression was observed. In the case of ASGPR-negative HeLa cells, ASF competition had, as expected, no influence on the transfection efficiency of any formulation. Surprisingly, this was also the case for ASGPR-positive Huh7 cells. Remaining gene transfer activity of targeted polyplexes despite ASF competition may be attributed to internalization via unspecific endocytosis pathways or insufficient blocking of the receptors over time. To investigate this possible time effect, the competition assay was repeated for Huh7 cells but polyplex incubation time was reduced to 45 min. After a total incubation time of 48 h, the cells were analyzed regarding their luciferase activity, revealing that the presence of ASF strongly decreased the transfection efficacy of the targeted polyplexes, especially for FDs of 25% (10-fold lower RLU values) and 50% (20-fold lower RLU values), while no differences of the unmodified and PEGylated polyplexes were observed (**Figure 3.13 D**). For a FD of 100%, presence of ASF reduced transfection efficiency by around 2-fold only, which might be attributed to the higher PEG content and thus overall less uptake after the short polyplex incubation time of 45 min. Altogether, these findings support the ASGPR targeting ability of the GalNAc-functionalized polyplexes.

3.4.3.2 Mannose-receptor-targeted polyplexes

Synthesis of mannose-ligand Gly-Ser(Man)-PEG$_{24}$-DBCO

To obtain improved and directed gene transfer to immune cells, the 4-arm polyplexes were functionalized with a novel mannose ligand to target mannose-specific receptors expressed on dendritic cells and macrophages. The two mannose-recognizing receptors CD206 (Mannose receptor) and CD209 (DC-SIGN, dendritic cell-specific intercellular adhesion molecule-3-grabbing non-integrin) are of particular interest for delivery of nucleic acids for tumor immunotherapy(482-484) or vaccination.(129, 137) CD206 is known to bind end-standing mannose units or dimannoside clusters,(128, 453, 485) whereas CD209 displays high affinity towards mannose-rich glycol-conjugates and branched mannoside structures.(486, 487) Crystal structure analyses revealed a particularly high affinity of a trimannose core structure (Man*α*1-3[Man*α*1-6]Man*α*) towards CD209,(488, 489) and multiple trimannose molecules on the nanoparticle surface turned out to be advantageous.(453, 488, 490)

Since spatial arrangement of mannose residues is subordinate to high mannose densities for high affinity towards mannose receptors, a novel mannose ligand was synthesized containing the carbohydrate motif, a PEG$_{24}$ shielding domain and a DBCO unit to enable the click reaction to azido-OAAs (for the description of the experimental procedure see chapter 3.3.3.4). For introducing the mannose motif to the ligand via Fmoc-based SPPS, a mannosylated serine

building block was developed in a two-step synthesis (**Figure 3.16**); identity and purity were confirmed via ESI-MS and ^{1}H-NMR (for spectra, see Appendix, 6.1.3.2). The final ligand was synthesized on a glycine-loaded, base-labile Tentagel HMBA (4-(hydroxymethyl)benzoic acid) resin. Using this synthesis strategy, the stability of the acetal connection between serine and mannose during the reaction steps could be guaranteed. In addition, the reaction process was shortened by one step, as saponification of acetyl protecting groups occurred *in situ* during the cleavage (**Figure 3.16**). The final ligand Gly-Ser(Man)-PEG$_{24}$-DBCO was characterized via MALDI-TOF MS (for the corresponding mass spectrum see Appendix, 6.1.3.2).

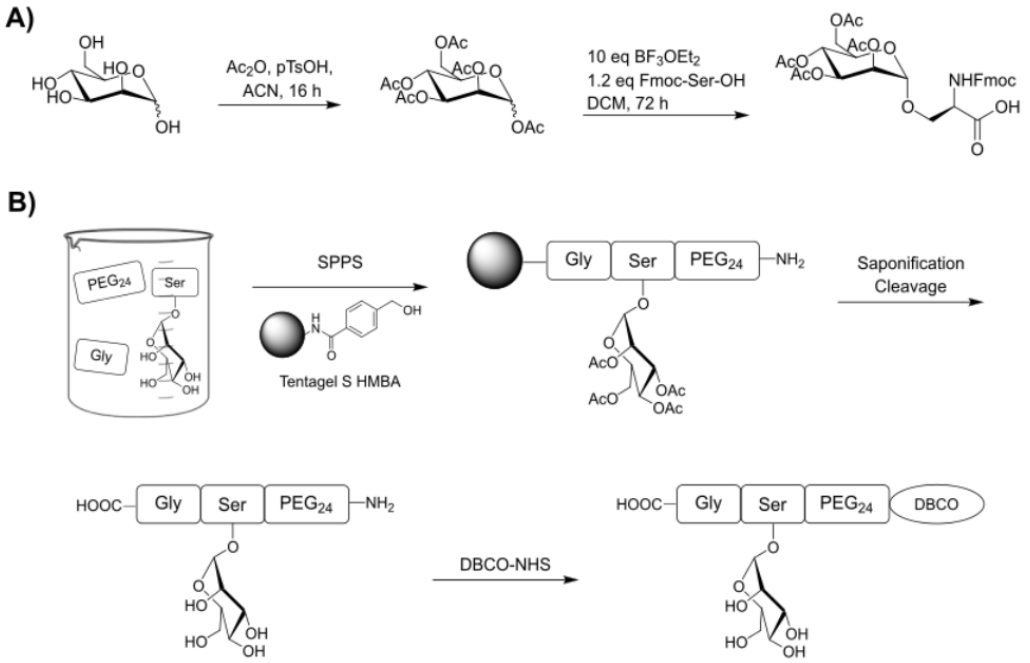

Figure 3.16. Synthesis scheme of Gly-Ser(Man)-PEG$_{24}$-DBCO ligand. A) Synthesis scheme for mannosylated serine building block Fmoc-Ser(O-α-Man(Ac)$_4$)-OH in a two-step reaction. B) Synthesis scheme for assembly of the ligand using SPPS and subsequent introduction of DBCO. The synthesis of Gly-Ser(Man)-PEG$_{24}$-DBCO is described in chapter 3.3.3.4.

Evaluation of mannosylated 4-arm polyplexes

The functionality of the novel mannose ligand Gly-Ser(Man)-PEG$_{24}$-DBCO was evaluated in dendritic cell (DC)-like DC2.4 cells as a proof-of-concept for active mannose receptor targeting. For this purpose, pDNA polyplexes formed with 4-arm carrier ***1463*** at an N/P ratio of 6 were modified with the mannose ligand or PEG$_{24}$ via the pre-click strategy. ***1463*** was selected based on a pre-screen in DC2.4 cells (**Figure 3.17**). Here, ***1463*** significantly outperformed (20- to 30-fold higher RLU values) the positive control LPEI and 4-arm carrier ***1494***, which demonstrated good transfection efficacies in tumor cells.

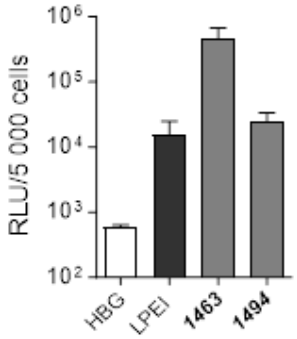

Figure 3.17. Transfection efficiency of 4-arm carriers ***1463*** and ***1494*** in the DC-like cell line DC2.4. Gene transfer activity was determined via luciferase gene expression assay (*n*=3; mean + SD) at 24 h after transfection with polyplexes formed at an N/P ratio of 6 and at a pFscnLuc concentration of 500 ng/well in comparison to LPEI polyplexes (N/P 6). The transfection and FACS experiment were conducted by Dr. Simone Berger (Pharmaceutical Biotechnology, LMU Munich).
Note: Instead of pCMVLuc, pFscnLuc was used in this experiment, which is a plasmid encoding *Photinus pyralis* firefly luciferase under the control of an optimized derivate of the human *fascin1* gene promoter, by this allowing DC-focused transcriptional targeting.(456)

Physicochemical characterization

First, the physicochemical properties of ***1463*** pDNA polyplexes, either unmodified, shielded (PEG_{24}-DBCO) or targeted (Gly-Ser(Man)-PEG_{24}-DBCO), were characterized. The polyplex preparation differed slightly from that used in the previous sections. To stress this, the formulations were termed differently. Pre-functionalization was performed with different amounts of shielding or targeting agent, respectively. Co-mixing of pre-clicked and unmodified carrier at different ratios was applied to obtain various FDs, ranging from *"1eq–50%"* over *"1eq–100%"* and *"4eq–50%"* to *"4eq–100%"* (*i.e.,* increasing FD). To delineate, "*1eq*" means that statistically one of the four azido groups of the 4-arm carrier ***1463*** was pre-clicked; "*4eq*" that all four azido groups were functionalized. "*50%*" means that 50% of pre-clicked and 50% of unmodified 4-arm carrier were used for polyplex formation; "*100%*" that only functionalized 4-arm carrier was used. All in all, *"1eq–50%"* corresponds to approx. 12.5% modified azides in the final polyplex formulation (*i.e.*, FD 12.5%); *"1eq–100%"* to FD 25%; *"4eq–50%"* to FD 50%; and *"4eq–100%"* to FD 100%. Only the *"4eq–100%"* polyplexes were formed in the same way as the FD 100% formulations of the previous sections.

Table 3.2. DLS and ELS measurements of 1463 pDNA polyplexes; unmodified, shielded or targeted.

		Z-average by intensity [nm]		Number mean [nm]		PDI		Zeta potential [mV]	
		mean	SD	mean	SD	mean	SD	mean	SD
unmodified		129.3	1.2	104.9	3.5	0.051	0.020	13.1	1.0
shielded	*1eq–50%*	1232.0	45.3	886.3	174.4	0.327	0.078	1.7	0.2
	1eq–100%	1476.0	52.1	1071.9	82.7	0.260	0.015	-0.5	0.1
	4eq–50%	1565.7	18.8	1290.7	339.2	0.242	0.071	-1.7	0.1
	4eq–100%	782.0	26.0	502.9	93.3	0.357	0.066	-3.3	0.2
targeted	*1eq–50%*	141.4	0.1	116.2	6.7	0.044	0.033	9.7	0.2
	1eq–100%	151.5	2.5	124.8	9.0	0.052	0.038	7.7	0.3
	4eq–50%	246.2	6.1	214.6	5.7	0.073	0.024	5.8	0.5
	4eq–100%	580.3	9.8	413.5	121.9	0.274	0.014	2.4	0.2

DLS and ELS measurements (*n*=3, mean ± SD) of pDNA polyplexes formed with 4-arm carrier ***1463*** in HBG buffer at an N/P ratio of 6 and at a pCMVLuc concentration of 25 µg/mL. Unmodified polyplexes in comparison to functionalized polyplexes, either pre-clicked with PEG_{24}-DBCO (shielded) or with Gly-Ser(Man)-PEG_{24}-DBCO (targeted) at indicated ratios, respectively. The DLS and ELS measurements were performed by Dr. Simone Berger (Pharmaceutical Biotechnology, LMU Munich).
Note: "*1eq*" means that statistically one of the four azido groups of 4-arm carrier ***1463*** is pre-clicked; "*4eq*" that all four azido groups are pre-clicked. "*50%*" means that 50% pre-clicked and 50% unmodified 4-arm carrier are used for polyplex formation; "100%" that only pre-clicked 4-arm carrier is used. All in all, *"1eq–50%"* corresponds to ~ 12.5% modified azides in the final polyplex formulation; *"1eq–100%"* to ~ 25%; *"4eq–50%"* to ~ 50%; and *"4eq–100%"* to ~ 100%.

DLS and ELS measurements revealed defined particles in all cases (**Table 3.2**). However, PEGylation mediated an up to approx. 10-fold size increase compared to unmodified polyplexes (780-1565 nm vs. 130 nm) but also led to strongly reduced zeta potentials of around 0 mV. In the case of targeted polyplexes, z-average diameters increased with increasing ligand content up to approx. 580 nm for the *"4eq–100%"* formulation. The surface charge decreased from 13 mV of unmodified polyplexes to almost neutrality, most likely due to the increasing amount of PEGylation, as the mannose ligand contains a PEG_{24} chain as well. At first glance, it was surprising that PEGylated polyplexes showed lower zeta potentials than their targeted counterparts, although both shielding agent and mannose ligand contained the same amount of PEG as well as a C-terminal carboxyl group (**Figure 3.16**). The different zeta potentials might mostly likely be attributed to the different polyplex stability, as indicated by the different sizes of shielded and targeted particles. In targeted polyplexes, sterical hindrance of mannose rings might reduce aggregation tendency, resulting in better polyplex assembly and smaller particles. At higher PEG content, this effect was less pronounced most probably due to the increasing destabilizing effects of PEG, leading to bigger, less compacted particles and lower zeta potentials. Noteworthy, the completely modified formulations (*i.e.*, *"4eq–100%")* of shielded and targeted polyplexes were most comparable regarding size and zeta potential.

Thus, screening in DC2.4 cells was done with these two (in the following referred to “shielded” and “targeted” polyplexes) in comparison to unmodified polyplexes.

Biological evaluation

DC2.4 cells were considered as suitable DC model cell line for mannose receptor targeting, as they express the mannose recognizing receptors CD206 (491) (macrophage mannose receptor) and CD209,(114, 492) which was confirmed via receptor staining of DC2.4 cells (**Figure 3.18**). As outlined above, high mannose densities on the nanoparticle surface are preferable for effective mannose receptor targeting.(486, 487) Therefore, it was assumed that the targeted *“4eq–100%”* polyplexes of the current study might be also recognized by both CD206 and CD209, since they contain multiple mannose moieties in terminal position, which may also form clusters due to the carrier architecture.

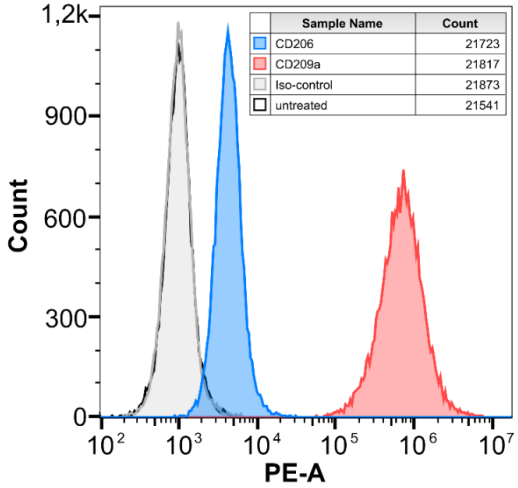

Figure 3.18. Receptor staining of DC2.4 cells. Receptor expression levels determined via flow cytometry after staining of the DC-like cell line DC2.4 with mannose receptor antibodies (anti-CD206-PE, blue; anti-CD209a-PE, red) in comparison to controls (isotype control antibody, grey; untreated control cells, white). This experiment was kindly performed by Dr. Simone Berger and Miriam Höhn (Pharmaceutical Biotechnology, LMU Munich).

Cellular uptake in DC2.4 cells, as determined by monitoring of Cy5-labeled pDNA via flow cytometry (**Figure 3.19 A**), was strongly reduced in the case of PEG shielding by more than 90% compared to unmodified polyplexes. Incorporation of mannose ligands restored and even improved cellular internalization by 1.5-fold over unmodified polyplexes. Similar results were obtained on the luciferase expression level (**Figure 3.19 B**). Transfection was completely hindered by PEGylation (RLU values at HBG buffer level) and targeting enhanced the gene-transfer activity, leading to 6-fold higher RLU values than unmodified polyplexes. All tested formulations were well tolerated by the DC2.4 cells (metabolic activity ≥70%, ISO-10993-5-2009; **Figure 3.19 C**).

The obtained transfection results so far demonstrated high activity of targeted polyplexes, suggesting a targeting effect mediated by the mannose ligand. However, DCs as antigen-

presenting cells are very efficient in internalization of particles of a broad size range by various uptake mechanisms.(493-495) Particles larger than 500 nm, for instance, can be taken up by phagocytosis and macropinocytosis. Thus, it is conceivable that the enhanced efficiency might also be mediated by size effects, as the tested targeted polyplexes exhibited a z-average of around 600 nm (**Table 3.2**). However, the shielded polyplexes which were at the same size range as the targeted polyplexes (**Table 3.2**) were completely ineffective for gene delivery. The zeta potential was comparable for both formulations as well (around 0 mV), ruling out benefits of charge-dependent uptake. Together, this suggests that the enhanced transfection efficiency observed for the targeted particles is a result of receptor-mediated uptake.

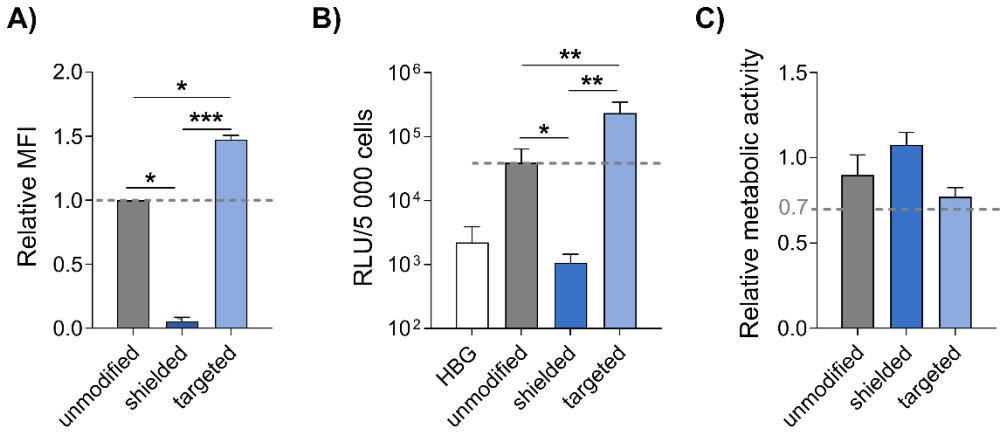

Figure 3.19. Gene-transfer performance of ***1463*** pDNA polyplexes in DC2.4 cells at 24 h after transfection. Comparison of unmodified vs. functionalized polyplexes, either "4eq–100%" pre-clicked with PEG_{24}-DBCO (shielded) or with Gly-Ser(Man)-PEG_{24}-DBCO (targeted), respectively. A) Cellular uptake, as determined via flow cytometry (n=6; mean + SD). Polyplexes were formed at an N/P ratio of 6 and at a pCMVLuc concentration of 200 ng (20% Cy5-labeled pDNA) per well (5000 cells). Data presented as mean fluorescence intensity (MFI) in Cy5-positive cells (Cy5-A) normalized to unmodified polyplexes. B) Transfection efficiency, as determined via luciferase gene expression assay (n=6; mean + SD); and C) metabolic activity in relation to HBG-treated control cells, as determined via CellTiter-Glo assay (n=3; mean + SD). Polyplexes were formed at an N/P ratio of 6 and at a pCMVLuc concentration of 500 ng/well (5000 cells). The presented experiments were performed by Dr. Simone Berger (Pharmaceutical Biotechnology, LMU Munich).
Significant differences: ns $p > 0.05$; * $p \leq 0.05$; ** $p \leq 0.01$; *** $p \leq 0.001$ (unpaired *t*-test with Welch's correction; GraphPad Prism™ 9.5.1). ns, not significant.

To investigate the targeting capability in more detail, transfections were performed in the presence of mannan, which acts as a competitor to the mannose ligand as it is recognized by mannose receptors as well.(468, 496) Mannan competition, however, showed no significantly relevant impact on the uptake in DC2.4 cells for any tested formulation (**Figure 3.20 A**). For the targeted polyplexes, a slightly reduced uptake (by ~15%) in the presence of the competitor mannan was observed, whereas for unmodified and shielded polyplexes, the presence of mannan even slightly improved uptake (by approx. 10% for shielded, and by approx. 25% for unmodified polyplexes). The most reasonable explanation might be that many different mechanisms are involved in the uptake process into DCs, enabling sufficient cellular internalization and gene transfer.(493-495, 497) Especially after longer incubation times, it is

likely that the particles are internalized not only by receptor-mediated endocytosis but also by several other routes.

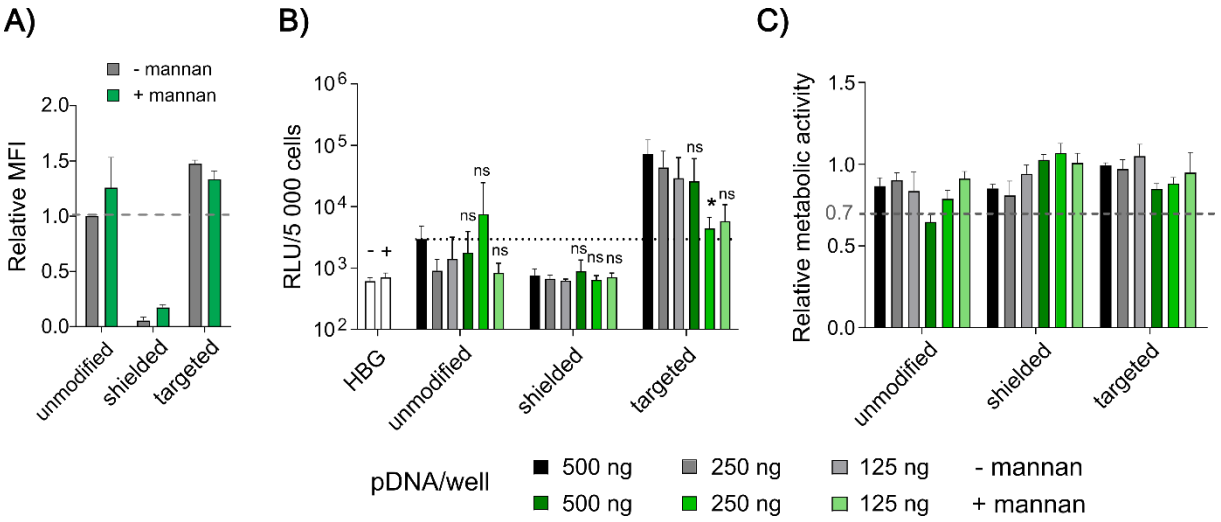

Figure 3.20. Gene-transfer performance of ***1463*** pDNA polyplexes in DC2.4 cells in the presence of competitor mannan (2 mg/mL) at 24 h after transfection. A) Cellular uptake, as determined via flow cytometry (n=6; mean + SD). Polyplexes were formed at an N/P ratio of 6 and at a pCMVLuc concentration of 200 ng (20% Cy5-labeled pDNA) per well (5000 cells). Data presented as mean fluorescence intensity (MFI) in Cy5-positive cells in relation to unmodified polyplexes. B) and C) Polyplexes were formed at an N/P ratio of 6 with a pCMVLuc concentration of 25 µg/mL and applied at different pCMVLuc concentrations (i.e., 500, 250, and 125 ng/well) by applying different polyplex volumes (5, 10, and 20 µL/well). HBG controls, "-" indicates transfection without mannan; "+" indicates transfection in presence of mannan. Comparison of unmodified vs. functionalized polyplexes, either "*4eq–100%*" pre-clicked with PEG_{24}-DBCO (shielded) or with Gly-Ser(Man)-PEG_{24}-DBCO (targeted), respectively. B) Transfection efficiency, as determined via luciferase gene expression assay (n=6; mean + SD). C) Relative metabolic activity of DC2.4 cells at 24 h after transfection of ***1463*** pDNA polyplexes in the presence of competitor mannan (2 mg/mL). Metabolic activity in relation to HBG-treated control cells, as determined via CellTiter-Glo assay (*n*=3; mean + SD) at 24 h after transfection. The experiments presented in this figure were performed by Dr. Simone Berger (Pharmaceutical Biotechnology, LMU Munich).
Significant differences: ns $p > 0.05$; * $p \leq 0.05$; ** $p \leq 0.01$; *** $p \leq 0.001$ (unpaired *t*-test with Welch's correction; GraphPad Prism™ 9.5.1). ns, not significant.

Nevertheless, in the luciferase gene expression assay, a minor mannose targeting effect could be observed (**Figure 3.20 B**). In the case of the targeted polyplexes, especially at lower pDNA doses, a strongly reduced transfection efficiency could be observed in presence of mannan (up to 10-fold decreased RLU values). In contrast, mannan had no influence on the performance of unmodified and PEGylated polyplexes, supporting the involvement of mannose receptors in the uptake process of the targeted polyplexes. In the case of PEG shielding, there was again no transfection efficiency, neither with nor without mannan. For all formulations, no considerable toxicity was observed (metabolic activity ≥70%, ISO-10993-5-2009; **Figure 3.20 C**).

Altogether, the obtained results indicate the involvement of mannose-receptor in the uptake of polyplexes functionalized with the novel mannose ligand. In addition to the effects of active targeting of mannose receptors on the surface of dendritic cells, size effects of polyplexes may

play a supporting role in the cellular internalization process. Nevertheless, the targeted polyplexes proved to be advantageous formulations promoting enhanced transfection efficiency compared to unmodified and shielded polyplexes.

3.5 Conclusion

The azido derivative ***1463*** of former published 4-arm OAA ***573***(71) proved to be an effective pDNA carrier. Further modifications by incorporation of tyrosines, tryptophans, or arginines provided no significant benefit on gene transfer activity. Introduction of shielding and targeting agents in the 4-arm pDNA polyplexes was achieved by conjugation via SPAAC, enabling a modular design, and thereby allowing high flexibility for variations and access to advanced ligand classes. In this work, the pre-functionalization approach was more favorable than post-functionalization in terms of nanoparticle formation and stability, shielding efficiency, and biological functionality. The PEG length as well as the functionalization degree were of great importance for well shielded polyplexes; in the case of ***1463*** nanoparticles, PEG_{24} and higher FDs (50-100%) were advantageous. Carbohydrate-based ligands for ASPGR and mannose receptor targeting demonstrated effectiveness in first proof-of-concept studies. However, the effects were not that clear-cut. The ligand-functionalized particles restored transfection efficacy compared to PEGylated polyplexes, and the participation of receptor-mediated endocytosis was indicated by competition assays and kinetic experiments. However, these observations were highly dependent on several parameters such as incubation times and cell lines which highlights the coexistence of multiple processes of polyplex uptake (esp. in DCs), including unspecific uptake alongside receptor-mediated endocytosis. Therefore, further improvements are recommended by careful ligand design (multivalency, spacers, architecture, alternatives to PEG, etc.), and/or optimized nanoparticles (choice of carrier and formulation such as polyplexes or lipoplexes/lipid nanoparticles, N/P ratio, FD, etc.). In addition to their targeting effects, carbohydrates can be used to enhance colloidal stability and biocompatibility of cationic polymers, as shown e.g., in numerous works on glycopolymers by Reineke and co-workers.(414, 498-501) Carbohydrates can also function simultaneously as both shielding and targeting moieties. Hyaluronic acid, for instance, shields nanoparticles by anionic coating and addresses CD44-positive cells such as endothelial and certain tumor cells.(94, 502-504) Altogether, this makes such carbohydrate-containing nanoparticles interesting nucleic acid delivery systems for future *ex vivo* or *in vivo* therapeutic applications, for example in directed nucleic acid delivery to antigen-presenting and immune cells, localized vaccinations, or systemic cancer immunotherapies.

Acknowledgements

We thank Teoman Benli-Hoppe and Urban Mate (both Department of Pharmacy, LMU Munich) for help in the synthesis of the 4-arm OAA library, as well as Wolfgang Rödl and Olga Brück (both Department of Pharmacy, LMU Munich) for technical and organizational support. Moreover, we acknowledge Dr. Céline Douat and Prof. Ivan Huc (both Department of Pharmacy, LMU Munich) for support in LCMS measurements, Melina Grau and Tobias Burghardt (both Department of Pharmacy, LMU Munich) for MALDI-TOF measurements, as well as Dr. Werner Spahl and colleagues (Department of Chemistry, LMU Munich) for ESI-MS measurements. The research was supported by the German Research Foundation (DFG) SFB1032 (project-ID 201269156) sub-project B4 and SFB1066 sub-project B5 (both to E. Wagner) as well as by a Faculty Study and Research grant of the Davidson College, North Carolina, USA (to N.L. Snyder). N.L. Fendler would like to thank the Beckman Foundation for their support through the Beckman Scholars Program. N.L. Snyder and L. Hartmann would also like to thank the National Science Foundation (NSF-IRES Award # 1854028) for partial support for this project. Illustrations were created with BioRender.com (Toronto, ON, Canada).

4 Modulating Efficacy and Cytotoxicity of Lipoamino Fatty Acid Nucleic Acid Carriers Using Disulfide or Hydrophobic Spacers

Ricarda C. Steffens[1,2], Sophie M. Thalmayr[1,3], Eric Weidinger[1], Johanna Seidl[1,3], Paul Folda[1], Miriam Höhn[1] and Ernst Wagner[1,2,3,]*

[1]Pharmaceutical Biotechnology, Department of Pharmacy, Ludwig-Maximilians-Universität (LMU) Munich, Butenandtstr. 5-13, 81377 Munich, Germany.

[2] Center for NanoScience (CeNS), LMU Munich, 80799 Munich, Germany

[3] CNATM – Cluster for Nucleic Acid Therapeutics Munich, Germany

* Correspondence: ernst.wagner@lmu.de

This chapter is adapted from a research paper published in Nanoscale, 2024 July 05, Volume 16, 13988-14005. DOI: 10.1039/d4nr01357c.(505)

Author contributions

Conceptualization, RCS and EWa; methodology, RCS, ST, EWe, MH; investigation, RCS, ST, EWe, JS, PF, MH, EWa; data curation, RCS, ST, EWe, EWa; formal analysis, RCS, ST, EWe; validation, RCS, ST, EWe, MH, EWa; visualization, RCS, ST, EWe, MH, EWa; writing – original draft, RCS, EWa; writing – review and editing, RCS, ST, EWe, EWa; funding acquisition, project administration, resources, supervision, EWa. All authors have read and agreed to the submitted version of the manuscript.

4.1 Abstract

Double pH-responsive xenopeptides comprising polar ionizable succinoyl tetraethylene pentamine (Stp) motifs and lipophilic ionizable lipoamino fatty acids (LAFs) were recently found to efficiently transfect mRNA and pDNA at low doses. However, potency was often accompanied with cytotoxicity at higher doses. Insertion of bioreducible disulfide building blocks (ssbb) or non-reducible hydrophobic spacers between polar and apolar ionizable domains of LAF–Stp carriers should mitigate toxicity of xenopeptides. Carriers showed stable nucleic acid complexation and endosomal pH-dependent lytic activities, both of which were abolished after reductive cleavage of ssbb-containing carriers. For pDNA, U-shaped carriers with one Stp and two LAF units or bundle carriers with two Stps and four LAFs displayed highest potency. For mRNA, best transfection was achieved with bundle carriers with one Stp and four LAFs. Both the ssbb and hydrophobic spacer containing analogs displayed improved metabolic activity, reduced membrane damage, and improved cell growth. The ssbb carriers were most beneficial regarding living cell count and low apoptosis rates. Mechanistically, inserted spacers decelerated the transfection kinetics and altered the requirement of endosomal protonation. Overall, mRNA and pDNA carriers with improved biocompatibility have been designed, with their high potency illustrated in transfection of various cell lines including low passage number colon carcinoma cells.

Graphical Abstract

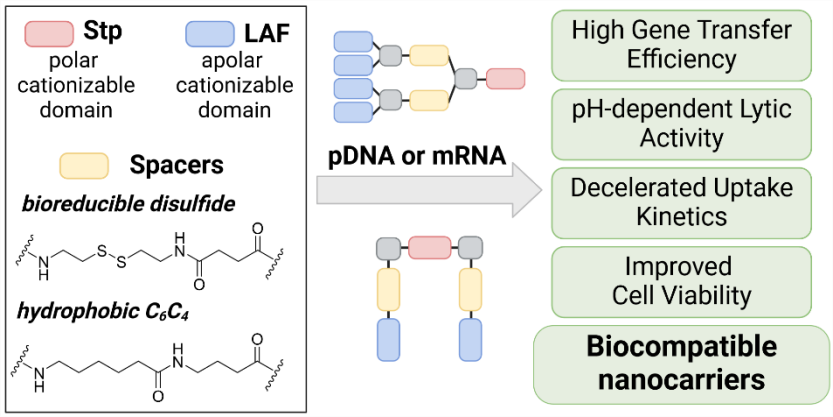

4.2 Introduction

Nucleic acid therapeutics present a novel frontier in medical science, offering immense potential for treating a wide range of diseases. Beyond their proven efficacy in vaccine development, nucleic acid delivery is a promising approach to cancer immunotherapy, gene and/or protein displacement therapies. Synthetic formulations including polyplexes, lipoplexes and lipid nanoparticles (LNPs) hold great potential for delivery of nucleic acids like DNA, mRNA, siRNA, and Cas9/sgRNA systems.(48, 54, 506, 507) The involved carriers offer

advantages such as relatively facile synthetic accessibility, the potential for precise modulation of nanoparticle features and minimal immunogenicity. However, limitations do exist, such as moderate efficacy requesting administration at very high nanoparticle per cell doses, associated with significant cytotoxicity, and challenges involve careful balancing between particle stability and dynamic nucleic acid release at the right cellular compartment.(508) To improve safety and efficacy of polyplexes for the various nucleic acid cargos, researchers have addressed these issues by continuous optimization of formulations and carrier molecules, e.g. by incorporating biocompatible building blocks.(28, 37, 50, 69, 173, 189, 467, 509-520)

Using a chemical evolution approach(58) based on solid phase assisted xenopeptide synthesis,(56, 61, 71, 521) our group recently developed novel nucleic acid carriers that have proven to be highly effective for delivering a variety of nucleic acid cargos including pDNA and mRNA.(162) These carriers are sequence-defined, double pH-responsive xenopeptides and comprise one or several hydrophilic units of cationizable artificial amino acid Stp (succinoyl tetraethylene pentamine)(61) and lipophilic, cationizable lipoamino fatty acids (LAFs).(162) The Stp units function as polar cationic counterparts to negatively charged nucleic acids, leading to polyplex formation through nucleic acid condensation via electrostatic interaction. The cationizable LAF residues combine advantageous qualities of lipophilic domains, permitting hydrophobic particle stabilization at physiological neutral pH, which is reversible upon protonation at mild acidic endosomal pH, resulting in a strongly enhanced endosomal escape and exceptionally high transfection efficacy. For certain LAF–Stp topologies, mRNA transfection was successful even at ultra-low doses of 3 picograms of mRNA, providing a nanoparticle potency comparable to viral vectors. Additionally, these carriers facilitate remarkable protein expression also in vivo, particularly in the spleen, tumor, lungs, and liver upon intravenous injection of mRNA polyplexes(162) or LNPs(107) in mice. Alongside with favorable efficacy of these novel LAF-carriers, in several cases high potency was observed to correlate with increased cytotoxicity. This can be compensated by application of low dosages,(162) nevertheless raises safety concerns regarding future therapeutic administration. While the superior ability of these nanoparticles to interact with cell membranes is highly desirable for nanoparticle uptake by endocytosis and endosomal escape, prolonged intracellular presence of membrane-active carriers may lead to reduced cell viability. Cytotoxicity induced by cationic polymers or lipids can be attributed to several causes. Carrier molecules and their metabolites may have the potential to cause cellular membrane disruption or nuclear damage, mitochondrial dysfunction, generation of reactive oxygen species (ROS), among other factors. For example, a two-stage cytotoxicity(66, 169) was reported for polyplexes consisting of polyethyleneimine (PEI)(28, 189, 512, 522), a most frequently used gold-standard for nucleic acid delivery. An early phase I toxicity resulting from compromised cellular membrane integrity, and a later phase II cytotoxicity due to a mitochondrial apoptotic

program was reported.(166) Additionally, PEI-based transfection efficiency and cytotoxicity was found to be associated with polymer size and type(173, 189, 517), and with permeabilization of nuclear membranes.(167, 415) Similar observations were made for a series of other cationic carriers; characteristics that favorably enhance intracellular transfer of nucleic acids across membrane barriers are likely to be also associated with increased cytotoxicity due to side effects of membrane disruption. The question has been raised whether the observed correlation of efficacy and cytotoxicity can be uncoupled. In fact, for polymeric cationic carriers it was already demonstrated that efficiency/cytotoxicity ratios can be modulated by either optimizing the size of the polymer(173, 189, 521) or its cationic subunits.(172, 510) For example, separating the efficient but also toxic multi-cationic structure of PEI into several small cationic (oligo)aminoethylene units resulted into highly potent but far less toxic polymers of similar sizes.(510) Molecular reasons are at least twofold; defined small subunits may have inherent favorable efficacy/toxicity properties(172) based on amphiphilicity or pKa profile, as observed and defined in the even-odd rule of oligoethylenimines.(523) Secondly, biodegradable linkages between the oligocationic subunits can be designed, reducing the persistence of polycationic molecules and this leading to favorable cytotoxicity profiles. Esters(467, 514, 515, 524), acetals(518, 525), or disulfides(513, 516, 519) were integrated into synthetic PEI carriers, ‘breaking up the correlation between efficacy and toxicity’.(516) Disulfide linkages have been applied to various other cationic carriers including ionizable lipids.(63, 70, 174, 526-533) Disulfide bonds are stable in the extracellular environment but are subsequently reduced within cells after endosomal release by high concentrations of cytosolic glutathione (GSH), leading to fragmentation of the carriers.(174) Hereby, both release of the nucleic acid cargo from the carrier is facilitated and cytotoxic effect associated with highly lytic properties of the carrier can be minimized.

In our previous work on sequence-defined T-shaped lipo-xenopeptides the introduction of a bioreducible disulfide bond between the cationic polar backbone and the standard, non-ionizable fatty acid domain was advantageous for mRNA and siRNA delivery,(63, 70) reducing cytotoxic effects and enhancing efficacy by solving the balancing act between extracellular polyplex stability and cytosolic nucleic acid release.(67, 70) The precise positioning of the disulfide cleavage site at the desired location was managed by design of a protected cystamine-based disulfide building block (ssbb) for use in solid-phase synthesis.(63)

In the current work, novel LAF carriers with U-shape or bundle topology were modified with bioreducible or non-reducible spacers that are integrated in the oligomer sequence at precise positions based on the rationale of separating cationic and lipophilic domains of the carrier oligomers. By introducing disulfide spacers, we aimed to maintain favorable characteristics of the polyplexes while consequently improving biocompatibility of the carriers after endosomal release. As the introduction of reducible linkers changes the geometry and distances between

lipophilic and hydrophilic subdomains of carriers, we also designed analogous carriers with isosteric hydrophobic nonreducible spacers. In the following we demonstrate the dynamic nucleic acid binding ability of the disulfide- modified carriers and polyplex destabilization as a result of the reductive cytosolic environment. Consequently, bioreducible carriers showed beneficial impact on cell viability while maintaining high nucleic acid transfer activity promoted by LAF carriers. Interestingly, introduction of hydrophobic non-reducible linkers also modulated the transfection/cytotoxicity profile. Altogether this highlights a beneficial influence of altered chemical topology plus optional biodegrading bonds on the biological carrier characteristics.

4.3 Materials and Methods

4.3.1 Materials

8-Aminooctanoic acid, glacial acetic acid, cystamine dihydrochloride, dodecanal, *N,N*-diisopropylethylamine (DIPEA), glutathione reduced (GSH), octanal, potassium permanganate, sodium citrate tribasic dihydrate, sodium cyanoborohydrate (NaBH3CN), succinic anhydride and super-DHB (9:1 mixture of 2,5-dihydrocybenzoic acid and 2-hydroxy-5-methoxybenzoic acid) were obtained from Sigma Aldrich (Munich, Germany). Sodium sulfatewas purchased from ORG Laborchemie (Bunde, Germany) and N-(9H-Fluoren-9-yl-methoxycarbonyloxy)-succinimide (Fmoc-OSu) from Iris Biotech (Marktredwitz, Germany). Acetonitrile, dichloromethane (DCM), dry methanol (MeOH), ethyl acetate (EtOAc), n-heptane, aqueous sodium hydroxide solution (1M) and tetrahydrofuran (THF) were purchased from Thermo Fisher Scientific (Schwerte, Germany). Solid-phase synthesis reactors (polypropylene reactors with polytetrafluoroethylene (PTFE) frits and Luer stopper) were purchased from Multi-SynTech (Witten, Germany). 2-Chlorotrityl chloride resin, dimethylformamide (DMF), piperidine, Fmoc-L-Lysine(Fmoc)-OH, Fmoc-L-Lysine(Dde)-OH, Fmoc-amino butanoic acid and Fmoc-amino hexanoic acid were obtained from Iris Biotech (Marktredwitz, Germany), benzotriazole-1-yl-oxytrispyrrolidino phosphonium hexafluorophosphate (PyBOP), 1-hydroxy-benzotriazole (HOBt), di-tert-butyl dicarbonate (Boc anhydride), hydrazine monohydrate, phenol, potassium cyanide and triisopropylsilane (TIS) from Sigma Aldrich (Munich, Germany). Ninhydrin was purchased from AppliChem (Darmstadt, Germany), pyridine and trifluoro acetic acid from Thermo Fisher Scientific (Schwerte, Germany) and ethanol absolute (EtOH) and aqueous hydrochloride solution (1M) from VWR (Darmstadt, Germany). Deuterated solvents were purchased from Eurisotop (Fluorochem, Hadfield, UK). Plasmid pCMVLuc (encoding Photinus pyralis firefly luciferase under the control of a cytomegalovirus promoter and enhancer) was obtained from Plasmid Factory GmbH (Bielefeld, Germany), CleanCap® Fluc mRNA (5 moU) and CleanCap EGFP mRNA (5moU) from Trilink Biotechnologies (San Diego, CA, USA) and EZ Cap™ Cy5 Firefly Luciferase mRNA (5-moUTP) from ApexBio (Apexbt

Technology LLC, Houston, USA). Agarose BioReagent low EEO, boric acid, bromophenol blue, ethidium bromide (EtBr) (1% solution in H2O), glycerol, RNase-free water, tris(hydroxymethyl) aminomethane hydrochloride (Tris-HCl) and triton X-100 were purchased from Sigma Aldrich (Munich, Germany), 4-(2-hydroxyethyl)-1-piperazineethanesulfonic acid (HEPES) from Biomol (Hamburg, Germany), GelRed (1000x) from VWR (Darmstadt, Germany) and D-(+)-glucose monohydrate and ethylene diaminetetraacetic acid (EDTA) from Merck (Darmstadt, Germany). Quant-iT™ RiboGreen RNA Assay-Kit was obtained from Thermo Fisher Scientific (Schwerte, Germany) and heparin (5000 I.U. mL-1) from B. Braun SE (Melsungen, Germany). Human blood was provided by the hospital of the Ludwig-Maximilians-Universität (Munich, Germany). All cell culture consumables were purchased from Faust Lab Science (Klettgau, Germany). HeLa cells (human adherent cervix carcinoma cell line) were obtained from the German Collection of Microorganisms and Cell Cultures (DSMZ, Braunschweig, Germany), N2a cells (murine neuroblastoma cell line Neuro2a) from the American Type Culture Collection (ATCC, Manassas, VA, USA) and human adherent hepatic carcinoma cell lines Huh7 wild-type from the Japanese Collection of Research Bioresources Cell Bank (Osaka, Japan). Dulbecco's Modified Eagle's medium (DMEM) low glucose, DMEM Ham's F12 medium, RPMI 1640 medium containing L-glutamine and sodium bicarbonate, fetal calf serum (FCS), stable glutamine, penicillin (100 U mL-1) and streptomycin (100 µg mL-1) were purchased from Sigma Aldrich (Munich, Germany) and PAN Biotech (Aidenbach, Germany). Adenosine 5'-triphosphate (ATP) disodium salt trihydrate was purchased from Roche Diagnostics GmbH (Mannheim, Germany), coenzyme A trilithium salt, dithiothreitol, glycylglycine, magnesium chloride ($MgCl_2$), para-formaldehyde and 4',6-diamidine-2'-phenylindole dihydrochloride (DAPI) were obtained from Sigma Aldrich (Munich, Germany). Cell lysis buffer 5x, luciferin sodium salt, CellTiter Glo® Luminescent Cell Viability Assay Kit and CytoTox96® nonradioactive cytotoxicity assay kit (LDH release assay) were purchased from Promega (Mannheim, Germany). Bafilomycin A1 and Collagen A were obtained from Merck KGaA (Darmstadt, Germany). µ-Slides 8 well ibidiTreat were obtained from ibidi GmbH (Gräfelfing, Germany) and TACS Annexin V-FITC Apoptosis Detection Kit from Bio-Techne GmbH (Wiesbaden, Germany).

LPEI 22 kDa and branched succinylated PEI (succPEI) were synthesized as reported previously.(70, 458) Starting materials (poly(2-ethyl-2-oxazoline) for linear PEI and branched PEI 25 kDa for succPEI) were obtained from Sigma Aldrich (Munich, Germany).

The syntheses of the disulfide building block (*N*-Fmoc, *N´*-succinoyl-cystamine, 'ssbb') and the lipoamino fatty acids 8Oc and 12Oc were performed analogously as described in Klein et al(63) and Thalmayr et al.(162) *N*-Fmoc, tri-Boc protected succinoyl tetraethylene pentamine (Stp) was prepared by in house synthesis according to previously published protocols.(61, 162)

4.3.2 Analytical methods

4.3.2.1 NMR spectroscopy

^{1}H-NMR spectra were recorded by using a Bruker Avance III HD 400 (400 MHz). Signals were calibrated to the residual, non-deuterated signals of the used solvent as an internal standard ($CDCl_3$ 7.26 ppm; methanol-d_4 4.87 (s) and 3.31 (p)). Chemical shifts (δ) were reported in parts per million (ppm). The spectra were analyzed by MestreNova (MestReLab Research x64, Version 10.0). Integration was performed manually. Multiplicities were abbreviated as follows: s, singlet; d, doublet; t, triplet; m, multiplet.

4.3.2.2 ESI-MS

ESI-MS was performed using a Thermo Scientific LTQ FT Ultra Fourier transform ion cyclotron and an IonMax source. Data is either shown as $[M+X]^z$ after positive ionization or $[M-X]^{-z}$ after negative ionization. Samples were kindly processed by Dr. Werner Spahl and colleagues from the analytical core facility at the Department of Chemistry, LMU Munich.

4.3.2.3 MALDI-TOF

MALDI-TOF mass spectrometry was conducted using an Autoflex II mass spectrometer (Bruker Daltonics, Germany). As matrix, a solution of 10 mg mL^{-1} super-DHB (9/1 (w/w) mixture of 2,5-dihydroxybenzoic acid and 2-hydroxy-5-methoxybenzoic acid) in 69.93/30/0.07 (v/v/v) H_2O/ACN/TFA was used. 1 µL of matrix solution was spotted on a MTP AnchorChip (Bruker Daltonics, Germany). Subsequently, 1 µL of sample solution dissolved in H_2O at a concentration of 1 mg mL^{-1}, was added onto the matrix, co-crystallized and analyzed. Spectra were recorded in positive ion mode. For MALDI-TOF analysis under reductive stress, the carrier was diluted with H_2O to a concentration of 1 mg mL^{-1} . 50 mM glutathione (GSH) stock solution was prepared in HBG, and pH was adjusted to 7.4 by addition of 1 M $NaOH_{aq}$. GSH stock solution was added to the oligomer solution to reach a final GSH concentration of 10 mM. The solution was incubated for 90 min at 37°C while shaking at 500 rpm. Afterwards, the sample was prepared and analyzed as described above.

4.3.3 Building block syntheses

4.3.3.1 Disulfide building block 1-(9H-fluoren-9-yl)-3,12-dioxo-2-oxa-7,8-dithia-4,11-diazapentadecan-15-oic acid

The synthesis of the disulfide building block was performed analogously as described in Klein et al.(63) In detail, 5.0 g of cystamine dihydrochloride (22.2 mmol, 1 eq.) were suspended in 50 mL of THF with 7.73 mL of DIPEA (44.4 mmol, 2 eq.) and cooled down to −78 °C. 6.0 g (17.8 mmol, 0.8 eq.) of Fmoc-OSu were dissolved in 70 mL of THF and added dropwise over the course of 3 h. The reaction was stirred for additional 1 hour at −78 °C, followed by stirring for 1 h at RT. Then, DIPEA (7.73 mL, 44.4 mmol, 2 eq.) was added and the reaction mixture

was cooled to 0 °C. Succinic anhydride (4.0 g, 40 mmol, 1.8 eq.) was dissolved in 50 mL of THF. This solution was added dropwise to the reaction mixture at 0 °C and stirred overnight. The reaction mixture was filtered and concentrated to approximately 200 mL, mixed with 200 mL of DCM and was washed 5× with 0.1 M sodium citrate buffer (pH 5.2). The organic phase was dried over sodium sulfate, concentrated, and purified by silica column chromatography using a n-heptane/EtOAc gradient (starting from 1:1 (v/v)) to elute Fmoc-byproducts, followed by a EtOAc/MeOH gradient to isolate the product. The solvent was removed under reduced pressure to give 2.95 g of a white solid (6.22 mmol, 28%).

4.3.3.2 Synthesis of lipoamino fatty acids (LAFs) 8Oc and 12Oc

The protocol was adapted from Thalmayr et al.(162) Briefly, 400 mg of 8-amino octanoic acid was dissolved in 50 mL of dry methanol (MeOH) and stirred for 15 min at RT. Then, 2.2 eq of the indicated fatty aldehyde (octanal and dodecanal, respectively), 2.5 eq of sodium cyanoborohydride ($NaBH_3CN$), and 0.8 eq acetic acid were added successively. The mixture was stirred for 48 hours at RT, before the solvent was removed under reduced pressure and the residual colorless oil was dried under high vacuum. Afterwards, excess of reducing agent was removed by re-dissolving the crude product in DCM and filtration. The filtrate was concentrated and purified by silica gel chromatography with a solvent gradient from 50:1 to 30:1 to remove unreacted starting material and by-products and 20:1 DCM/MeOH (v/v) to isolate the desired product. Elution of products was detected by thin-layer chromatography and staining by basic potassium permanganate ($KMnO_4$) solution and careful warming. Products were characterized by ESI-MS (electrospray ionization mass spectrometry) and ^{1}H-NMR. Analytical data are in accordance with literature.(162)

4.3.4 Synthesis of LAF Stp xenopeptides – General procedure

Resin loading. The LAF containing carriers were synthesized by solid phase assisted synthesis using an acid-labile 2-chlorotrityl resin (theoretical loading: 1.55 mmol g^{-1}). 50 mg of resin were transferred to a syringe reactor and swelled in dry DCM for 20 min. The solvent was ejected and the first amino acid or building block (0.3 eq) was dissolved in dry DCM. After addition of 0.9 eq DIPEA, the solution was immediately added to the resin and allowed to react for 60 minutes at RT while shaking. Afterwards, free reaction sites were capped. Therefore, the resin was incubated with a capping solution consisting of 1 mL dry DCM, 0.75 mL MeOH and 0.125 mL DIPEA to the resin for 30 min. Then, the solution was discarded, and the resin was washed with DMF and DCM (5 x 2 mL each) and dried under reduced pressure. Resin loading was determined by UV/Vis spectrometry by detection of the absorbance of free fulvene product resulting from Fmoc deprotection. Therefore, 5-10 mg of the resin was treated with 1 mL of Fmoc deprotection solution consisting of 20% piperidine in DMF (v/v) for 60 min while shaking at 500 rpm. After centrifugation at 10,000 rpm for 20 sec, 25 µL of the supernatant

were diluted in 975 µL of DMF, transferred to a cuvette and absorbance was measured by a multiwell photometer at 301 nm against 20% piperidine in DMF (v/v) as blank. Resin loading was calculated by using the following equation:

Resin loading [mmol g^{-1}] = (A x 1000) x (m [mg] x 7800 x df)$^{-1}$ with df = dilution factor.

Fmoc deprotection. After loading determination, the resin was swelled in dry DCM and Fmoc-protective groups were removed. Therefore, the resin was treated with Fmoc-deprotection solution (20% piperidine in DMF) for 10 minutes. Then, the solution was drained, and the procedure was repeated 3 times. Afterwards, the resin was washed with DMF and DCM (5 x 2 mL).

Coupling of Fmoc-protected amino acids and artificial building blocks. For successive assembly of desired structures, amino acids and artificial building blocks were coupled to the resin in the indicated sequences. Symmetrical branching points were introduced by using Fmoc-*L*-Lys(Fmoc)-OH and asymmetrical branching points were introduced using Fmoc-*L*-Lys(Dde)-OH, for introducing redox cleavage sites, a suitable disulfide-containing, Fmoc-protected building block was used and dimers of Fmoc-amino butanoic acid and Fmoc-amino hexanoic acid served as spacers. For manual coupling, 4 eq of the Fmoc-protected amino acid or artificial building block were dissolved in 500 µL DCM and mixed with 4 eq PyBOP and 4 eq HOBt, both dissolved in 500 µL DMF. After addition of 8 eq of DIPEA, the mixture was added to the resin and incubated for 90 minutes, followed by washing with DMF and DCM (5 x 1 mL each) and removal of Fmoc-group as described above.

Bocylation. Prior to removal of Dde protecting group, terminal free amino groups were temporarily protected by Boc protecting group. Therefore, 10 eq of Boc anhydride and 10 eq of DIPEA were dissolved in DMF and incubated with the resin for 90 min. Completion of Bocylation was confirmed by Kaiser test.

Dde-deprotection. Subsequent removal of the Dde protecting group, [*N*-(1-(4,4-dimethyl-2,6-dioxocyclohexylidene)ethyl)], for asymmetrical synthesis was achieved by treatment with 2% hydrazine in DMF (v/v) for 15 cycles of 2 min each. Afterwards, the resin was washed with DMF, 10% DIPEA in DMF (v/v), DMF and DCM (5 x 2 mL each).

LAF coupling. For coupling of LAFs, 4 eq of the indicated LAF per deprotected, resin bound amino group and 8 eq of DIPEA were dissolved in DMF, and 4 eq of PyBOP and 4 eq of HOBt were dissolved in DCM. Both solutions were subsequently added to the resin and the reaction time was extended to 36 hours.

Kaiser test. Completion of both coupling and deprotection steps, was confirmed by performing Kaiser tests. After washing the resin with DCM (5 x 2 mL), a small sample of DCM was transferred into an Eppendorf reaction tube. One drop of each Kaiser test solution was added to the resin: first, 80% (w/v) phenol in EtOH, followed by 5% (w/v) ninhydrin in EtOH and 20 µM potassium cyanide (KCN) in pyridine (1 mL aqueous KCN solution, c = 1 mM in 49 mL pyridine). The tube was incubated under shaking at 500 rpm at 99°C for 4 min. The presence of free

amines was indicated by dark blue color of both resin beads and reaction solution. Absence of free amines was indicated by no change of color.

Cleavage from resin. Once the desired sequence was obtained, the resin was dried in vacuo prior to cleavage. For cleavage and in situ removal of acid-labile protecting groups, a cleavage cocktail consisting of TFA/TIS/H_2O (95/2.5/2.5 v/v/v) was added to the resin and allowed to react for 45 minutes. The cleavage solution was drained and collected, the resin was washed first with 500 µL of TFA, followed by 1 mL of DCM and the solutions were combined. The collected solutions were dried under nitrogen flow.

Purification. The dried pellet was dissolved in EtOH or EtOH/H_2O (1:1, v/v). The clear solutions were dialyzed against EtOH overnight at room temperature, followed by dialysis against H_2O for additional 24 hours at 4°C. For dialysis, Spectra/Por® Dialysis Membranes (Carl Roth, Karlsruhe, Germany), the suitable molecular weight cut-off (MWCO) 1 kDa or 2 kDa were used, depending on the molecular weight of the synthesized sequence. Afterwards, the compounds were diluted with water and lyophilized. Final products were characterized by MALDI-TOF-MS and ^{1}H NMR spectroscopy (see **Table 4.1** and **appendix, chapter 6.1.5)**.

Table 4.1. Summarizing table with mass data for all LAF-Stp oligomers.

ID	Sequence (N to C)	EtOH/ H_2O (v/v)[(a)]	Formula	Calculated mass	Found mass (MALDI-TOF-MS)
Bundles 8Oc-B2-1:4					
1621	[K(8Oc)$_2$]$_2$-K-Stp	9:1*	$C_{126}H_{251}N_{15}O_{10}$	2136.43	2133.46 (162)
1791	[K(8Oc)$_2$]$_2$-K-ssbb-Stp	9:1	$C_{134}H_{265}N_{17}O_{12}S_2$	2369.01	2365.02
1792	[K(8Oc)$_2$-ssbb]$_2$-K-Stp	9:1	$C_{142}H_{279}N_{19}O_{14}S_4$	2603.06	2598.83
1793	[K(8Oc)$_2$]$_2$-K-C$_6$-C$_4$-Stp	9:1	$C_{136}H_{269}N_{17}O_{12}$	2333.10	2329.12
1794	[K(8Oc)$_2$-C$_6$-C$_4$]$_2$-K-Stp	9:1	$C_{146}H_{287}N_{19}O_{14}$	2531.23	2526.97
Bundles 8Oc-B2-2:4					
1730	[K(8Oc)$_2$]$_2$-K-Stp$_2$	9:1	$C_{138}H_{276}N_{20}O_{12}$	2407.85	2401.93
1823	[K(8Oc)$_2$]$_2$-K-ssbb-Stp$_2$	9:1	$C_{146}H_{290}N_{22}O_{14}S_2$	2640.21	2635.71
1824	[K(8Oc)$_2$-ssbb]$_2$-K-Stp$_2$	9:1	$C_{154}H_{304}N_{24}O_{16}S_4$	2874.26	2869.16
1825	[K(8Oc)$_2$]$_2$-K-C$_6$-C$_4$-Stp$_2$	9:1	$C_{148}H_{294}N_{22}O_{14}$	2604.03	2599.98
1826	[K(8Oc)$_2$-C$_6$-C$_4$]$_2$-K-Stp$_2$	9:1	$C_{158}H_{312}N_{24}O_{16}$	2802.43	2811.57
U-shapes 12Oc-U1-1:2					
1611	K(12Oc)-Stp-K(12Oc)	1:1	$C_{88}H_{177}N_{11}O_7$	1501.42	1499.15
1821	K(ssbb-12Oc)-Stp-K(ssbb-12Oc)	10:0	$C_{104}H_{205}N_{15}O_{11}S_4$	1968.48	1965.63
1822	K(C$_4$-C$_6$-12Oc)-Stp-K(C$_4$-C$_6$-12Oc)	10:0	$C_{108}H_{213}N_{15}O_{11}$	1896.66	1894.01

[(a)] solvent for dissolution; abbreviations: ID, identification number; EtOH, ethanol, MALDI-TOF-MS, matrix-assisted laser desorption ionization – time of flight – mass spectrometry; 8Oc, LAF based on 8-aminooctanoic acid and two octyl chains; 12Oc, LAF based on 8-aminooctanoic acid and two dodecyl chains, K, lysine; Stp, succinoyl tetraethylene pentamine; ssbb, disulfide building block; C_6, spacer building block based on 6-aminohexanoic acid; C_4, spacer building block based on 4-aminobutyric acid. *Dissolved in ethanol/HCl_{aq}

4.3.5 Polyplex formation

Polyplex formation was performed as follows: the respective nucleic acid was diluted in HBG (HEPES buffered glucose, 20 mM HEPES, 5% glucose (w/v), pH 7.4) and the calculated amount of LAF carrier at the indicated N/P (nitrogen/phosphate) ratio was diluted in Millipore water from a LAF carrier stock solution (10 mg mL^{-1} in $EtOH/H_2O$ at carrier-specific solvent ratios, for details see **Table 4.1**). For calculation of the N/P ratio, secondary amines of Stp units (3 amines per Stp), terminal primary amines and tertiary amines of the LAF residues were considered. Polyplexes were formed upon addition of equal volumes of nucleic acid solution (in HBG) to the LAF carrier solution (in water), followed by rapid pipetting and incubation for 40 min at room temperature (RT) in a closed Eppendorf tube. In case of control polyplexes, *i.e.*, LPEI (N/P 6) for pDNA polyplexes and succPEI (weight/weight (w/w) ratio of 4) for mRNA polyplexes, the respective carrier was diluted in HBG before mixing with the nucleic acid solution as described above. Final concentrations of nucleic acid were 12.5 µg mL^{-1} for mRNA and 10 µg mL^{-1} for pDNA.

4.3.6 Physico-chemical evaluation

4.3.6.1 Experiments under reductive conditions

For experiments mimicking cytosolic reductive environment, the polyplexes were prepared at the indicated N/P ratio in the required volume with a pDNA concentration of 12.5 µg mL^{-1} and a mRNA concentration of 15.6 µg mL^{-1}. After polyplex formation, GSH solution (50 mM GSH in HBG, pH adjusted to 7.4 by addition of 1 M $NaOH_{aq}$) was added to the to the polyplex solution to obtain a final GSH concentration of 10 mM. For negative controls, the respective volume of HBG was added to the polyplex solutions. The samples were incubated at 37 °C for 90 min while being placed on a mechanical shaker at 500 rpm before further evaluation.

4.3.6.2 Agarose gel shift assay

1% (w/v) agarose gel was prepared by microwave-assisted heating of agarose in TBE buffer (18.0 g of tris(hydroxymethyl)aminomethane, 5.5 g of boric acid, 2 mM EDTA at pH 8 in 1 L of water). After cooling down to about 50 °C, 1000× GelRed (0.001% (v/v)) was added to the solution. Afterwards, the solution was casted into an electrophoresis unit and cooled down for gelation. Polyplexes were formulated as described in section 4.3.5 with a pDNA concentration of 10 µg mL^{-1} and mRNA concentration of 12.5 µg mL^{-1}, respectively. After 40 min of incubation, loading buffer (6×; prepared from 6 mL of glycerol, 1.2 mL of 0.5 M EDTA, 2.8 mL of H_2O, 0.02 g of bromophenol blue) was added to the polyplex solution to obtain a 1 : 6 dilution. 20 µL (pDNA polyplexes) or 18 µL (mRNA polyplexes) of the samples were loaded to the gel and electrophoresis was performed at 120 mV for 70 min in 1× TBE buffer. Free pDNA (c = 10 µg mL^{-1}) or mRNA (c = 12.5 µg mL^{-1}) diluted in HBG was used as control.

4.3.6.3 Ethidium bromide exclusion assay

Quantification of EtBr fluorescence was carried out using a microplate reader (Spark, Tecan, Männedorf, Switzerland) with an excitation wavelength λ_{ex} = 535 nm and an emission wavelength λ_{em} = 590 nm. Polyplexes were prepared as described in section 4.3.5 with a total volume of 50 µL at a final pDNA concentration of 10 µg mL^{-1}. After the indicated incubation time, 250 µL of aqueous EtBr solution (c = 0.5 µg mL^{-1}) were added to the polyplexes. After additional incubation for 10 min at room temperature, 260 µL of each sample were transferred into a TPP-ft 96-well-plate and fluorescence intensity was measured. A calibration curve with free pDNA (linear concentration range from 0 to 10 µg mL^{-1}) diluted in HBG was used for quantification. The amount of free, *i.e.*, non-compacted pDNA was calculated based on the calibration of free pDNA and displayed as percentage of EtBr fluorescence in relation to 100% of free pDNA.

4.3.6.4 Complexation efficiency of mRNA polyplexes with and without reductive conditions

Quant-iT™ RiboGreen RNA Assay-Kit (Thermo Fisher Scientific) was used to determine the encapsulation efficiency [ee (%)] of mRNA polyplexes. Polyplexes were formulated as described in section 4.3.5 at a concentration of 15.6 µg mL^{-1}. For stress testing, HBG or GSH solution (50 mM, section 4.3.6.1) were added to a final mRNA concentration of 12.5 µg mL^{-1} and a GSH concentration of 10 mM. The samples were incubated for 90 min at 37 °C under constant shaking at 400 rpm. Unstressed control samples were prepared as described above with addition of HBG and without further incubation. All samples were diluted with 1× TE (10 mM Tris–HCl, 1 mM EDTA, pH 7.5 in RNase-free water) to an mRNA concentration of 2 µg mL^{-1}. 50 µL of the diluted samples were mixed with 50 µL of 1× TE as 'untreated samples'. For complete release of mRNA, unstressed samples were diluted with 50 µL of 1× TE containing 2% (v/v) Triton X-100 and 250 IU mL^{-1} heparin to a final mRNA concentration of 2 µg mL^{-1} (*i.e.*, 'Triton sample'). All samples were incubated for 10 min at 37 °C under constant shaking at 150 rpm. After cooling down at RT for 5 min, 100 µL of RiboGreen reagent diluted 200-fold in 1× TE were added to each sample. After 5 min under light protection, the fluorescence intensity was measured in a Tecan microplate reader (Spark, Tecan, Männedorf, Switzerland) at excitation/emission wavelength of 485/535 nm in duplicates. Background was measured for the respective conditions (*i.e.* HBG or HBG with GSH 10 mM) in 1× TE, or in 1× TE supplemented with Triton X-100 and heparin, treated in the same manner as the respective polyplex samples. The following formula was used to calculate encapsulation efficiency after background subtraction of each sample:

$$ee(\%) = 100\% - \frac{mean\ emission_{untreated\ sample}}{mean\ emission_{Triton\ sample}} \times 100\%$$

4.3.6.5 Dynamic light scattering (DLS)

Measurements were performed using a Zetasizer Nano ZS (Malvern Instruments, Malvern, Worcestershire, United Kingdom) using a folded capillary cell (DTS1070) by dynamic and electrophoretic laser light scattering (DLS, ELS). For determination of particle size and polydispersity index (PDI), 100 µL of pDNA polyplex solutions or 80 µL of mRNA polyplex solutions were formed as described above at a pDNA concentration of 10 µg mL^{-1} or an mRNA concentration of 12.5 µg mL^{-1}, respectively, and measured with the settings as follows: 30 s of equilibration time, temperature of 25 °C, refractive index 1.330, viscosity 0.8872 mPa s.
Each sample was measured three times with six sub-runs per measurement. For determination of zeta potential, the polyplex solution was diluted with HBG to a final volume of 800 µL immediately prior to measurement. Measurement parameters were identical to size determination, with an increase of equilibration time to 60 s. Each sample was measured with 15 sub-runs (10 s each) and zeta potential were calculated by Smoluchowski equation. All values (size, PDI and zeta potential) were displayed as mean ± SD of these measurements.

4.3.7 Biological evaluation

4.3.7.1 Erythrocyte leakage assay

The erythrocyte leakage assay was performed following a protocol published by Krhac Levacic et al.(70) Erythrocytes were isolated by repeated washing of fresh, citrate buffered (25 mM citrate) human blood with a solution of phosphate buffered saline (PBS) supplemented with 25 mM citrate and subsequent centrifugation (800 rcf, 10–15 min at 4 °C). Washing was considered as completed when the supernatant was clear after centrifugation. The cell pellet was then diluted to 5×10^7 erythrocytes per mL with PBS at different pH values (pH 5.5, 6.5 and 7.4) and stored on ice. The oligomers were diluted with PBS at the indicated pH value to a concentration of 2.5 µM and pipetted into a V-bottom 96-well plate as quadruplicate (75 µL per well). For evaluation of lytic potential after incubation under reductive conditions, the oligomers were incubated with 10 mM GSH (final concentration) in HEPES (20 mM, pH 7.4) at the indicated pH value for 90 minutes at 37 °C while shaking at 500 rpm, followed by pipetting into the V-bottom 96-well plate. 75 µL of the erythrocyte suspension at the same pH value was added to each well. Then, the V-bottom 96-well plates were incubated under slow constant shaking for 60 min at 37 °C. Afterwards, the samples were centrifuged (800 rcf, 4 °C, 10 min), and 100 µL of the supernatant were transferred to a TPP-ft 96-well plate. To determine the lytic activity, the samples were analyzed for hemoglobin release at wavelength λ = 405 nm using a microplate reader (Spark, Tecan, Männedorf, Switzerland). PBS at the indicated pH values was used as negative control (0% value) and samples treated with 1% Triton X-100 at the indicated pH value served as positive control (100% value). Data are presented as mean value (±SD) out of quadruplicates.

4.3.7.2 Cell culture

HeLa (human adherent cervix carcinoma cell line), HeLa-Gal8-mRuby stably expressing a galectin8-mRuby3 fusion protein(154, 534, 535) and N2a (murine neuroblastoma cell line Neuro2a) cells were cultured in Dulbecco's Modified Eagle Medium (DMEM) low glucose (1 g L^{-1} glucose). Huh7 wt cells (human adherent hepatic carcinoma cell line) were cultured in DMEM Ham's F12 medium. Cell culture media were supplemented with 10% fetal calf serum (FCS), 4 mM of stable glutamine, 100 U mL^{-1} penicillin and 100 µg mL^{-1} streptomycin. Cells were cultured at 37 °C with 5% CO_2 and a relative humidity of 95% in an incubator. Human colon carcinoma COGA-2 and COGA-12 low passage cell lines,(536) generated in a previous clinical study approved by local ethical committee with written, informed consent from all patients and molecularly characterized in great detail, were cultured in RPMI 1640 medium containing L-glutamine and sodium bicarbonate, supplemented with 10% FCS, 100 U mL^{-1} penicillin and 100 µg mL^{-1} streptomycin). COGA-2 cells were cultured in flasks manually pre-coated with collagen A (1:10 (v/v) in PBS).

4.3.7.3 Transfection screening

5000 HeLa, 10 000 N2a, 8000 Huh7 or 10 000 COGA-2 or COGA-12 cells were seeded in a 96-well plate about 24 hours prior to transfection. For COGA-2 cells, plates were coated with collagen A (1:10 (v/v) in PBS) before seeding. Polyplexes were prepared as described in section 4.3.5. Prior to treatment, cell culture medium was replaced by suitable amounts of fresh medium to obtain a final volume of 100 µL per well after transfection. Different doses of nucleic acid per well were evaluated. Each polyplex was added to the wells as triplicate. For pDNA, indicated doses of pDNA polyplex solution containing 10 µg mL^{-1} pCMVLuc (Plasmid Factory GmbH, Bielefeld, Germany) were prepared as described in section 2.2. From this polyplex solution, required volumes (in the range of 5–20 µL) were added to the wells; for detailed information see indicated doses in the figures. LPEI (MW = 22 kDa) polyplex solution (N/P 6) was used as positive control at indicated pDNA doses. For mRNA, indicated doses of mRNA polyplexes containing 12.5 µg mL^{-1} CleanCap® FLuc mRNA (5moU) (Trilink Biotechnologies, San Diego, CA, USA) (*i.e.* suitable volumes in a range of 1.25–20 µL) of polyplex solution were transferred to the corresponding wells. As positive control, succinylated branched PEI (succPEI) at a w/w ratio of 4 was used at indicated doses. Each well was filled up with the corresponding volume of HBG to reach a final volume of 100 µL per well.

4.3.7.4 Luciferase expression assay

Transfection efficacy of the polyplexes was evaluated after incubation for 24 hours at 37 °C. The medium was removed, and the cells were lysed with 0.5× lysis buffer (100 µL per well) and stored at −80 °C at least overnight. Before determination of luciferase expression, plates were allowed to come up to RT and incubated for 1 hour. For luciferase activity of mRNA-treated cells, the cell lysate was diluted in PBS at a ratio of 1:100. Luciferase activity was

measured using a Centro LB 960 plate reader luminometer (Berthold Technologies GmbH & Co. KG, Bad Wildbad, Germany). Hereto, 35 µL of the cell lysate were measured for 10 s after automatic addition of 100 µL LAR buffer (20 mM glycylglycine; 1 mM $MgCl_2$; 0.1 mM ethylenediaminetetraacetic acid; 3.3 mM dithiothreitol; 0.55 mM adenosine 5′-triphosphate; 0.27 mM coenzyme A, pH 8–8.5) supplemented with 5% (v/v) of a mixture of 10 mM luciferin and 29 mM glycylglycine. Transfection efficiency was calculated for the seeded number of cells and presented as relative light units (RLU) per well. In case of mRNA, data was presented after background subtraction (*i.e.*, HBG-treated control cells). In the case of pDNA polyplexes, the HBG background was not subtracted but depicted in the related graphs.

4.3.7.5 Cell metabolic activity by CellTiter-Glo®

Transfections were performed as described in section 4.3.7.3. The supernatant was removed at 24 h after transfection, and 25 µL of medium mixed with 25 µL of CellTiter-Glo® Reagent (Promega) were added to each well. After incubation on an orbital shaker for 30 min at RT, luminescence was recorded using a Centro LB 960 plate reader luminometer (Berthold Technologies, Bad Wildbad, Germany). The luminescence signals (in RLU) of the samples were set in relation to the luminescence signal of the negative control (HBG buffer-treated control cells). Experiments were performed as triplicates.

4.3.7.6 Confocal laser scanning microscopy (CLSM)

15 000 HeLa Gal8 mRuby cells(154, 534, 535) per well were seeded one day prior to transfection in ibidi µ-slide 8-well ibidiTreat chamber slides and cultured at 37 °C, with 5% CO_2 and 95% relative humidity. Polyplexes were formed as described in section 4.3.5 at a Luc-mRNA concentration of 12.5 µg mL^{-1} with 20% (w/w) Cy5 labelled firefly luciferase mRNA. Medium was changed prior to transfection with adequate volumes to reach a final volume of 300 µL per well after transfection with indicated doses of mRNA polyplexes. After transfection, the cells were incubated for 2 h or 4 h. Medium was removed, cells were washed twice with PBS and fixed with 4% (w/v) paraformaldehyde in PBS for 1 h at RT in the dark. Subsequently, cells were washed twice with PBS and nuclei were stained with DAPI (1 µg mL^{-1} in PBS) for 30 min at RT in the dark. The staining solution was replaced with fresh PBS and cells were stored under light protection at 4 °C until imaging. Imaging was performed with a Leica-TCS-SP8 CLSM equipped with an HC PL APO 63× 1.4 objective and images were processed with the LAS X software from Leica.

4.3.7.7 Bafilomycin A1 assay

5000 HeLa cells were seeded into 96-well plates one day prior to transfection. 30 min before transfection, medium was replaced with either fresh medium or medium containing bafilomycin A1 (BafA1) (0.1 µg mL^{-1} in DMSO) to reach a final concentration of 200 nM BafA1 after polyplex addition. Polyplexes were formed as described above and indicated doses of

pCMVLuc pDNA or Luc-mRNA polyplexes were subjected to the cells. After 4 h of incubation, cells treated with mRNA polyplexes were lysed and evaluated *via* luciferase expression assay as described in section 4.3.7.4. For pDNA, medium was replaced by fresh medium without BafA1 after 4 h and incubated further 20 h before analysis. Transfections were performed in triplicates.

4.3.7.8 Cell viability by LDH cytotoxicity assay

LDH cytotoxicity assay was performed according to the manufacturers' protocol (Promega). Briefly, 5000 HeLa cells per well were seeded into a 96-well plate one day prior to transfection. Polyplexes were prepared as described in section 4.3.5. After replacement of medium with suitable amounts of fresh medium, the test compounds were added to the cells in the indicated concentration (*i.e.*, 100 ng per well for pDNA polyplexes and 63 ng per well for mRNA polyplexes) to reach a final volume of 100 µL per well. As control groups, cells treated with the indicated amount of HBG buffer or 20 µL of either LPEI polyplexes containing 10 µg mL^{-1} pDNA or succPEI polyplexes containing 12.5 µg mL^{-1} mRNA were used. Cells without any treatment (neither polyplex nor HBG) served as negative control. After transfection, the cells were incubated at 37 °C for the desired exposure time (*i.e.*, 8 h, 12 h, 16 h, 24 h). 45 min before the end of the incubation time and addition of CytoTox® reagent, a triplicate of untreated cells was treated with 10 µL of 10× lysis solution as maximum LDH release control. Then, 50 µL of the supernatant of each well was transferred to a fresh transparent, flat-bottom 96-well plate, followed by addition of 50 µL of CytoTox® reagent and incubation in the dark for 30 min at RT while slowly shaking. After 30 min, 50 µL of stop solution was added to each well and the absorbance was immediately measured at 490 nm (OD_{490}) using a multiplate reader (Spark, Tecan, Männedorf, Switzerland). For calculation of released LDH, the average values of the untreated cells was subtracted from all values of experimental cells. From the corrected experimental values, the following equation was used to calculate the percentage of LDH release:

$$LDH\ release\ (\%) = 100 \times \frac{sample\ LDH\ release\ (OD_{490})}{maximum\ LDH\ release\ (OD_{490})}$$

4.3.7.9 Microscope Images

The polyplexes were prepared as described in section 4.3.5 and transfected to the cells as described in section 4.3.7.3. Subsequently the cells were incubated for 24 hours after transfection, and then examined microscopically by an Axiovert 200 (Zeiss, Oberkochen, Germany). Photographic images were taken by a INFINITY2-3C (3.3 Megapixel Color CCD Camera USB2.0), Lumenera Corporation/Ottawa (purchased from FRAMOS GmbH, Taufkirchen, Germany) and processed by Infinity Capture Software

4.3.7.10 Cell Watcher analysis

For the cell watcher analysis, HeLa cells were seeded 24 hours prior to transfection to a 48-well plate (5000 cells per well) and monitored by Cellwatcher M (PHIO Scientific GmbH, Munich, Germany). Confluency was calculated by the corresponding software. 24 hours after seeding, medium was replaced by fresh, pre-warmed medium and the cells were transfected with polyplex solution at indicated doses. Cell growth was monitored for a total incubation time of 48 hours after transfection.

4.3.7.11 Flow cytometer analysis

40 000 HeLa cells per well were seeded 24 hours prior to transfection. Polyplexes were prepared as described in section 4.3.5 and transfected to the cells with 100 ng per well for pDNA polyplexes (pDNA concentration of 10 µg mL^{-1}) and 63 ng per well for mRNA polyplexes (mRNA concentration of 12.5 µg mL^{-1}). After 24 hours of incubation, the medium was removed, and the cells were gently washed with cold PBS (4 °C) and trypsinized for 5 minutes at 37 °C. The cell suspension was diluted with FACS buffer (10% FBS in PBS, 0.1% (v/v) DAPI) and transferred to a FACS tube. Cells were analyzed by flow cytometry using a CytoFLEX S Flow Cytometer (Beckman Coulter, Brea, CA, USA) over 60 seconds at a flow rate of 170 µL min^{-1}. Flow cytometry data were analyzed using FlowJo™ v10.8 flow cytometric analysis software by FlowJo, LLC (Becton, 20 Dickinson and Company, USA).

4.3.7.12 Kinetics of cellular association and expression

To evaluate the cell association and expression kinetics, 18 000 HeLa cells per well were seeded in a 24 well-plate 24 h prior to transfection. Polyplexes were prepared at N/P 24 with a w/w mixture of 20% (w/w) EZ Cap Cy5 Firefly Luciferase mRNA (5moUTP) and 80% (w/w) CleanCap® EGFP mRNA (5moU) at a total mRNA concentration of 12.5 µg mL^{-1}. The cells were transfected in duplicates with a dose of 100 ng total mRNA and incubated for 30 min, 2 h, 4 h, 6 h, 24 h and 48 h. After incubation, the cells were prepared for flow cytometer measurement as described in section 4.3.7.11, without the addition of DAPI. The measurement was performed using a CytoFLEX S Flow Cytometer (Beckman Coulter, Brea, CA, USA) at suitable flow rates and times of acquisition. However, at least 8000 cells per analysis were recorded. Flow cytometry data were analyzed using FlowJo™ v10.8 flow cytometric analysis software by FlowJo, LLC (Becton, 20 Dickinson and Company, U.S.).

4.3.7.13 Annexin V/propidium iodide assay

Polyplex treatments were performed in duplicates in 24-well plates. HeLa cells were seeded 24 h prior to transfection in a 24-well-plate (40 000 cells per well). Immediately prior to transfection, the medium was replaced with 475 µL of fresh medium containing 10% (v/v) FBS for pDNA polyplexes and with 487.5 µL for mRNA polyplexes. The nanoparticles were prepared as described in section 4.3.5. Transfection was performed with 12.5 µL of polyplexes

containing 125 ng per well pDNA or 6.3 µL polyplex solution containing 78 ng per well mRNA, respectively. HBG was then added to reach a final volume of 500 µL per well, *i.e.*, 12.5 µL per well for cells transfected with pDNA polyplexes and 6.2 µL for cells treated with mRNA polyplexes. HBG buffer (25 µL per well for pDNA polyplexes and 12.5 µL per well for mRNA polyplexes) was used as negative control. After 24 h of incubation, the cells were collected and incubated with annexin V incubation reagent (prepared according to manufacturer's protocol of Bio-Techne GmbH, Wiesbaden, Germany) for 10 min before flow cytometer analysis using a CytoFLEX S Flow Cytometer (Beckman Coulter, Brea, CA, USA). Cells were analyzed with a flow rate of 170 µL min^{-1} until 10 000 events were counted. Gates were set compared to control measurements with HBG-buffer treated cells and with exclusion of cell debris. Annexin V and propidium iodide negative cells were considered as healthy cells. Cells shifted to the annexin V and propidium iodide positive gate indicated late apoptotic cells, whereas cells shifted to only annexin V-positive gate were considered as early apoptotic, and PI-positive, but annexin-V-negative cells were not viable. Flow cytometry data were analyzed using FlowJo™ v10.8 flow cytometric analysis software by FlowJo, LLC (Becton, 20 Dickinson and Company, U.S.).

4.3.8 Statistical analysis

Experimental results are presented as arithmetic mean of triplicates, if not stated otherwise, with error bars displaying the standard deviation (SD). Statistical analysis of the results (mean ± SD) was performed by applying unpaired Student's two-tailed *t*-test with Welch's correction. Calculations and graphical presentation were performed with Prism 10.1.2 (GraphPad Software Inc.). ns (statistically not significant) $p > 0.05$; *$p \leq 0.05$; **$p \leq 0.01$; ***$p \leq 0.001$; ****$p \leq 0.0001$.

4.4 Results and Discussion

4.4.1 Design and synthesis of disulfide and hydrophobic spacer analogs

In recent work, our group has developed a library of novel nucleic acid carriers with versatile sequences and topologies.(162) The novel xenopeptides are comprised of protonatable Stp units, derived from amino ethylene units of PEI, enabling nucleic acid compaction and providing endosomal buffer capacity, α,ε-amidated lysines as branching points and lipoamino fatty acids (LAF) with central tertiary amines, which display favorable, pH-dependent properties supporting polyplex stabilization by lipophilic characteristics at extracellular pH and particle disassembly upon protonation in endosomal environment. The LAFs used in the new study were 8Oc (based on reductive bisalkylation of 8-aminooctanoic acid with octanal) and 12Oc (obtained by the reductive amination of dodecanal with 8-aminooctanoic acid), see **Scheme 4.1**. Variations of the lipophilic chain length and the position of the tertiary amine have been used to tailor endosomal escape by endosomolytic activity. Each LAF-xenopeptide was assigned to a distinct, consecutive ID number, and an additional nomenclature, providing information about type of LAF, topology (B2 bundle, or U-shape) and the Stp/LAF ratio (*e.g.* ***1621***: LAF = 8Oc, topology = B2, Stp/LAF = 1 : 4). Among the xenopeptides of the library, the carriers ***1621*** (8Oc-B2-1 : 4) and ***1611*** (12Oc-U1-1 : 2) have demonstrated great potencies for the delivery of mRNA and DNA, respectively. Especially for mRNA, both carriers exhibited excellent transfection efficacies, even at ultra-low mRNA doses. For B2 bundle topology,

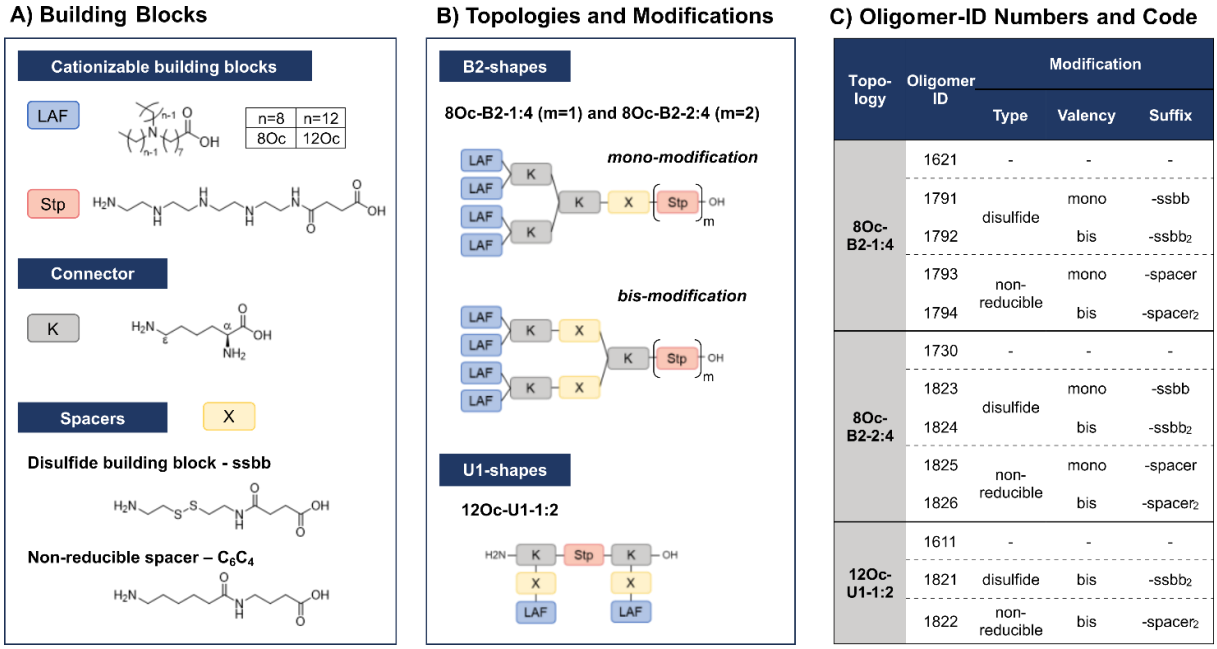

Topology	Oligomer ID	Modification: Type	Modification: Valency	Modification: Suffix
8Oc-B2-1:4	1621	-	-	-
	1791	disulfide	mono	-ssbb
	1792		bis	-ssbb$_2$
	1793	non-reducible	mono	-spacer
	1794		bis	-spacer$_2$
8Oc-B2-2:4	1730	-	-	-
	1823	disulfide	mono	-ssbb
	1824		bis	-ssbb$_2$
	1825	non-reducible	mono	-spacer
	1826		bis	-spacer$_2$
12Oc-U1-1:2	1611	-	-	-
	1821	disulfide	bis	-ssbb$_2$
	1822	non-reducible	bis	-spacer$_2$

Scheme 4.1. Library design of lipoamino fatty acid containing LAF–Stp carriers containing reducible (ssbb) and non-reducible (C_6C_4) spacer domains. (A) Building blocks used in solid phase assisted assembly (displayed in unprotected form). (B) Different topologies and positioning of bioreducible or non-reducible building blocks. (C) Summarized overview of the library and its identification (ID) numbers.

shorter LAFs such as 8Oc in ***1621*** were favorable for transfection efficiency compared to the longer 12Oc LAF units, although cytotoxicity was observed for ***1621*** at high doses. In case of pDNA polyplexes, formulations with a higher Stp/LAF ratio (1 : 2) as present in U-shape carrier ***1611*** are more effective in terms of gene transfer.(162) This is consistent with the hypothesis that the PEI-like Stp units are beneficial for DNA condensation into polyplexes.(37, 71, 521).

Based on these considerations we converted the sequence of B2-1:4 ***1621*** into the B2-2:4 carrier ***1730***. As demonstrated here, DNA polyplexes formed with ***1730***, providing two Stp units, showed superior properties over ***1621*** (**Figure 4.1**). For example, polyplex size was reduced from 220 nm to 80 nm at N/P 12 and transfection efficiency on N2a cells was 108-times increased compared to ***1621*** (**Figure 4.1C**). However, cell viability, determined by a CellTiter Glo® assay, was still reduced compared to LPEI, but improved over ***1621*** at high N/P ratios (**Figure 4.1D**). Altogether, these new findings make ***1730*** a highly promising LAF carrier for pDNA delivery.

Due to their great potential for nucleic acid delivery, xenopeptides ***1611***, ***1621*** and ***1730*** were selected for further sequence-defined chemical evolution by introduction of spacers between the Stp and LAF units. Previous work demonstrated that topologies between or within the

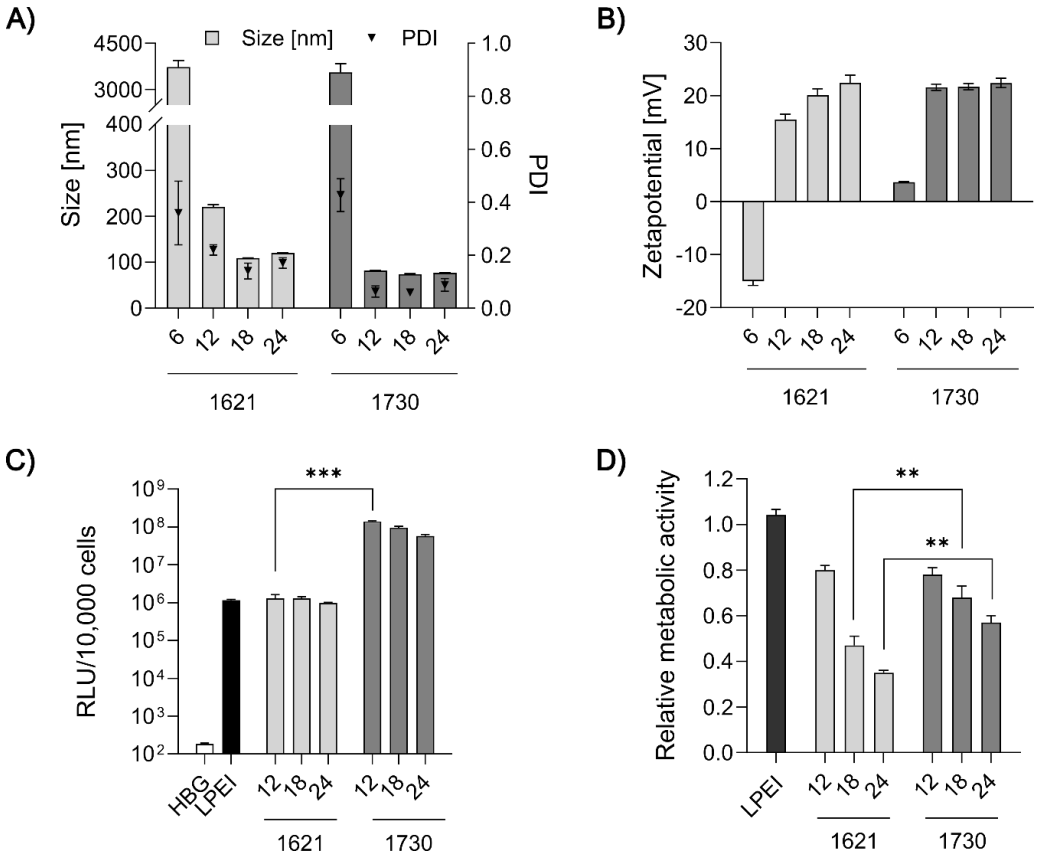

Figure 4.1. Evaluation of pDNA polyplexes after chemical evolution from 8Oc-B2-1:4 (***1621***) to 8Oc-B2-2:4 (***1730***). A) and B) Evaluation of different N/P ratios on physico-chemical properties of pDNA polyplexes by DLS and ELS measurements. C) and D) *In vitro* evaluation on N2a cells (n = 3, mean + SD). Cellular transfection efficiency was determined by luciferase gene expression assay (C). Cell viability at 24 hours after transfection was determined by CellTiter Glo® Assay in relation to control wells treated with HBG (D).The results of the screening were kindly provided by Johanna Seidl (Pharmaceutical biotechnology, LMU Munich).

various subunits ('LAF nitrogen catwalk') can modulate potency but also cytotoxicity of carriers. Based on established Fmoc solid-phase assisted synthesis with protected artificial amino acids,(56, 61, 71, 521) we now generated novel spacer-containing xenopeptides as listed in **Scheme 4.1** and **Table 4.1**. As spacers, either Fmoc-protected succinoyl-cystamine as a solid-phase-synthesis compatible disulfide building block (ssbb)(63, 537) or an analogous non-reducible amino hexanoic acid-amino-butanoic acid dipeptide spacer (C_6C_4) was used, providing comparable spatial distance (ssbb = 20.6 Å *vs.* C_6C_4 = 19.6 Å) and similar hydrophilic/hydrophobic characteristics.

The incorporation of the disulfide building blocks provides carriers with redox-responsive cleavage sites for degradation in the intracellular, reductive cytosolic environment with increased concentration of GSH.(174, 538, 539) Cytosolic carrier cleavage is expected to destabilize the polyplexes and to abolish the amphiphilic and potentially lytic character of the xenopeptides. Both spacer- and disulfide-analogs were set in comparison with their original LAF–Stp structures regarding their nucleic acid compaction ability and resulting physico-chemical properties (size, polydispersity, surface charge) as well as their potency to deliver pDNA and mRNA to various cell lines without having a cytotoxic influence on the cells. For carriers of the U1-1:2 topology, the disulfide modification was introduced in the lysine side chain before coupling of 12Oc for maintaining symmetry and generating a system that is cleaved in small fragments of mostly hydrophilic and lipophilic properties upon disulfide reduction (see **Scheme 4.1**). For bundle structures, multiple options for the positioning of the disulfide-motifs were possible, leading to various cleavage products. At first, the ssbb was positioned behind the cationic Stp unit. Upon disulfide reduction, fragmentation into a cationic Stp-domain and a large, mostly hydrophobic LAF domain will occur. As a second option, the disulfide was integrated after the first branching lysine. In this case, disulfide reduction would lead to fragmentation into a Stp-lysine fragment and two smaller LAF fragments. As a last option, the ssbb was introduced directly before the LAF, leading to a structure with four cleavage sites. However, synthetic issues regarding disulfide instability occurred during the assembly of tetra-ssbb analogs (data not shown) and prevented the synthesis. The identity of all synthesized carriers was confirmed by MALDI-TOF mass spectrometry and ^{1}H-NMR spectroscopy. The analytical data are summarized in the appendix, section 6.1.5.

In order to investigate the biodegradability of the reducible carriers under reductive stress, MALDI-TOF analysis was performed after incubation with the physiological antioxidant GSH (c = 10 mM). To mimic intracellular reducing conditions, the disulfide-containing oligomers were dissolved in HBG and incubated with GSH at a final concentration of 10 mM for 90 min at 37 °C. Oligomer fragments of GSH-induced disulfide reduction were subsequently detected by MALDI analysis, besides small peaks of intact oligomer (**Table 4.2** and **Figure 4.2**). In case of the exemplarily presented mass spectrum, mass peaks associated with the Stp backbone after

partial and complete disulfide reduction were found, as well as the mass peaks of the hydrophobic LAF arm.

Table 4.2. Summarizing table with mass data for disulfide-containing LAF- Stp oligomers after incubation with 10 mM glutathione (GSH) for 90 minutes at 37°C.

Oligomer	Fragment structures (N → C)	calculated $[M+H]^+$	found	comment
8Oc-B2-1:4				
1791	$[K(8Oc)_2]_2$-K-ssbb-Stp	2370.0	2365.9	$[M+H]^+$
	$[K(8Oc)_2]_2$-K-SH	1922.8	1915.2	$[M+H]^+$
	SH-Stp	449.3	n.d.	outside detection range
1792	$[K(8Oc)_2$-ssbb$]_2$-K-Stp	2604.1	2598.9	$[M+H]^+$
	$K(8Oc)_2$- SH	936.9	934.5	$[M+H]^+$
	$[K(8Oc)_2$-ssbb]-K(SH)-Stp	1670.2	1667.0	$[M+H]^+$
	Stp-K-$(SH)_2$	736.4	n.d.	outside detection range
8Oc-B2-2:4				
1823	$[K(8Oc)_2]_2$-K-ssbb-Stp_2	2641.2	2635.9	$[M+H]^+$
	$[K(8Oc)_2]_2$-K-SH	1923.8	1915.2	$[M+H]^+$
	SH-Stp_2	720.5	1435.9	$[2M+H]^+$
1824	$[K(8Oc)_2$-ssbb$]_2$-K-Stp_2	2875.3	2871.2	$[M+H]^+$
	$K(8Oc)_2$-SH	936.9	934.5	$[M+H]^+$
	$[K(8Oc)_2$-ssbb]-K(SH)-Stp_2	1941.4	1937.9	$[M+H]^+$
	(SH)-K-Stp_2	1007.6	n.d.	not detected
12Oc-U1-1:2				
1821	K-ε(ssbb-12Oc)-Stp-K-ε(ssbb-12Oc)	1969.5	1965.5	$[M+H]^+$
	12Oc-SH	555.5	1105.2	$[2M+H]^+$
	K-ε(ssbb-12Oc)-Stp-K-ε(SH)	1417.0	1413.6	$[M+H]^+$
	K-ε(SH)-Stp-K-ε(SH)	864.5	858.4, 1718.1	$[M+H]^+$, $[2M+H]^+$

K, lysine; Stp, succinoyl tetraethylene pentamine; ssbb, disulfide building block; 8Oc, LAF based on 8-aminooctanoic acid and two octyl chains; 12Oc, LAF based on 8-aminooctanoic acid and two dodecyl chains; n.d., not detected.

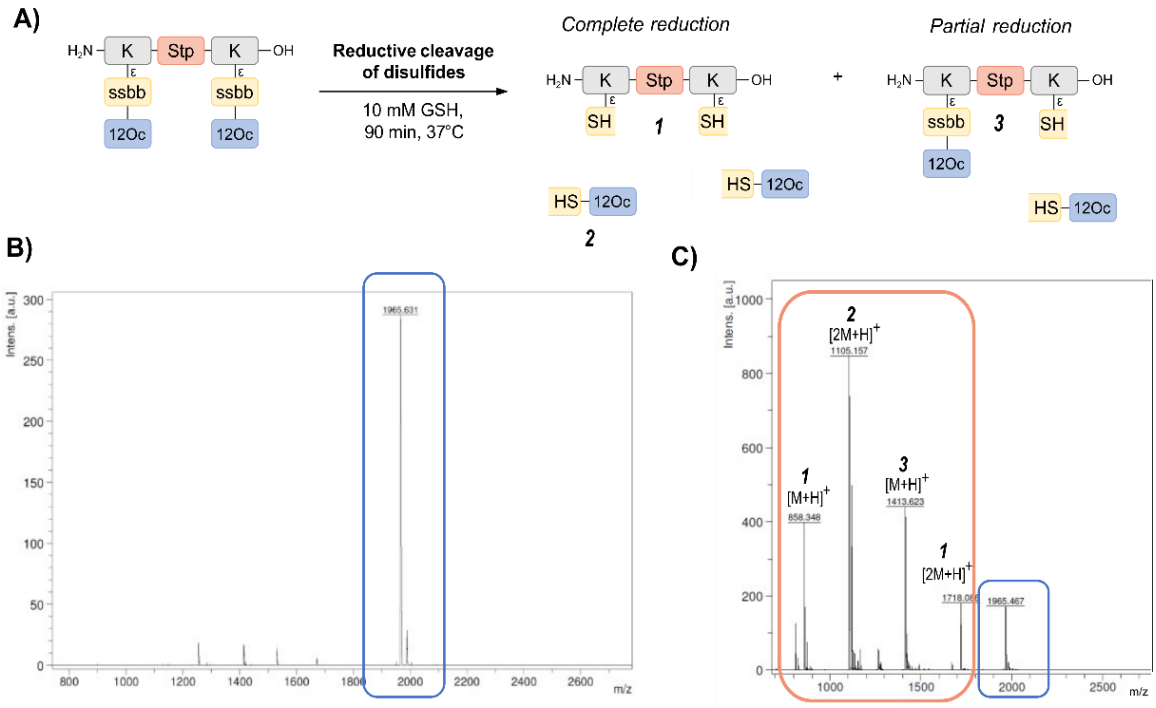

Figure 4.2. MALDI analysis before and after incubation with glutathione (GSH). (A) Scheme of disulfide-containing LAF-oligomer ***1821*** with 12Oc-U1-1:2 topology before and after GSH-induced reduction of disulfides with possible cleavage products upon complete or partial reduction. Representative MALDI mass spectra of disulfide-LAF-oligomer ***1821*** before (B) and after (C) treatment with 10 mM GSH for 90 min at 37 °C. The mass spectrum after GSH-treatment contains additional peaks (**1**, **2** and **3**) assigned to cleavage products upon disulfide reduction.

4.4.2 Physico-chemical evaluation of pDNA and mRNA polyplexes

4.4.2.1 Nanoparticle formation

In a first screening of the novel carriers, polyplexes were formed with either pCMVLuc DNA or CleanCap® FLuc mRNA (5moU) at different N/P ratios to identify optimum conditions for polyplex formation. Size and polydispersity of the resulting polyplexes, as well as zeta potential were evaluated. The N/P ratio describes the ratio between protonatable amines (N) of the oligomer to phosphates of the nucleic acid (P). For determination of the number of protonatable amines, three secondary amines per Stp unit, one tertiary amine per LAF, and terminal primary amines (exist only in U1 shapes) are taken into consideration. Note that the majority of amines (LAF amines and two thirds of Stp secondary amines) are not protonated at neutral pH. After an incubation time of 40 min at room temperature, DLS and ELS measurements were performed (**Figure 4.3**, **Figure 4.4**). Small polyplex sizes, preferably < 200 nm, with PDI values ≤ 0.2 and positive zeta potential were considered as successful formulation.

pDNA. Polyplexes were formed with pCMVLuc DNA at N/P ratios 6, 12, 18 and in the case of bundle LAF carriers also 24, to identify the N/P ratio necessary for polyplex formation (**Figure 4.3**). N/P ratio of 6 was not sufficient for most carriers to form stable and nano-sized polyplexes, independent of their topology, accompanied by mostly negative zeta potential which was not favorable for attachment to negatively charged cell membranes (**Figure 4.3 B**). For the carriers

following the 12Oc-U1-1:2 topology (***1611*** and its analogs), N/P 12 was sufficient for polyplex formation, and a further decrease of particle size was observed for ***1611*** by increasing the N/P ratio to 18. In the U1-series, most comparable particles regarding their size and zeta potential were obtained at N/P 18. For 8Oc-B2-1:4 (***1621*** series), a minimum N/P 18 was required to obtain stable polyplexes for all analogs. In comparison to ***1621***, ***1730*** contains a second Stp unit, which is considered to support DNA compaction.(521) This is underlined by slightly reduced particle sizes compared with ***1621*** and its analogs at N/P 18. In addition, the ***1730*** series formed stable nanoparticles at N/P 12. This finding is in line with previous work by Nie and co-workers, demonstrating the importance of a well-balanced lipophilic–hydrophilic ratio of bioreducible nucleic acid carrier constructs comprised of large cationic headgroups and lipophilic tails.(529)

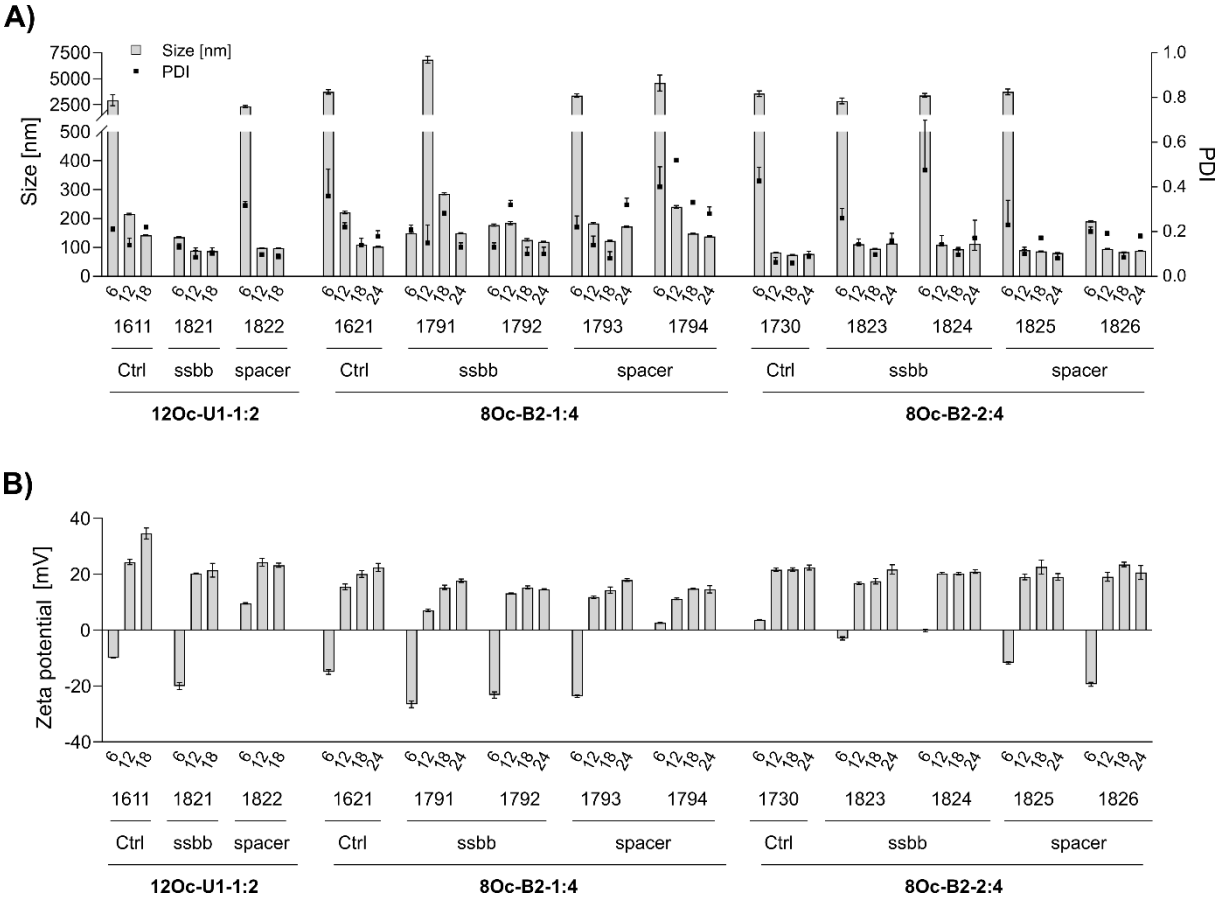

Figure 4.3. DLS and ELS measurements of pDNA polyplexes. Polyplexes were formed with different LAF-Stp carriers at the indicated N/P ratios and a pCMVLuc concentration of 10 µg mL^{-1} (n=3, mean ± SD) and evaluated by A) DLS- measurements for determination of Z-average and PDI and B) ELS measurements to determine zeta potential.

mRNA. The whole set of xenopeptides was also evaluated regarding its ability to form mRNA polyplexes (**Figure 4.4**). In previous studies, ***1611*** and ***1621*** proved to form stable and reproducible particles at N/P 18.(162) For the new disulfide and C_6C_4 spacer analogs, N/P 12

was also evaluated (**Figure 4.4 A, B**). The 12Oc-U1-1:2 analogs, ***1821*** (ssbb) and ***1822*** (C_6C_4), formed stable mRNA particles already at N/P 12, with positive zeta potential of 15-18 mV.

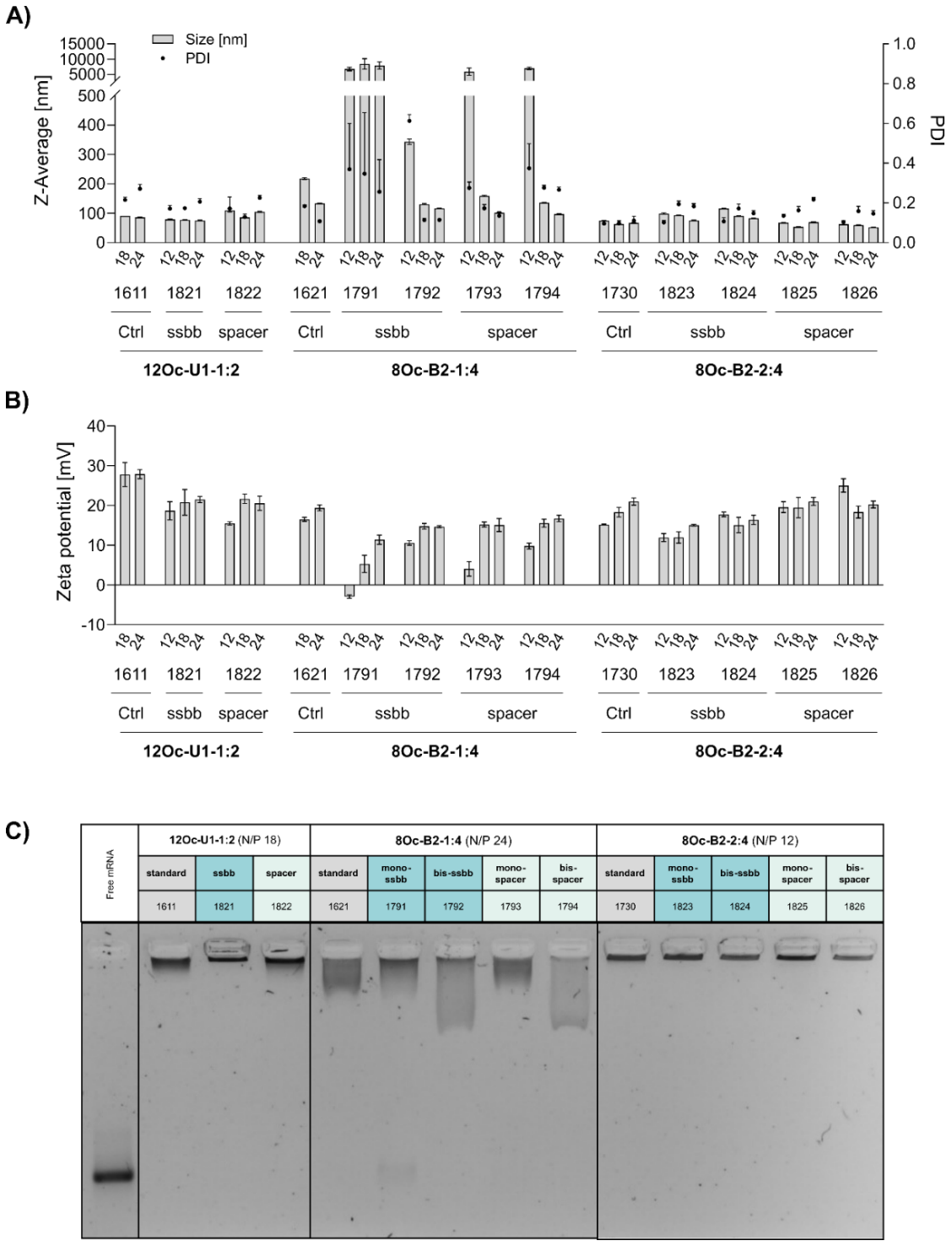

Figure 4.4. Physico-chemical characterization of mRNA polyplexes. Polyplexes were formed with different LAF-Stp carriers at the indicated N/P ratios and an mRNA concentration of 12.5 µg mL^{-1} (n=3, mean ± SD) and evaluated by A) DLS measurements for determination of Z-average and PDI and B) ELS measurements to determine zeta potential. C) Agarose gel shift assay of mRNA polyplexes. The experimental results were kindly provided by Sophie Thalmayr (Pharmaceutical Biotechnology, LMU Munich).

Comparable to the original structure ***1621***, the 8Oc-B2-1:4-analogs formed nanosized polyplexes at N/P ≥ 18, except for the mono-ssbb analog ***1791*** which was unable to generate stable mRNA polyplexes at any N/P ratio. This observation was confirmed by an agarose gel shift assay, where free mRNA was detected for formulation with ***1791***, but not for other LAF-carriers (**Figure 4.4 C**). The corresponding C_6C_4 spacer analog ***1793*** showed no aggregation at N/P ≥ 18. All 8Oc-B2-2:4 carriers of the ***1730*** series formed desirable mRNA nanoparticles at N/P 12, which were smaller in size than ***1621***.

4.4.2.2 Nucleic acid binding ability

The ability of the carriers to condense pDNA and mRNA was determined under standard polyplex formation conditions after 40 min of incubation, as well as under reductive conditions assessing polyplex instability after forced disulfide degradation upon incubation with GSH for 90 min at 37 °C (**Figure 4.5**, **Figure 4.6**, **Figure 4.7**). To exclude possible polyplex instability as a result of treatment conditions, a second control group was included without reductive environment.

pDNA. The compaction ability was determined by an ethidium bromide (EtBr) exclusion assay and agarose gel shift assay (**Figure 4.5**). A pre-experiment confirmed absence of disturbing effects like potential DNA degradation as a result of the treatment conditions (37 °C for 90 min, +/- 10 mM GSH) on free DNA (**Figure 4.6**). Under standard conditions, all polyplex formulations showed favorable DNA compaction ability under non-reductive conditions, with

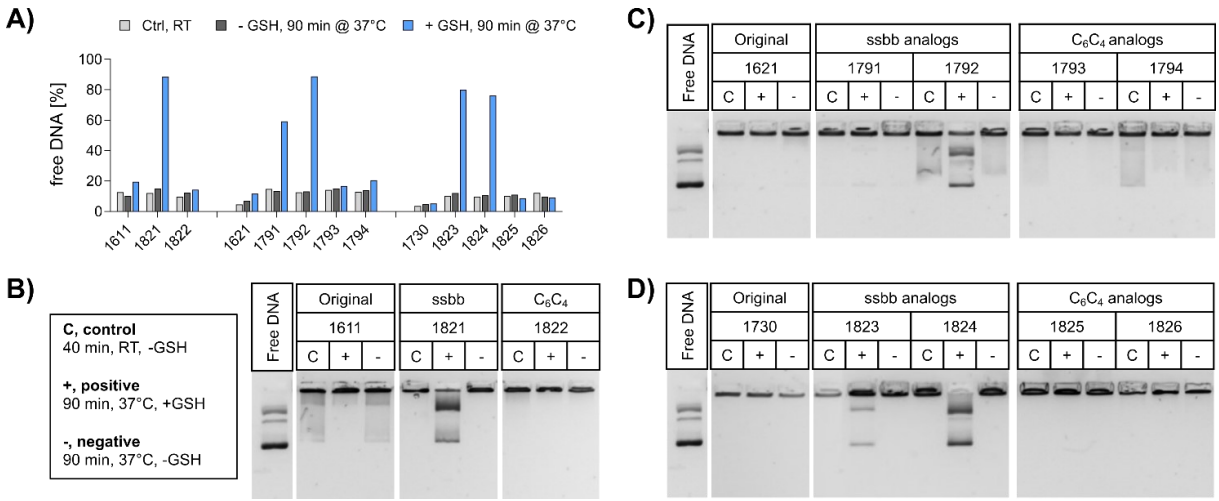

Figure 4.5. DNA compaction ability and cargo release of LAF-Stp carriers before and after GSH treatment. A) Ethidium bromide assay pf pDNA polyplexes formed with the indicated carriers at N/P 18. The carriers were incubated with GSH (blue) or with HBG (dark grey) for 90 min at 37°C prior to EtBr assay or incubated in absence of GSH for 40 min at RT (light grey). The fluorescence intensity of EtBr correlates with the amount of free and non-compacted pDNA, as pDNA only in this state is accessible for EtBr intercalation. 100% EtBr fluorescence refers to the fluorescence of free pDNA without carrier in the same concentration as used for polyplex formation. B-D) DNA compaction and release ability of polyplexes formed at N/P 18 was determined in an agarose gel shift assay (1% w/v agarose) after 90 min incubation at 37°C under reducing (+) and non-reducing (-) conditions. Lanes 'C' refer to standard control polyplexes without preincubation at 37°C.

less than 20% of free DNA detected (**Figure 4.5A**). In the case of ***1730*** (two Stp units), compaction was even stronger than for ***1621*** (one Stp unit). After exposure to a reducing environment (10 mM GSH, 90 min, 37 °C), decompaction of DNA was detected exclusively for disulfide-containing analogs, while no effect on DNA compaction was observed for non-reducible xenopeptides. This was found for all reducible analogs of the ***1621*** B2 bundle series (mono-disulfide ***1791***, bis-disulfide ***1792***), ***1730*** B2 bundle series (***1823*** and ***1824***), and the U-shape disulfide analog ***1821***.

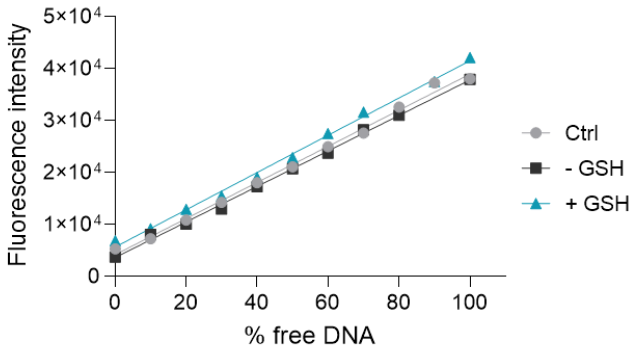

Figure 4.6. Calibration curve for EtBr assay. Free DNA was incubated either for 40 min at RT in HBG (Ctrl) or for 90 min at 37°C with or without GSH (+/- GSH), before addition of ethidium bromide and subsequent measurement.

Agarose gel shift assays (**Figure 4.5 B-D**) were performed to confirm the findings of the ethidium bromide exclusion assay. For 12Oc-U1-1:2 polyplexes, original ***1611*** polyplexes showed a minor release of DNA, but like polyplexes of the C_6C_4 spacer analog ***1822***, were not affected by reductive GSH. In contrast, the disulfide analog ***1821*** showed GSH-dependent destabilization of polyplexes (**Figure 4.5 B**). DNA release was also observed for all disulfide containing B2 bundle xenopeptides after exposure to reductive environment. This effect was stronger for bis-disulfide analogs ***1792*** and ***1824*** than mono-disulfide analogs (**Figure 4.5 C, D**). It has to be noted that the gel shift assay indicates free pDNA that is not enclosed into nanoparticles. In contrast the EtBr assay detects also barely compacted pDNA by intercalation of the dye also in loose particles.

mRNA. Encapsulation efficiency (ee) of mRNA polyplexes was determined via RiboGreen assay for a selected set of ***1621*** and the bis-modified analogs ***1792*** ($ssbb_2$) and ***1794*** ($(C_6C_4)_2$) at N/P 24 (**Figure 4.7**). Under standard conditions, the ee for all tested formulations was >85%, in case of ***1621*** and ***1792*** even >90%. Subsequent to incubation with the reductive GSH for 90 min at 37 °C, ee of the disulfide-containing analog ***1792*** was about 30% reduced, verifying polyplex destabilization under bioreducible conditions, while ee of non-reducible analogs, ***1621*** and ***1794***, remained unchanged.

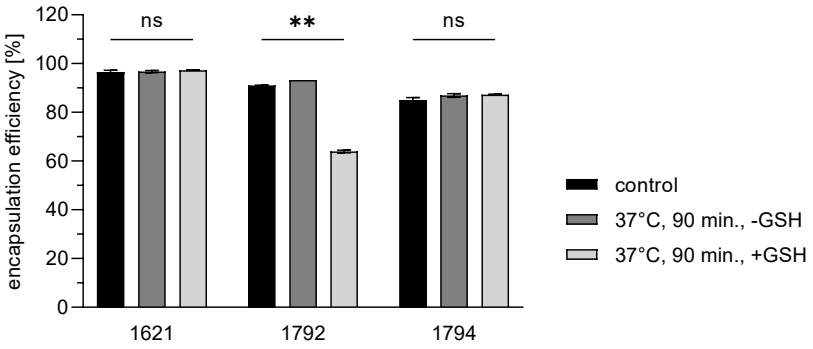

Figure 4.7. Encapsulation efficiency of mRNA polyplexes formed with different LAF-Stp carriers at N/P 24 and a Luc-mRNA concentration of 12.5 µg mL^{-1} (*n*=2). Besides the control group (40 min at RT in absence of GSH), stressed polyplexes (90 min at 37°C +/- GSH) were evaluated. Fluorescence of free mRNA interacting with RiboGreen reagent in intact polyplexes in comparison to polyplexes treated with 1% Triton X-100 and 250 IU mL^{-1} heparin. The encapsulation efficiency was determined by Sophie Thalmayr (Pharmaceutical Biotechnology, LMU Munich).

4.4.3 Biological and transfection activity

4.4.3.1 Erythrocyte leakage assay

Carriers ***1611*** and ***1621*** display favorable pH-dependent lytic activity at pH 6.5 and 5.5 mimicking different stages of endosomal uptake, which is considered to enhance endosomal escape into cytosol resulting in high transfection efficacy.(162) Significant lytic activities at pH 7.4, however, may also explain cytotoxicity due to undesired membrane damage.(153, 167) By incorporating biodegradable disulfides that are reduced by the high cytosolic GSH levels, lytic activity after endosomal release should be attenuated. Erythrocyte leakage assays are displayed in **Figure 4.8**. In case of the ***1611*** series, the additional spacing, either by the disulfide or the non-reducible spacer dimer, had only a minor impact on lytic potential under standard conditions, regardless of a larger hydrophobic domain in the oligomer. For the ***1621*** series, an increase of lytic potential under standard conditions was observed for the bis-analogs (***1792*** and ***1794***) over ***1621***, probably due to a significant increase of the hydrophobic ratio by the additional building blocks (both, ssbb and C_6C_4), but limited to pH 6.5 and 5.5. Comparable observations were made for ***1730***, promoting again a stronger lytic activity for the bis-analogs. In a direct comparison of the bundle structures, the B2-2:4 ***1730*** series showed about 30% increase in lytic activity over ***1621*** series, despite the less lipophilic Stp/LAF ratio of 2:4 instead of 1:4. However, the negative charge of erythrocyte membranes must be noted, where cationic amphiphiles display advantageous leakage effects.(153, 540, 541) Similar tendencies as the increase of lytic activity at pH 6.5 among the modified, both reducible and non-reducible LAF carriers, were observed also for the B2-2:4 series. These findings are consistent with our previous work investigating the lytic activity of different U-shapes, where not only an increase of the lipidic domain, but also the amount of Stp caused an increase of

lytic activity (U1-1:2 < U1-2:2 < U1-2:4). In the case of disulfide-containing structures, the lytic activity was abolished after reductive cleavage by incubation with GSH for 90 minutes. This effect might have positive consequences on biocompatibility at later time points beyond entry.

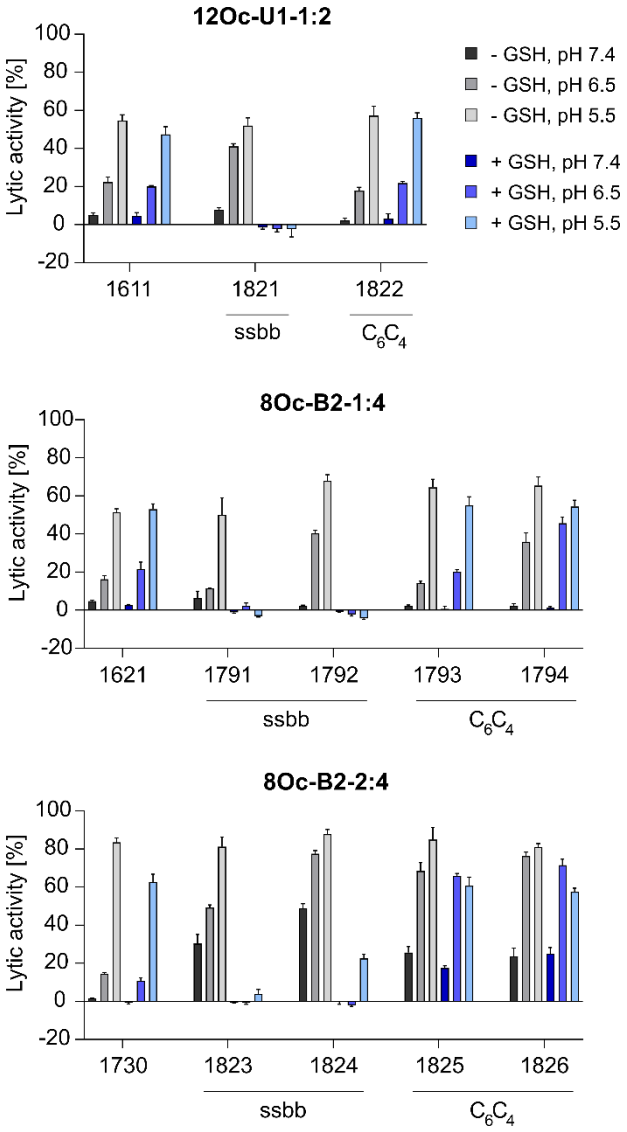

Figure 4.8. Lytic potential of free LAF xenopeptides evaluated in an erythrocyte leakage assay (n = 4; mean ± SD) at a concentration of 1.25 µM LAF carrier at three different physiological relevant pH values (pH 7.4, 6.5, 5.5). GSH treated xenopeptides were incubated with 10 mM GSH in PBS adjusted to the indicated pH at 37 °C for 90 min. PBS-treated erythrocytes were set to 0% lytic activity. 1% Triton X-100 served as positive control and was set to 100% lytic potential.

4.4.3.2 pDNA and mRNA transfection efficacy

The novel xenopeptides of the ***1611***, ***1621*** and ***1730*** series were screened as pDNA and mRNA polyplexes in luciferase expression assays. The cervix carcinoma cell line HeLa, known to possess high intracellular concentrations of glutathione,(528) was selected as first cell line of choice to evaluate the transfection efficiency and biocompatibility of the reducible and non-reducible carriers (**Figure 4.9**). Similar as outlined for the physico-chemical properties,

demands on the xenopeptide carrier differ significantly between pDNA transfer (**Figure 4.9 A, B**) and mRNA transfer (**Figure 4.9 C, D**). In the current work, with the 8Oc-B2-2 : 4 bundle structure ***1730*** a superior pDNA carrier was identified, whereas ***1730*** cannot meet the known high mRNA transfection efficiency of 8Oc-B2-1 : 4 bundle structure ***1621***.

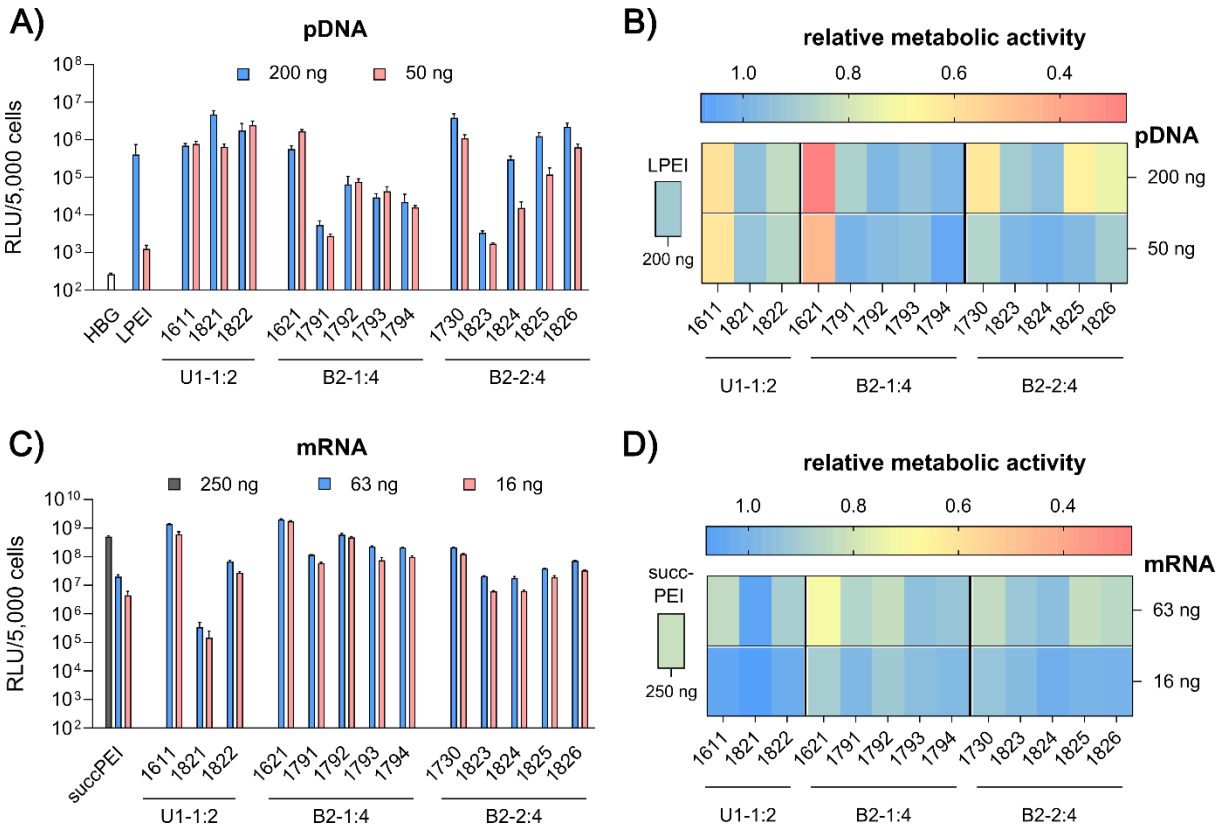

Figure 4.9. *In vitro* screening of the library of LAF–Stp xenopeptides applied in pDNA polyplexes (A and B) or mRNA polyplexes (C and D) on HeLa cells. pDNA polyplexes were formed at N/P 18 and mRNA polyplexes were formed at N/P 18 (12Oc-U1-1 : 2 carriers), N/P 24 (8Oc-B2-1 : 4 carriers) and N/P 12 (8Oc-B2-2 : 4 carriers). LPEI polyplexes were formed at N/P 6 and succPEI polyplexes were formed at w/w ratio 4. Polyplexes were transfected at the indicated nucleic acid doses per well. (A and C) Transfection efficiency determined by luciferase expression assay after 24 hours of incubation (n = 3 ± SD). (B and D) Cell viability measured by CellTiter Glo® assay in relation to control wells treated with HBG (n = 3 ± SD). The biological evaluation of mRNA polyplexes was kindly performed by Sophie Thalmayr (Pharmaceutical Biotechnology, LMU Munich)

pDNA. pCMVLuc polyplexes were formed at N/P 18, since at this ratio all carriers form stable, nano-sized polyplexes (**Figure 4.3**), and tested in 200 ng high and 50 ng low pDNA doses on HeLa cells (**Figure 4.9 A, B**). The 'gold standard' for pDNA transfections, LPEI (189, 522), was included for comparison and mediated the expected high luciferase gene expression, but at the high dose only. At this dose, no toxicity was observed. The standard U1-shape ***1611*** shows similar high transfection levels at both high and low dose. Metabolic activity of ***1611*** polyplexes, as determined by CellTiter Glo® assay, however, was significantly reduced (**Figure 4.9 B**) but could be recovered to >80% relative metabolic activity with the novel reducible and non-reducible spacer xenopeptide analogs (***1821*** and ***1822***, respectively) while maintaining high

transfection efficacy at both dose levels. In fact, the bioreducible carrier ***1821*** mediated a 11.6-fold higher gene transfer than LPEI at the same dose. The ***1611*** series was also screened for transfecting N2a cells as well as Huh7 cells at 200 ng pDNA dose (**Figure 4.10**). Here, neither standard ***1611*** nor the novel analogs did considerably affect metabolic activity of cells, and the ***1611*** series mediated a transfection activity outperforming LPEI by 5- to ~100-fold. The novel 8Oc-B2-2 : 4 carrier ***1730*** exceeded the transfection efficiency of both LPEI and ***1621*** on all investigated cell lines (HeLa, **Figure 4.9**; N2a and Huh7 cells, **Figure 4.10**). Furthermore, ***1730*** reaches or even exceeds transfection efficiencies of ***1611*** polyplexes. The disulfide-spacer analogs (***1823*** and ***1824***) loose transfection activity on HeLa cells, whereas the non-reducible spacer analogs (***1825*** and ***1826***) display activity similar as ***1730***. Spacer effects are less pronounced in the other cell lines (**Figure 4.10**). The ***1621*** series was least suitable for pDNA apart from standard ***1621***, which however displayed cytotoxicity. Analogs with disulfide or non-reducible spacer improved metabolic activity at the expense of reduced pDNA transfection efficiency (**Figure 4.9 B** and **Figure 4.10 D**).

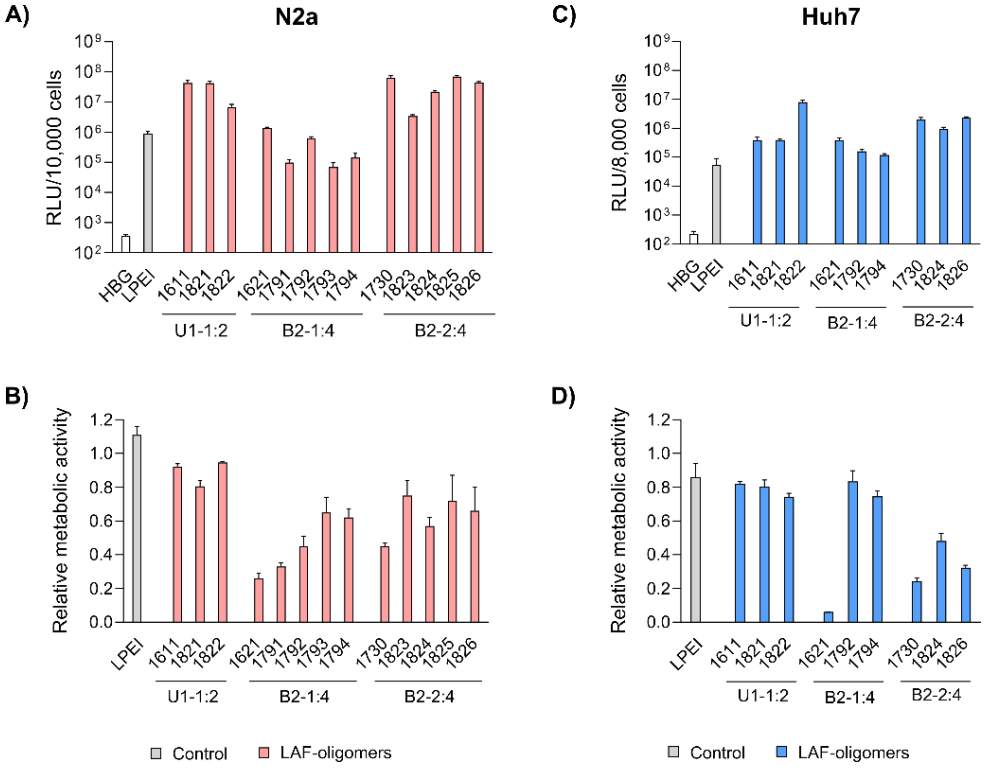

Figure 4.10. *In vitro* screening of pDNA polyplexes containing LAF-Stp oligomers. Polyplexes were formed with the carriers of the library formed at N/P 18 on N2a cells (A and B; 10,000 cells/well) and Huh7 cells (C and D; 8000 cells/well). As control, LPEI (at N/P 6) was transfected. All polyplexes contained 200 ng pDNA per well. Transfection efficiency was determined by luciferase expression assay and cell viability was determined by CellTiter Glo® assay (n=3 +SD), both after 24 hours of incubation. Experiments to evaluate transfection activity and cell viability of Huh7 cells were performed by Eric Weidinger (Pharmaceutical biotechnology, LMU Munich).

mRNA. Carrier demands were significantly different for mRNA delivery. The novel carriers were tested at the low doses of 63 ng or 16 ng FLuc mRNA. SuccPEI was used as established positive control(70, 517) also including a higher, non-toxic 250 ng mRNA dose.

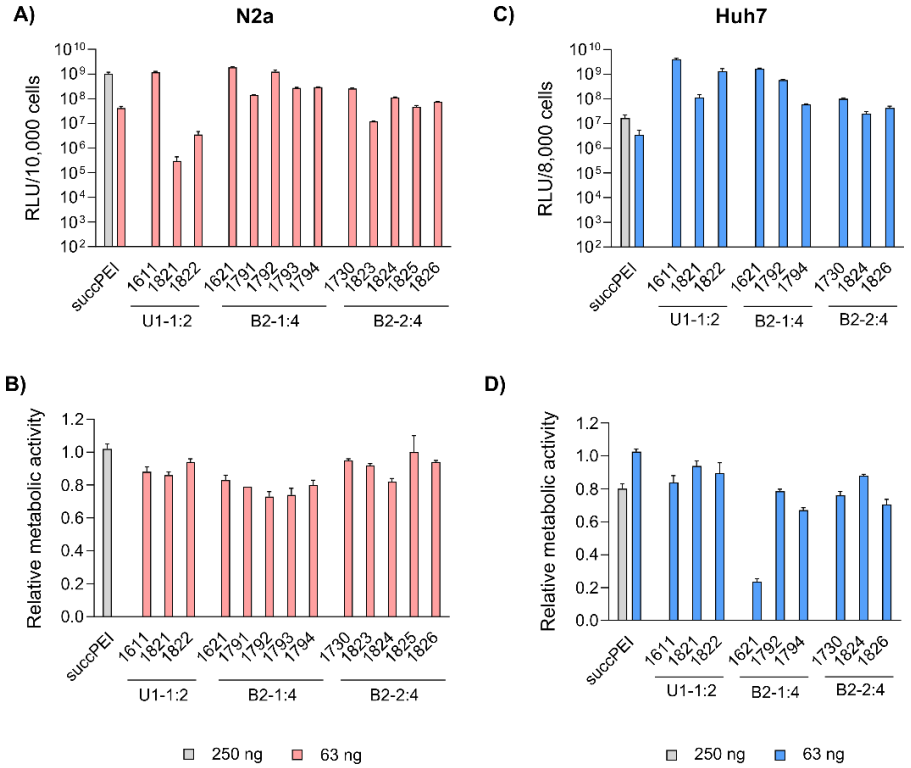

Figure 4.11 *In vitro* screening of mRNA polyplexes containing LAF-Stp oligomers of the library. The polyplexes were formed at N/P 18 (12Oc-U1-1:2 carriers), N/P 24 (8Oc-B2-1:4 carriers) and N/P 12 (8Oc-B2-2:4 carriers) containing 63 ng mRNA per well or with succPEI (w/w ratio 4) containing either 250 ng or 63 ng mRNA per well and transfected to N2a and (A and B; 10,000 cells/well) and Huh7 cells (C and D; 8000 cells/well). Transfection efficiency was determined by luciferase expression assay and cell viability was measured by CellTiter Glo® assay (n=3 +SD), both after 24 hours of incubation. The data were kindly provided by Sophie Thalmayr and Eric Weidinger (Pharmaceutical biotechnology, LMU Munich).

The carriers ***1611*** (12Oc-U1-1 : 2) and ***1621*** (8Oc-B2-1 : 4) had outstanding potential for the delivery of mRNA at low and ultra-low doses, with RLU values greater than 10^9 on N2a and Huh7 cells (**Figure 4.11**), consistent with previous findings,(162) whereas ***1730*** (B2-2 : 4) showed slightly reduced mRNA transfection efficacies along all cell lines. Luciferase expression was diminished after modification of the 12Oc-U1-1 : 2 ***1611*** carrier with both, reducible and non-reducible building blocks on HeLa and N2a cells (**Figure 4.9 C** and **Figure 4.11 A, B**), probably as a consequence of the enhanced spacing between the LAF residues and Stp domain. For transfections to Huh7 cells, the non-reducible spacer was beneficial (**Figure 4.10 B** and **Figure 4.11 D**). Even though the modifications had beneficial effects on cell viability of HeLa cells, the disulfide xenopeptide ***1821*** and the non-reducible analog ***1822*** was not or less suitable for mRNA delivery (**Figure 4.9 C, D** and **Figure 4.11 A**). In sharp contrast, regarding the B2 bundles, the 8Oc-B2-1 : 4 ***1621*** series showed overall favorable mRNA transfection efficiency compared to 8Oc-B2-2 : 4 ***1730*** series, making ***1621*** and its

analogs the most promising candidates for mRNA delivery in this study (**Figure 4.9 C** and **Figure 4.11 A, C**). As observed also for pDNA polyplexes, luciferase activity of ***1791*** (B2-1 : 4-ssbb) was substantially reduced, but for ***1792*** (B2-1 : 4-ssbb$_2$) transfection efficacy was high both on HeLa as well as N2a cells (**Figure 4.9 C** and **Figure 4.11 A, C**). The C_6C_4 spacer analogs of the bundles were comparable to the disulfide analogs; dose reduction to 16 ng mRNA per well had no large impact on transfection efficacy on HeLa cells. Relative metabolic activity (**Figure 4.9 D**) was improved for disulfide- and also non-reducible spacer analogs over ***1621*** on HeLa and Huh7 cells (**Figure 4.9 D** and **Figure 4.11 D**). The mRNA transfection efficiency of ***1730*** was lower than ***1621*** across all cell lines, and additional spacing, either by disulfide or non-reducible spacer, leads to slight decrease of transfection efficacy. The disulfide-oligomers ***1823*** and ***1824*** showed reduced cytotoxicity against HeLa over both, original ***1730*** and non-reducible spacer-analogs ***1825*** and ***1826***. Overall, less effects on metabolic activity were observed than for pDNA polyplexes, which might be due to overall lower doses of mRNA.

In summary, the particular characteristics of each cell line influenced both transfection efficiency and metabolic activity of cells. The reducible and non-reducible analogs of ***1611*** (12Oc-U1-1 : 2) and ***1730*** (8Oc-B2-2 : 4) were identified as promising candidates for efficient pDNA delivery with improved metabolic cell activity. In case of mRNA, ***1792*** and ***1794***, the bis-modified analogs to ***1621***, were defined as encouraging oligomers with improved cell viability. A strong benefit of the disulfide spacer was most clearly found on HeLa cells, which are known for their high intracellular GSH levels. In the case of Huh7 and N2a cells other intracellular mechanisms causing or preventing cytotoxicity may apply which are independent of bioreduction. This hypothesis is further stressed by the positive impact of the non-reducible spacers on both transfection efficacy and cell viability.

4.4.3.3 Transfections of human colon carcinoma cells

Human colorectal carcinoma cell lines (COGA) had been established in a previous clinically approved study from human tumors, cultivated to low passage numbers and characterized in detail.(536) They show high level of similarity to their original cancers, resembling in key characteristics such as phenotype and marker expression. For this reason, they represent suitable cell materials for evaluating non-viral carriers for gene therapy of colon cancer. Two types of COGA cells were used in the present study, both expressing epithelial markers CK8, CK19 and CK20 and having tumorigenic properties. COGA-2 represents poorly differentiated cells with a ‘rounded-up’ morphology, lacking E-cadherin at plasma membrane and epithelial adherent junctions, containing p53 and K-ras mutations, and activated Wnt-signaling/nuclear β-catenin. COGA-12 cells accumulate in a ‘piled-up’ morphology, express E-cadherin displayed at plasma membrane, lacking p53 and K-ras mutations or activated Wnt signaling.

Optimized lipo-polyplexes containing a mixture of PEI and cationic lipids have been previously reported to be effective for gene transfer to COGA cells.(542) Thus, our LAF–Stp xenopeptides presenting amphiphilic, double pH-responsive characteristics combining the benefits of the former carrier systems were hypothesized as promising gene transfer agents for COGA cells. In fact, using the best performing carriers from previous screening we were able to achieve efficient transfection both with pDNA (**Figure 4.12 A**) and mRNA (**Figure 4.12 B**).

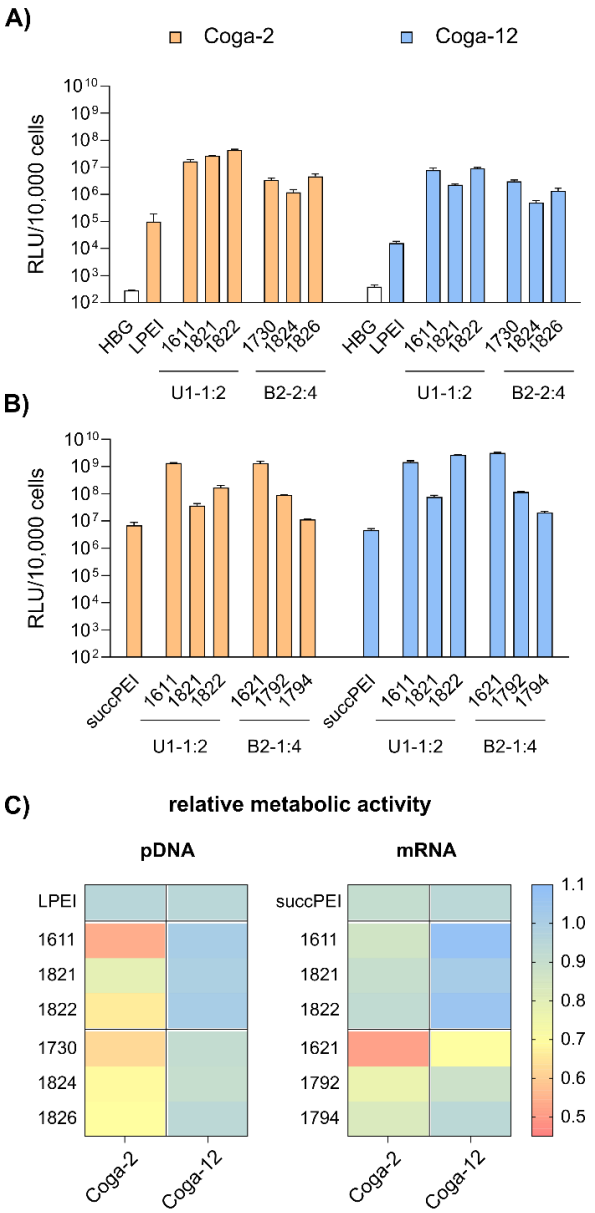

Figure 4.12. Transfections of LAF carriers on Coga-2 and Coga-12 colon carcinoma cells. (A) Luciferase gene expression of colon carcinoma cells at 24 hours after transfection of pDNA polyplexes (n = 3, mean + SD). The polyplexes were formed at N/P 18 and contained 50 ng pDNA per well with a concentration of 10 µg mL^{-1} pDNA. As control, LPEI polyplexes (N/P 6) were used. (B) Luciferase gene expression of colon carcinoma cells at 24 hours after transfection of mRNA polyplexes (n = 3, mean + SD). The cells were treated with polyplexes formed at N/P 18 (12Oc-U1-1 : 2) or N/P 24 (8Oc-B2-1 : 4) containing 31 ng mRNA per well with a concentration of 12.5 µg mL^{-1}. As control, succPEI (w/w ratio 4) was used. (C) Relative metabolic activity of Coga-2 and Coga-12 cells treated with pDNA- (left) or mRNA-polyplexes (right) at 24 hours after transfection determined by CellTiter Glo® assay (n = 3). The experiments were performed by Sophie Thalmayr and Miriam Höhn (Pharmaceutical biotechnology, LMU Munich).

The LAF carriers outperformed LPEI/pDNA and succPEI/mRNA polyplexes, respectively, on both cell lines up to >100-fold (**Figure 4.12**). Only COGA-2 but not COGA-12 cells displayed significantly reduced metabolic activity upon transfection with the xenopeptides ***1611***, ***1621*** and ***1730*** lacking inserted spacers. Importantly, similar as observed with HeLa cells, spacer-modified xenopeptides improved metabolic activity profiles.

4.4.4 Cellular mechanisms of transfection

4.4.4.1 Cellular association and GFP expression

HeLa cells were treated with the top performing mRNA polyplexes from the initial screening (***1621***, ***1792*** and ***1794***). Cellular association and uptake, as well as transfection efficacy were evaluated by flow cytometer analysis at indicated time points between 30 min and 48 hours after polyplex treatment (**Figure 4.13 A, B**). Cell association of polyplexes containing Cy5-labelled mRNA was detected for over 60% of the cells for ***1621*** and ***1792*** within just 30 min, while ***1794*** demonstrated slower cell association and uptake kinetics. Once an almost complete cell association and uptake was achieved, both non-reducible LAF-carriers, ***1621*** and ***1794***, maintained a high level of Cy5-positive cells, whereas the ratio decreased for ***1792***, indicating the degradation of the bioreducible carrier, polyplex dissociation and the then more exposed Cy5-labeled mRNA cargo.

The kinetics of the cell association and uptake showed a strong correlation with the expression of GFP. After polyplex treatment, ***1621*** showed a rapid increase in GFP-expression, with 100% GFP-positive cells after 4 hours. Although the modified analogs exhibited moderately delayed (***1792***) or slow (***1794***). GFP-expression kinetics, both ultimately generated GFP-fluorescence in approx. 90% of the cells at 24 hours after transfection. Regarding ***1792***, GFP expression was found to decrease at 48 hours, providing further support for the previous findings of the cell association study.

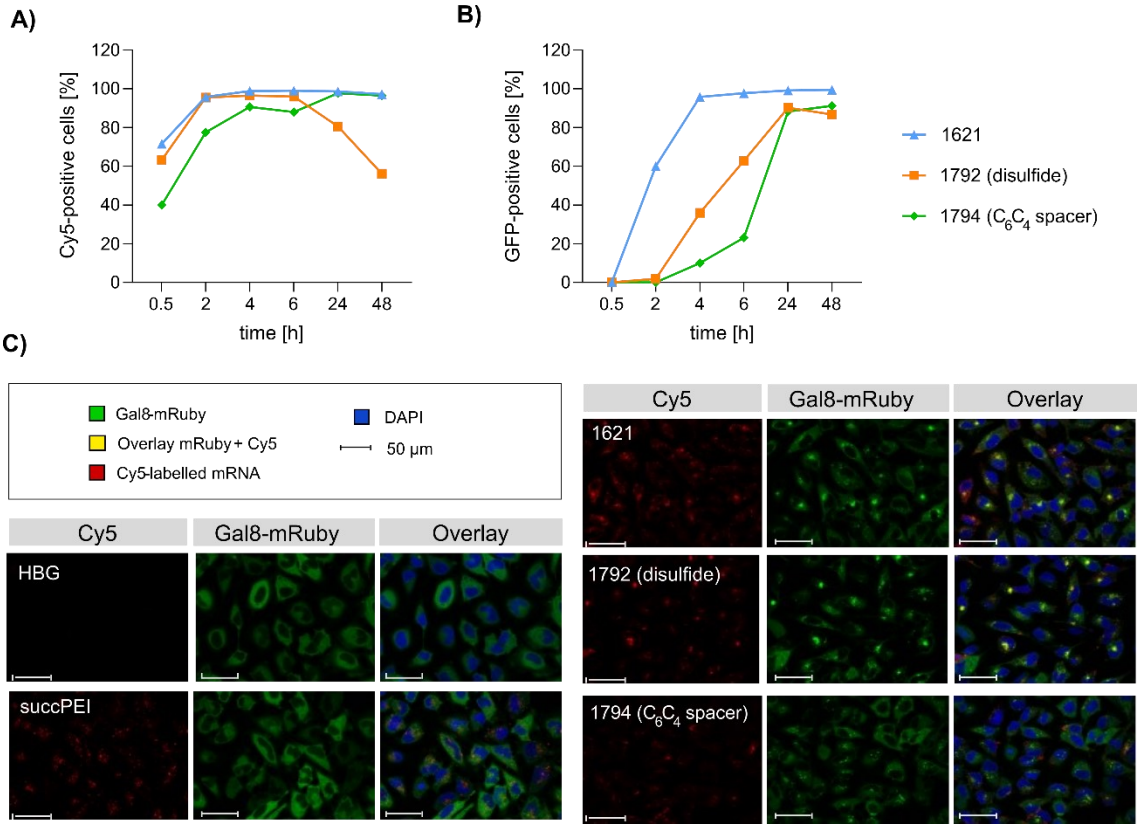

Figure 4.13. Mechanistic studies. (A and B) Flow cytometry analysis of HeLa cells treated with mRNA polyplexes. The polyplexes were formed with the indicated xenopeptides and 100 ng per well of cargo containing Cy5-Luc mRNA (20% (w/w)) and GFP-mRNA (80% (w/w)) with an N/P ratio of 24 (12.5 µg mL^{-1} total mRNA) and transfected to 18 000 HeLa cells per well. Cells were analyzed by flow cytometry at the indicated time points. (A) Cell association and cellular uptake of mRNA polyplexes by HeLa cells presented by Cy5-positive cells. (B) GFP expression as measure of transfection efficacy. (C) Endosomal disruption evaluated in HeLa-Gal8-mRuby cells treated with mRNA polyplexes formed with the indicated xenopeptide in comparison to succPEI (w/w 4) at a mRNA dose of 47 ng at 4 hours after transfection by confocal laser scanning microscopy (CLSM). Redistribution of cytosolic Gal8-mRuby fluorescence (green) from cytosol (see HBG control) to an intracellular punctuate vesicle pattern represents endosomal membrane disruption. The experimental data were kindly provided by Sophie Thalmayr, Eric Weidinger and Miriam Höhn (Pharmaceutical biotechnology, LMU Munich).

4.4.4.2 Galectin-8 assay monitoring endosomal destabilization

Confocal laser scanning microscopy of HeLa-Gal8-mRuby cells(154, 534, 535) revealed an enhanced endosomolytic activity of ***1621*** and ***1792*** over succPEI and ***1794*** mRNA polyplexes (**Figure 4.13 C** and **Figure 4.14**). This was indicated by the punctuate green fluorescent pattern of the galectin-8 mRuby fusion protein, which is caused by the interaction of Gal8 with galactans presented on the inside of disrupted endosomal membranes. The signal increased from 2 hours to 4 hours post transfection, especially for LAF carriers ***1621*** and ***1792***, as cellular trafficking and endosomal release progressed. Without treatment, Gal8-mRuby cannot contact intravesicular galactans and is evenly distributed within the cytosol (compare HBG buffer control). The overlay of Cy5 mRNA and Gal8 signals further reveals high endosomal uptake of ***1621*** and ***1792*** polyplexes at a low mRNA dose of 47 ng. A weaker Cy5 mRNA signal was detected by CLSM for succPEI and ***1794*** mRNA polyplexes. Nevertheless, flow cytometry demonstrated that over 80% of HeLa cells were Cy5-positive after treatment with only 10%

were GFP positive after 4 hours, supporting the observation of a retarded ***1794*** polyplex uptake.

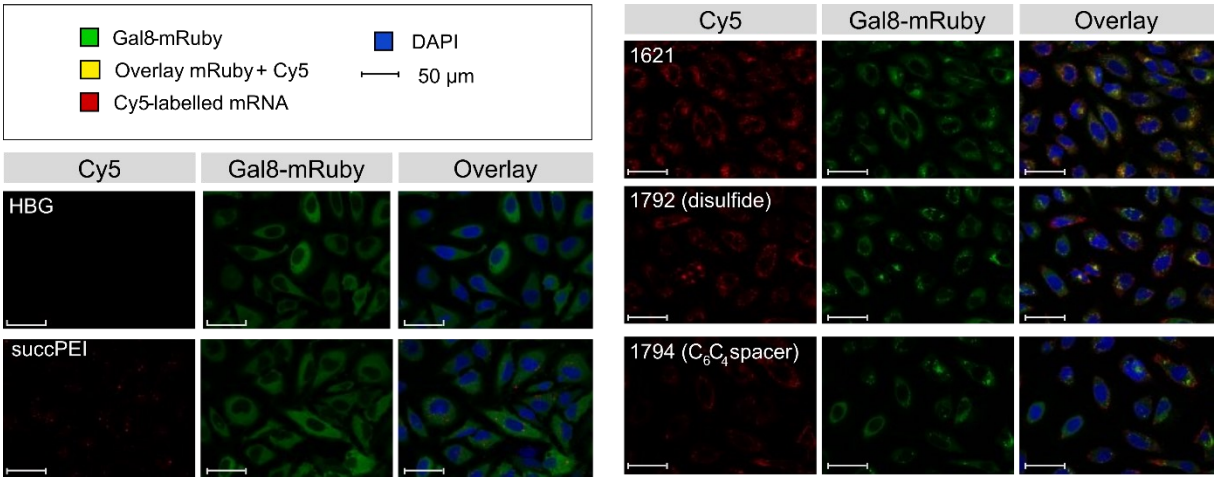

Figure 4.14. Endosomal disruption evaluated in HeLa-Gal8-mRuby cells treated with mRNA-polyplexes formed with the indicated LAF-oligomers in comparison to succPEI (w/w 4) at an mRNA dose of 47 ng at 2 hours after transfection by confocal laser scanning microscopy (CLSM). Punctuate redistribution of cytosolic Gal8–mRuby fluorescence (green) represents endosomal membrane disruption. The experimental data were kindly provided by Sophie Thalmayr and Miriam Höhn (Pharmaceutical biotechnology, LMU Munich).

4.4.4.3 Bafilomycin A1 assay addressing the role of endosomal acidification

In addition to the mechanistic studies investigating the kinetics of cellular uptake and gene transfer activity, transfection efficiency was tested in the presence of bafilomycin A1 (BafA1) (**Table 4.3** and **Figure 4.15**). BafA1 prevents the acidification during endosomal maturation by inhibiting the endo/lysosomal vacuolar-type H^+-ATPase, which can lead to decreased endosomal escape and transfection efficiency. Previous studies have shown that LAF carriers with a higher Stp content and certain topologies, especially U-shapes, are more dependent on acidification to achieve high transfection levels.(107, 162)

Table 4.3. Effect of bafilomycin A1 on transfection efficiency.

Cargo	Carrier [ID]	Dosis [ng]	Fold decrease -BafA1/+BafA1
mRNA	succPEI	250	156
	1621	63	1
	1792		39
	1794		11
pDNA	LPEI	200	2384
	1611	100	3
	1821		502
	1822		12
	1730	100	324
	1824		122
	1826		39

HeLa cells were pre-incubated with BafA1 30 min prior to polyplex treatment and transfected with the indicated LAF-Stp polyplexes (mRNA: LAF polyplexes at N/P 24, succPEI w/w 4; pDNA: LAF polyplexes at N/P 18, LPEI N/P 6). Luciferase activity of cells treated with mRNA polyplexes was determined at 4 hours after transfection. pDNA polyplexes were allowed to incubate for further 20 h in BafA1-free medium (after 4 hours incubation with BafA1) before read-out by luciferase expression assay. The fold decrease of relative light units detected in cells treated with BafA1 compared to cells without BafA1 treatment was calculated.

This was confirmed by the present work, where the B2-2 : 4 bundle ***1730*** showed high sensitivity to BafA1, with a 324-fold decreased gene transfer activity in presence of BafA1, whereas ***1621*** (B2-1 : 4) was independent of the pH value. This observation is in accordance with the results of the erythrocyte leakage assay, where the lytic activity of B2-2 : 4 carriers was also strongly pH dependent (compare **Figure 4.8**). ***1730*** has a stronger interaction and consequently denser compaction of DNA than ***1621***, due to the additional protonatable Stp unit (as supported by the EtBr exclusion assay, **Figure 4.5**). This, in turn, leads to a greater dependence on lower pH values for xenopeptide solubilization and efficient release of the cargo. In accordance with the lytic potential towards erythrocytes, the analogs of ***1730*** were less sensitive to BafA1. ***1611*** polyplexes were moderately dependent of endosomal acidification (3-fold inhibition by bafilomycin), as previously observed also in other cell lines(162). ***1611*** and ***1621*** spacer analogs, however, were more dependent on endosomal acidification, especially the disulfide-containing xenopeptides (39- and 502-fold inhibition by bafilomycin).

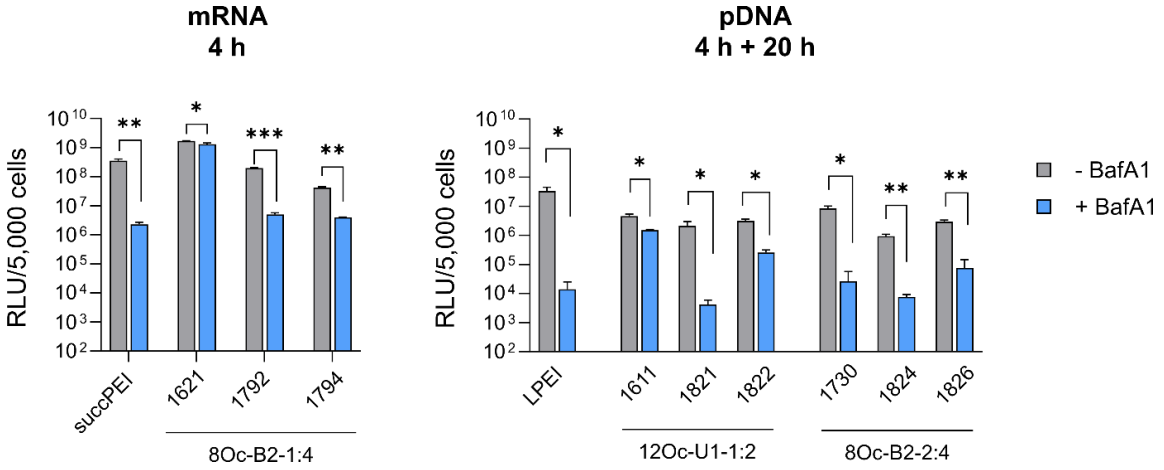

Figure 4.15. Luciferase expression of 5000 HeLa cells/well treated with the indicated polyplexes in absence or presence of Bafilomycin A1 (BafA1) for evaluation of the influence of endosomal acidification on transfection efficiency. The cells were transfected with mRNA or pDNA polyplexes in the presence of 200 nM BafA1. A) The mRNA polyplexes were formed with LAF-carriers of the 8Oc-B2-1:4 topology (***1621*** – original, ***1792*** – disulfide, ***1794*** – spacer) at N/P 24 containing 31 ng Luc-mRNA per well, compared to succPEI (w/w 4, 250 ng mRNA) and incubated for 4 hours in presence of BafA1. Read-out after 4 h via luciferase expression assay (n = 3; mean ± SD). B) pDNA polyplexes were formed with the carriers of either 12Oc-U1-1:2 (***1611*** – original, ***1821*** – disulfide, ***1822*** – spacer) or 8Oc-B2-2:4 (***1730*** – original, ***1824*** – disulfide, ***1826*** – spacer) topology at N/P 18 containing 100 ng pDNA, compared to LPEI (N/P 6, 200 ng). The polyplexes were incubated on the cells in presence of BafA1 for 4 h, followed by medium change and further 20 h of incubation before readout via luciferase expression assay. Significance levels: ns $p > 0.05$; *$p \leq 0.05$; **$p \leq 0.01$; ***$p \leq 0.001$; ****$p \leq 0.0001$. The bafilomycin assay was kindly performed by Sophie Thalmayr (Pharmaceutical biotechnology, LMU Munich).

4.4.5 Investigations on cell viability and proliferation

Preceding screening experiments revealed that the outstanding potential of LAF–Stp carriers is often associated with reduced metabolic activity of transfected cells. While cells treated with HBG and LPEI exhibited unaltered cell proliferation, those transfected with polyplexes of the original xenopeptides ***1611*** and ***1621*** demonstrated a reduced confluency after a 24-hour incubation period (**Figure 4.16**). In contrast, cells treated with disulfide spacer-containing xenopeptide polyplexes showed similar confluency as the non-toxic controls HBG and LPEI, supporting favorable effects of the biodegradable carriers, which became only moderately evident by the metabolic activity assay thus far. In addition to the initial evaluation of cell viability with the results gleaned from CellTiter-Glo® assays, supplementary assays were performed to develop a deeper understanding about the influence of the LAF–Stp xenopeptides on cell viability.

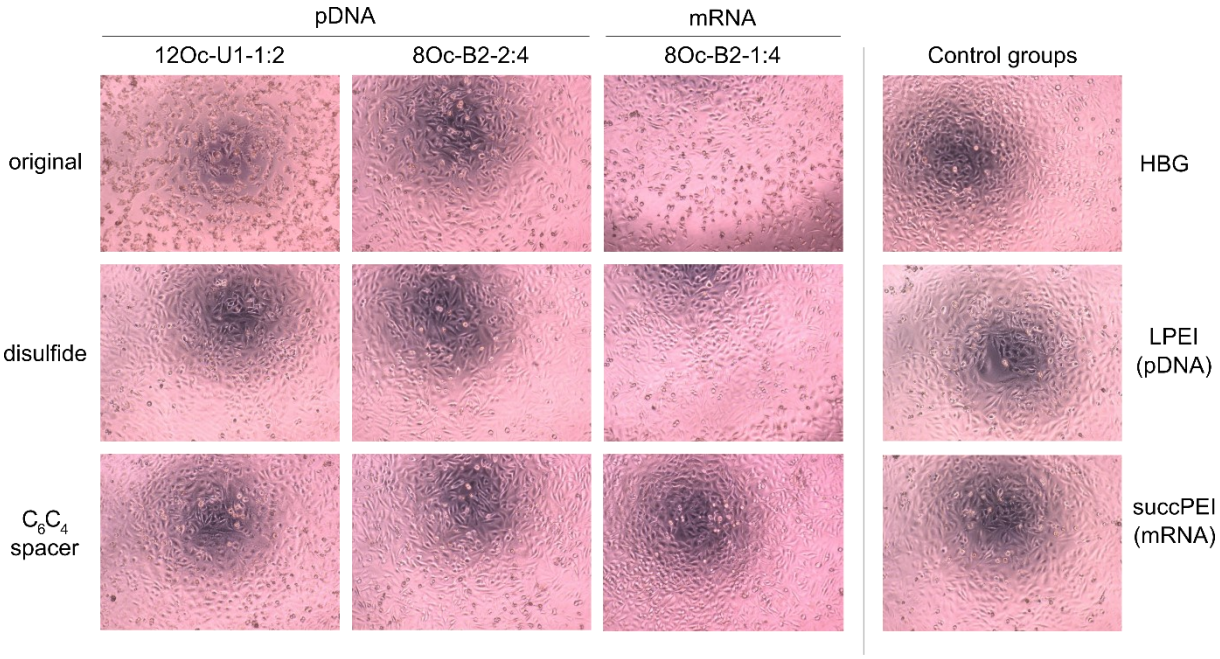

Figure 4.16. Microscopic pictures of HeLa cells at 24 hours after transfection with pDNA- and mRNA-polyplexes in comparison to controls. DNA-polyplexes were formed with the indicated carriers at N/P 18 for LAF-polyplexes and N/P 6 for LPEI (100 ng pDNA/well) and mRNA-polyplexes were formed at N/P 24 for LAF-polyplexes and w/w 4 for succPEI (63 ng mRNA/well). Cells were covered with DMEM low glucose medium.

4.4.5.1 LDH release assay

While the CellTiter Glo® assay detects metabolically active cells by ATP-dependent formation of oxyluciferin, the LDH release assay is based on colorimetric quantification of lactate dehydrogenase (LDH), a cytosolic enzyme that is released upon impairment of cellular membrane integrity into the surrounding medium. Membrane damage was indicated by the appearance of cellular debris 24 hours after polyplex treatment in connection with reduced confluency during microscopic examination in case of the original xenopeptide structures

(**Figure 4.15**). To perceive insights in time-dependent dynamics of plasma membrane disruption following polyplex transfection, LDH release assays were conducted at multiple time points including 8, 12, 16 and 24 hours after transfection (**Figure 4.17**).

Intriguingly, no LDH release was detected at 8 hours, suggesting that the carriers do not induce immediate membrane damage upon cellular exposure, or shortly after endosomal escape which started after about 4 hours, as indicated by CLSM analysis (**Figure 4.13 C**). For 12Oc-U1-1 : 2-pDNA polyplexes lacking bio-degradable domains, *i.e.*, ***1611*** and the spacer analog ***1822***, LDH release became detectable at 12 hours after transfection. While LDH release continued to rise for ***1611*** up to the 24 hours-mark, cells treated with the ***1822*** (12Oc-U1-1 : 2-spacer) exhibited a decline after reaching a peak at 16 hours. In contrast, for the bio-reducible polyplexes formed with ***1821***, no release of LDH was prompted, emphasizing the beneficial effect of the disulfide spacer (**Figure 4.17 A**). For the 8Oc-B2-2 : 4 analogs, LDH release was absent in case of the disulfide analog ***1824***, but to some extent measurable for polyplexes with the non-reducible ***1730*** and ***1826*** xenopeptides after 24 hours post-transfection (**Figure 4.17 B**). Notably, cells treated with mRNA polyplexes of the ***1621*** series demonstrated an LDH release profile comparable to those transfected with the structurally similar ***1730*** series, even though they delivered different cargo molecules. Within the ***1621*** series, the original xenopeptide exhibited the highest LDH release, and modification with disulfide spacers led to a moderate reduction in cytotoxicity, while the non-reducible spacer displayed no membrane damage at all (**Figure 4.17 C**). These findings support prior observations derived from the CellTiter-Glo® assay. By the LDH release assay, a disulfide dependent benefit on cell viability became evident at least for cells treated with pDNA polyplexes. Additionally, cell viability was improved for spacer-modified carriers in mRNA polyplexes, irrespective of reducible or non-reducible chemistry.

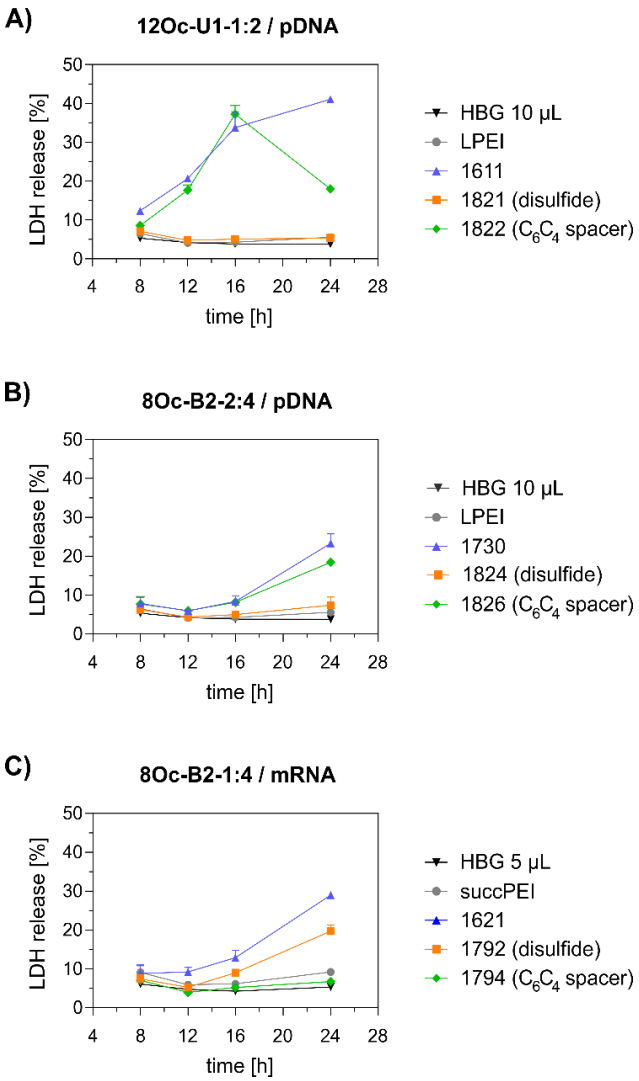

Figure 4.17. LDH release after transfection of HeLa cells with pDNA polyplexes (12Oc-U1-1 : 2 and 8Oc-B2-2 : 4 series) formed at N/P 18 at a dose of 100 ng pDNA per well (A and B) and with mRNA polyplexes (8Oc-B2-1 : 4 analogs) formed at N/P 24 at a mRNA dose of 63 ng per well (C). LDH release was detected at 8, 12, 16 and 24 hours after transfection by an enzymatic reaction with iodonitrotetrazoliumchlorid leading to formation a purple formazan product. Each polyplex was transfected as triplicate. Absorbance of the formazan product was determined at 490 nm. LDH release was calculated in relation to cells treated with lysis buffer (representing maximum LDH release). This experiment was performed in collaboration with Sophie Thalmayr (Pharmaceutical biotechnology, LMU Munich)

4.4.5.2 Cell proliferation after polyplex treatment

As the microscopic images recorded at 24 hours after polyplex treatment and the selected cell viability assays (CellTiter Glo® and LDH release assay) have demonstrated a positive influence of the disulfide and hydrophobic spacer xenopeptides on cell viability, the cells were further analyzed by monitoring the cell growth.

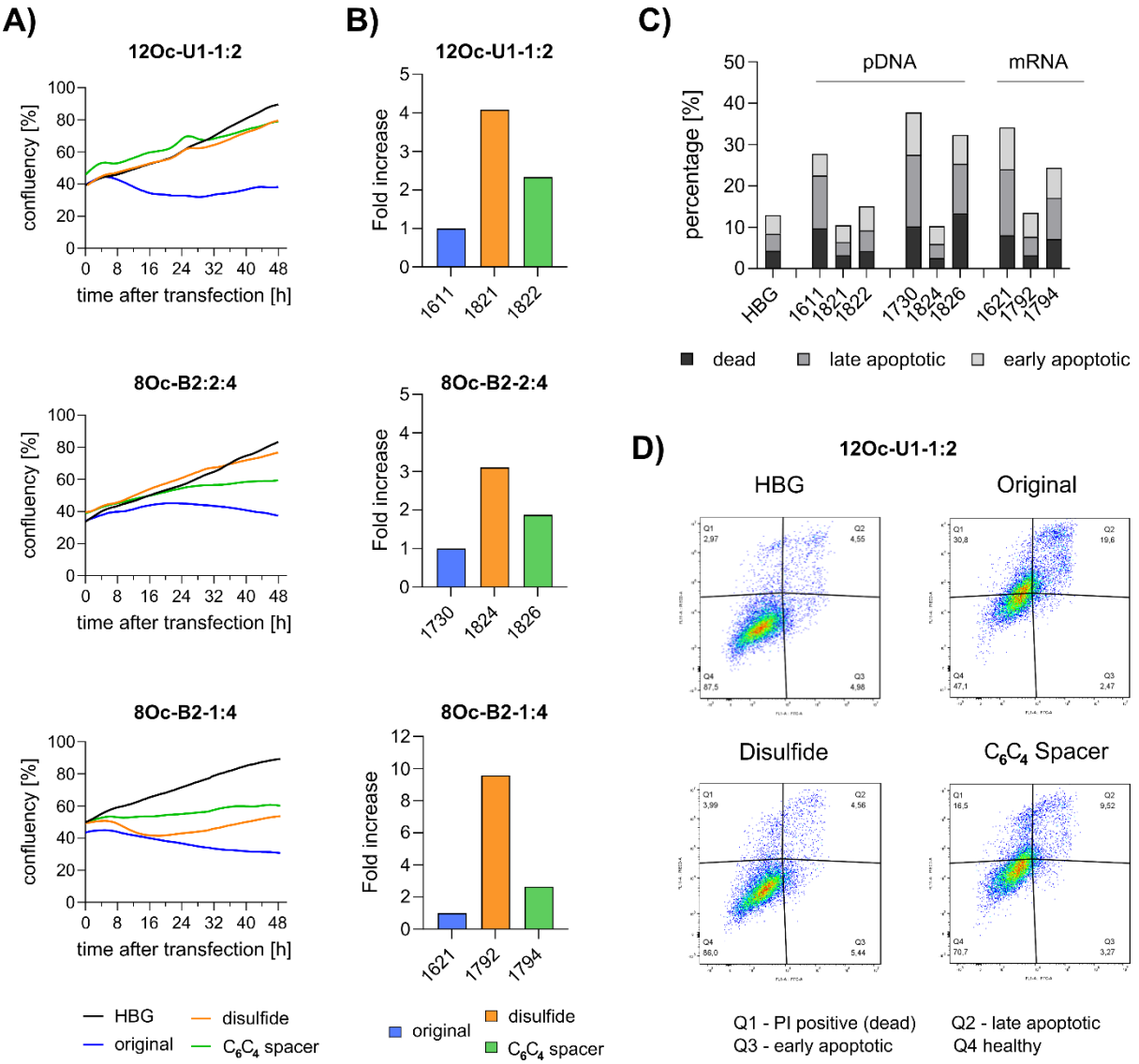

Figure 4.18. Cell proliferation after polyplex treatment. A) Time-dependent monitoring of cell growth using Cell Watcher M (PHIO Scientific, Munich, Germany) over 48 hours after transfection of polyplexes. 12Oc-U1-1:2 and 8Oc-B2-2:4: pDNA polyplexes at N/P 18, 8Oc-B2-1:4: mRNA polyplexes at N/P 24. Confluency of cells was determined automatically every 30 minutes. Black: HBG control; blue: original xenopeptide; orange: disulfide-spacer; green: non-reducible spacer xenopeptide. B) Flow cytometer analysis of HeLa cells at 24 hours after transfection. Cells were treated with pDNA-polyplexes formed with analogs of 12Oc-U1-1:2 topology or 8Oc-B2-2:4 carriers at N/P 18 or mRNA polyplexes formed with 8Oc-B2-1:4 carriers at N/P 24. HeLa cells were analyzed for a constant time of 60 seconds and a flow rate of 170 µL min-1. Only DAPI-negative cells were counted. C) and D) Annexin/PI assay on HeLa cells (40,000 cells/well in a 24-well plate) at 24 hours after treatment with pDNA polyplexes formed with either 12Oc-U1-1:2-analogs or 8Oc-B2-2:4-analogs at N/P 18 in comparison to HBG-buffer treated cells (pDNA dose = 125 ng/well) or mRNA polyplexes formed with 8Oc-B2-1:4-analogs at N/P 24 in comparison to HBG-buffer treated cells (mRNA dose = 78 ng/well). C) Overview of the complete data set. D) Exemplarily dot plot of selected data set of 12Oc-U1-1:2 polyplexes at a pDNA dose of 125 ng/well. The experiments were conducted in collaboration with Sophie Thalmayr and Eric Weidinger (Pharmaceutical biotechnology, LMU Munich).

First, for a detailed investigation of the cell proliferation subsequent to transfection, the cells were monitored in a time-resolved manner using a Cell Watcher Instrument (**Figure 4.18 A**). For the ***1611*** series, decline of cell growth was observed beginning 6 hours after transfection, whereas the ***1821*** and ***1822*** showed confluency curves similar to HBG-treated cells. In case

of the bundle structures, cells treated with polyplexes consisting of the original xenopeptides complexed with either pDNA (8Oc-B2-2 : 4) or mRNA (8Oc-B2-1 : 4), cell growth was inhibited as observed by an about 8 to 20 hours shifted increase in confluency after transfection. This finding supports the hypothesis that toxicity occurs not directly upon polyplex exposure but after internalization and probably endosomal escape, starting after 4 hours incubation for ***1621*** and ***1792***. The xenopeptide spacer analogs of ***1621*** showed also a decelerated, almost stagnated cell proliferation. Overall, the proliferation of cells incubated with pDNA polyplexes formed with disulfide-analogs of either 8Oc-B2-2 : 4 or 12Oc-U1-1 : 2 occurred in a similar manner as HBG-treated control cells with a constant increase. An exception is the ***1792*** mRNA polyplex (8Oc-B2-1 : 4-ssbb$_2$), which, in contrast to other disulfide analogs, showed a decrease in confluence at 8 hours post transfection, but recovered after 16 hours, highlighting the results of the LDH assay.

Second, at 24 hours after transfection, viable cells were counted by flow cytometry (**Figure 4.18 B**). The analysis revealed an about three to four-fold increase of healthy cells for disulfide-spacer xenopeptide pDNA polyplexes formed with 12Oc-U1-1 : 2 or 8Oc-B2-2 : 4 carriers. For mRNA polyplexes, an about 10-fold increase in number of healthy cells was found upon transfection with ***1792*** (8Oc-B2-1 : 4-ssbb$_2$). In all cases, a slight increase (approx. 2-fold) of viable cell numbers was detected for non-reducible spacer xenopeptide analogs of each topology, independent of the nucleic acid cargo.

4.4.5.3 Influence of xenopeptide spacers on apoptotic pathways

The results of the experiments monitoring cell proliferation indicated a spacer-dependent influence on cell growth after polyplex treatment. An annexin V/propidium iodide assay was performed to gain additional insights in the pathway causing reduced cell viability of the non-reducible (both, spacer-modified and unmodified) LAF–Stp polyplexes (**Figure 4.18 B, C** and **Figure 4.19**). The assay revealed (slightly) increased ratio of late apoptotic or necrotic cells at 24 hours after treatment with standard LAF–Stp xenopeptide polyplexes independent of the nucleic acid payload, but stronger promoted for xenopeptides with bundle topology, as determined by flow cytometry analysis at a constant cell count. An increase of apoptotic cells might be traced back to mitochondrial damage caused by the original xenopeptide carriers which subsequently initiates signaling cascades resulting in apoptosis. The bioreducible xenopeptides, in contrast, showed largely improved biocompatibility with a maximum of 10% of apoptotic or necrotic cells for HeLa cells treated with pDNA polyplexes and less than 15% for mRNA-treated cells. This further highlights the beneficial effect of GSH-induced biodegradability of the disulfide-spacer carriers.

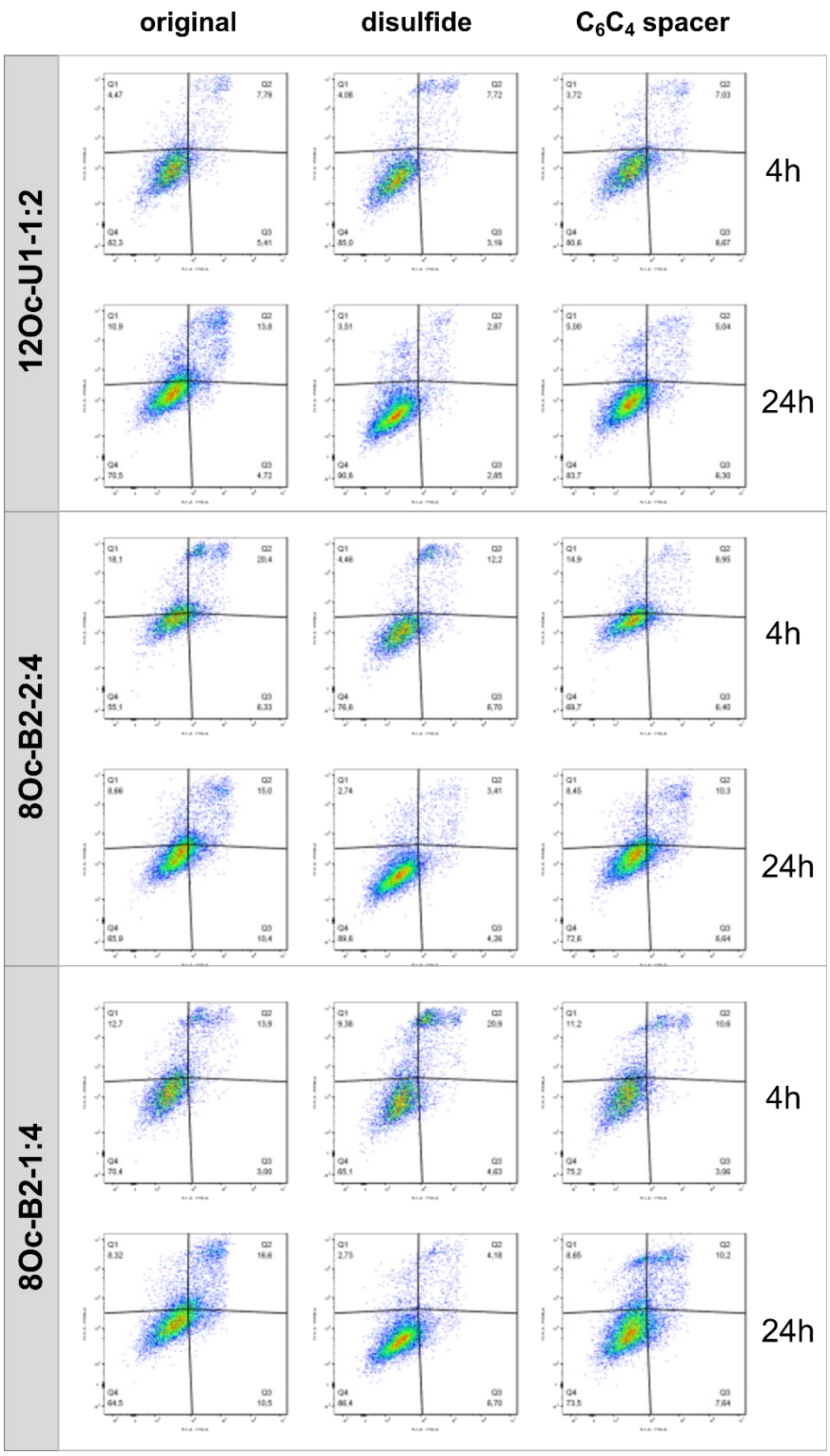

Figure 4.19. Annexin V/propidium iodide assay. Dot plots of flow cytometer analysis of HeLa cells (40,000 cells/well in a 24-well plate) at 4 and 24 hours, respectively after treatment with pDNA polyplexes formed with either 12Oc-U1-1:2-analogs or 8Oc-B2-2:4-analogs at N/P 18 in comparison to HBG-buffer treated cells (125 ng DNA per well) or mRNA polyplexes formed with 8Oc-B2-1:4-analogs at N/P 24 in comparison to HBG-buffer treated cells (78 ng mRNA per well). The experiment was performed together with Eric Weidinger (Pharmaceutical biotechnology, LMU Munich).

4.5 Conclusions

Three different classes of LAF–Stp xenopeptides with proven high efficacy for either pDNA or mRNA delivery were further optimized by inserting bioreducible disulfide spacers and isosteric non-reducible spacers. Interestingly, both types of linkages were found to be effective in modulating transfection efficacy and cellular metabolic responses. The initial physico-chemical and biological screening highlighted the differing demands of either pDNA or mRNA cargo on the xenopeptide Stp/LAF ratio, sequence and topology for polyplex performance. The potency of xenopeptides and their effects on cellular metabolic activity were also found to strongly depend on the selected cell lines. Favorable individual xenopeptide/nucleic acid cargo/target cell combinations were identified for five different cancer cell lines, including low passage number human colorectal carcinoma cells. In some cases, high transfection efficacy was strictly coupled with cytotoxicity at higher dose; modifications relieving toxicity also abolished potency of transfection, suggesting an underlying toxic delivery mechanism. In other cases, inserted spacers improved metabolic cell activity but also maintained or even improved transfection activity. Closer analysis revealed topology-dependent differences between unmodified and spacer-modified carriers regarding cellular association, uptake, dependence on endosomal acidification, and expression kinetics. Spacer xenopeptide based polyplexes showed reduced post-transfection cell membrane damage as detected by LDH release assays. Time-resolved cell growth monitoring detected post-transfection inhibition of cellular proliferation with original LAF xenopeptides and apoptotic events that could be attenuated by spacer integration. Thus, this study gained insights in mechanisms of potent LAF–Stp xenopeptide carriers and options for improving their biocompatibility, thereby paving the way for the development of safe and effective nucleic acid delivery systems.

Conflicts of interest

There are no conflicts to declare.

Acknowledgements

The authors acknowledge support by the German Research Foundation (DFG) SFB1032 (project-ID 201269156) sub-project B4 (to E. Wa.), and BMBF Cluster for Future ‘CNATM – Cluster for Nucleic Acid Therapeutics Munich’ project-ID 03ZU1201AA (to E. Wa.).

We thank Melina Grau, Lun Peng and Janin Germer for providing previously established transfection reagents, Melina Grau and Tobias Burghardt for MALDI measurements, Simone Berger, Janin Germer and Mina Yazdi for scientific discussions, Wolfgang Rödl and Olga Brück for technical and organizational support.

5 Summary

During the last decades, nucleic acid-based therapies have entered numerous fields of therapeutic applications. While viral vectors have traditionally been favored for their high transfection efficacy, nonviral vectors are increasingly explored and gaining importance due to their improved safety profiles and reduced immunogenicity. However, several challenges in efficient delivery remain which include particle stability, cellular uptake, endosomal escape and cargo release. To address these challenges, sophisticated strategies have been developed to enhance the efficacy and specificity of therapeutic cargo delivery. Continuous optimization, achieved by 'chemical evolution' of synthetic carriers, is crucial in refining the carrier systems, focusing on enhancing both their efficacy and safety for clinical applications.

In the first part of this thesis a modular carrier system was evaluated for its potential to be functionalized with complex carbohydrate-based targeting ligands. The study also focused on the influence of two polyplex modification strategies on particle formation and biological activity. A suitable OAA for pDNA delivery was selected from a small library of six 'four-arm' carriers, each synthesized by solid phase assisted synthesis tailored for pDNA delivery. The carriers featured structural variations, including azido-lysines to allow carrier modification by alkyne-bearing glyco-ligands via SPAAC. One carrier, featuring repeated alternating motifs of Stp and histidine exhibited favorable characteristics for pDNA delivery, as demonstrated *in vitro* across various cell lines and was subsequently selected as suitable candidate for functionalization with DBCO-equipped ligands.

Two approaches for polyplex modification – pre- and post-functionalization – were evaluated using PEG_n-DBCO ligands with varying PEG lengths (n = 12, 24, 48, or 96). Physicochemical and *in vitro* analyses revealed that both the PEG length and the chosen polyplex modification strategy had significant influence on the physicochemical properties and biological performance of the shielded carriers. Pre-PEGylation with PEG length ≥24 reduced transfection efficacy by minimizing the ability to interact with cell membranes as a consequence of shielding the positive surface charge and thereby reducing electrostatic interactions. However, this strategy positively influenced polyplex formation by maintaining small particle sizes and preventing aggregation, while the zeta potential was strongly decreased.

Leveraging the modular nature of the azido-functionalized carrier system, which allows for the attachment of various ligands, the selected carrier was further decorated with either GalNAc or mannose ligands containing a PEG_{24} shielding domain by using the pre-functionalization approach. This carrier modification was intended to facilitate receptor-mediated delivery of pDNA polyplexes to lectin-presenting cells, specifically targeting hepatocarcinoma cell lines

HepG2 and Huh7, which express ASGPR, and the dendritic-like cell line DC2.4, which expresses mannose receptors.

Functionalization with GalNAc enhanced the transfection efficacy compared to the shielded polyplexes, a result attributed to the presence of the ligand and the positive surface charge of the particles. Kinetic studies showed accelerated uptake by receptor-positive hepatocytes, while receptor-negative cells did not exhibit this enhancement. An inhibition assay using asialofetuin, a natural competitor, confirmed the involvement of ASGPR in the uptake of GalNAc-functionalized polyplexes. This receptor-mediated uptake was specific to the GalNAc-decorated particles, as neither unmodified nor shielded polyplexes showed similar involvement of the receptor.

The mannose-modified polyplexes showed a significantly improved cellular uptake and gene expression compared to their unmodified and shielded counterparts. This effect was particularly pronounced in polyplexes with a high degree of functionalization. However, the uptake of these mannose-modified polyplexes appeared to be mediated by multiple internalization pathways, including nonspecific endocytosis. This conclusion was supported by the observation that inhibition with the receptor-specific competitor mannan only minimally affected cellular uptake, indicating that also mannose-independent mechanisms contribute to polyplex internalization beyond receptor-specific pathways.

These findings demonstrate that the polyplex modification strategies, effectively influence particle formation and biological activity. More specifically pre-functionalization with GalNAc and mannose ligands could be used to achieve targeted and enhanced gene delivery.

The second part of this thesis aimed for improving the cellular tolerability of highly potent carriers for pDNA and mRNA delivery comprised of LAF-Stp xenopeptides. This was achieved by incorporating either reducible disulfide building blocks or hydrophobic, non-reducible spacers of the same length at precise positions within the carrier molecules.

The strategy was applied to LAF-Stp xenopeptides of different topologies, which have shown to be favorable for either pDNA or mRNA transfection activity in previous studies. However, in some cases, their high transfection efficacy was intrinsically linked cytotoxicity at elevated doses. Physicochemical characterization identified suitable LAF-Stp xenopeptide/cargo combinations and optimum N/P ratios for particle formation, proving once more the individual requirements of each cargo. Furthermore, GSH-dependent disulfide cleavage was detected for bioreducible carriers. In the case of polyplexes, this feature enabled reduction cargo release, as determined by suitable assays. In addition to that, the lytic activity of the carriers alone was modulated by spacer insertion and abolished for the reducible spacers after GSH treatment.

The biological activity of the modified carriers was assessed *in vitro* using five different cancer cell lines. The transfection potency and the cellular tolerability towards the polyplexes were found to be highly cell line-dependent. The use of disulfide modified xenopeptides have shown to improve metabolic activity and reduce cellular membrane disruption after transfection, but also non-reducible spacers had an influence on transfection activity and cell viability. Additional mechanistic studies were performed aiming to elucidate underlying mechanisms promoting reduced cell viability. These analyses indicated a decelerated cellular processing of the spacer-modified polyplexes. The cellular uptake, endosomal release as well as expression kinetics were observed to be slowed down in comparison to the original xenopeptide carriers. At the same time, it became apparent that the slower kinetics of the spacer modified polyplexes supported cell proliferation similar to untreated or buffer-treated cells and prevented apoptotic events.

The incorporation of reducible disulfide and non-reducible hydrophobic spacers into LAF-Stp xenopeptide carriers was found to successfully improve cellular tolerability by reducing cytotoxicity while maintaining transfection efficacy. These modifications demonstrated that carrier optimization, in this case accomplished by spacer integration, can effectively balance transfection efficiency with enhanced biocompatibility.

6 Appendix

6.1 Analytical Data

6.1.1 Analytical data of the azido 4-arm library

573: AK[HK(H-(Stp-H)$_3$-C)$_2$]$_2$

Calculated molecular weight (MW in Da): 6611.00

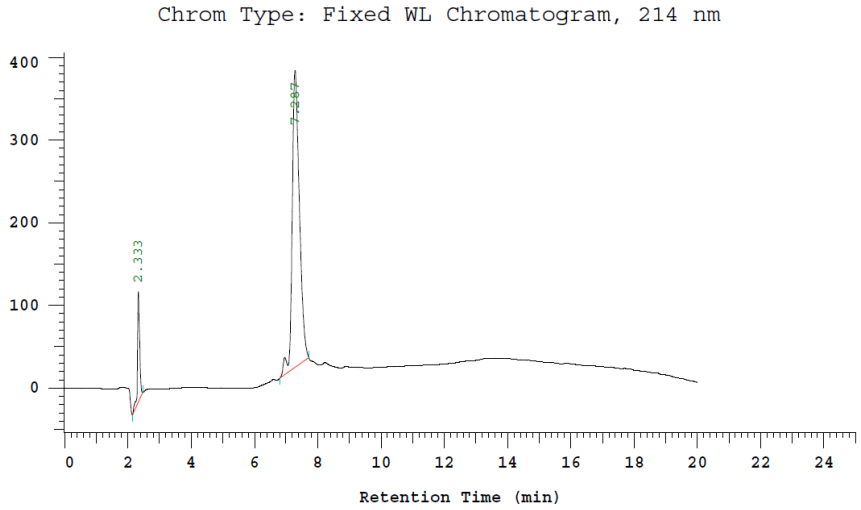

RP-HPLC Chromatogram of OAA ***573*** [ACN/H_2O with 0.1% TFA, 95/5 (v/v) – 0/100 (v/v) in 20 min] over 20 min at 25°C.

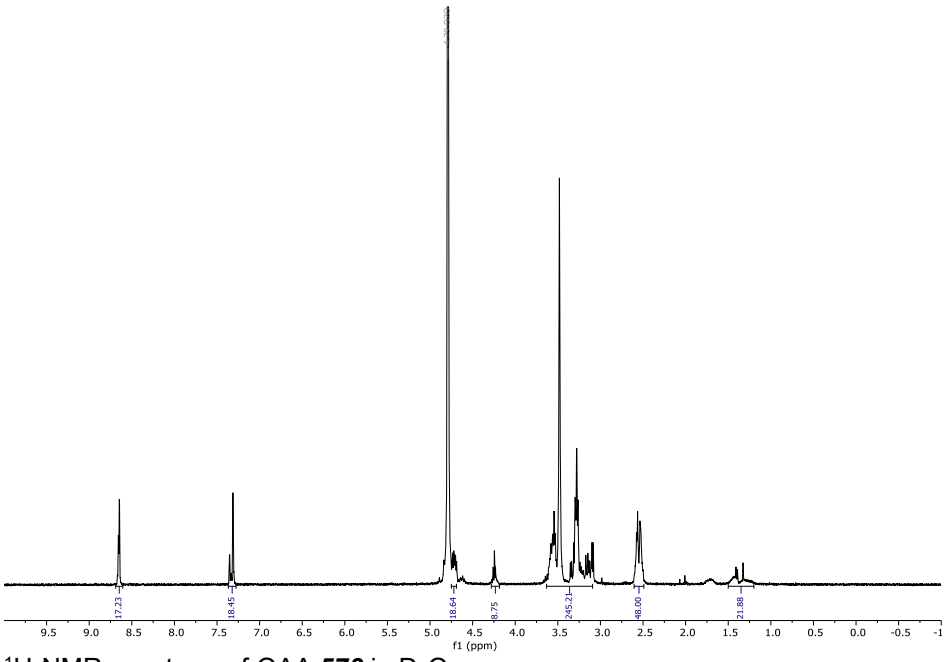

^{1}H-NMR spectrum of OAA ***573*** in D_2O.

δ (ppm) = 1.0-1.5 (m, 21 H, βH alanine, βγδH lysine), 2.3-2.6 (m, 48 H, -CO-CH_2-CH_2-CO- succinic acid), 2.8-3.6 (m, 242 H, -CH_2- tepa, βH cysteine, βH histidine, εH lysine), 4.0-4.3 (m, 8 H, αH alanine, αH cysteine, αH lysine), 4.4-4.7 (m, 18H, αH histidine), 4.79 (s, HDO), 7.2-7.4 (m, 18H, imidazole), 8.4-8.7 (d, 18H, imidazole).

1463: **A-K-[H-K-(H-Stp)$_3$-C-K(N$_3$)]$_2$]$_2$**

Calculated molecular weight (MW in Da): 7227.68

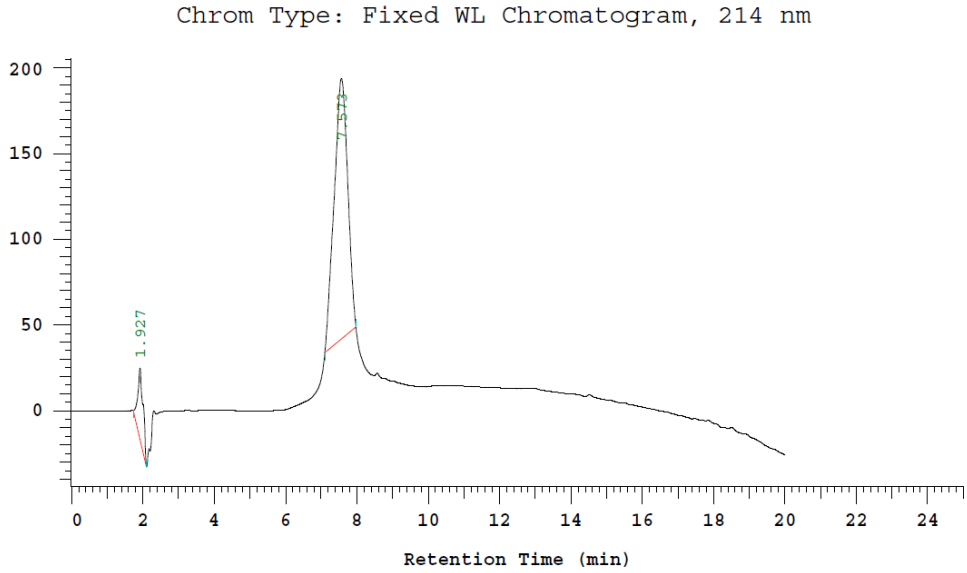

RP-HPLC Chromatogram of OAA ***1463*** [ACN/H$_2$O with 0.1% TFA, 95/5 (v/v) – 0/100 (v/v)] over 20 min at 25°C.

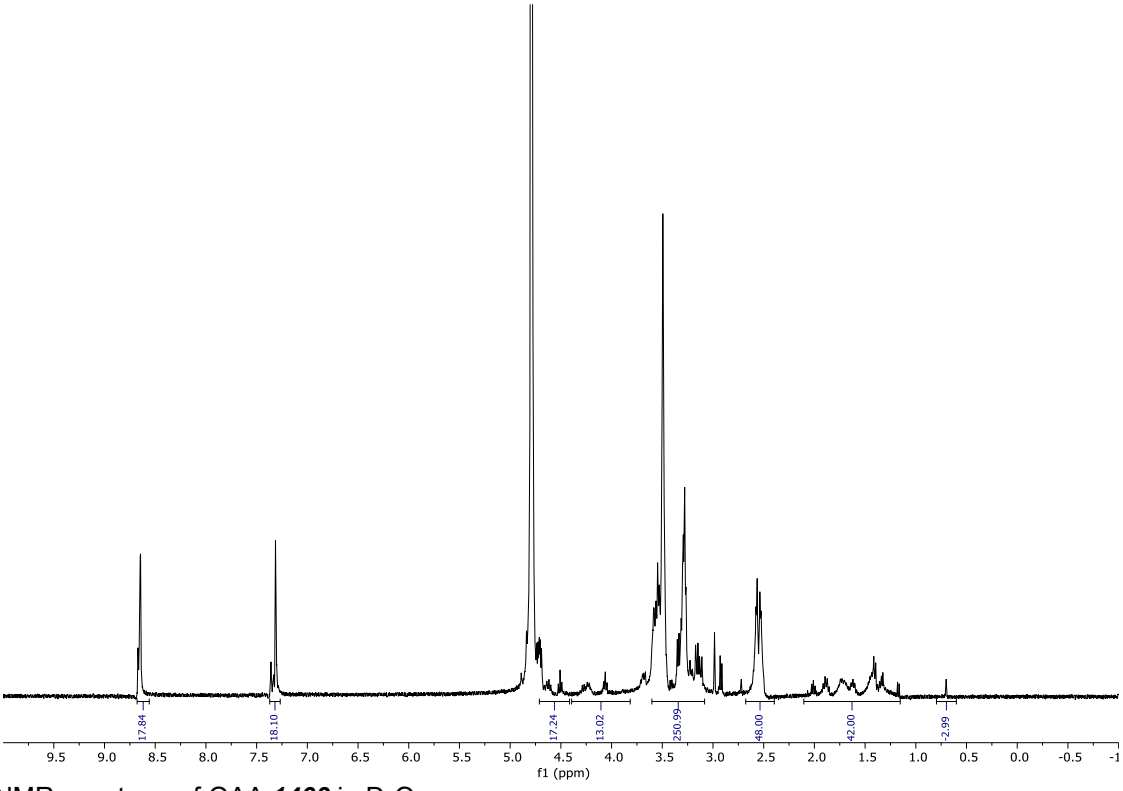

^{1}H-NMR spectrum of OAA ***1463*** in D$_2$O.

δ (ppm) = 0.5-1 (m, 3H, βH alanine), 1.0-2.0 (m, 42 H, βγδH lysine), 2.3-2.6 (m, 48 H, -CO-CH$_2$-CH$_2$-CO- succinic acid), 2.8-3.6 (m, 250 H, -CH$_2$- tepa, βH cysteine, βH histidine, εH lysine), 4.0-4.3 (m, 12H, αH alanine, αH cysteine, αH lysine), 4.4-4.7 (m, 18H, αH histidine), 4.79 (s, HDO), 7.2-7.5 (m, 18H, imidazole), 8.5-8.7 (d, 18H, imidazole).

***1479*: A-K-[H-K-(H-Stp)$_3$-Y$_3$-C-K(N$_3$)]$_2$]$_2$**

Calculated molecular weight (MW in Da): 9185.76

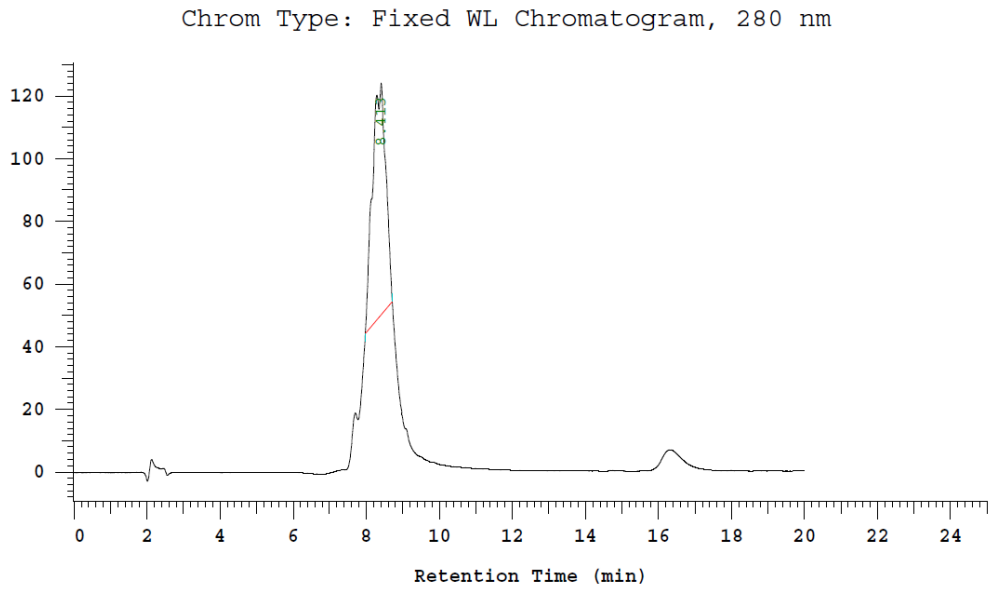

RP-HPLC Chromatogram of OAA ***1479*** [ACN/H_2O with 0.1% TFA, 95/5 (v/v) – 0/100 (v/v)] over 20 min at 25°C.

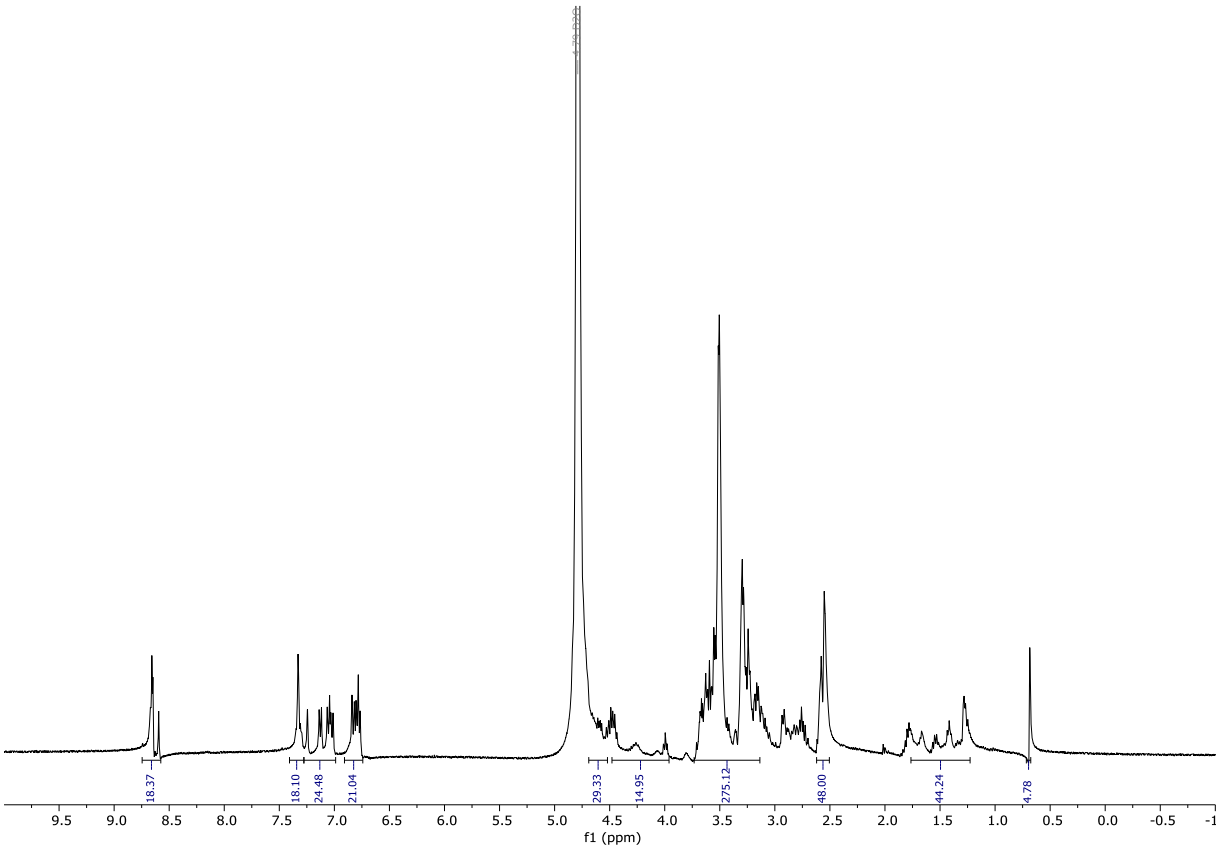

^{1}H-NMR spectrum of OAA ***1479*** in D_2O.

δ (ppm) =0.5-1 (m, 3H, βH alanine), 1.0-1.5 (m, 42 H, βγδH lysine), 2.3-2.6 (m, 48 H, -CO-CH_2-CH_2-CO- succinic acid), 3.2-3.6 (m, 274 H, -CH_2- tepa, βH cysteine, βH tyrosine, βH histidine, εH lysine), 4.0-4.3 (m, 12 H, αH alanine, αH cysteine, αH lysine), 4.5-4.7 (m, 30H, αH histidine, αH tyrosine), 4.79 (s, HDO)), 6.6-6.9 (m, 24H, benzene), 7.0-7.2 (m, 24H, imidazole), 6.9-7.5 (m, 18H, imidazole), 8.4-8.7 (m, 18H, imidazole).

***1482*: A-K-[H-K-(H-Stp)$_3$-W$_3$-C-K(N$_3$))$_2$]$_2$**

Calculated molecular weight (MW in Da): 9462.20

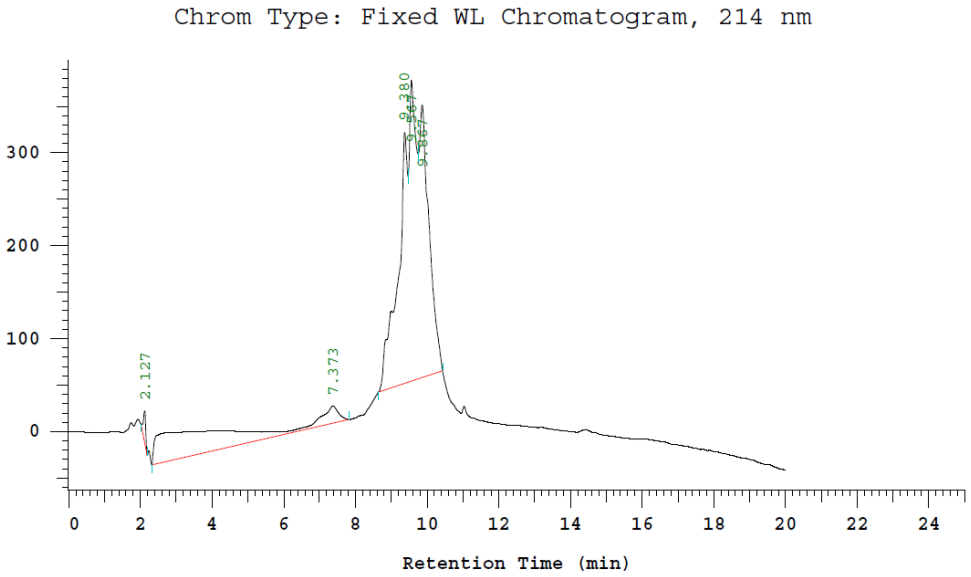

RP-HPLC Chromatogram of OAA ***1482*** [ACN/H$_2$O with 0.1% TFA, 95/5 (v/v) – 0/100 (v/v)] over 20 min at 25°C.

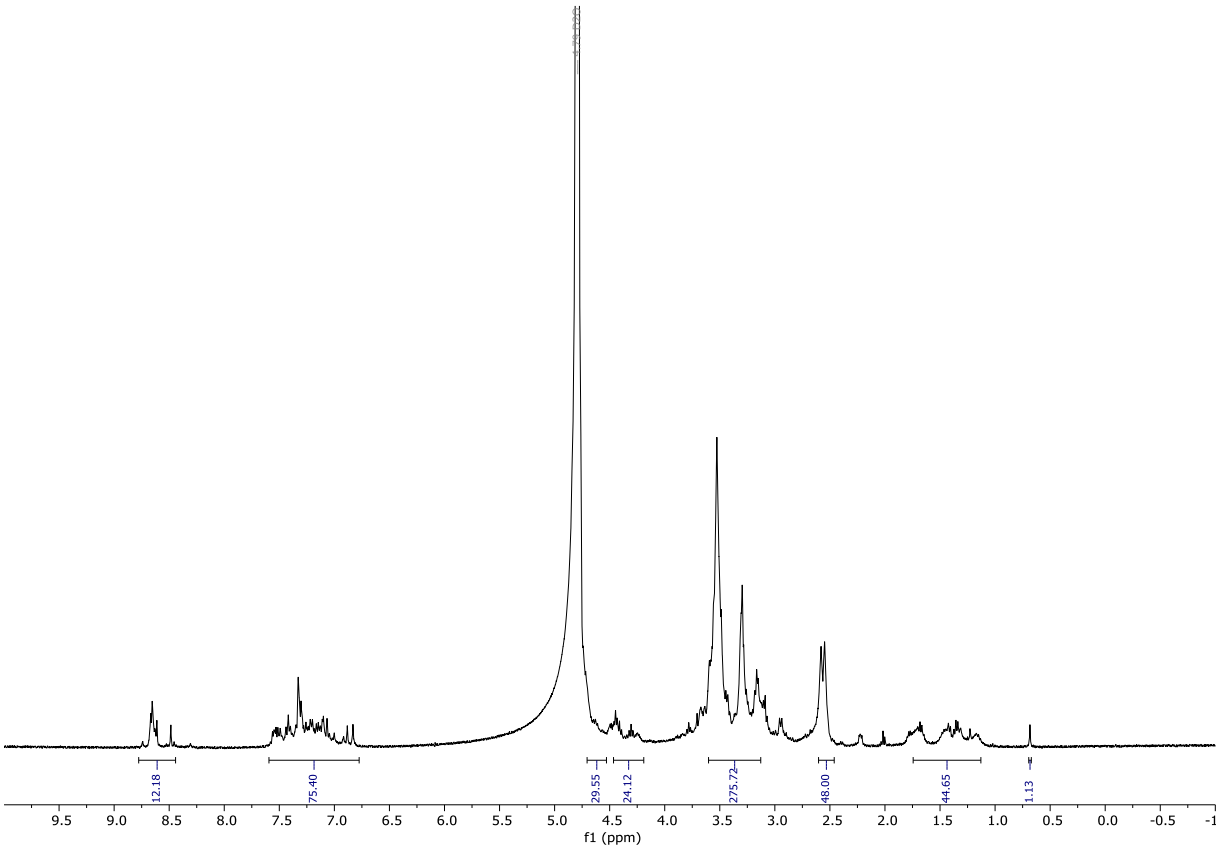

^{1}H-NMR spectrum of OAA ***1482*** in D$_2$O.

δ (ppm):0.5-1 (m, 3H, βH alanine), 1.0-1.5 (m, 42 H, βγδH lysine), 2.3-2.6 (m, 48 H, -CO-CH$_2$-CH$_2$-CO- succinic acid), 3.0-3.5 (m, 274 H, -CH$_2$- tepa, βH cysteine, βH tyrosine, βH histidine, βH tryptophan, εH lysine,), 4.2-4.4 (m, 24 H, αH alanine, αH cysteine, αH lysine), 4.4-4.7 (m, 30H, αH histidine, αH indole), 4.79 (s, HDO), 6.6-7.5 (m, 78 H, indole, imidazole), 8.4-8.7 (d, 18H, imidazole).

***1494*: A-K-[H-K-(H-Stp-W)$_3$-C-K(N$_3$))$_2$]$_2$**

Calculated molecular weight (MW in Da): 9460.18

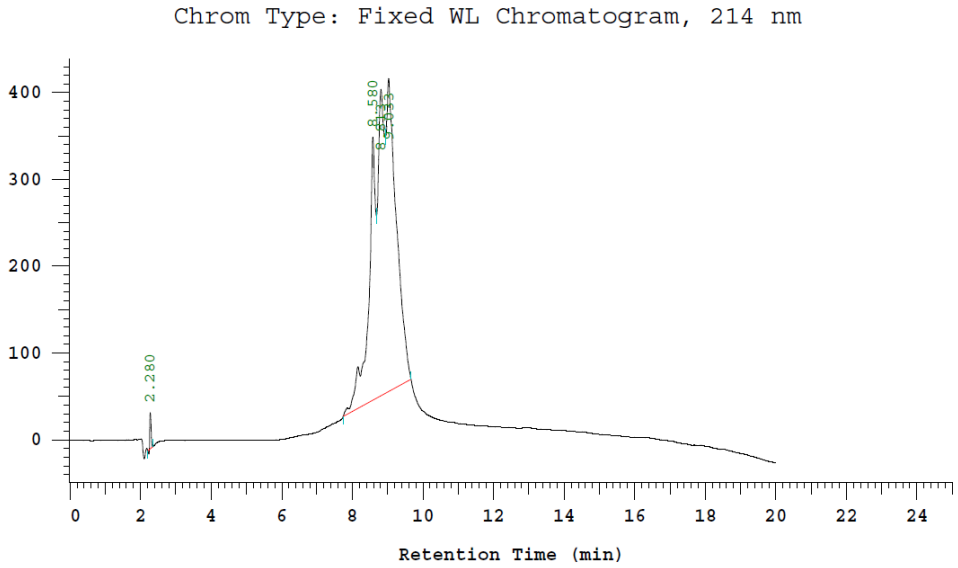

RP-HPLC Chromatogram of OAA ***1494*** [ACN/H_2O with 0.1% TFA, 95/5 (v/v) – 0/100 (v/v)] over 20 min at 25°C.

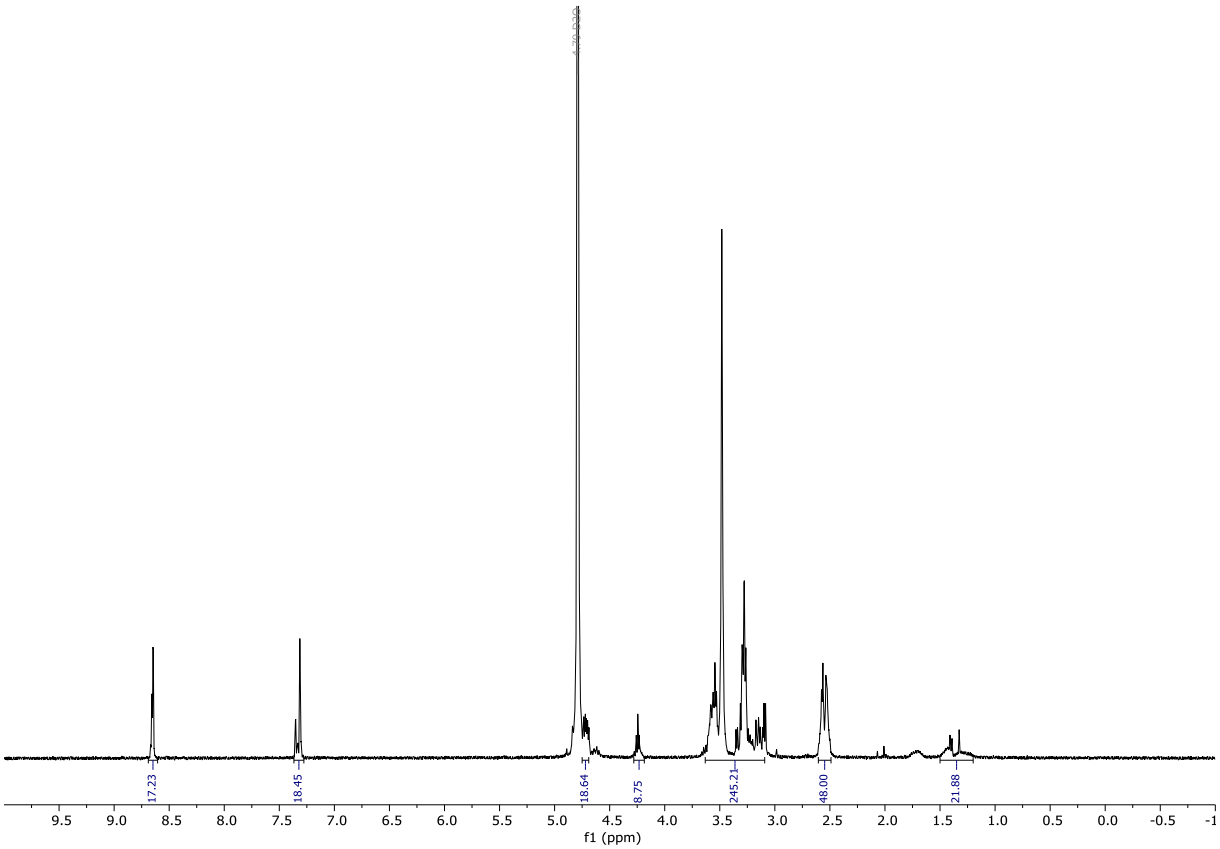

^{1}H-NMR spectrum of OAA ***1494*** in D_2O.

δ (ppm) =0.5-1 (m, 3H, βH alanine), 1.0-2.0 (m, 42 H, βγδH lysine), 2.3-2.6 (m, 48 H, -CO-CH_2-CH_2-CO- succinic acid), 3.0-3.6 (m, 274 H, -CH_2- tepa, βH cysteine, βH tyrosine, βH histidine, βH tryptophan, εH lysine,), 3.8-4.2 (m, 24 H, αH alanine, αH cysteine, αH lysine), 4.4-4.7 (m, 30H, αH histidine, αH indole), 4.79 (s, HDO), 7.0-7.7 (m, 60 H, indole), 7.4-7.6 (m, 18H, imidazole), 8.4-8.7 (d, 18H, imidazole).

***1493*: A-K-[H-K-(H-Stp-R)$_3$-C-K(N$_3$))$_2$]$_2$**

Calculated molecular weight (MW in Da): 9131.97

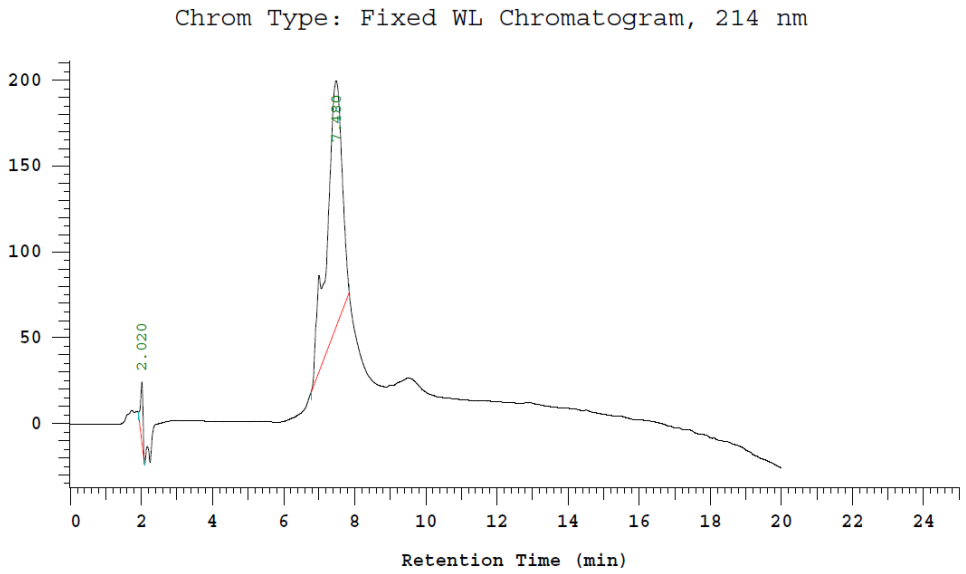

RP-HPLC Chromatogram of OAA ***1493*** [ACN/H$_2$O with 0.1% TFA, 95/5 (v/v) – 0/100 (v/v)] over 20 min at 25°C.

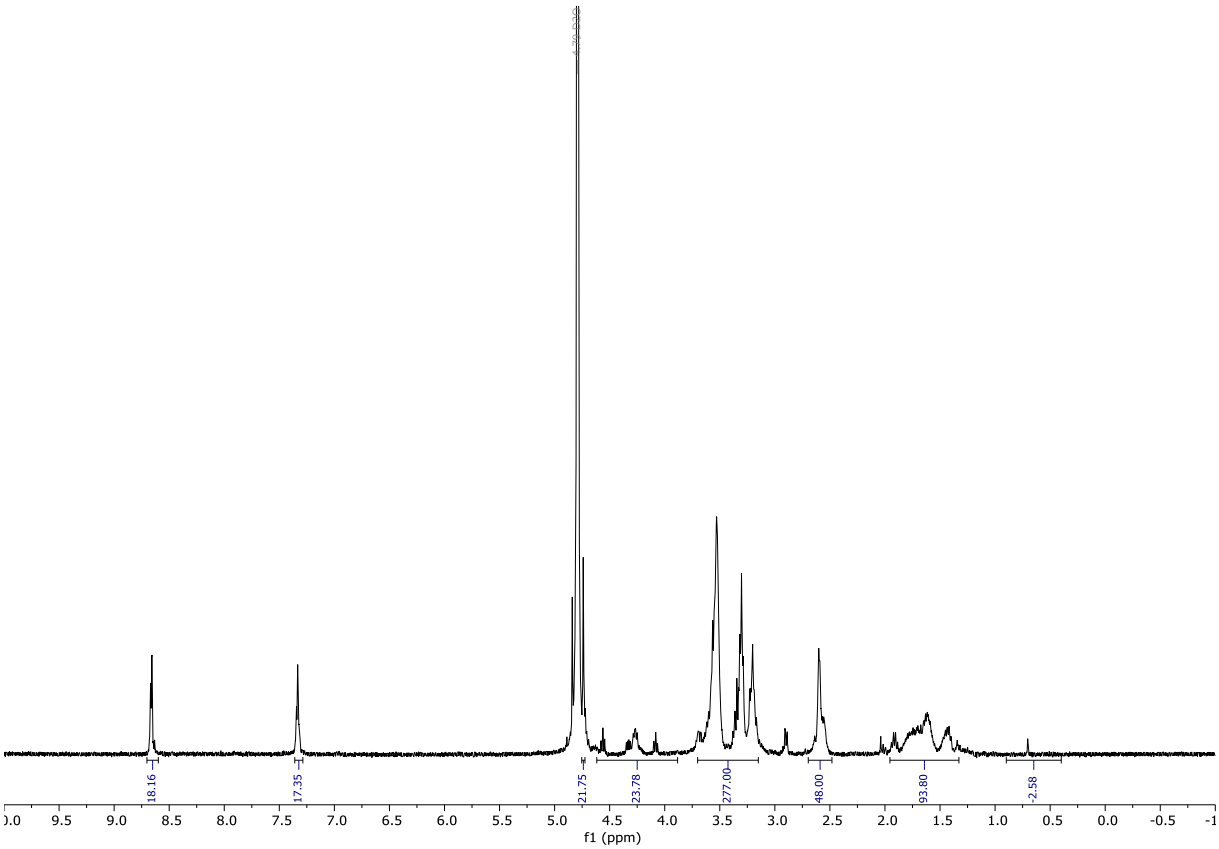

^{1}H-NMR spectrum of OAA ***1493*** in D$_2$O.

δ (ppm) =0.5-1 (m, 3H, βH alanine), 1.0-1.9 (m, 90 H, βγδH lysine, β-γ-arginine), 2.3-2.7 (m, 48 H, -CO-CH$_2$-CH$_2$-CO- succinic acid), 2.8-3.7 (m, 274 H, -CH$_2$- tepa, βH cysteine, βH tyrosine, βH histidine, βH tryptophan, εH lysine,), 4.0-4.3 (m, 24 H, αH alanine, αH cysteine, αH lysine), 4.5-4.7 (m, 18H, αH histidine), 4.79 (s, HDO), 7.3-7.5 (m, 18H, imidazole), 8.8-8.7 (d, 18H, imidazole).

***1495*: A-K-[H-K-(H-Stp)$_3$-R$_3$-C-K(N$_3$))$_2$]$_2$**

Calculated molecular weight (MW in Da): 9101.91

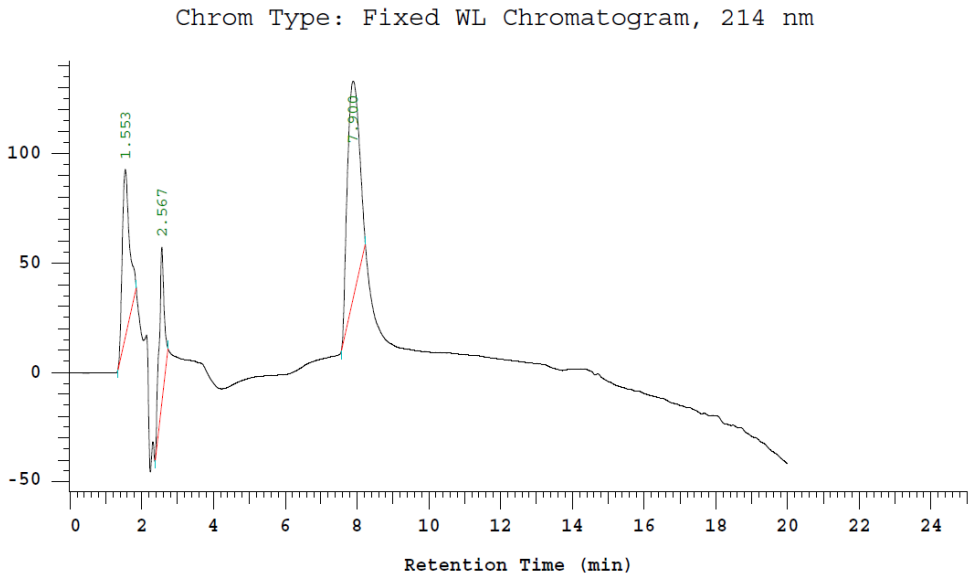

RP-HPLC Chromatogram of OAA ***1495*** [ACN/H$_2$O with 0.1% TFA, 95/5 (v/v) – 0/100 (v/v)] over 20 min at 25°C.

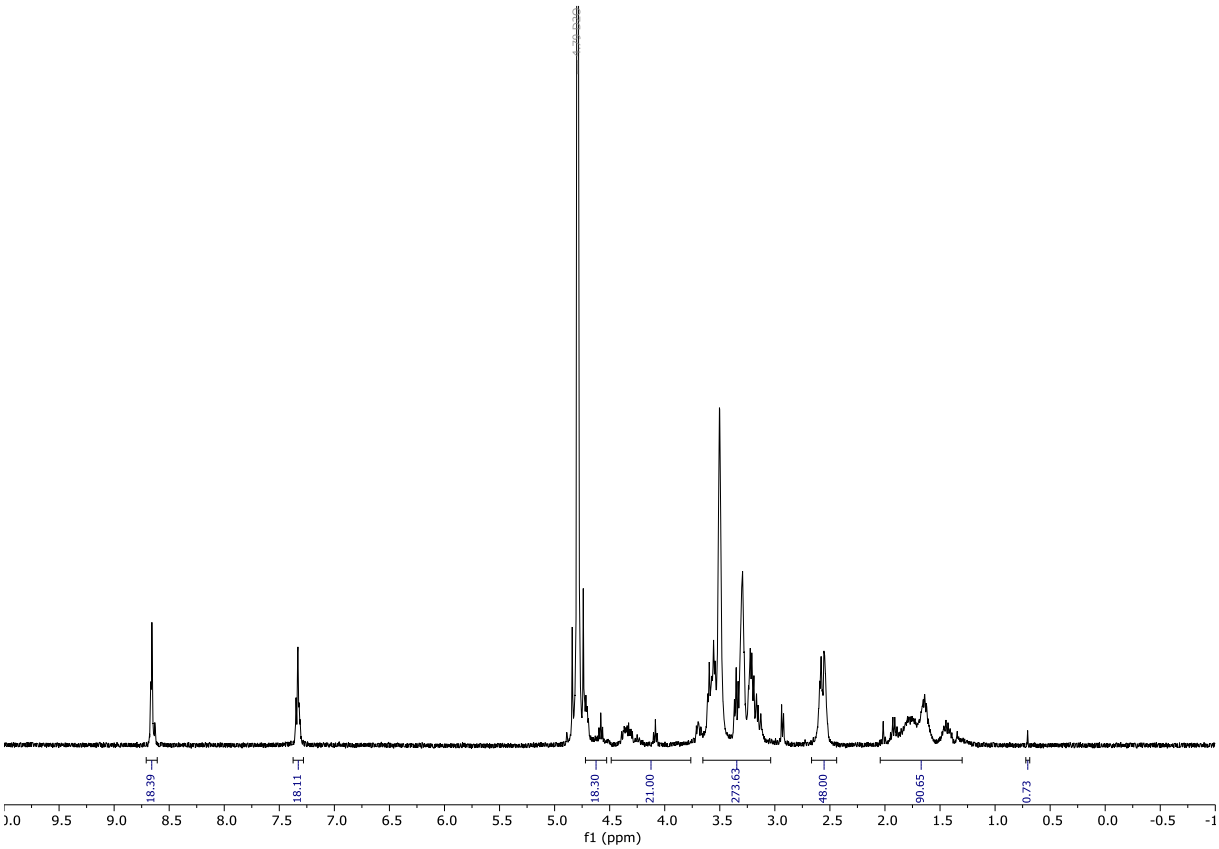

^{1}H-NMR spectrum of OAA ***1495*** in D$_2$O.

δ (ppm) =0.5-1 (m, 3H, βH alanine), 1.0-2.0 (m, 90 H, βγδH lysine, βγ arginine), 2.3-2.6 (m, 48 H, -CO-CH$_2$-CH$_2$-CO- succinic acid), 3.0-3.6 (m, 274 H, -CH$_2$- tepa, βH cysteine, βH tyrosine, βH histidine, βH tryptophan, εH lysine), 3.8-4.3 (m, 24 H, αH alanine, αH cysteine, αH lysine), 4.5-4.7 (m, 18H, αH histidine), 4.79 (s, HDO), 6.9-7.5 (m, 18H, imidazole), 8.4-8.7 (d, 18H, imidazole).

6.1.2 Analytical data of the PEG_n-DBCO shielding agents

PEG_{12}-DBCO

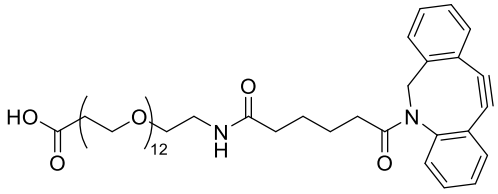

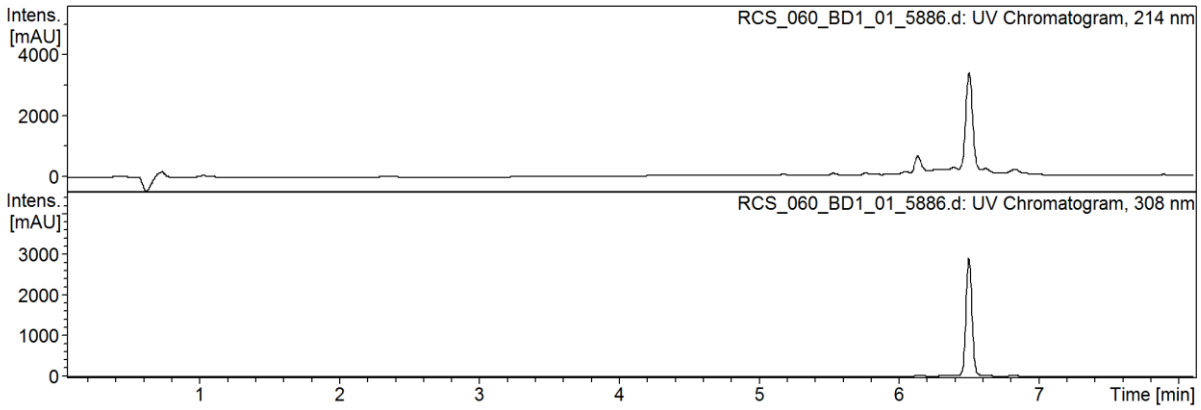

RP-UPLC chromatogram of PEG_{12}-DBCO from 95/5 to 5/95 (v/v) H_2O/ACN + 0.1% formic acid in 8 min at 25°C.

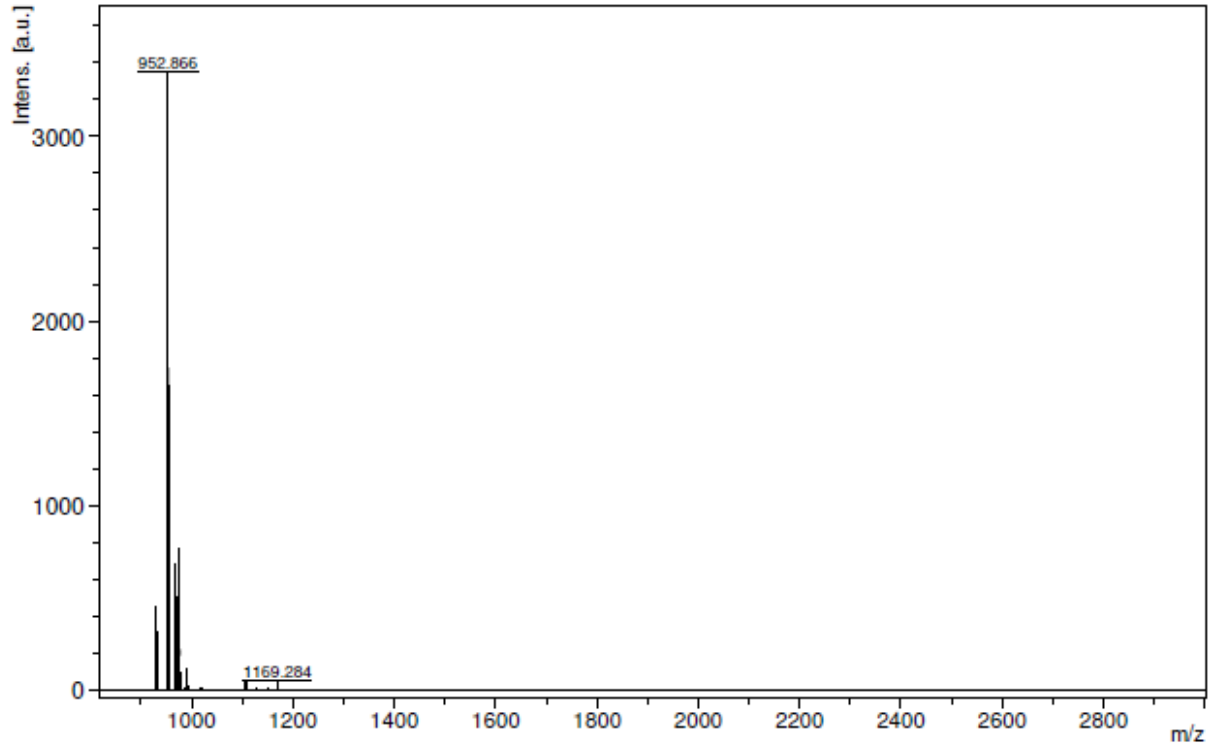

MALDI-TOF spectrum of PEG_{12}-DBCO. MW [Da] calc. $[M+Na]^+$ 955.08; found 952.87.

PEG_{24}-DBCO

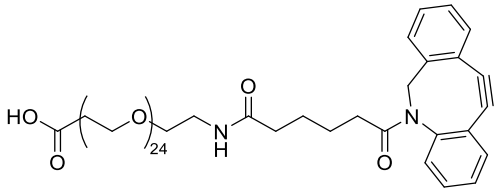

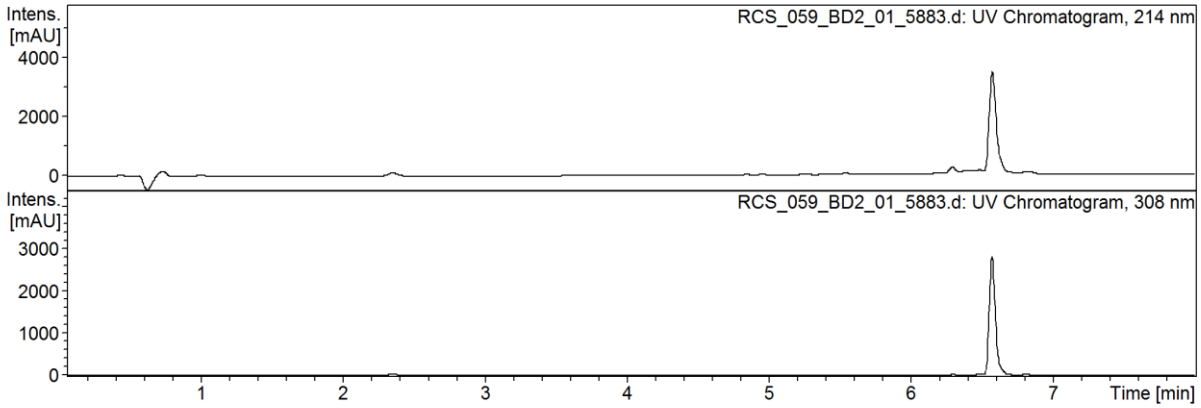

RP-UPLC chromatogram of PEG_{24}-DBCO from 95/5 to 5/95 (v/v) H_2O/ACN + 0.1% formic acid in 8 min at 25°C.

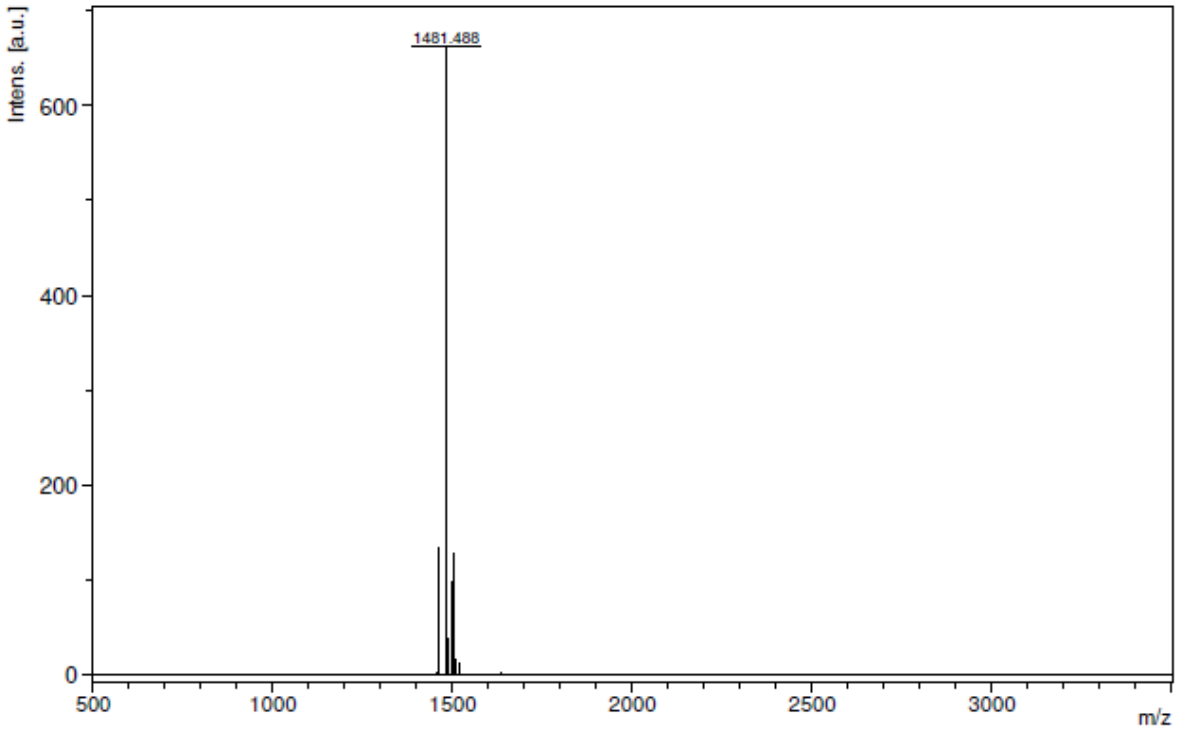

MALDI-TOF spectrum of PEG_{24}-DBCO. MW [Da] calc. $[M+Na]^+$ 1483.72; found 1481.49.

PEG_{48}-DBCO

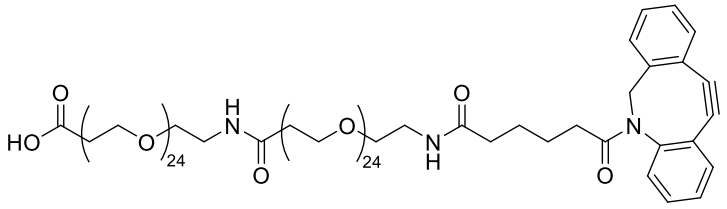

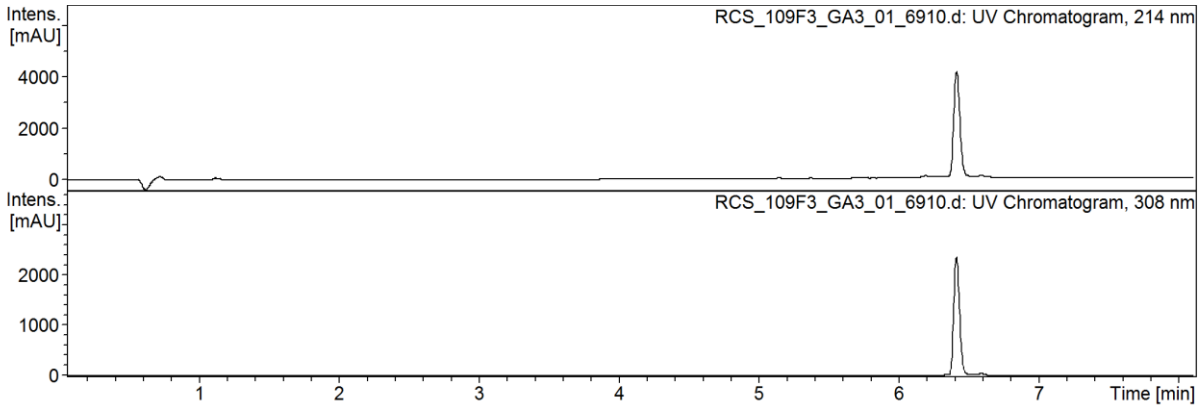

RP-UPLC chromatogram of PEG_{48}-DBCO from 95/5 to 5/95 (v/v) H_2O/ACN + 0.1% formic acid in 8 min at 25°C.

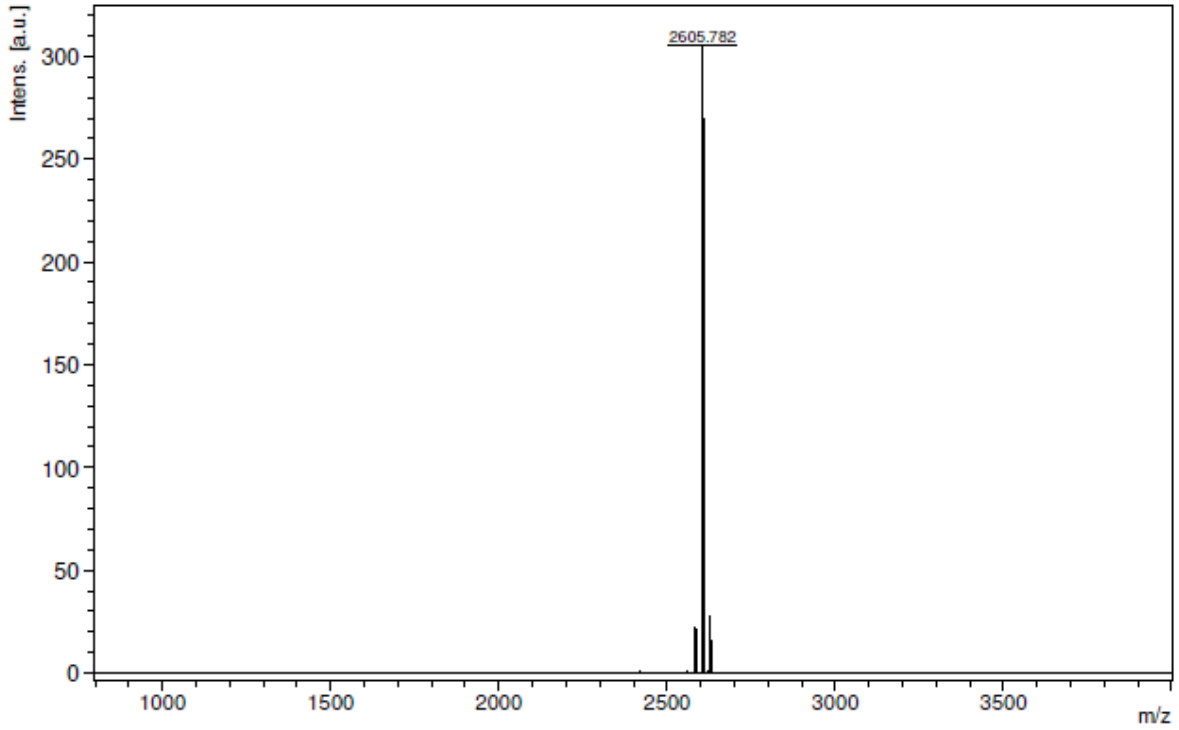

MALDI-TOF spectrum of PEG_{48}-DBCO. MW [Da] calc. $[M+Na]^+$ 2612.07; found 2605.78.

PEG_{96}-DBCO

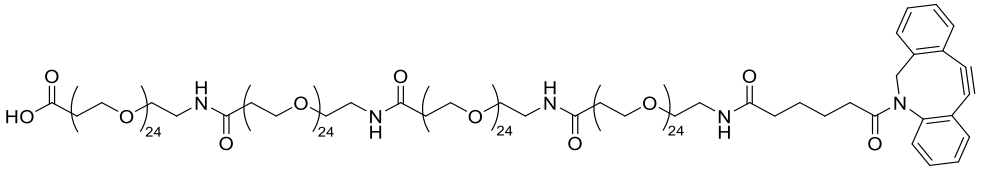

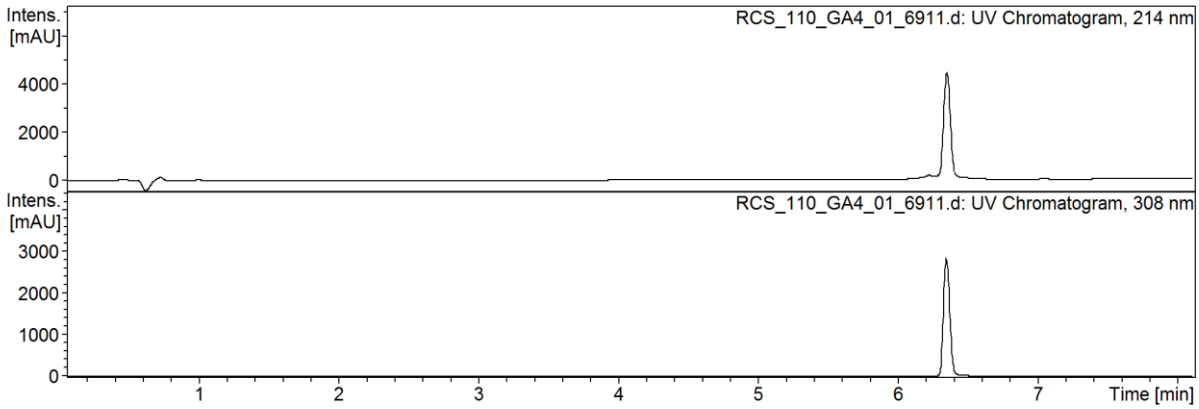

RP-UPLC chromatogram of PEG_{96}-DBCO from 95/5 to 5/95 (v/v) H_2O/ACN + 0.1% formic acid in 8 min at 25°C.

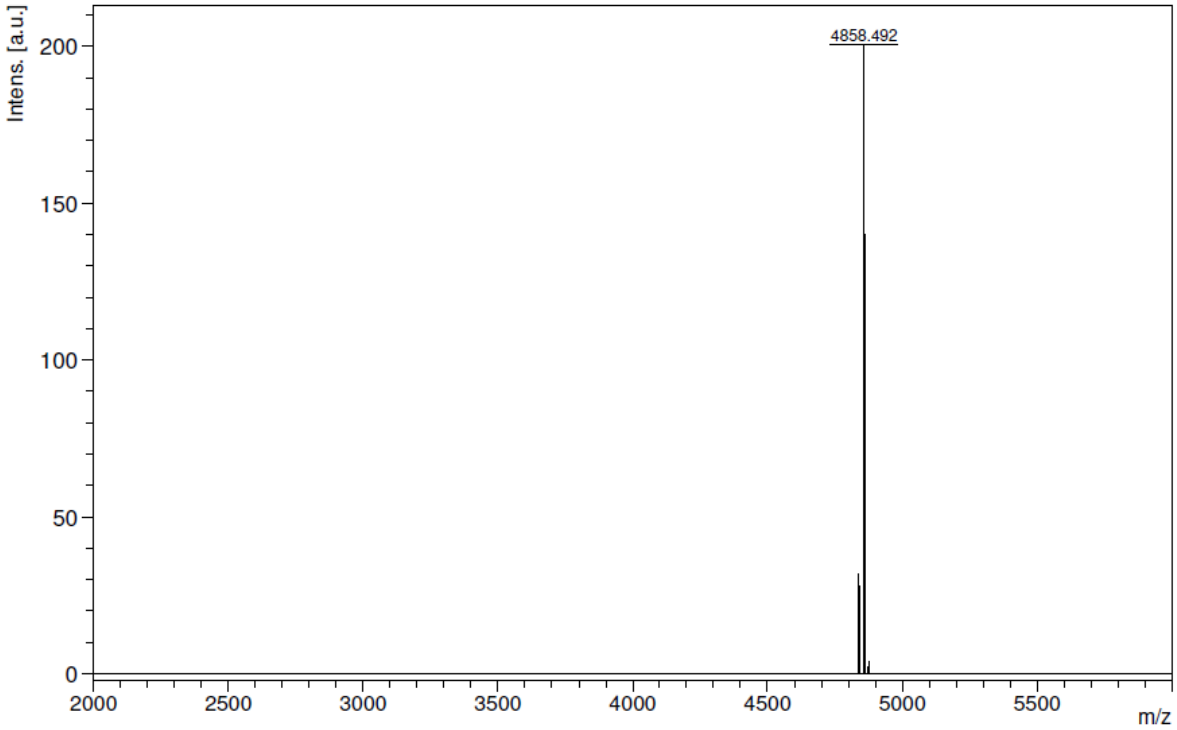

MALDI-TOF spectrum of PEG_{96}-DBCO. MW [Da] calc. $[M+Na]^+$ 4868.77; found 4858.49.

6.1.3 Analytical data of the carbohydrate-PEG$_{24}$-DBCO ligands

6.1.3.1 (GalNAc)$_3$-PEG$_{24}$-DBCO

(GalNAc)$_3$-amine

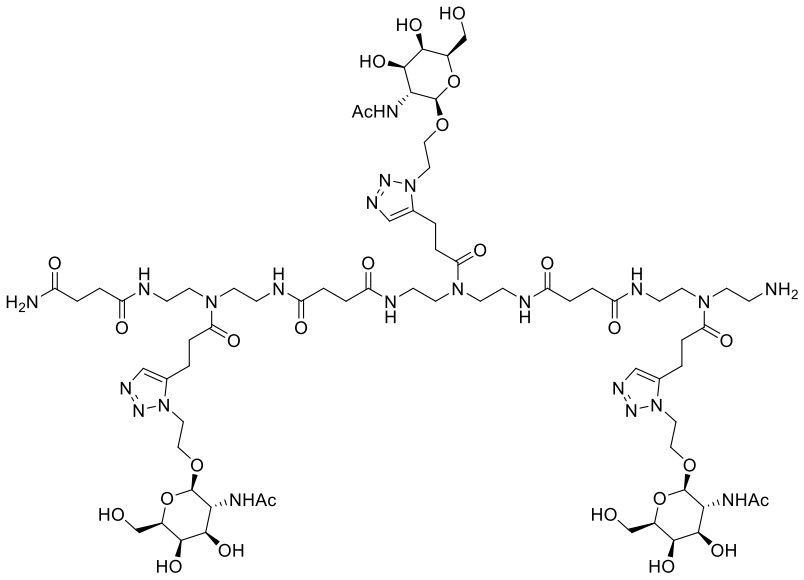

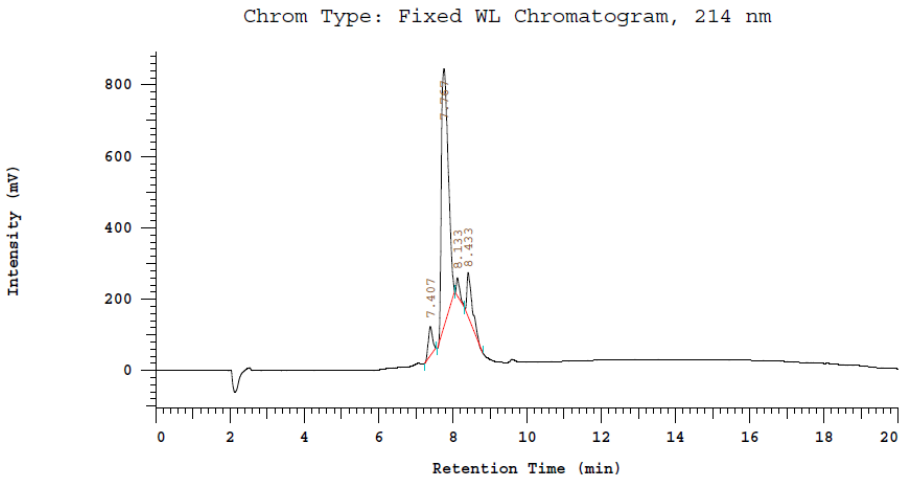

RP-HPLC Chromatogram of (GalNAc)$_3$-TDS$_3$-amine [ACN/H_2O with 0.1% TFA, 95/5 (v/v) – 0/100 (v/v)] over 20 min at 25°C.

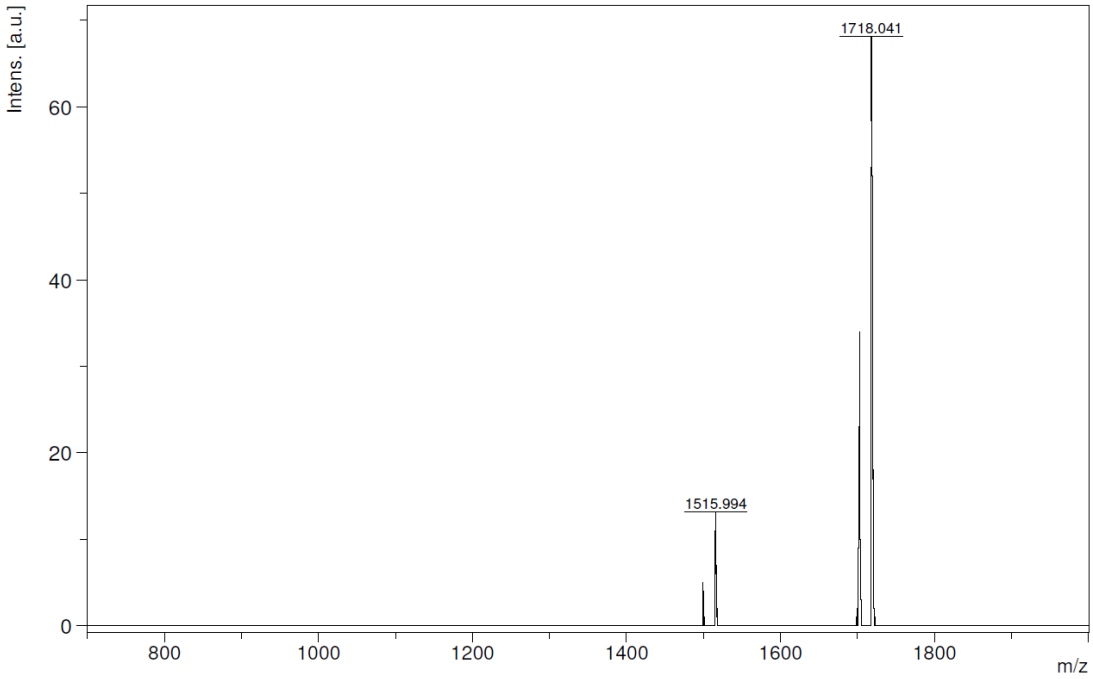

MALDI-TOF spectrum of $(GalNAc)_3$-TDS_3-amine. MW [Da] calc. $[M+Cl]^-$ 1717.792; found: 1718.041.

Note: The second peak at 1515.994 Da refers to $[M–carbohydrate+Cl]^-$, which represents most presumably an artefact of the ionization process as the UPLC chromatogram confirms high purity of the product. Thus, this peak can be neglected.

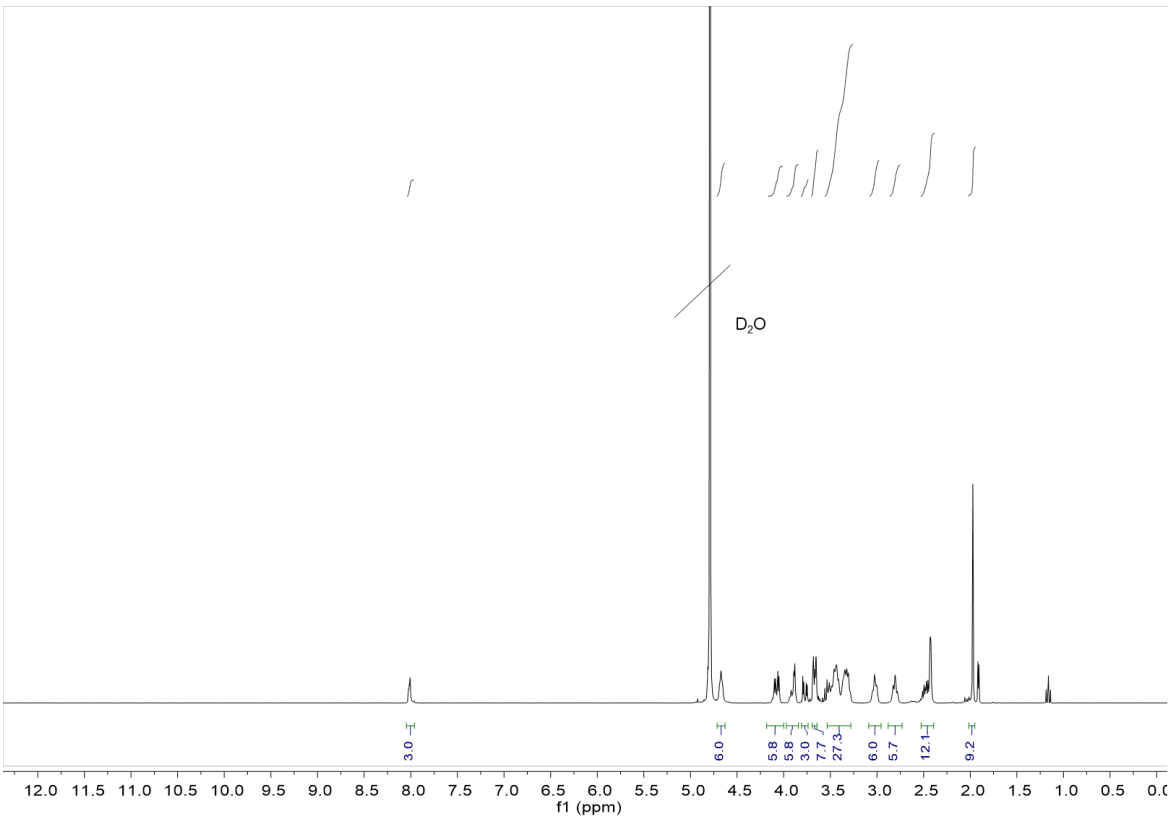

^{1}H-NMR spectrum of $(GalNAc)_3$-TDS_3-amine in D_2O.

^{1}H NMR (300 MHz, D_2O): δ 8.04 – 7.97 (m, 3H, triazole), 4.67 (s, 6H, triazole linker), 4.16 – 4.01 (m, 6H, triazole linker), 3.97 – 3.84 (m, 6H, H5 and H4 GalNAc), 3.77 (dd, *J* = 11.0, 3.2 Hz, 3H, H2 GalNAc), 3.70 – 3.63 (m, 7H, carbohydrate), 3.56 – 3.26 (m, 27H, TDS backbone, carbohydrate), 3.01 (t, *J* = 7.0 Hz, 6H, TDS linker), 2.80 (t, *J* = 7.0 Hz, 6H, TDS linker), 2.53 – 2.38 (m, 12H, succinyl), 1.97 (s, 9H, acetyl).

(GalNAc)$_3$-PEG$_{24}$-DBCO

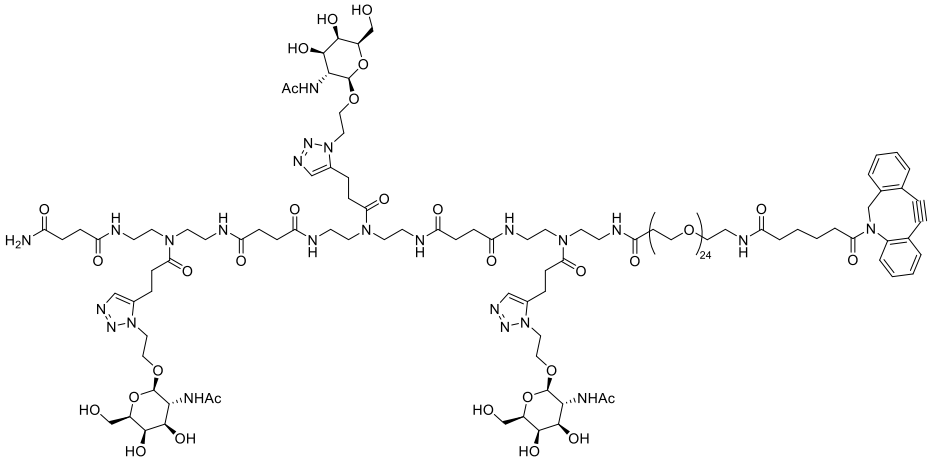

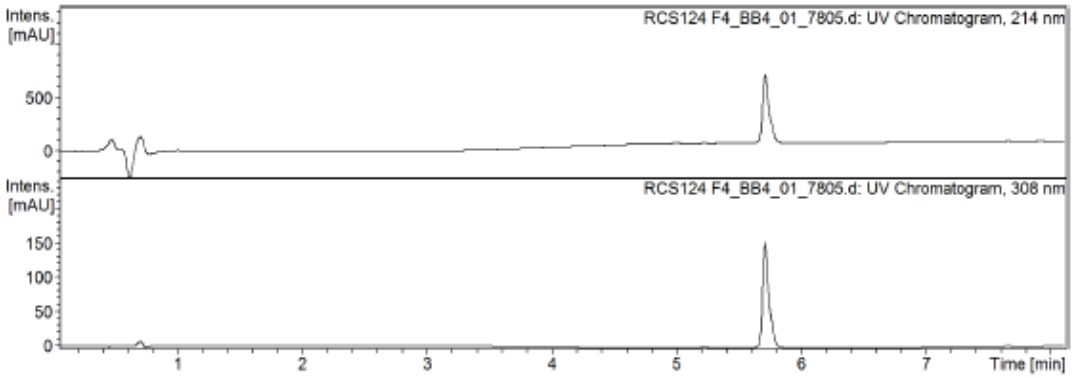

RP-UPLC chromatogram of (GalNAc)$_3$-PEG$_{24}$-DBCO from 95/5 to 5/95 (v/v) H_2O/ACN + 0.1% formic acid in 8 min at 25°C.

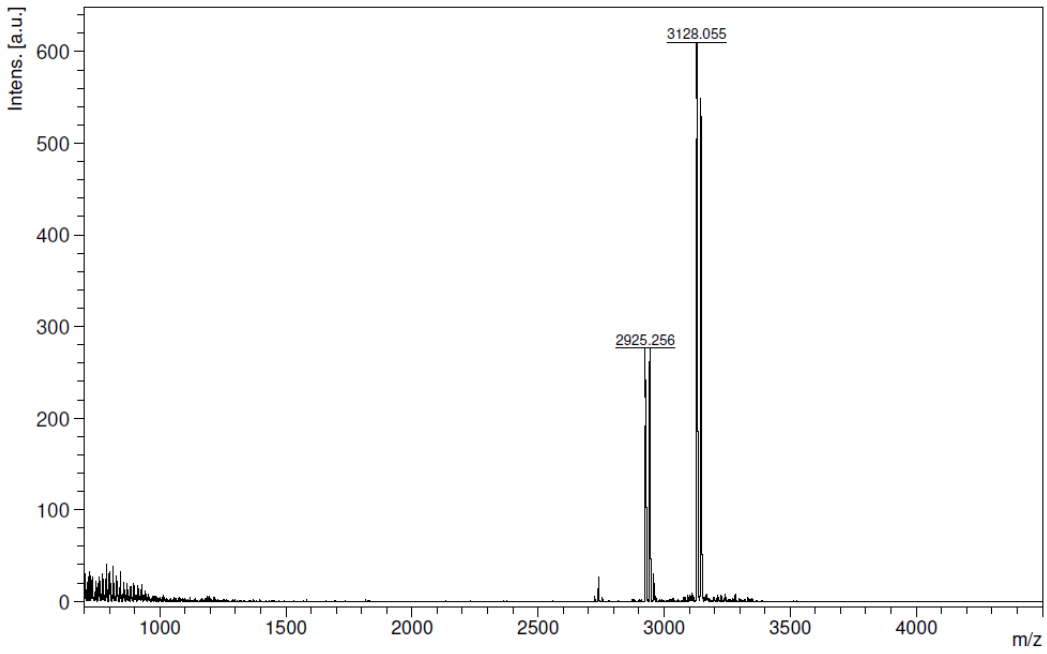

MALDI-TOF spectrum of (GalNAc)$_3$-PEG$_{24}$-DBCO. MW [Da] calc. $[M+H]^+$ 3127.521; found: 3128.055.

Note: The second peak at 2925.256 Da refers to [M–carbohydrate]+, which represents most presumably an artefact of the ionization process as the UPLC chromatogram confirms high purity of the product. Thus, this peak can be neglected.

6.1.3.2 Analytical data of Gly-Ser(Man)-PEG$_{24}$-DBCO

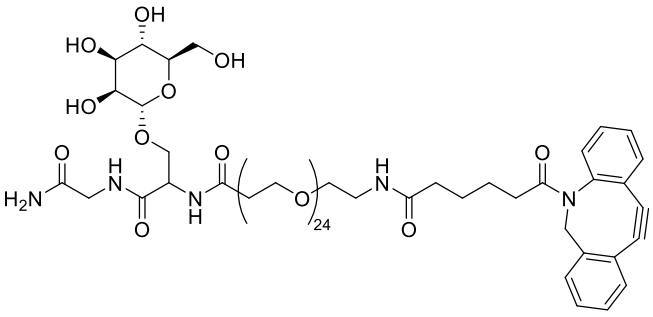

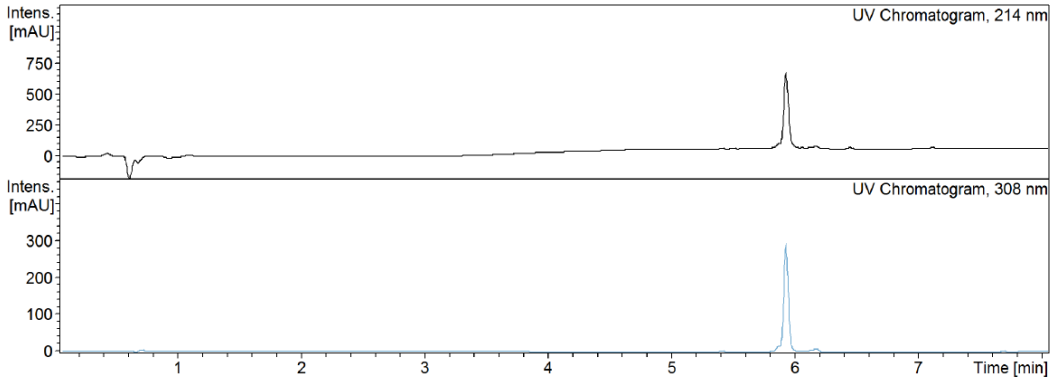

RP-UPLC chromatogram of Gly-Ser(Man)-PEG$_{24}$-DBCO from 95/5 to 5/95 (v/v) H_2O/ACN + 0.1% formic acid in 8 min at 25°C.

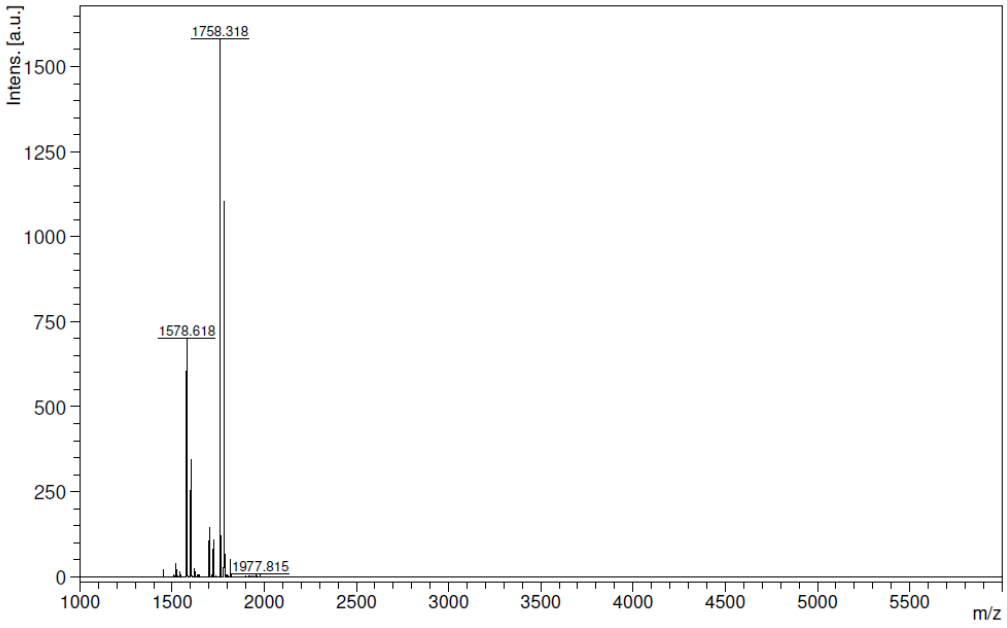

MALDI-TOF spectrum of Gly-Ser(Man)-PEG$_{24}$-DBCO. MW [Da] calc. $[M+H]^+$ 1767.025; found $[M+H]^+$ 1758.318.

Note: The second peak at 1578.618 Da refers to $[M–carbohydrate]^+$, which represents most presumably an artefact of the ionization process. as the UPLC chromatogram confirms high purity of the product. Thus, this peak can be neglected

6.1.4 Analytical data of building blocks

6.1.4.1 Disulfide building block 1-(9H-fluoren-9-yl)-3,12-dioxo-2-oxa-7,8-dithia-4,11-diazapentadecan-15-oic acid

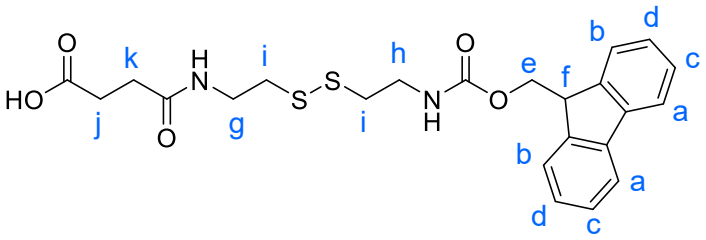

ESI-MS: calculated for $C_{23}H_{26}N_2O_5S_2$ = 474.128; found: $[M+Na]^+$ = 497.118 and $[M-H]^-$ = 473.121

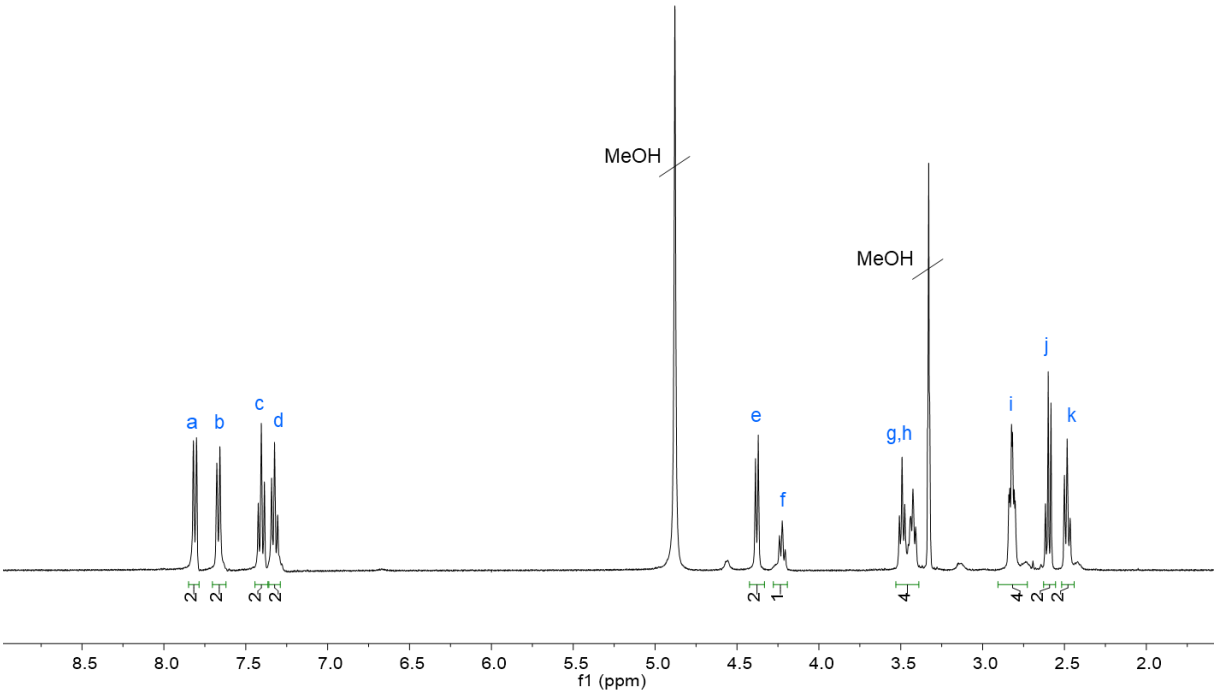

^{1}HNMR (400 MHz, Methanol-d_4) δ_H (ppm) = 7.81 (d, *J* = 7.5 Hz, 2H, a), 7.67 (d, *J* = 7.5 Hz, 2H, b), 7.41 (d, *J* = 7.4 Hz, 2H, c), 7.37 – 7.28 (m, 2H, d), 4.38 (d, *J* = 6.9 Hz, 2H, e), 4.22 (t, *J* = 6.9 Hz, 1H, f), 3.46 (dt, *J* = 26.6, 6.6 Hz, 4H, g, h), 2.82 (td, *J* = 6.8, 2.8 Hz, 4H, i), 2.60 (dd, *J* = 7.3, 6.1 Hz, 2H, j), 2.48 (t, *J* = 6.9 Hz, 2H, k).

6.1.4.2 Lipoamino fatty acid building block 8Oc

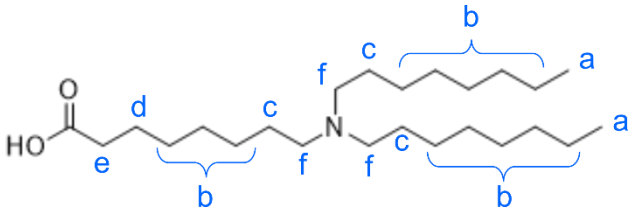

Yield: 320.9 mg, 33%

ESI-MS: calculated for $C_{24}H_{50}NO_2$ $[M+H]^+$ = 384.38361; found $[M+H]^+$ = 384.38325

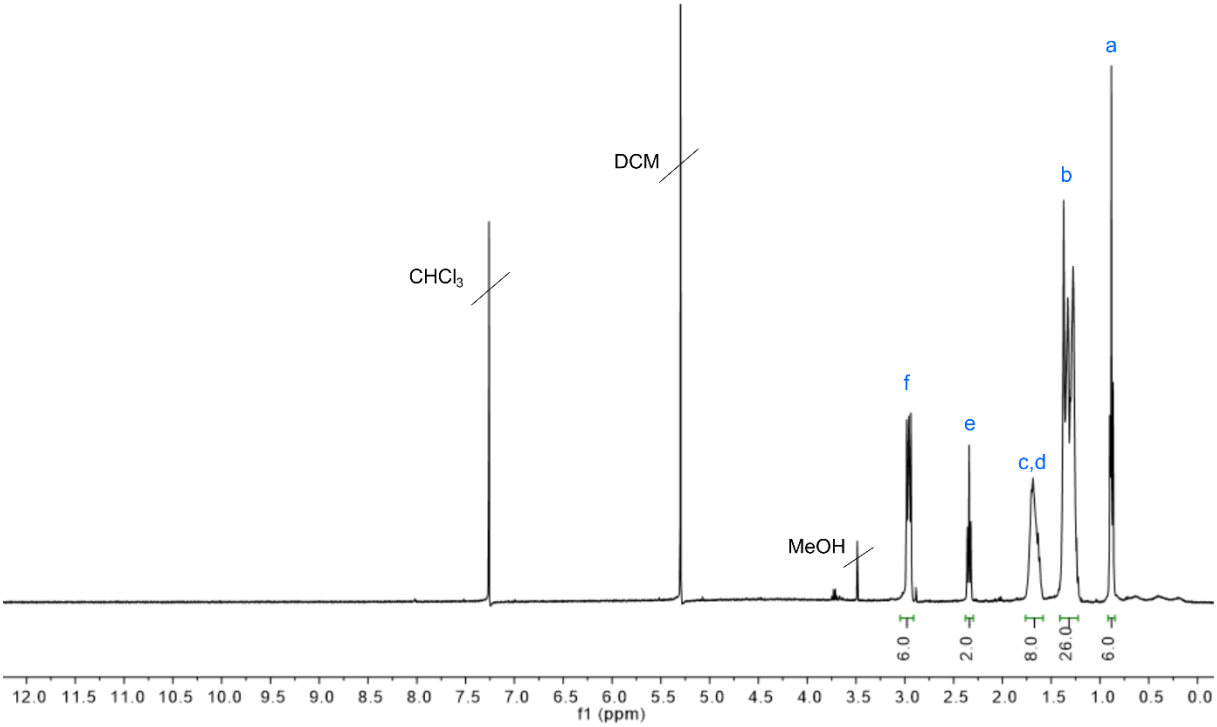

^{1}H NMR (400 MHz, Chloroform-*d*) δ_H (ppm) = 3.03 – 2.93 (m, 6H, f), 2.34 (t, *J* = 7.3 Hz, 2H, e), 1.67 (t, *J* = 14.1 Hz, 8H, c, d), 1.42 – 1.21 (m, 28H, b), 0.92 – 0.84 (m, 6H, a).

6.1.4.3 Lipoamino fatty acid building block 12Oc

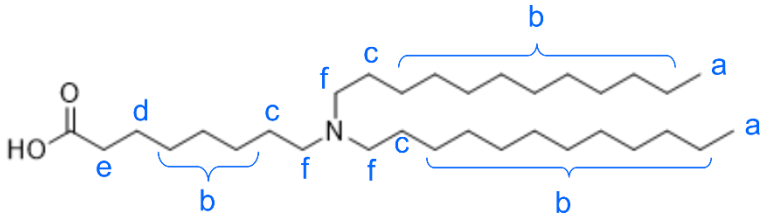

Yield: 623.7 mg, 51 %;

^{1}H NMR (400 MHz, Chloroform-*d*) δ_H (ppm) = 3.01 – 2.91 (m, 6H, f), 2.34 (t, *J* = 7.3 Hz, 2H, e), 1.66 (dt, *J* = 21.2, 7.8 Hz, 8H, c, d), 1.31 (d, *J* = 45.2 Hz, 42H, b), 0.91 – 0.84 (m, 6H, a).

ESI-MS: calculated for $C_{32}H_{66}NO_2$ $[M+H]^+$ = 496.50881; found $[M+H]^+$ = 496.51

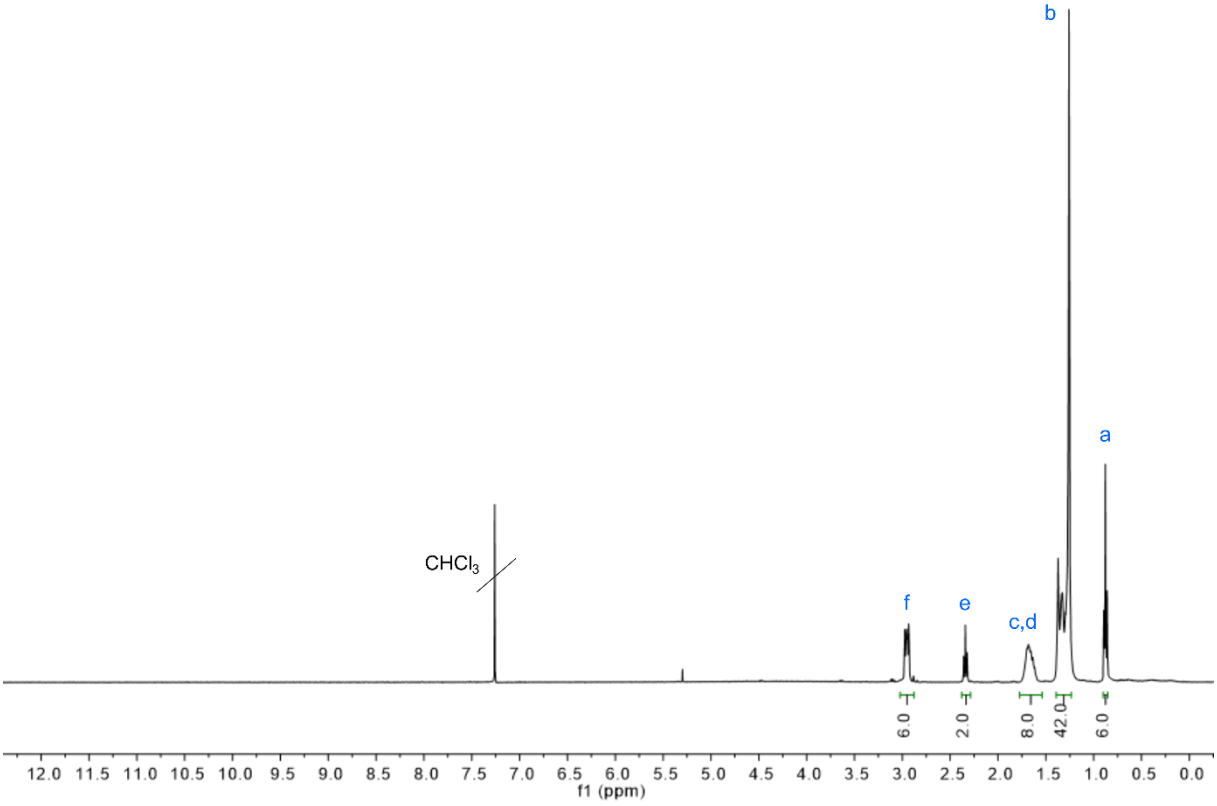

6.1.5 Analytical data of LAF Stp xenopeptides

6.1.5.1 8Oc-B2-1:4 library

1791 (8Oc-B2-1:4-ssbb)

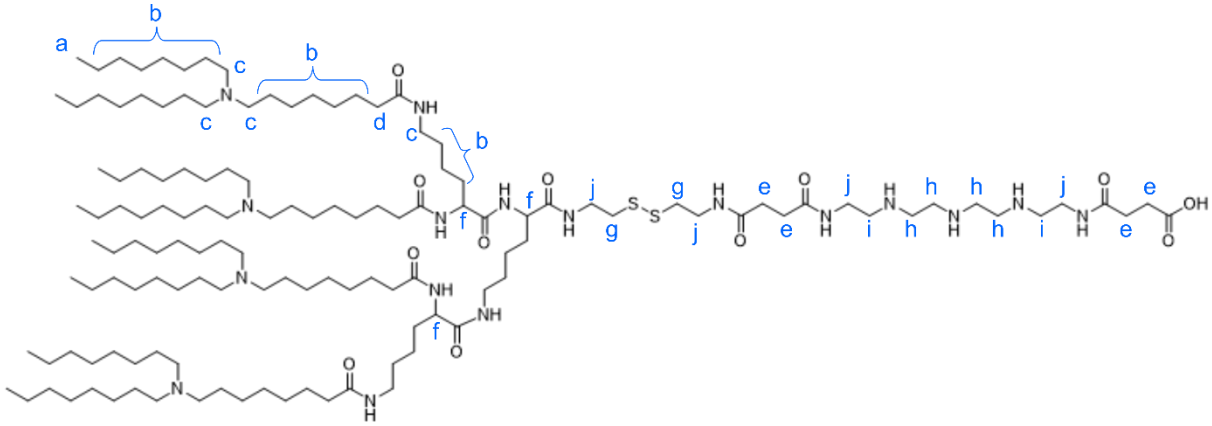

Yield: 26.7 mg (82%)

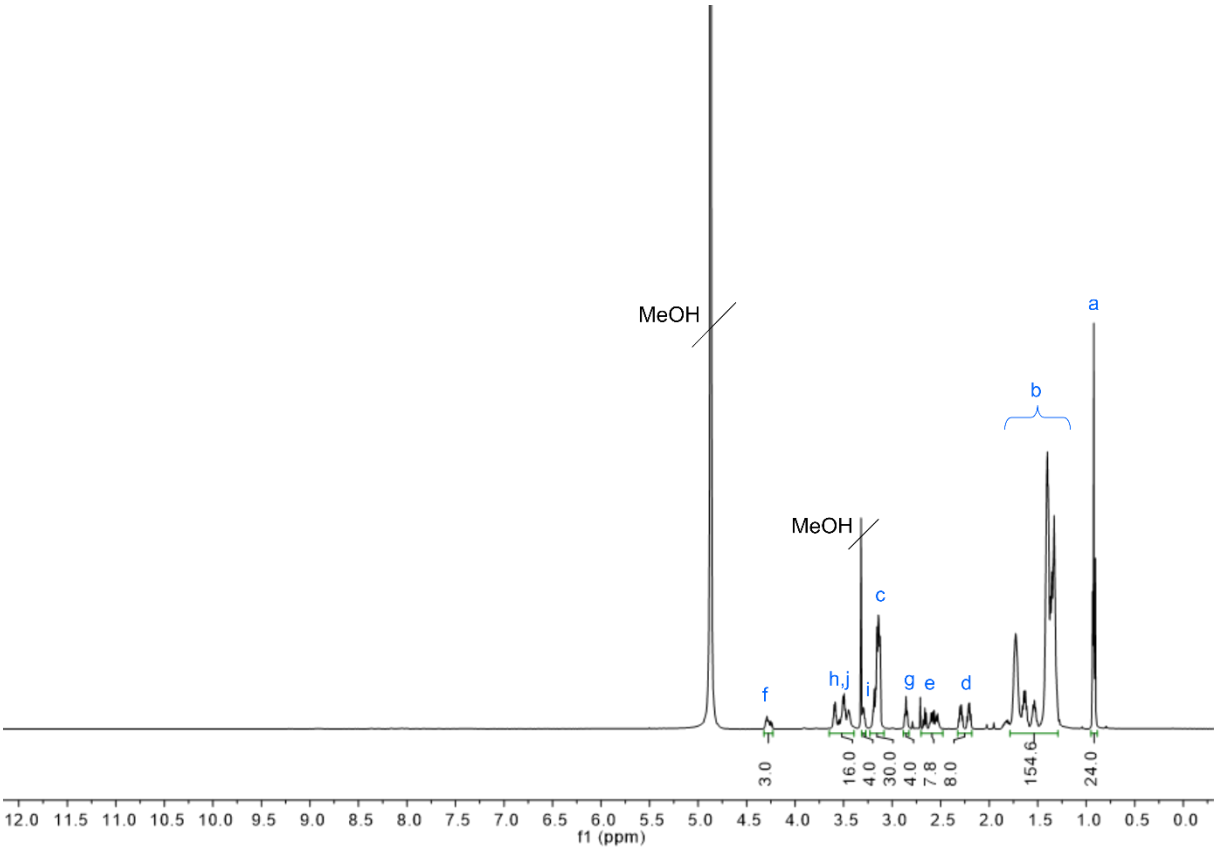

^{1}H NMR (500 MHz, Methanol-d_4) δ_H (ppm) = 4.28 (ddt, J = 19.6, 9.0, 4.0 Hz, 3H, f), 3.64 – 3.39 (m, 16H, h, j), 3.31 – 3.27 (m, 4H, i), 3.22 – 3.07 (m, 30H, c), 2.86 (dd, J = 7.7, 5.3 Hz, 4H, g), 2.70 – 2.48 (m, 8H, e), 2.25 (dtd, J = 42.9, 7.4, 4.7 Hz, 8H, d), 1.80 – 1.26 (m, 154H, b), 0.96 – 0.88 (m, 24H, a).

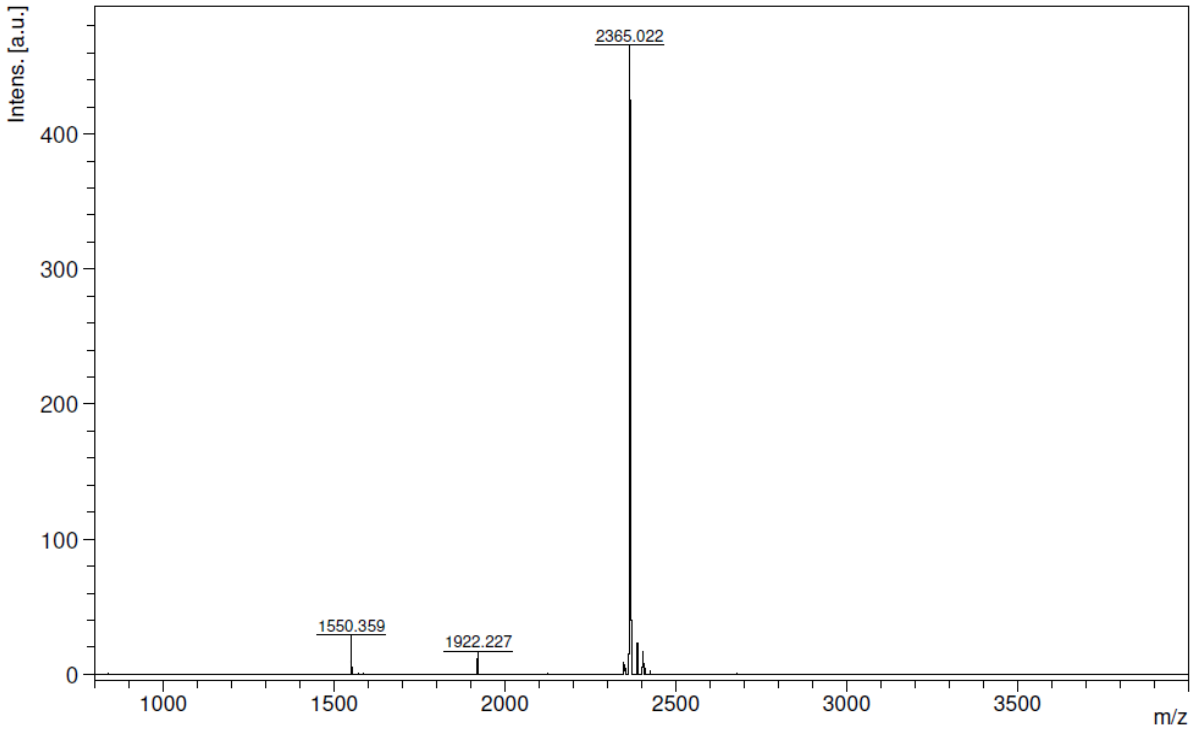

MALDI-TOF-MS: calculated for $C_{134}H_{266}N_{17}O_{12}S_2$ $[M+H]^+$: 2370.82; found $[M+H]^+$: 2365.02

1792 (8Oc-B2-1:4-ssbb$_2$)

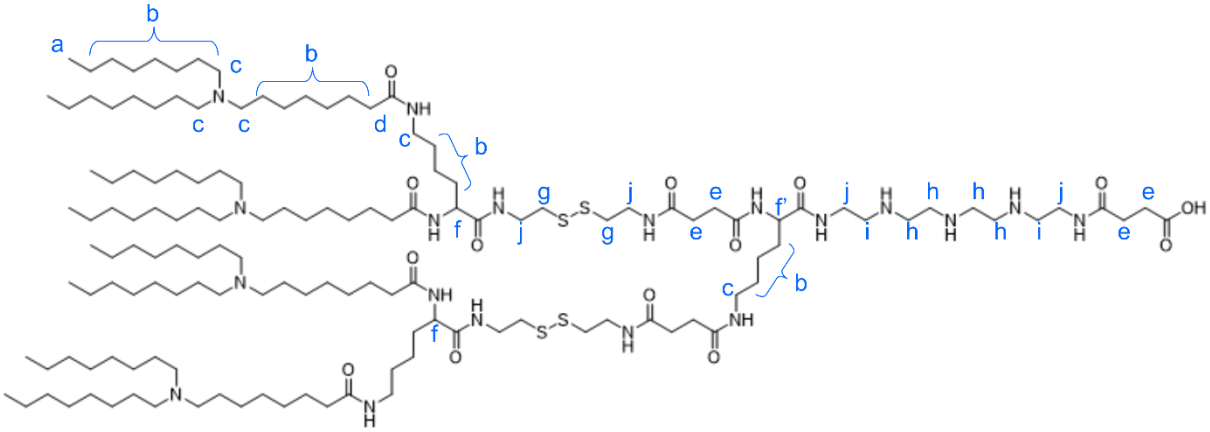

Yield: 18.6 mg (52%),

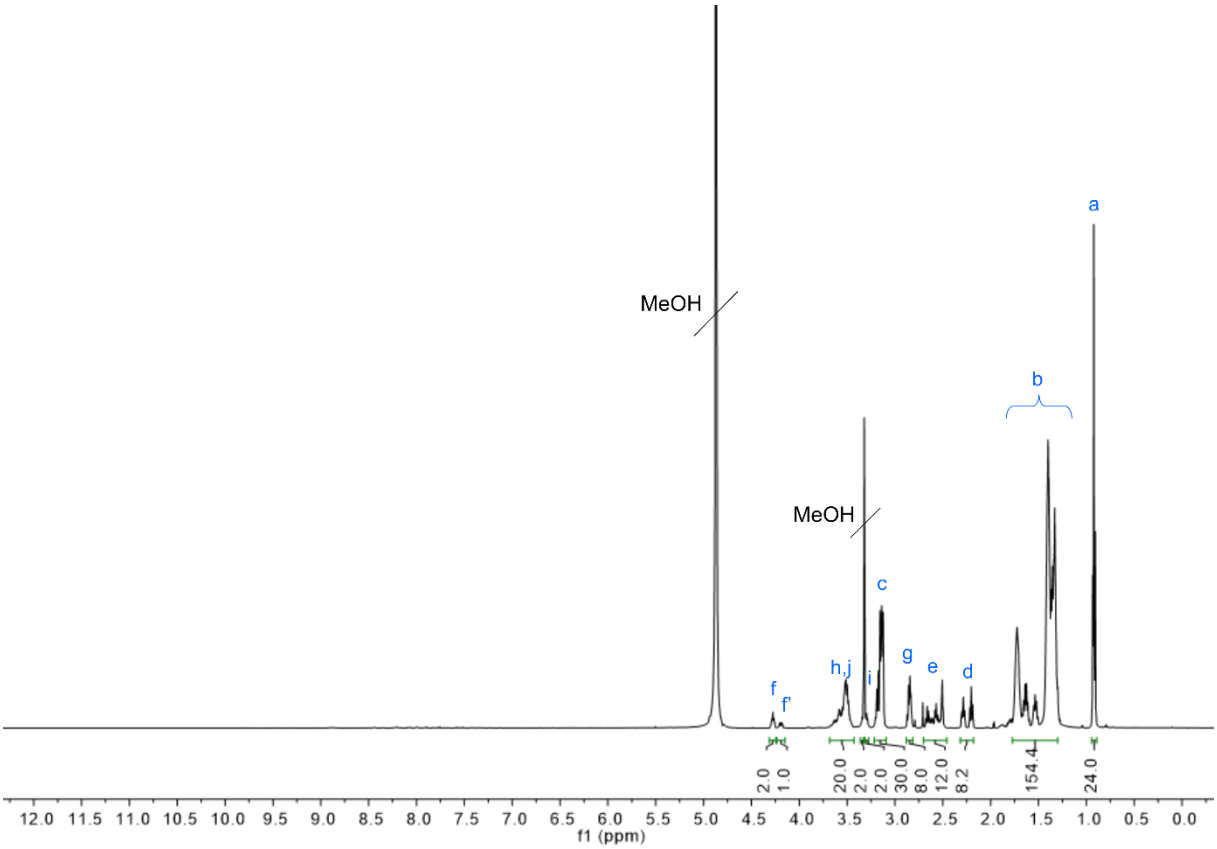

^{1}H NMR (500 MHz, Methanol-d_4) δ_H (ppm) = 4.28 (m, 2H, f), 4.19 (dd, J = 9.1, 5.1 Hz, 1H, f'), 3.69 – 3.43 (m, 20H, h, j), 3.32 (m, 4H, i, overlapping signal of solvent residue), 3.22 – 3.09 (m, 30H, c), 2.89 – 2.81 (m, 8H, g), 2.71 – 2.47 (m, 12H, e), 2.32 – 2.13 (m, 8H, d), 1.77 – 1.26 (m, 154H, b), 0.95 – 0.88 (m, 24H, a).

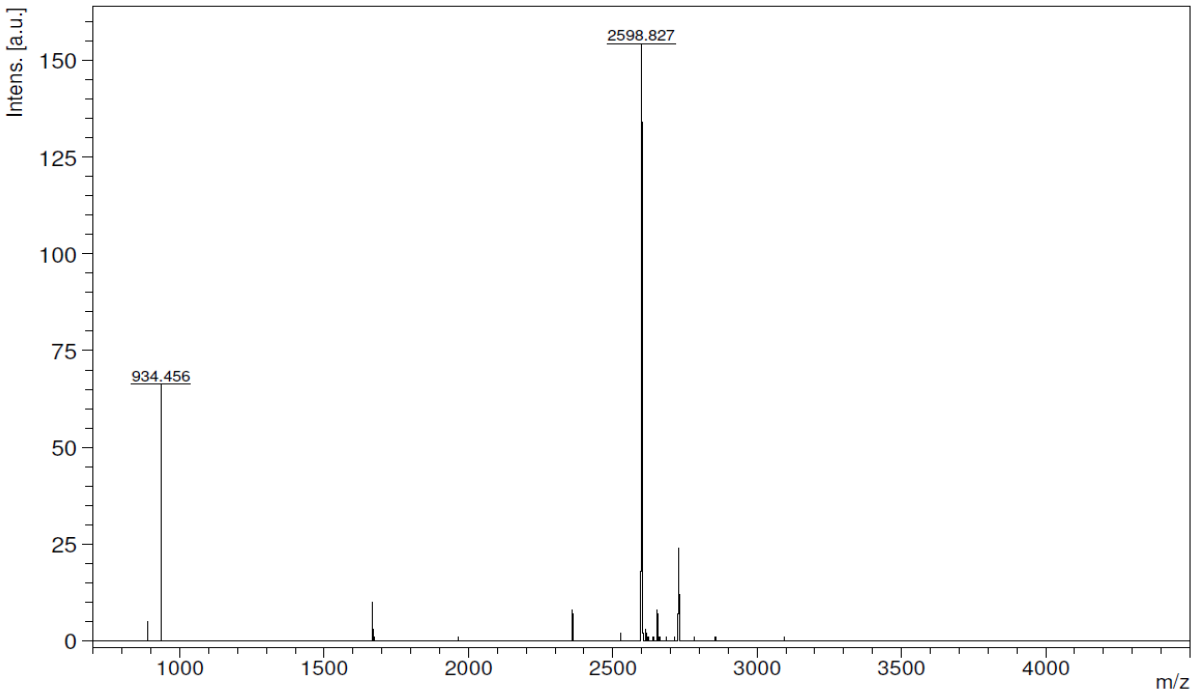

MALDI-TOF-MS: m/z calculated for $C_{142}H_{279}N_{19}O_{14}S_4$ $[M+H]^+$: 2604.07; found $[M+H]^+$: 2598.83

1793 (8Oc-B2-1:4-spacer)

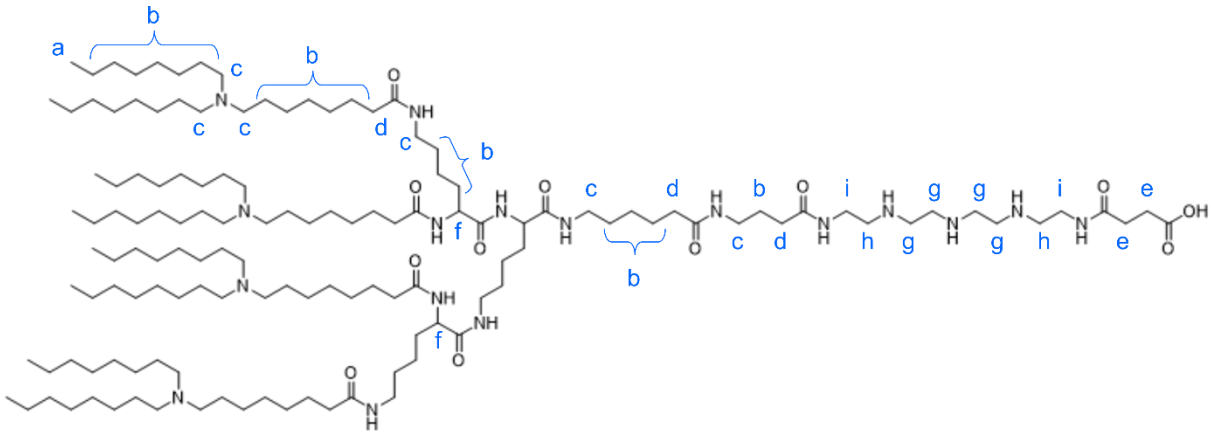

Yield: 14.9 mg, 44%

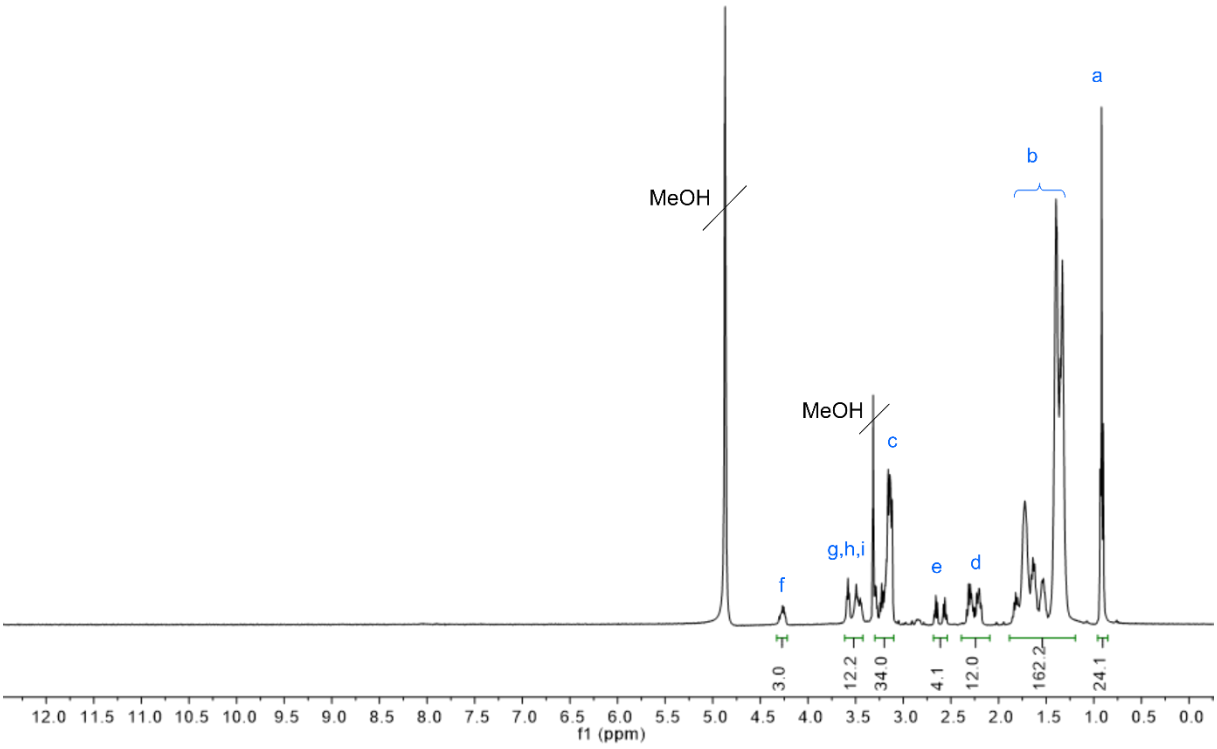

^{1}H NMR (400 MHz, Methanol-d_4) δ_H (ppm) = 4.33 – 4.21 (m, 3H, f), 3.63 – 3.38 (m, 12H, g, h, i), 3.31 – 3.09 (m, 34H, c), 2.70 – 2.54 (m, 4H, e), 2.37 – 2.14 (m, 12H, d), 1.88 – 1.19 (m, 162H, b), 0.95 – 0.87 (m, 24H, a).

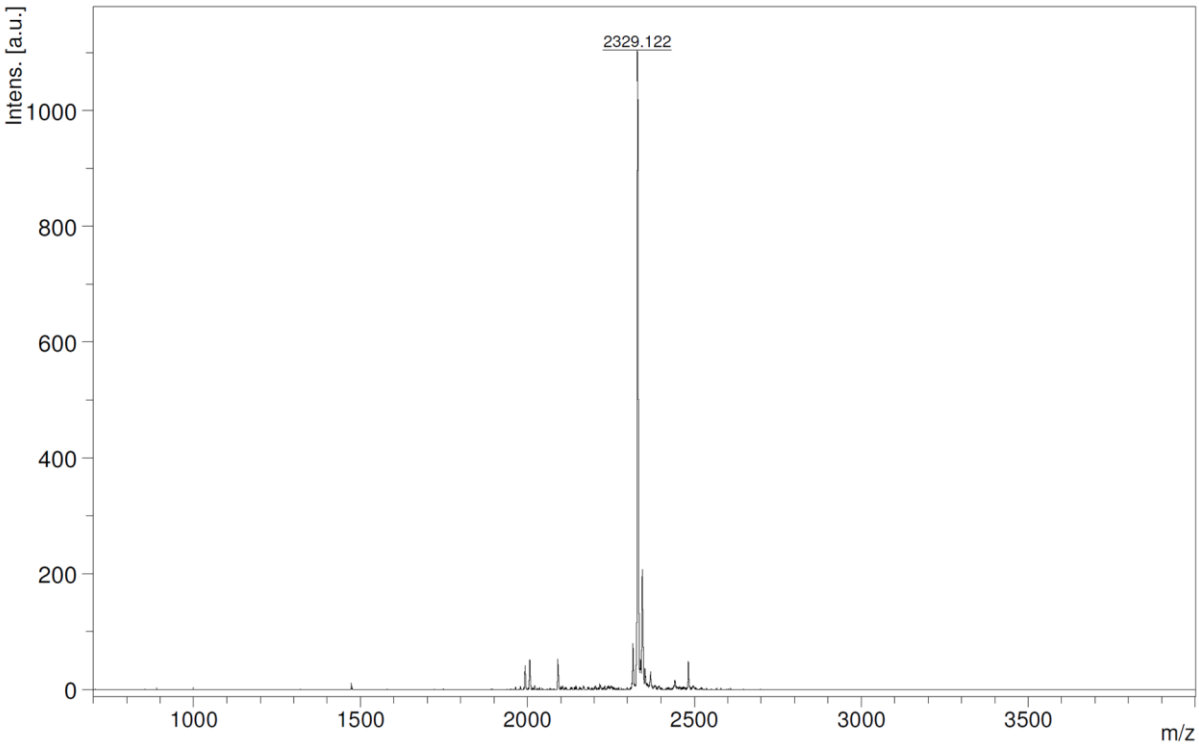

MALDI-TOF-MS m/z calculated for $C_{136}H_{269}N_{17}O_{12}$ $[M+H]^+$: 2334.11; found $[M+H]^+$: 2329.12

1794 (8Oc-B2-1:4-spacer$_2$)

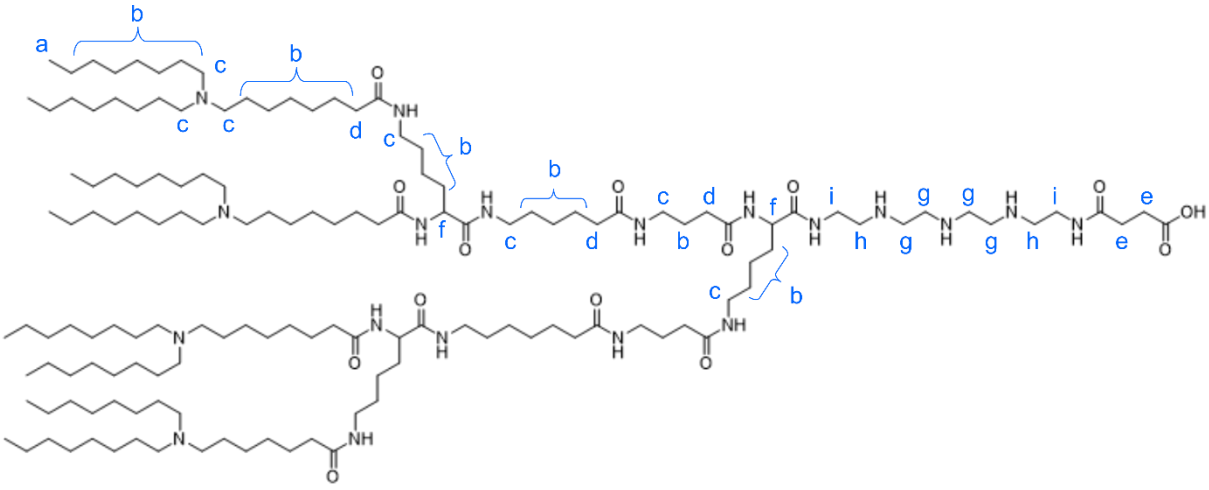

Yield: 19.6 mg, 45%

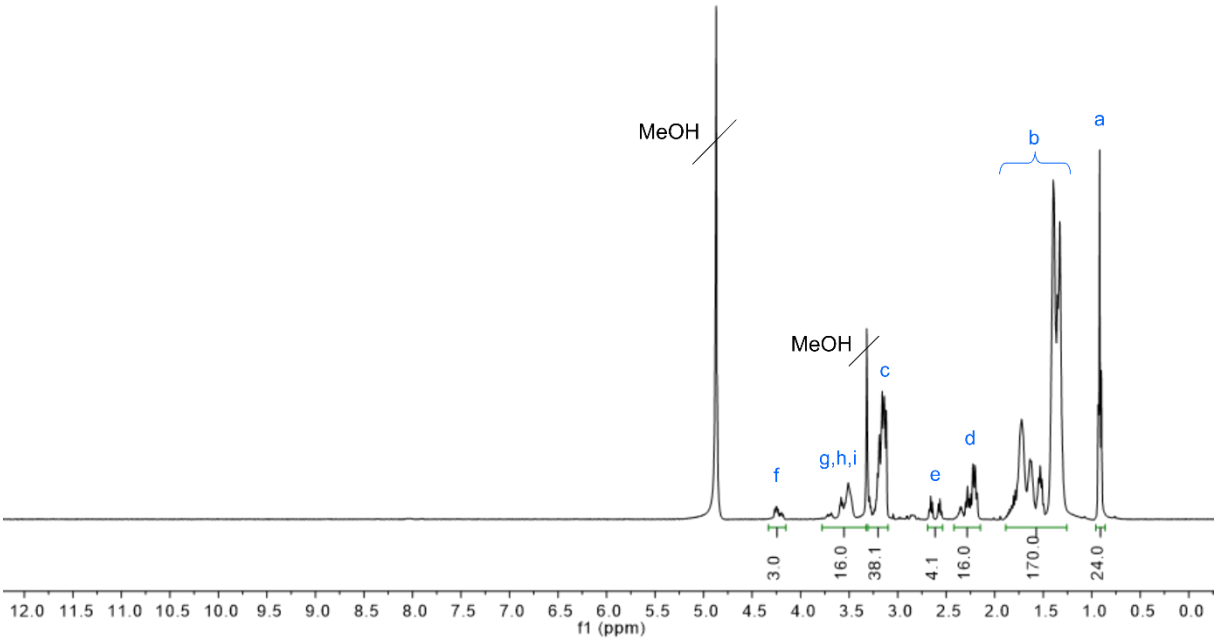

^{1}H NMR (400 MHz, Methanol-d_4) δ_H (ppm) = 4.31 – 4.17 (m, 3H, f), 3.77 – 3.38 (m, 16H, g, h, i), 3.30 – 3.10 (m, 38H, c), 2.69 – 2.55 (m, 4H, e), 2.41 – 2.15 (m, 16H, d), 1.91 – 1.26 (m, 170H, b), 0.96 – 0.87 (m, 24H, a).

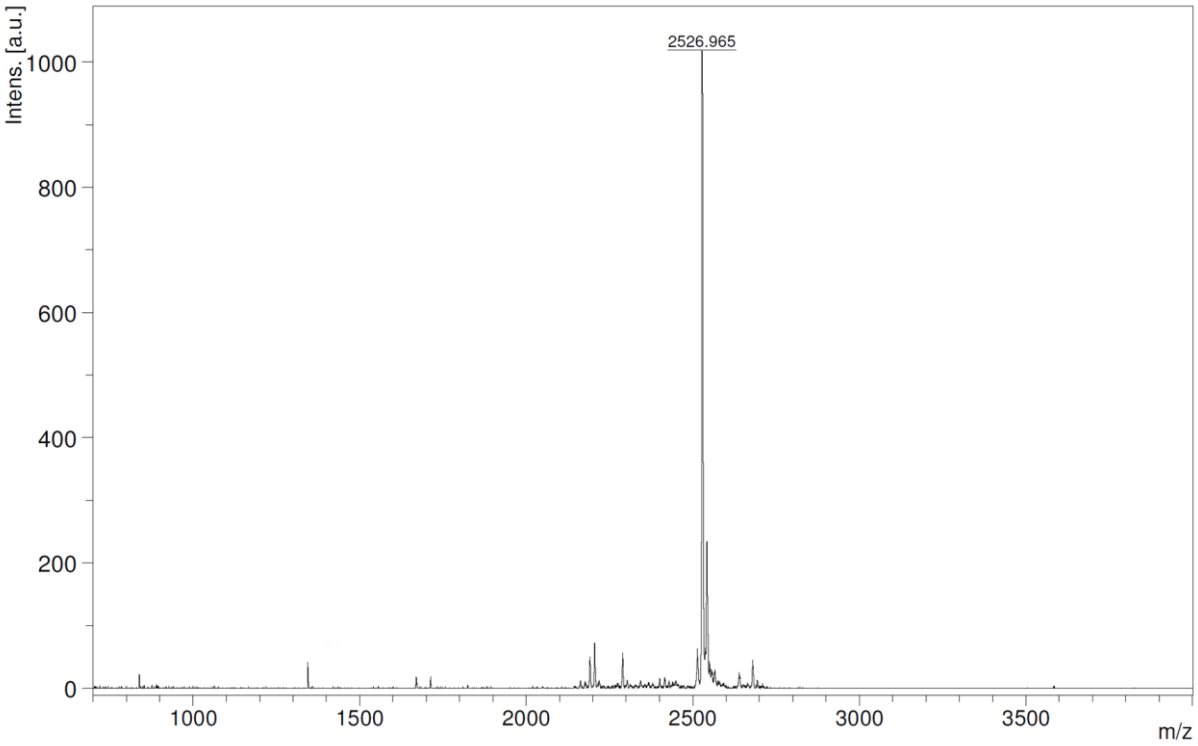

MALDI-TOF-MS m/z calculated for $C_{146}H_{287}N_{19}O_{14}$ $[M+H]^+$ 2532.24; found $[M+H]^+$ 2526.97

6.1.5.2 8Oc-B2-2:4 library

1730 **(8Oc-B2-2:4)**

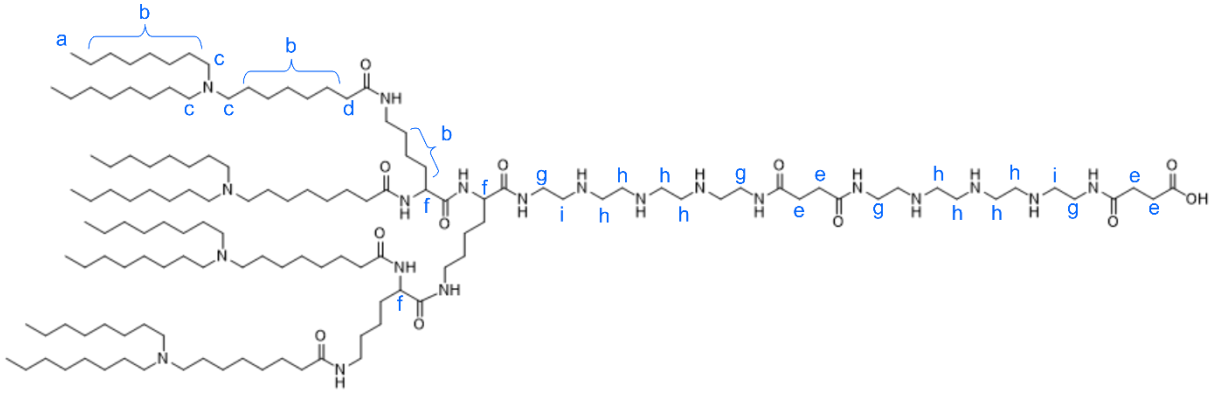

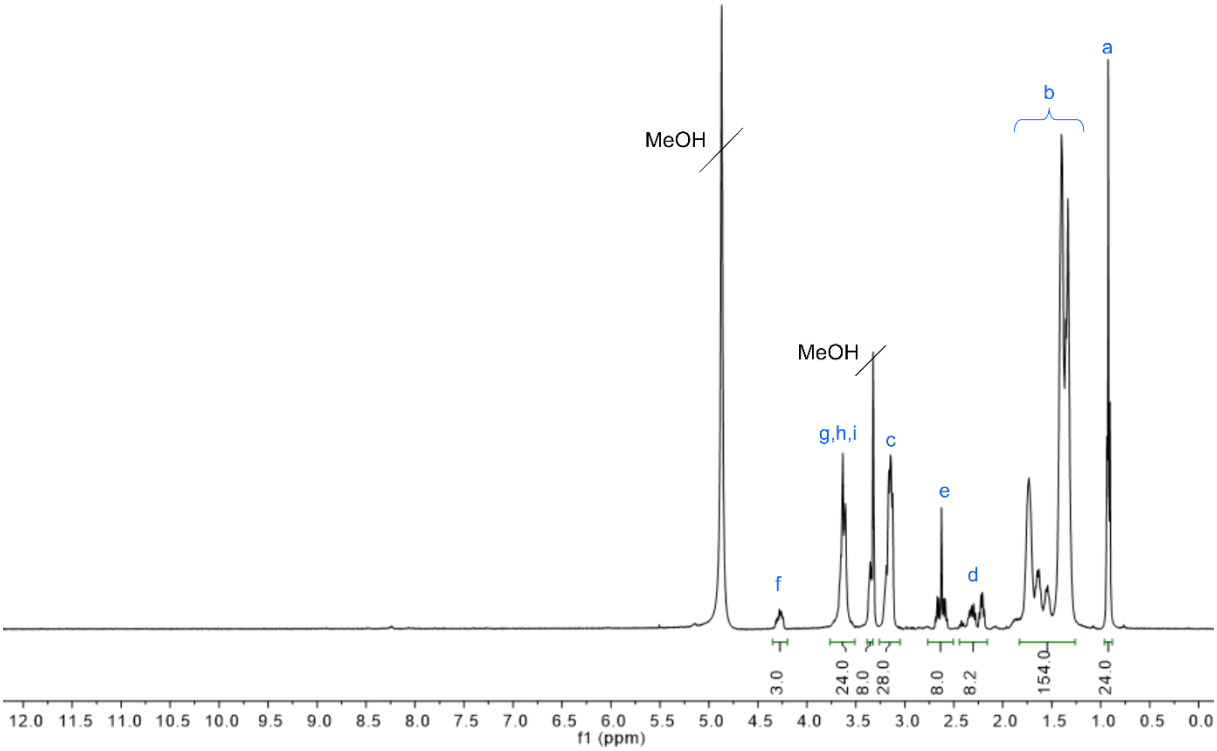

^{1}H NMR (400 MHz, Methanol-d_4) δ_H (ppm) = 4.36 – 4.23 (m, 3H, f), 3.64 (td, J = 11.3, 4.6 Hz, 24H, g, h), 3.35 (m, 8H, i), 3.16 (td, J = 11.7, 10.0, 4.5 Hz, 28H, c), 2.72 – 2.57 (m, 8H, e), 2.46 – 2.13 (m, 8H, d), 1.83 – 1.25 (m, 154H, b), 1.00 – 0.86 (m, 24H, a).

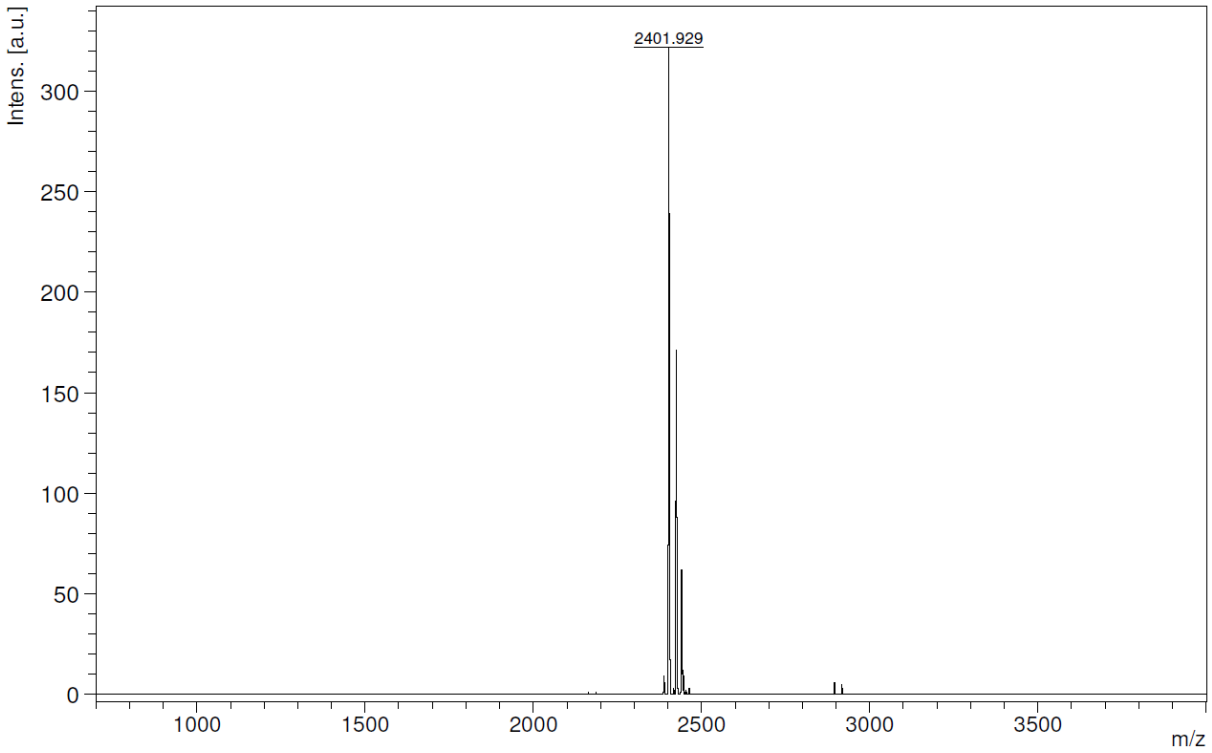

MALDI-TOF-MS m/z calculated for $C_{138}H_{276}N_{20}O_{12}$ $[M+H]^+$ 2408.86; found $[M+H]^+$ 2401.93

1823 (8Oc-B2-2:4 ssbb)

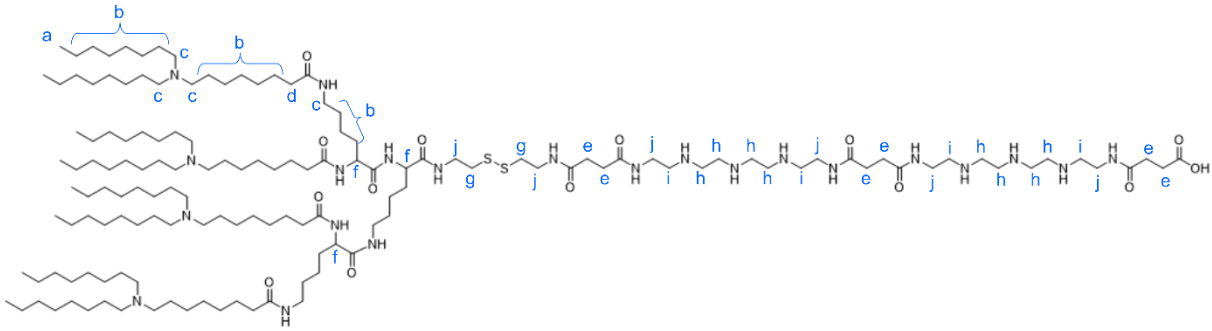

Yield: 15.8 mg, 41%

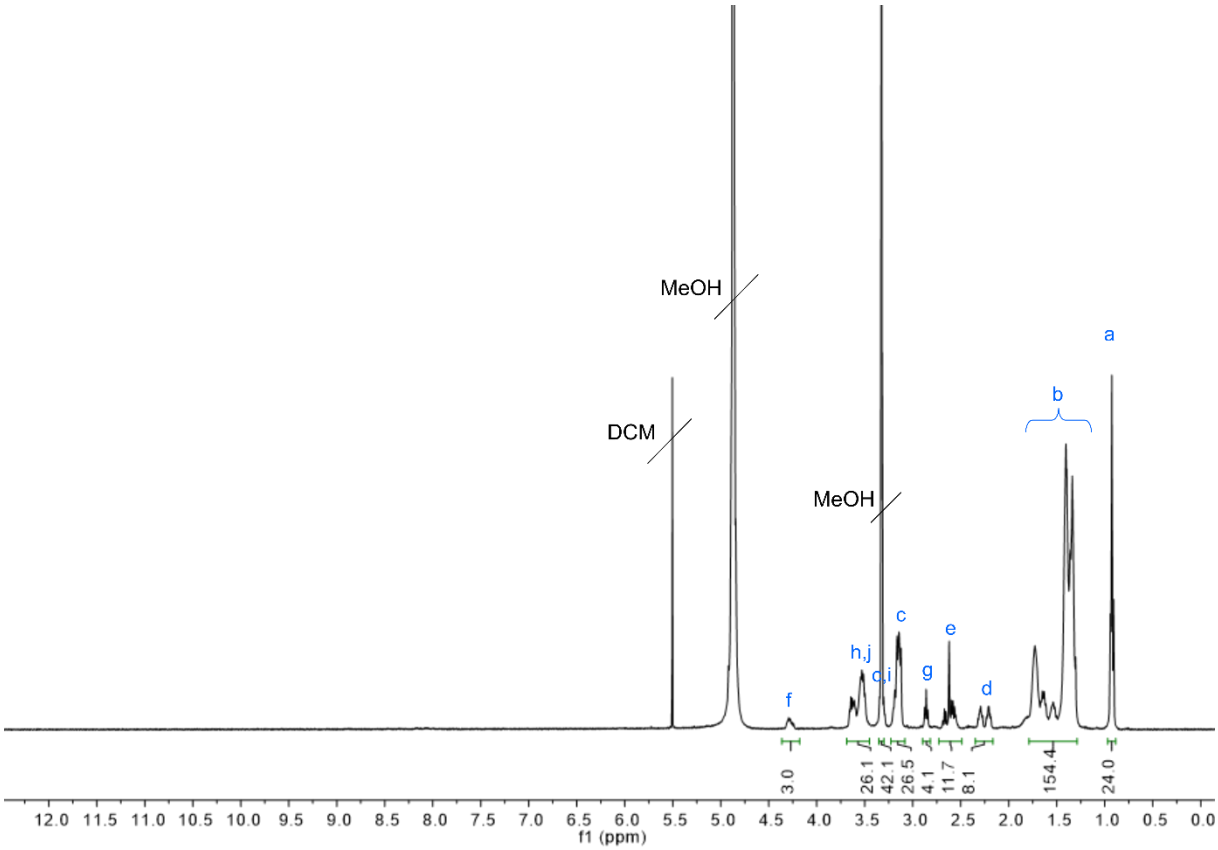

^{1}H NMR (400 MHz, Methanol-d_4) δ_H (ppm) =4.34 – 4.22 (m, 3H, f), 3.69 – 3.47 (m, 26H, h,j), 3.33 (m, 12H, c,i, overlapping signal of solvent residue), 3.23 – 3.09 (m, 26H, c), 2.86 (t, J = 6.7 Hz, 4H, g), 2.72 – 2.53 (m, 12H, e), 2.34 – 2.17 (m, 8H, d), 1.80 – 1.28 (m, 154H, b), 0.98 – 0.89 (m, 24H, a).

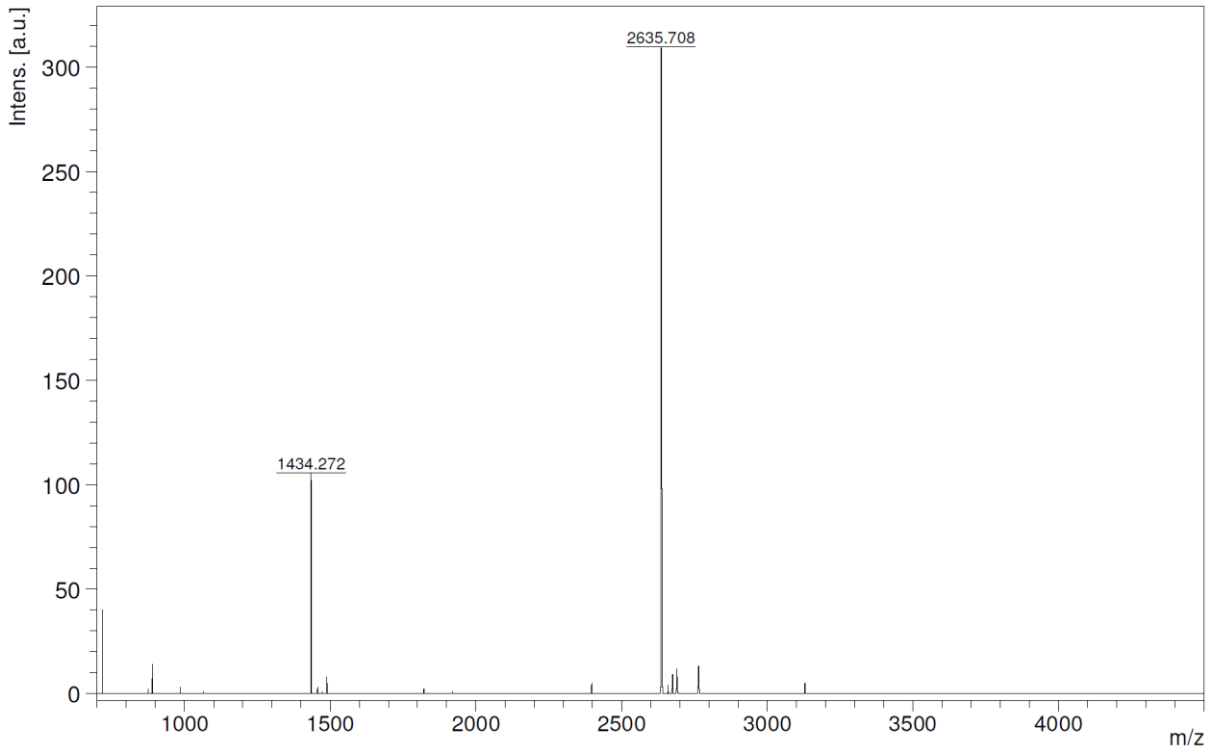

MALDI-TOF-MS m/z calculated for $C_{146}H_{290}N_{22}O_{14}S_2$ $[M+H]^+$: 2641.22; found $[M+H]^+$: 2635.71

1824 (8Oc-B2-2:4 -ssbb$_2$)

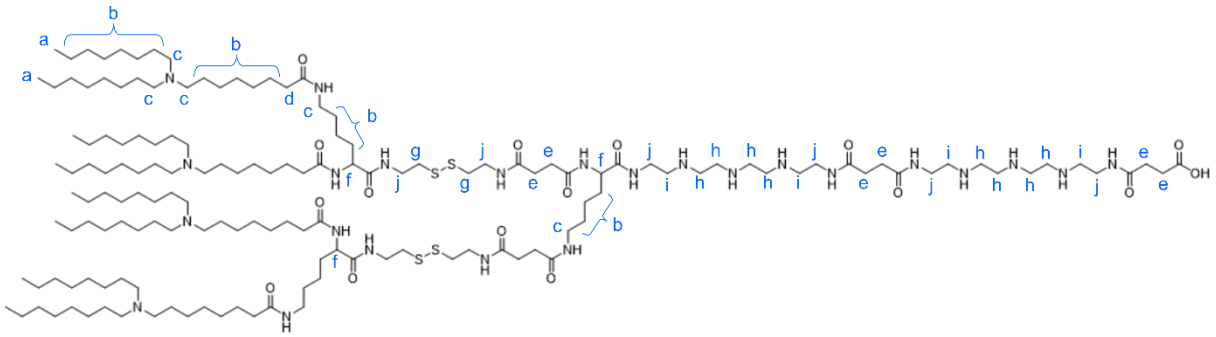

Yield: 25.6 mg, 62%

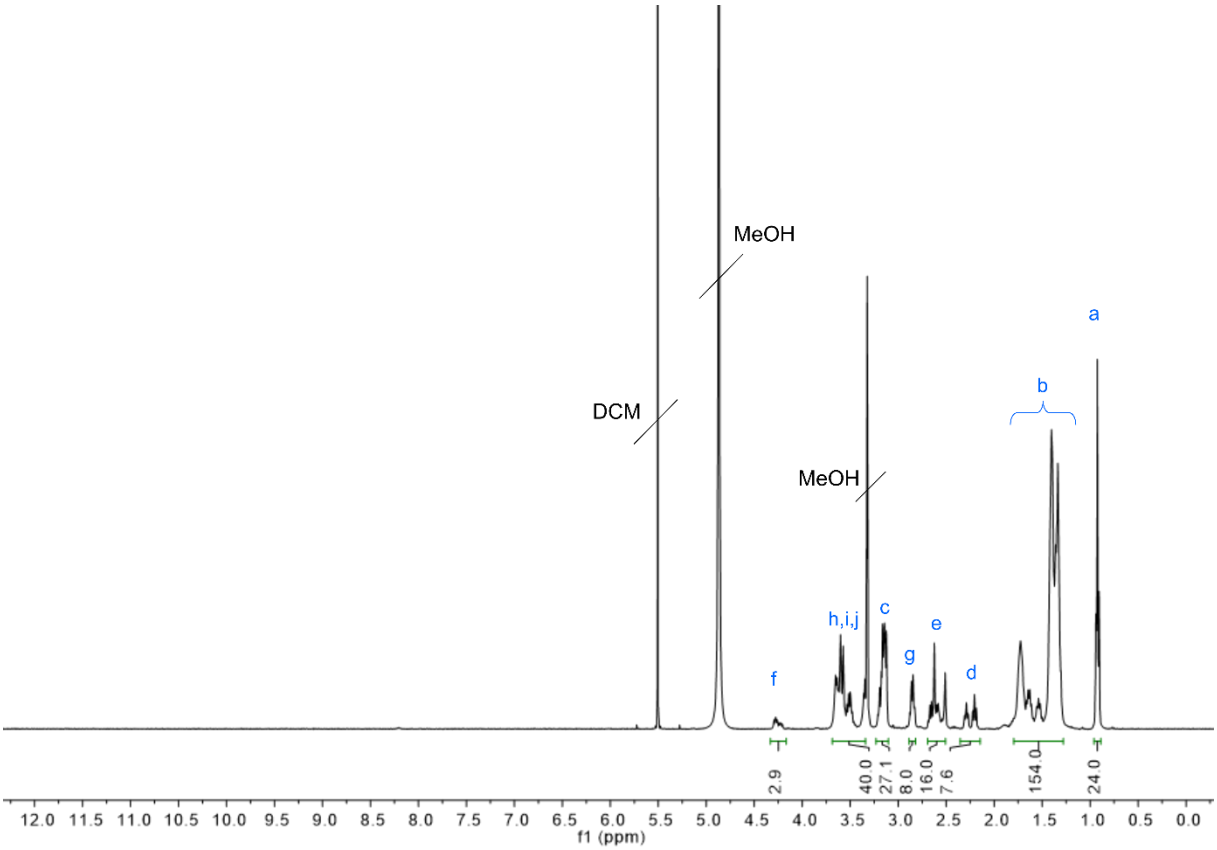

^{1}H NMR (500 MHz, Methanol-d_4) δ_H (ppm) =4.33 – 4.19 (m, 3H, f), 3.70 – 3.34 (m, 40H, h, i, j), 3.24 – 3.09 (m, 27H, c), 2.90 – 2.81 (m, 8H, g), 2.70 – 2.49 (m, 16H, e), 2.34 – 2.15 (m, 8H, d), 1.80 – 1.27 (m, 154H, b), 0.96 – 0.89 (m, 24H, a).

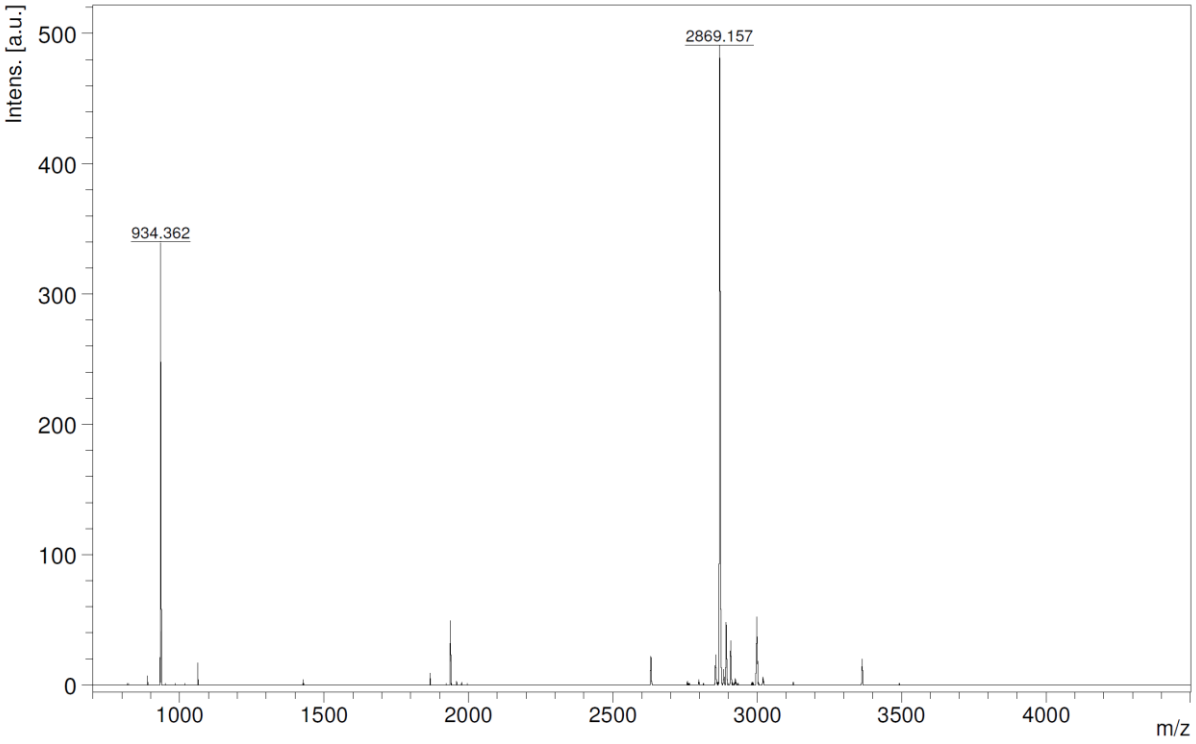

MALDI-TOF-MS m/z calculated for $C_{154}H_{304}N_{24}O_{16}S_4$ $[M+H]^+$: 2874.26; found $[M+H]^+$: 2869.157

1825 (8Oc-B2-2:4 -spacer)

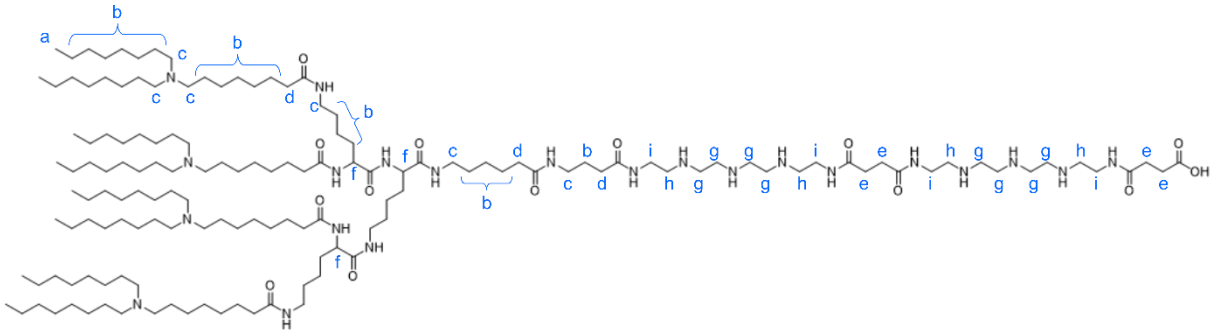

Yield: 28.0 mg, 74%

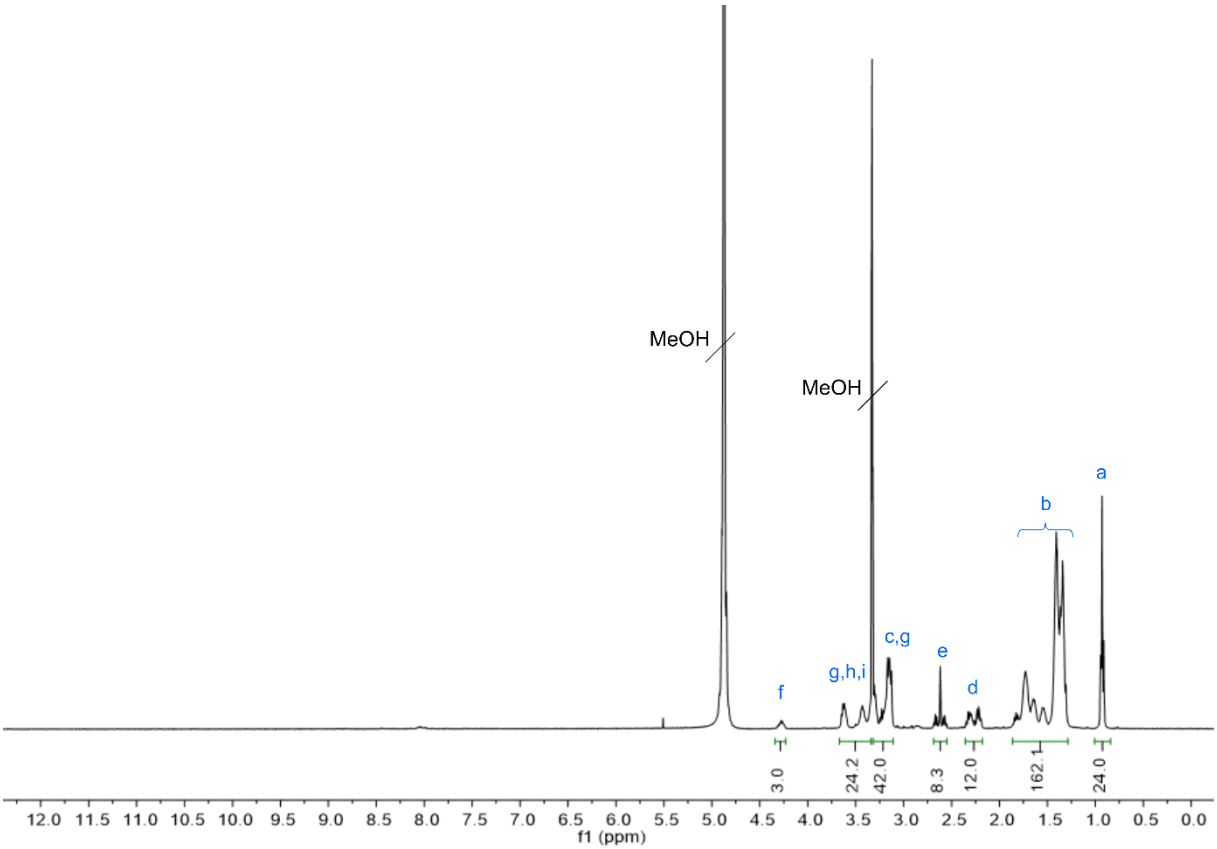

^{1}H NMR (400 MHz, Methanol-d_4) δ_H (ppm) = 4.34 – 4.23 (m, 3H, f), 3.68 – 3.34 (m, 24H, g, h, i, overlapping signal of solvent residue), 3.32 – 3.10 (m, 42H, c, g), 2.70 – 2.54 (m, 8H, e), 2.36 – 2.18 (m, 12H, d), 1.87 – 1.28 (m, 162H, b), 1.00 – 0.87 (m, 24H, a).

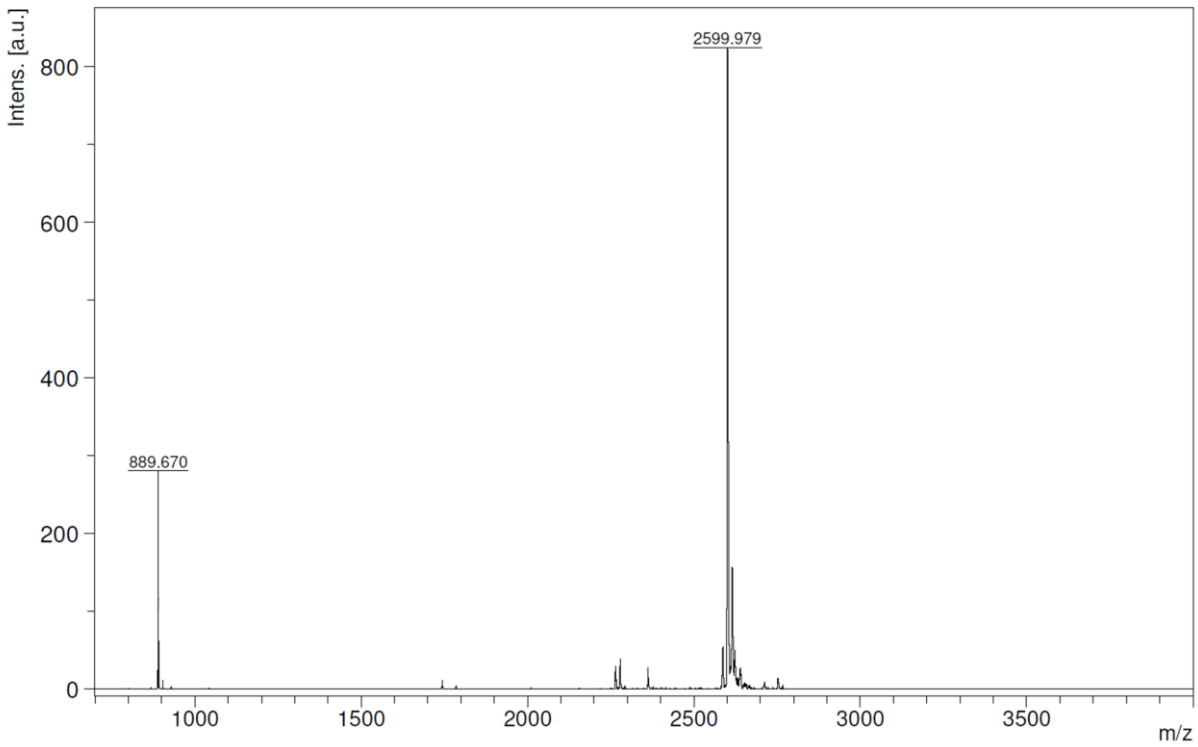

MALDI-TOF-MS m/z calculated for $C_{148}H_{294}N_{22}O_{14}$ $[M+H]^+$: 2604.30; found for $[M+H]^+$: 2599.98

1826 (8Oc-B2-2:4 -spacer$_2$)

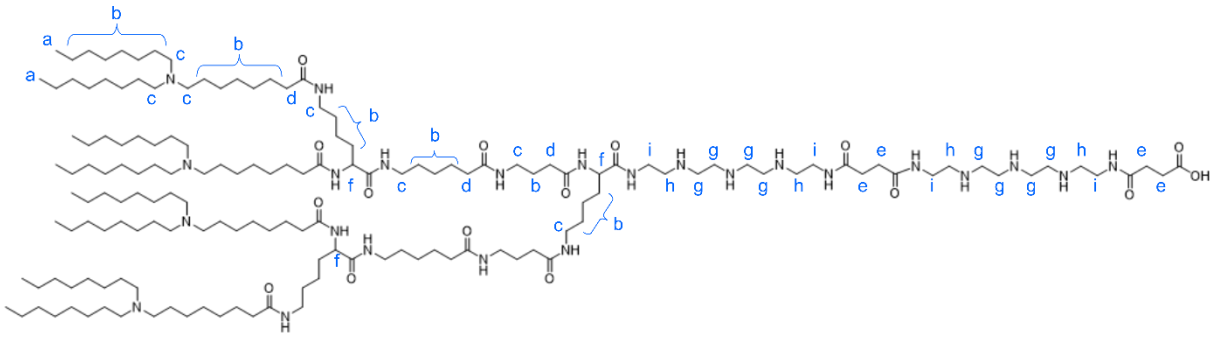

Yield: 14.8 mg, 39%

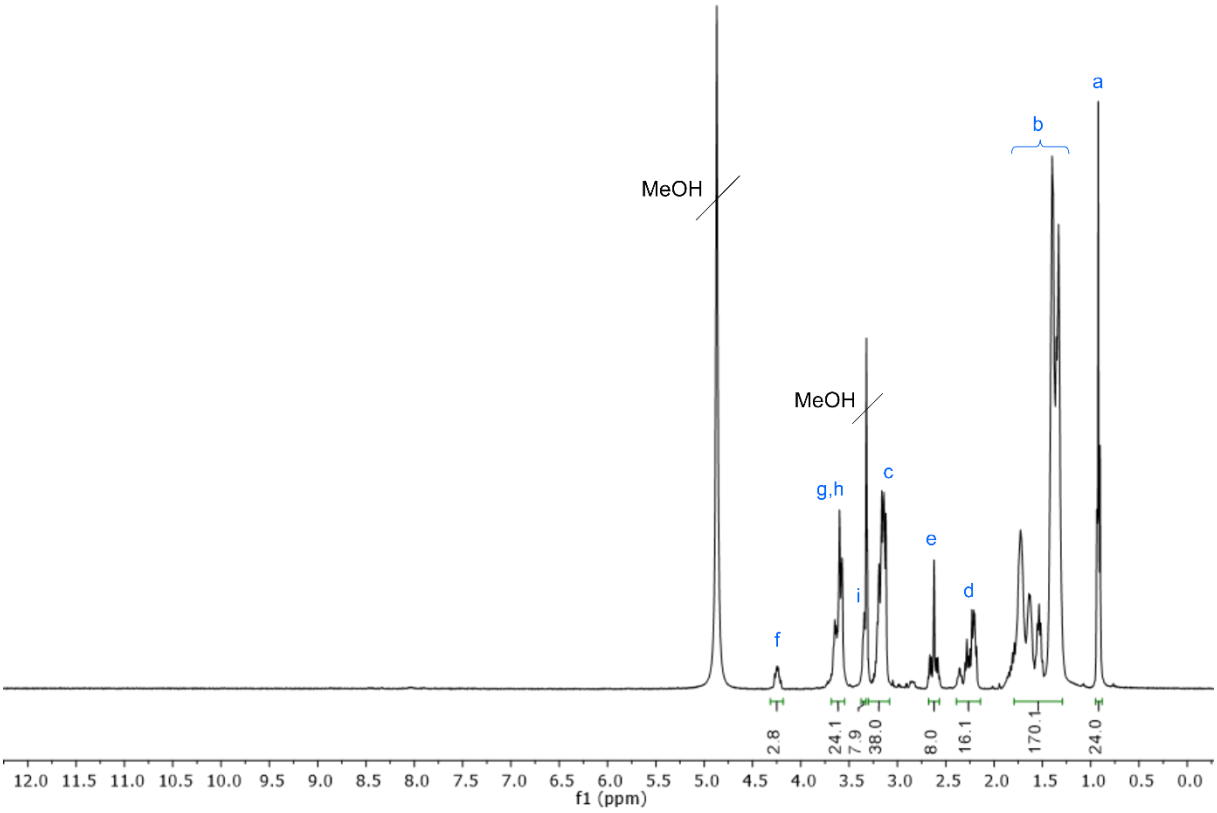

^{1}H NMR (400 MHz, Methanol-d_4) δ_H (ppm) =4.24 (td, J = 9.9, 5.6 Hz, 3H, f), 3.74 – 3.50 (m, 24H, g, h), 3.38 – 3.33 (m, 8H, i), 3.25 – 3.05 (m, 38H, c), 2.68 – 2.53 (m, 8H, e), 2.41 – 2.15 (m, 16H, d), 1.81 – 1.26 (m, 170H, b), 1.00 – 0.88 (m, 24H, a).

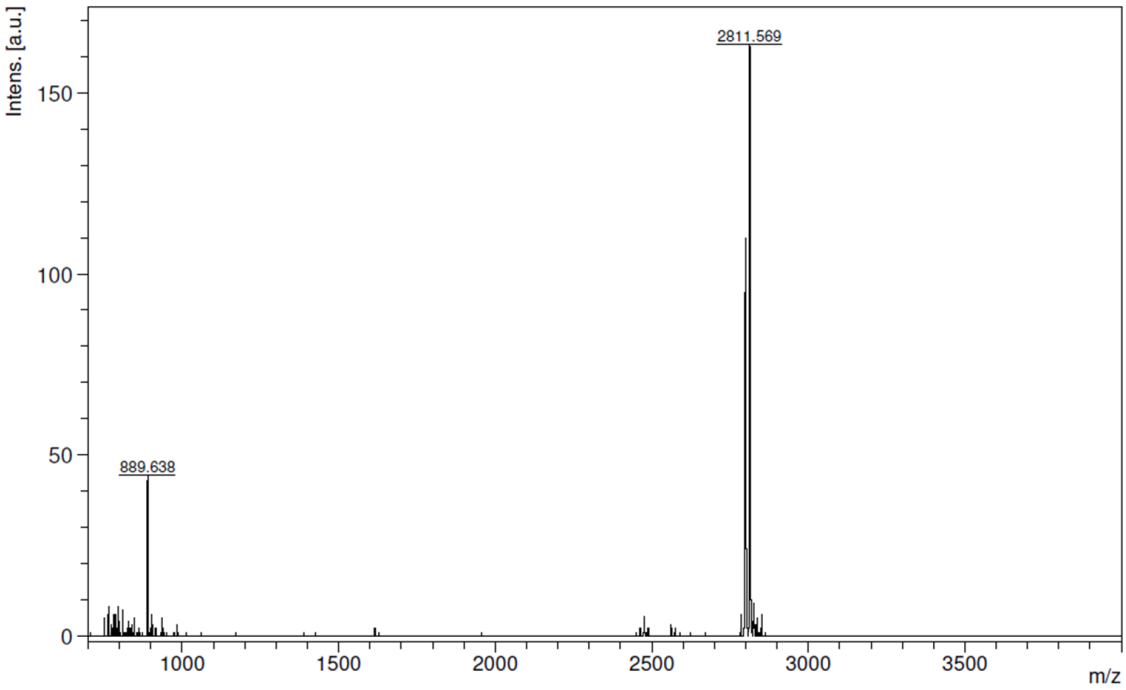

MALDI-TOF-MS m/z calculated for $C_{158}H_{312}N_{24}O_{16}$ $[M+H]^+$: 2802.43; found $[M+H]^+$: 2811.569.

6.1.5.3 12Oc-U1-1:2 analogs

1821 (12Oc-U1-1:2-ssbb)

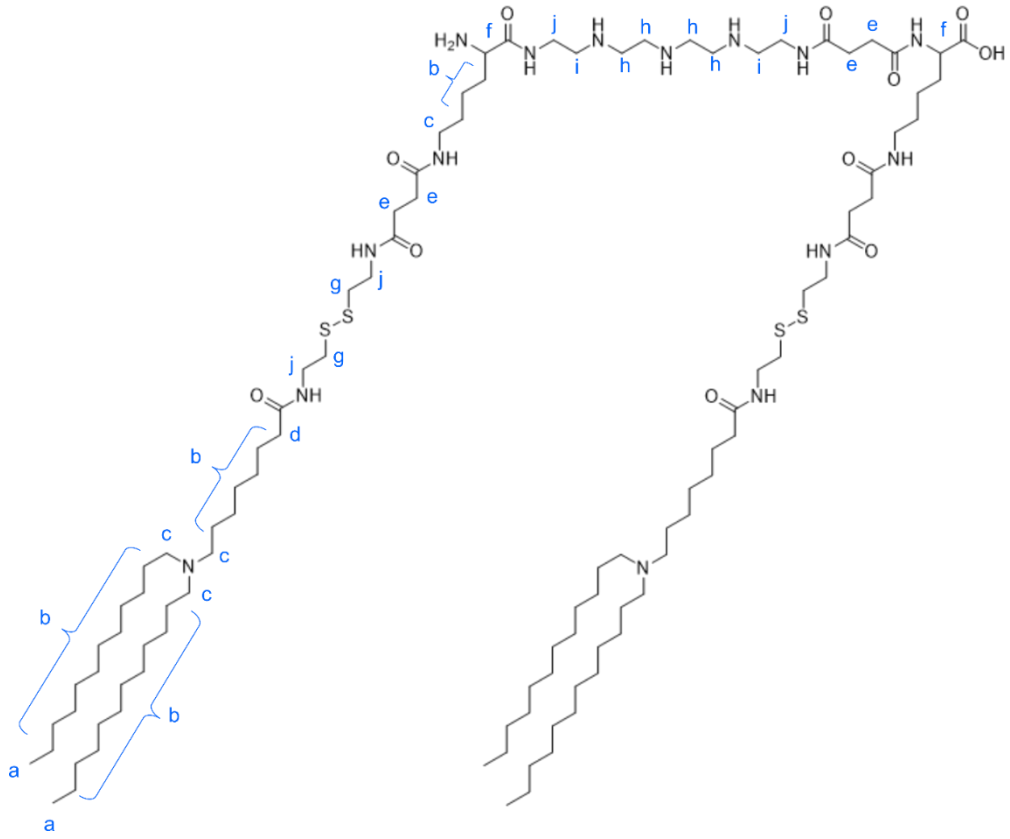

Yield: 17.7 mg, 73%

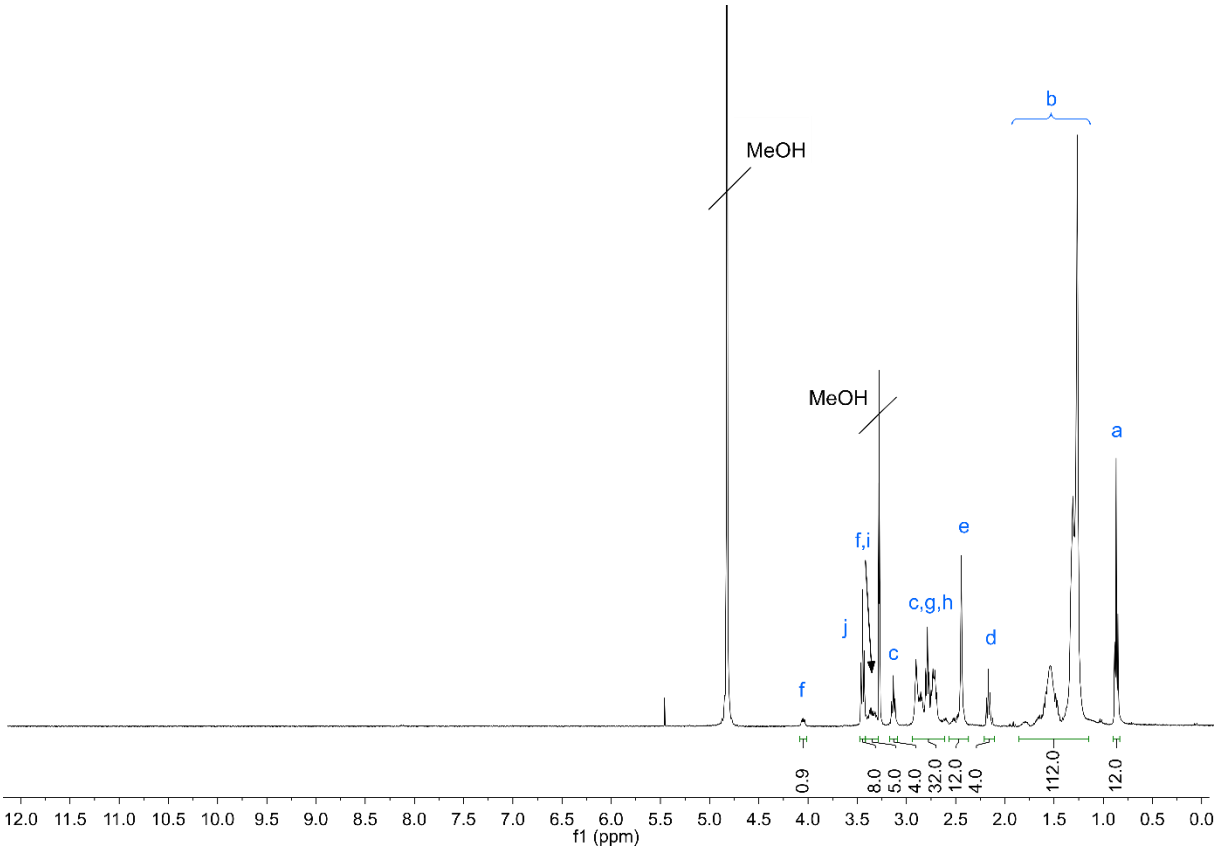

^{1}H NMR (400 MHz, Methanol-d_4) δ_H (ppm) = 4.14 – 4.05 (m, 1H, f), 3.49 (t, J = 6.7 Hz, j), 3.44 – 3.33 (m, 5H, f, i), 3.18 (t, J = 6.9 Hz, 4H, c), 3.00 – 2.65 (m, 32H, c, g, h), 2.49 (s, 12H, e), 2.21 (t, J = 7.4 Hz, 4H, d), 1.90 – 1.19 (m, 112H, b), 0.94 – 0.86 (m, 12H, a).

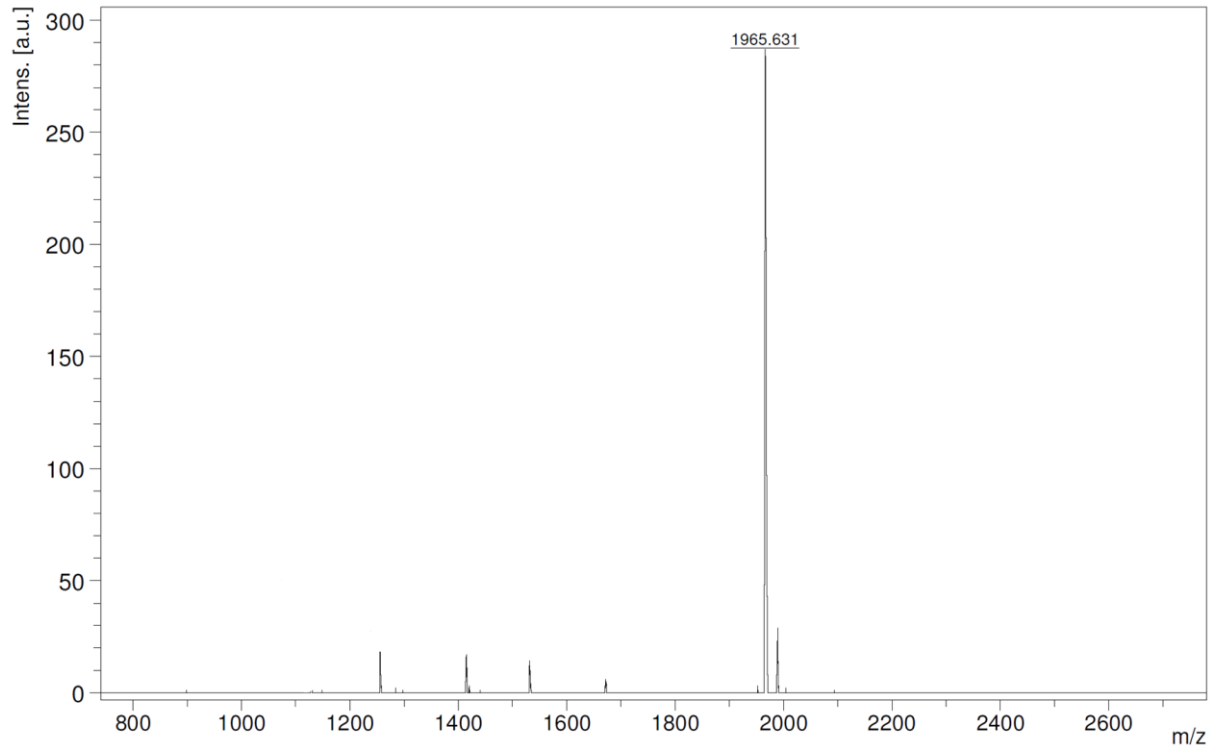

MALDI-TOF-MS m/z calculated for $C_{158}H_{312}N_{24}O_{16}$ $[M+H]^+$: 1968.483; found $[M+H]^+$: 1965.631

1822 (12Oc-U1-1:2-spacer)

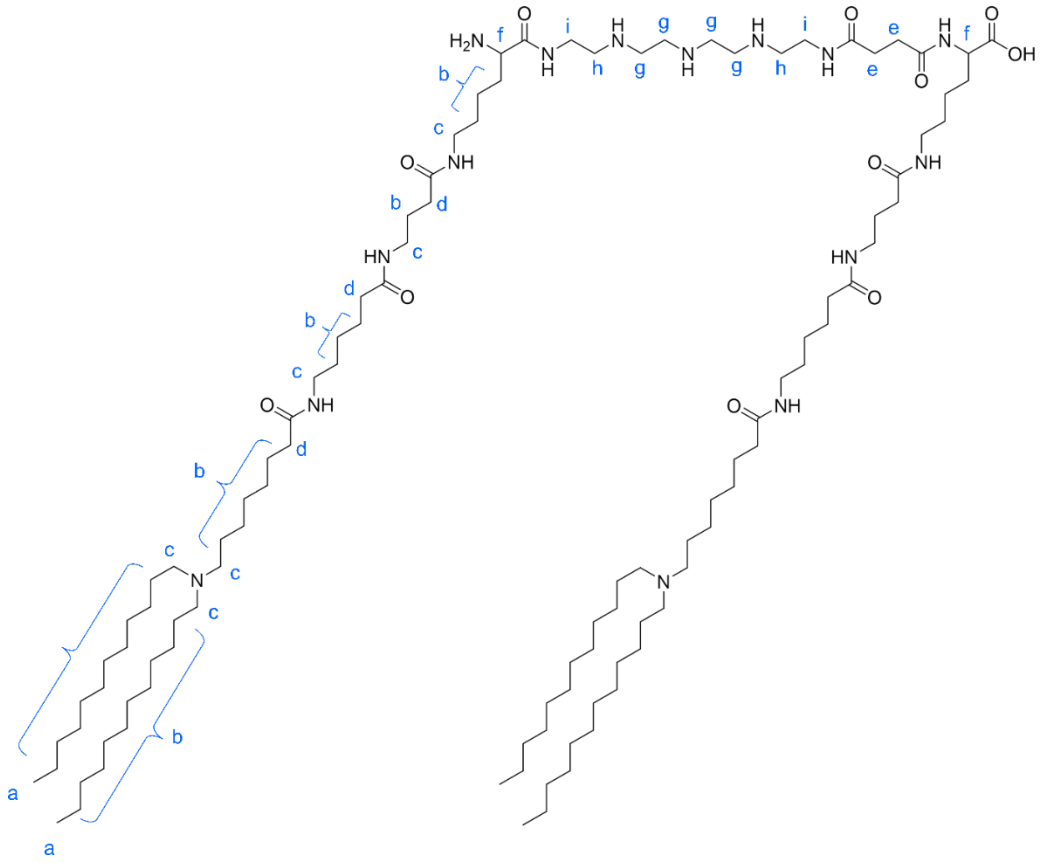

Yield: 15.3 mg, 52%

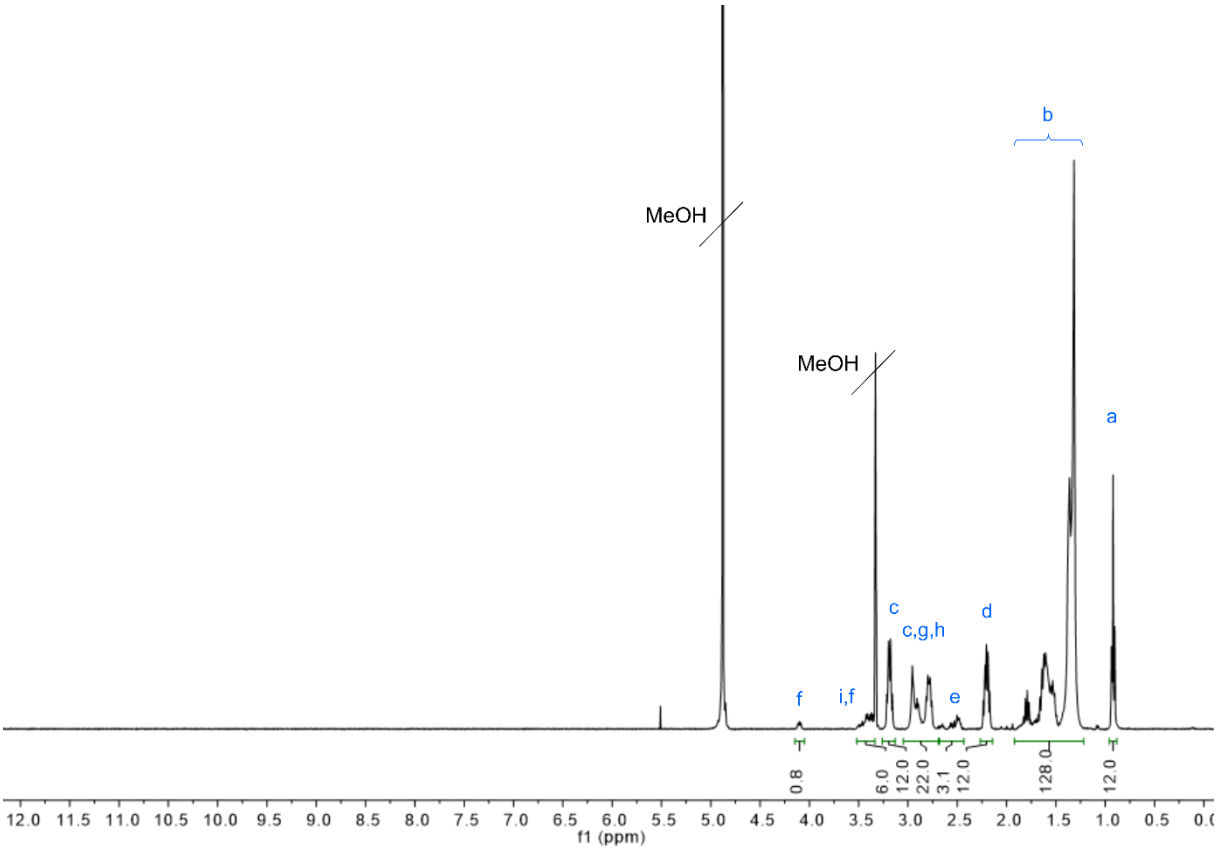

^{1}H NMR (400 MHz, Methanol-d_4) δ_H (ppm) = 4.10 (dd, J = 8.6, 4.7 Hz, 1H, f), 3.52 – 3.33 (m, 5H, f, i), 3.24 – 3.13 (m, 12H, c), 3.03 – 2.70 (m, 22H, g, h, c), 2.68 – 2.42 (m, 4H, e), 2.26 – 2.16 (m, 12H, d), 1.92 – 1.23 (m, 128H, b), 0.97 – 0.87 (m, 12H, a).

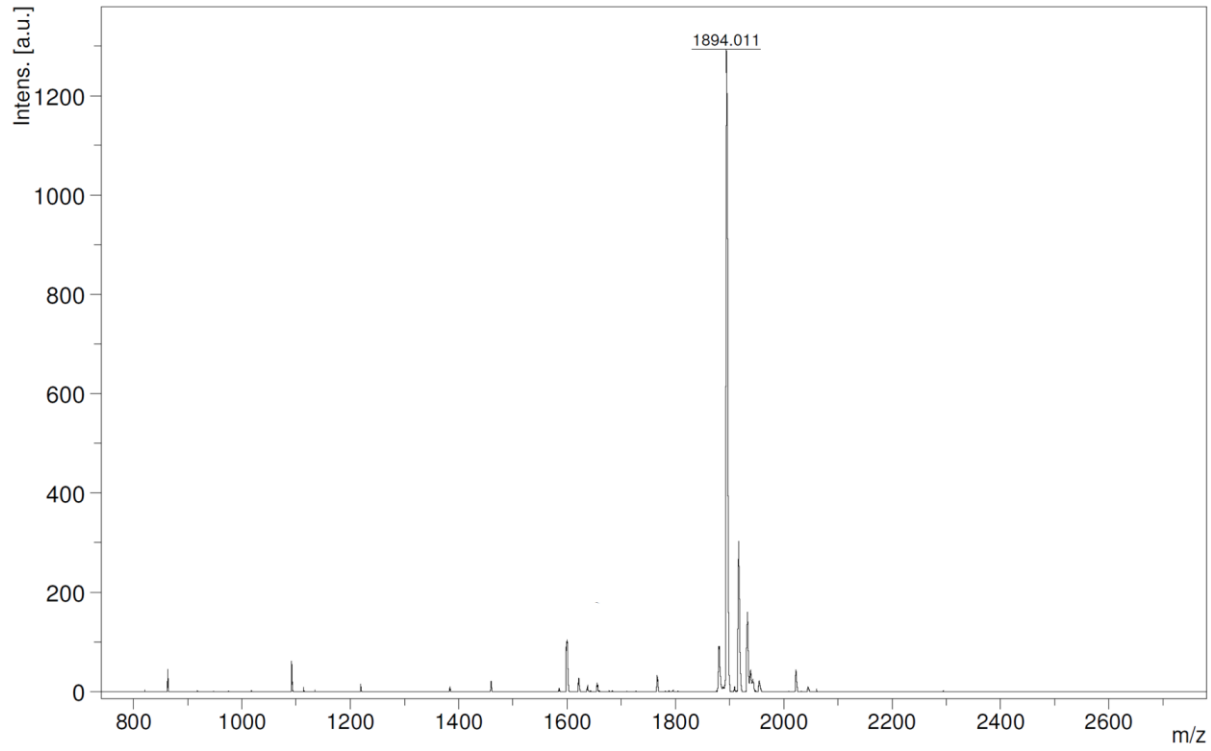

MALDI-TOF-MS m/z calculated for $C_{108}H_{213}N_{15}O_{11}$ $[M+H]^+$: 1896.66; found $[M+H]^+$: 1894.011

6.2 Abbreviations

Ac	acetylated
ACN	acetonitrile
ALAS-1	aminolevulinic acid synthase 1
ALS	amyotrophic lateral sclerosis
APC	antigen-presenting cells
ApoB	apolipoprotein B
ApoE	apolipoprotein E
ASF	asialofetuin
ASGCT	American Society of Gene and Cell Therapy
ASGPR	asialo glycoprotein receptor
ASO	antisense oligonucleotide
ASOR	asialorosomucoid
ATP	adenosin triphosphate
Au-NPs	gold nanoparticles
BafA1	bafilomycin A1
BBB	blood-brain barrier
BCEC	brain capillary endothelial cell
Boc	tert-butoxycarbonyl
C_6C_4	dipeptide spacer
CD206	mannose receptor
CLSM	confocal laser scanning microscopy
CMT	carrier-mediated transcytosis
CNS	central nervous system
COPD	chronic obstructive pulmonary disease
COVID-19	corona virus disease
CRD	Carbohydrate recognition domain
CRISPR	clustered regularly interspaced short palindromic repeats
CTG	CellTiterGlo®
Ctrl	Control
CuAAC	Copper catalyzed alkyne-azide cycloaddition
$CuSO_4$	copper sulfate
Cy5	Cyanine5
D2O	deuterated H2O
DAD	diode array detector
DAPI	4',6-diamidino-2'-phenylindole
DBCO	dibenzocyclooctyne
DC	dendritic cell
DCA	docosanoic acid
DCM	dichlormethan
DC-SIGN	dendritic cell-specific intercellular adhesion molecule-3-grabbing non integrin
Dde	[*N*-(1-(4,4-dimethyl-2,6-dioxocyclohexylidene)ethyl)]
DFG	german research foundation
DIC	diisopropylcarbodiimide
DIPEA	N,N-diisopropylethylamine
Dlin-MC3 DMA	Dilinoleyl-methyl-4-dimethylaminobutyrate
DLS	dynamic light scattering
DMAP	4-dimethylaminopyridine
DMEM	Dulbecco's modified Eagle medium
DMF	dimethylformamide
DMSO	dimethylsulfoxide
DNA	desoxyribonucleic acid
DOTAP	dioleoyl-3-trimethylammonium propane
DSPC	1,2-distearoyl-sn-glycero-3-phosphocholine
DSPG	1,2-distearoyl-sn-glycero-3-phosphoglycerol
EDTA	ethylene diaminetetraacetic acid
ee	encapsulation efficiency
EGFR	epidermal growth factor receptor
ELS	electrophoretic light scattering
EMA	european medicine agency
EO	ethylene oxide
eq	equivalents
ESI	eletrospray ionization
et al	et alii
EtBr	ethidium bromide
EtOAc	ethyl acetate

EtOH	ethanol
FACS	fluorescence activated cell sorting
FBS	fetal bovine serum
FCS	fetal calf serum
FD	functionalization degree
FDA	food and drug administration
FITC	fluorescein isothiocyanate
Fmoc	N(9H-fluoren-9-yl-methoxycarbonyloxy)
GABA	gamma-aminobutyric acid
GalNAc	N-acetyl galactosamine
GFP	green fluorescent protein
GLUT1	glucose transporter 1
Gly-Ser(Man)	Glycyl serine(mannose)
GSH	glutathione
H+-ATPase	proton adenosine triphosphatase
HA	Hyaluronic acid
HBG	HEPES buffered glucose
HCE	human corneal epithelial
HEPES	(4-(2-hydroxyethyl)-1-piperazineethanesulfonic acid
HMBA	4-(hydroxymethyl)benzoic acid
HSC	hepatic stellate cell
i.m	intramuscular
i.v.	intravenous
IgR	immunoglobin receptor
IRBP	interphotoreceptor retinoid binding protein
KC	Kupffer cell
K_d	dissociation constant
kDa	kilo Dalton
kg	kilogram
LAF	lipoamino fatty acid
LCA	Leber's congenital amaurosis
LC-MS	liquid chromatography mass spectrometry
LDH	lactate dehydrogenase
LDL	low-density lipoprotein
LDLR	low-density lipoprotein receptor
Lf	Lactoferrin
LfR	lactoferrin receptor
LNP	lipid nanoparticle
LPEI	linear PEI
LRP1	Low density lipoprotein receptor-related protein 1
LSEC	liver sinusoidal endothelial cells
mAB	monoclonal antibody
MALDI	matrix assisted laser desorption ionization
mbar	millibar
MeOH	methanol
MFI	mean fluorescence intensity
mg	milligram
MHz	mega Hertz
miRNA	micro RNA
mmol	millimol
mRNA	messenger RNA
MS	mass spectrometry
MTBE	methyl tertbutyl ether
MTT	(3-[4,5-dimethylthiazol-2-yl]-2,5 diphenyl tetrazolium bromide)
mV	millivolt
MWCO	moleculare weight cut-off
N/P	nitrogen to phosphate ratio
Na_2SO_4	sodium sulfate
NaOH	sodium hydroxide
ng	nanogram
NHS	N-hydroxysuccinimide
nm	nanometer
NMR	nuclear magnetic resonance
OAA	oligoaminoamide
OD	optical density
PAMAM	polyamidoamines
PBAE	poly-(ß-amino ester)
PBS	phosphate buffered saline

pCMVLuc	encoding Photinus pyralis firefly luciferase under the control of cytomegalovirus promoter and enhancer
PDI	polydispersity index
pDNA	plasmid DNA
PECAM	platelet endothelial cell adhesion molecule
PEG	polyethylene glycol
PEI	polyethylene imine
pH	potentia hydrogenii
PH1	primary hyperoxaluria 1
pHPMA	poly(N-(2-hydroxypropyl)methacrylamide
PI	propidium iodide
pKa	acid dissociation constant
PLL	poly-L-Lysine
pM	picomolar
PMO	phosphoramidate morpholino oligomer
polyAsp(DET)	poly(aspartic acid) diethylenetriamine
pPB	cyclic peptide ligand
ppm	parts per million
PyBOP	benzotriazole-1-yl-oxytrispyrrolidino phosphonium hexafluorophosphate
rcf	relative centrifugal force
RES	reticuloendothelial system
RGD	Arginine-glycine-aspartic acid
RLU	relative light units
RMT	receptor-mediated transcytosis
RNA	ribonucleic acid
RNAi	RNA interference
RNP	ribonucleoprotein
ROS	reactive oxygen species
RPE	retinal pigment endothelium
RP-HPLC	reversed phase high performance liquid chromatography
rpm	rotations per minute
RT	room temperature
RVG	rabies virus glycoprotein
RVG29	rabies virus glycoprotein derived protein
s.c.	subcutaneous
SARS-CoV-2	severe acute respiratory symptome coronavirus 2
SD	standard deviation
SDTC	sodium diethyl dithiocarbamate
sgRNA	single guide RNA
shRNA	short hairpin RNA
siRNA	short-interfering RNA
SORT	selective organ targeting
SPAAC	strain-promoted azide-alkyne cycloaddition
SPPS	solid phase peptide synthesis
ssbb	disulfide building block
Stp	Succinoyl tetraethylene pentamine
succPEI	succinylated PEI
TDS	triple bond diethylene triamine succinyl
TEM	transmission electron microscopy
Tf	Transferrin
TFA	trifluoro acetic acid
TFP	tetrafluorophenyl
TfR	Transferrin receptor
THF	tetrahydrofuran
TIPS	triisopropylsilane
TOF	time of flight
TrkA	tropomyosin receptor kinase A
TTR	transthyretin
UPLC	ultra performance liquid chromatography
UV/Vis	ultra violet/ visible
v/v	volume to volume ratio
VCAM-1	vascular cell adhesion molecule-1
VEGFR	vascular endothelial growth factor receptor
VIPER	virus-inspired polymer for endosomal release
w/w	weight to weight ratio
wt	wildtype

7 References

1. Belgrad J, Fakih HH, Khvorova A. Nucleic Acid Therapeutics: Successes, Milestones, and Upcoming Innovation. Nucleic Acid Ther. 2024;34(2):52-72.
2. Buning H, Fehse B, Ivics Z, Kochanek S, Koehl U, Kupatt C, Mussolino C, Nettelbeck DM, Schambach A, Uckert W, Wagner E, Cathomen T. Gene Therapy "Made in Germany": A Historical Perspective, Analysis of the Status Quo, and Recommendations for Action by the German Society for Gene Therapy. Hum Gene Ther. 2021;32(19-20):987-996.
3. Friedmann T, Roblin R. Gene therapy for human genetic disease? Science. 1972;175(4025):949-955.
4. Mulligan RC. The basic science of gene therapy. Science. 1993;260(5110):926-932.
5. Sun W, Shi Q, Zhang H, Yang K, Ke Y, Wang Y, Qiao L. Advances in the techniques and methodologies of cancer gene therapy. Discov Med. 2019;27(146):45-55.
6. Huayamares SG, Loughrey D, Kim H, Dahlman JE, Sorscher EJ. Nucleic acid-based drugs for patients with solid tumours. Nat Rev Clin Oncol. 2024;21(6):407-427.
7. Doudna JA, Charpentier E. Genome editing. The new frontier of genome engineering with CRISPR-Cas9. Science. 2014;346(6213):1258096.
8. Lin Y, Wagner E, Lachelt U. Non-viral delivery of the CRISPR/Cas system: DNA versus RNA versus RNP. Biomater Sci. 2022;10(5):1166-1192.
9. Elbashir SM, Lendeckel W, Tuschl T. RNA interference is mediated by 21- and 22-nucleotide RNAs. Genes Dev. 2001;15(2):188-200.
10. Zimmermann TS, Lee AC, Akinc A, Bramlage B, Bumcrot D, Fedoruk MN, Harborth J, Heyes JA, Jeffs LB, John M, Judge AD, Lam K, McClintock K, Nechev LV, Palmer LR, Racie T, Rohl I, Seiffert S, Shanmugam S, Sood V, Soutschek J, Toudjarska I, Wheat AJ, Yaworski E, Zedalis W, Koteliansky V, Manoharan M, Vornlocher HP, MacLachlan I. RNAi-mediated gene silencing in non-human primates. Nature. 2006;441(7089):111-114.
11. Uhlmann EP, A. Antisense oligonucleotides: a new therapeutic principle. Chem Rev. 1990;90(4):543-584.
12. Ruger J, Ioannou S, Castanotto D, Stein CA. Oligonucleotides to the (Gene) Rescue: FDA Approvals 2017-2019. Trends Pharmacol Sci. 2020;41(1):27-41.
13. Stein CA, Castanotto D. FDA-Approved Oligonucleotide Therapies in 2017. Mol Ther. 2017;25(5):1069-1075.
14. Kowalski PS, Rudra A, Miao L, Anderson DG. Delivering the Messenger: Advances in Technologies for Therapeutic mRNA Delivery. Mol Ther. 2019;27(4):710-728.
15. Parhiz H, Atochina-Vasserman EN, Weissman D. mRNA-based therapeutics: looking beyond COVID-19 vaccines. Lancet. 2024;403(10432):1192-1204.
16. ASGCT Gene, Cell, & RNA Therapy Landscape Report, Q2. In: Citeline ASoGCTa, editor.; 2024.
17. Lundstrom K. Viral Vectors in Gene Therapy. Diseases. 2018;6(2).
18. Kulkarni JA, Witzigmann D, Thomson SB, Chen S, Leavitt BR, Cullis PR, van der Meel R. The current landscape of nucleic acid therapeutics. Nat Nanotechnol. 2021;16(6):630-643.
19. Hoy SM. Patisiran: First Global Approval. Drugs. 2018;78(15):1625-1631.
20. Adams D, Gonzalez-Duarte A, O'Riordan WD, Yang CC, Ueda M, Kristen AV, Tournev I, Schmidt HH, Coelho T, Berk JL, Lin KP, Vita G, Attarian S, Plante-Bordeneuve V, Mezei MM, Campistol JM, Buades J, Brannagan TH, 3rd, Kim BJ, Oh J, Parman Y, Sekijima Y, Hawkins PN, Solomon SD, Polydefkis M, Dyck PJ, Gandhi PJ, Goyal S, Chen J, Strahs AL, Nochur SV, Sweetser MT, Garg PP, Vaishnaw AK, Gollob JA, Suhr OB. Patisiran, an RNAi Therapeutic, for Hereditary Transthyretin Amyloidosis. N Engl J Med. 2018;379(1):11-21.
21. Baden LR, El Sahly HM, Essink B, Kotloff K, Frey S, Novak R, Diemert D, Spector SA, Rouphael N, Creech CB, McGettigan J, Khetan S, Segall N, Solis J, Brosz A, Fierro C, Schwartz H, Neuzil K, Corey L, Gilbert P, Janes H, Follmann D, Marovich M, Mascola J, Polakowski L, Ledgerwood J, Graham BS, Bennett H, Pajon R, Knightly C, Leav B, Deng W, Zhou H, Han S, Ivarsson M, Miller J, Zaks T, Group CS. Efficacy and Safety of the mRNA-1273 SARS-CoV-2 Vaccine. N Engl J Med. 2021;384(5):403-416.
22. Sahin U, Muik A, Derhovanessian E, Vogler I, Kranz LM, Vormehr M, Baum A, Pascal K, Quandt J, Maurus D, Brachtendorf S, Lorks V, Sikorski J, Hilker R, Becker D, Eller AK, Grutzner J, Boesler C, Rosenbaum C, Kuhnle MC, Luxemburger U, Kemmer-Bruck A, Langer D, Bexon M, Bolte S, Kariko K, Palanche T, Fischer B, Schultz A, Shi PY, Fontes-Garfias C, Perez JL, Swanson KA, Loschko J, Scully IL, Cutler M, Kalina W, Kyratsous CA, Cooper D, Dormitzer PR, Jansen KU, Tureci O. COVID-19 vaccine BNT162b1 elicits human antibody and TH1 T cell responses. Nature. 2020;586(7830):594-599.
23. Polack FP, Thomas SJ, Kitchin N, Absalon J, Gurtman A, Lockhart S, Perez JL, Perez Marc G, Moreira ED, Zerbini C, Bailey R, Swanson KA, Roychoudhury S, Koury K, Li P, Kalina WV, Cooper D, Frenck RW,

Jr., Hammitt LL, Tureci O, Nell H, Schaefer A, Unal S, Tresnan DB, Mather S, Dormitzer PR, Sahin U, Jansen KU, Gruber WC, Group CCT. Safety and Efficacy of the BNT162b2 mRNA Covid-19 Vaccine. N Engl J Med. 2020;383(27):2603-2615.

24. Wu Y, Yu S, de Lazaro I. Advances in lipid nanoparticle mRNA therapeutics beyond COVID-19 vaccines. Nanoscale. 2024;16(14):6820-6836.
25. Chen Y, Li Y, Li C, Zhang D, Liu Y, Zhang J, Guan S, Ding X, Xiao Q. The current perspective and opportunities of small nucleic acid-based therapeutics. Drug Dev Res. 2024;85(2):e22164.
26. Gupta A, Andresen JL, Manan RS, Langer R. Nucleic acid delivery for therapeutic applications. Adv Drug Deliv Rev. 2021;178:113834.
27. Ingle RG, Fang WJ. An Overview of the Stability and Delivery Challenges of Commercial Nucleic Acid Therapeutics. Pharmaceutics. 2023;15(4).
28. Boussif O, Lezoualc'h F, Zanta MA, Mergny MD, Scherman D, Demeneix B, Behr JP. A versatile vector for gene and oligonucleotide transfer into cells in culture and in vivo: polyethylenimine. Proc Natl Acad Sci U S A. 1995;92(16):7297-7301.
29. Winkeljann B, Keul DC, Merkel OM. Engineering poly- and micelleplexes for nucleic acid delivery - A reflection on their endosomal escape. J Control Release. 2023;353:518-534.
30. Dowdy SF, Setten RL, Cui XS, Jadhav SG. Delivery of RNA Therapeutics: The Great Endosomal Escape! Nucleic Acid Ther. 2022;32(5):361-368.
31. Dowdy SF. Endosomal escape of RNA therapeutics: How do we solve this rate-limiting problem? RNA. 2023;29(4):396-401.
32. Chatterjee S, Kon E, Sharma P, Peer D. Endosomal escape: A bottleneck for LNP-mediated therapeutics. Proc Natl Acad Sci U S A. 2024;121(11):e2307800120.
33. Singh RP, Srivastava AK, Yang YJ, Manchanda G, Kumar A, Yerpude ST, Rai AR, Dubey RC. Nucleic Acid Nanotechnology: Trends, Opportunities and Challenges. Curr Pharm Biotechnol. 2023;24(1):50-60.
34. Nayerossadat N, Maedeh T, Ali PA. Viral and nonviral delivery systems for gene delivery. Adv Biomed Res. 2012;1:27.
35. Zhang Y, Satterlee A, Huang L. In vivo gene delivery by nonviral vectors: overcoming hurdles? Mol Ther. 2012;20(7):1298-1304.
36. Wang T, Upponi JR, Torchilin VP. Design of multifunctional non-viral gene vectors to overcome physiological barriers: dilemmas and strategies. Int J Pharm. 2012;427(1):3-20.
37. Scholz C, Wagner E. Therapeutic plasmid DNA versus siRNA delivery: common and different tasks for synthetic carriers. J Control Release. 2012;161(2):554-565.
38. Blakney AK, Yilmaz G, McKay PF, Becer CR, Shattock RJ. One Size Does Not Fit All: The Effect of Chain Length and Charge Density of Poly(ethylene imine) Based Copolymers on Delivery of pDNA, mRNA, and RepRNA Polyplexes. Biomacromolecules. 2018;19(7):2870-2879.
39. Peng L, Wagner E. Polymeric Carriers for Nucleic Acid Delivery: Current Designs and Future Directions. Biomacromolecules. 2019;20(10):3613-3626.
40. Albanese A, Tang PS, Chan WC. The effect of nanoparticle size, shape, and surface chemistry on biological systems. Annu Rev Biomed Eng. 2012;14:1-16.
41. Kunath K, von Harpe A, Fischer D, Petersen H, Bickel U, Voigt K, Kissel T. Low-molecular-weight polyethylenimine as a non-viral vector for DNA delivery: comparison of physicochemical properties, transfection efficiency and in vivo distribution with high-molecular-weight polyethylenimine. J Control Release. 2003;89(1):113-125.
42. Hassett KJ, Higgins J, Woods A, Levy B, Xia Y, Hsiao CJ, Acosta E, Almarsson O, Moore MJ, Brito LA. Impact of lipid nanoparticle size on mRNA vaccine immunogenicity. J Control Release. 2021;335:237-246.
43. Hoshyar N, Gray S, Han H, Bao G. The effect of nanoparticle size on in vivo pharmacokinetics and cellular interaction. Nanomedicine (Lond). 2016;11(6):673-692.
44. Mandl HK, Quijano E, Suh HW, Sparago E, Oeck S, Grun M, Glazer PM, Saltzman WM. Optimizing biodegradable nanoparticle size for tissue-specific delivery. J Control Release. 2019;314:92-101.
45. Hager S, Wagner E. Bioresponsive polyplexes - chemically programmed for nucleic acid delivery. Expert Opin Drug Deliv. 2018;15(11):1067-1083.
46. Degors IMS, Wang C, Rehman ZU, Zuhorn IS. Carriers Break Barriers in Drug Delivery: Endocytosis and Endosomal Escape of Gene Delivery Vectors. Acc Chem Res. 2019;52(7):1750-1760.
47. Duncan R, Richardson SC. Endocytosis and intracellular trafficking as gateways for nanomedicine delivery: opportunities and challenges. Mol Pharm. 2012;9(9):2380-2402.
48. Felgner PL, Barenholz Y, Behr JP, Cheng SH, Cullis P, Huang L, Jessee JA, Seymour L, Szoka F, Thierry AR, Wagner E, Wu G. Nomenclature for synthetic gene delivery systems. Hum Gene Ther. 1997;8(5):511-512.

49. Bloomfield VA. DNA condensation by multivalent cations. Biopolymers. 1997;44(3):269-282.

50. Lachelt U, Wagner E. Nucleic Acid Therapeutics Using Polyplexes: A Journey of 50 Years (and Beyond). Chem Rev. 2015;115(19):11043-11078.

51. Mislick KA, Baldeschwieler JD. Evidence for the role of proteoglycans in cation-mediated gene transfer. Proc Natl Acad Sci U S A. 1996;93(22):12349-12354.

52. Semple SC, Akinc A, Chen J, Sandhu AP, Mui BL, Cho CK, Sah DW, Stebbing D, Crosley EJ, Yaworski E, Hafez IM, Dorkin JR, Qin J, Lam K, Rajeev KG, Wong KF, Jeffs LB, Nechev L, Eisenhardt ML, Jayaraman M, Kazem M, Maier MA, Srinivasulu M, Weinstein MJ, Chen Q, Alvarez R, Barros SA, De S, Klimuk SK, Borland T, Kosovrasti V, Cantley WL, Tam YK, Manoharan M, Ciufolini MA, Tracy MA, de Fougerolles A, MacLachlan I, Cullis PR, Madden TD, Hope MJ. Rational design of cationic lipids for siRNA delivery. Nat Biotechnol. 2010;28(2):172-176.

53. Sakaguchi N, Kojima C, Harada A, Koiwai K, Kono K. The correlation between fusion capability and transfection activity in hybrid complexes of lipoplexes and pH-sensitive liposomes. Biomaterials. 2008;29(29):4029-4036.

54. Cullis PR, Hope MJ. Lipid Nanoparticle Systems for Enabling Gene Therapies. Mol Ther. 2017;25(7):1467-1475.

55. Uchida S, Kinoh H, Ishii T, Matsui A, Tockary TA, Takeda KM, Uchida H, Osada K, Itaka K, Kataoka K. Systemic delivery of messenger RNA for the treatment of pancreatic cancer using polyplex nanomicelles with a cholesterol moiety. Biomaterials. 2016;82:221-228.

56. Schaffert D, Troiber C, Salcher EE, Frohlich T, Martin I, Badgujar N, Dohmen C, Edinger D, Klager R, Maiwald G, Farkasova K, Seeber S, Jahn-Hofmann K, Hadwiger P, Wagner E. Solid-phase synthesis of sequence-defined T-, i-, and U-shape polymers for pDNA and siRNA delivery. Angew Chem Int Ed Engl. 2011;50(38):8986-8989.

57. Frohlich T, Edinger D, Klager R, Troiber C, Salcher E, Badgujar N, Martin I, Schaffert D, Cengizeroglu A, Hadwiger P, Vornlocher HP, Wagner E. Structure-activity relationships of siRNA carriers based on sequence-defined oligo (ethane amino) amides. J Control Release. 2012;160(3):532-541.

58. Freitag F, Wagner E. Optimizing synthetic nucleic acid and protein nanocarriers: The chemical evolution approach. Adv Drug Deliv Rev. 2021;168:30-54.

59. Wang Y, Wagner E. Non-Viral Targeted Nucleic Acid Delivery: Apply Sequences for Optimization. Pharmaceutics. 2020;12(9).

60. Merrifield RB. Solid phase synthesis. I. The synthesis of a tetrapeptide. Journal of the American Chemical Society. 1963;85(14): 2149-2154.

61. Schaffert D, Badgujar N, Wagner E. Novel Fmoc-polyamino acids for solid-phase synthesis of defined polyamidoamines. Org Lett. 2011;13(7):1586-1589.

62. Krhac Levacic A, Morys S, Wagner E. Solid-phase supported design of carriers for therapeutic nucleic acid delivery. Biosci Rep. 2017;37(5).

63. Klein PM, Reinhard S, Lee DJ, Muller K, Ponader D, Hartmann L, Wagner E. Precise redox-sensitive cleavage sites for improved bioactivity of siRNA lipopolyplexes. Nanoscale. 2016;8(42):18098-18104.

64. Chu DS, Johnson RN, Pun SH. Cathepsin B-sensitive polymers for compartment-specific degradation and nucleic acid release. J Control Release. 2012;157(3):445-454.

65. Dohmen C, Edinger D, Frohlich T, Schreiner L, Lachelt U, Troiber C, Radler J, Hadwiger P, Vornlocher HP, Wagner E. Nanosized multifunctional polyplexes for receptor-mediated siRNA delivery. ACS Nano. 2012;6(6):5198-5208.

66. Hall A, Lachelt U, Bartek J, Wagner E, Moghimi SM. Polyplex Evolution: Understanding Biology, Optimizing Performance. Mol Ther. 2017;25(7):1476-1490.

67. Berger S, Krhac Levacic A, Horterer E, Wilk U, Benli-Hoppe T, Wang Y, Ozturk O, Luo J, Wagner E. Optimizing pDNA Lipo-polyplexes: A Balancing Act between Stability and Cargo Release. Biomacromolecules. 2021;22(3):1282-1296.

68. Troiber C, Edinger D, Kos P, Schreiner L, Klager R, Herrmann A, Wagner E. Stabilizing effect of tyrosine trimers on pDNA and siRNA polyplexes. Biomaterials. 2013;34(5):1624-1633.

69. Goncalves C, Akhter S, Pichon C, Midoux P. Intracellular Availability of pDNA and mRNA after Transfection: A Comparative Study among Polyplexes, Lipoplexes, and Lipopolyplexes. Mol Pharm. 2016;13(9):3153-3163.

70. Krhac Levacic A, Berger S, Muller J, Wegner A, Lachelt U, Dohmen C, Rudolph C, Wagner E. Dynamic mRNA polyplexes benefit from bioreducible cleavage sites for in vitro and in vivo transfer. J Control Release. 2021;339:27-40.

71. Lachelt U, Kos P, Mickler FM, Herrmann A, Salcher EE, Rodl W, Badgujar N, Brauchle C, Wagner E. Fine-tuning of proton sponges by precise diaminoethanes and histidines in pDNA polyplexes. Nanomedicine. 2014;10(1):35-44.

72. Plank C, Mechtler K, Szoka FC, Jr., Wagner E. Activation of the complement system by synthetic DNA complexes: a potential barrier for intravenous gene delivery. Hum Gene Ther. 1996;7(12):1437-1446.

73. Monopoli MP, Aberg C, Salvati A, Dawson KA. Biomolecular coronas provide the biological identity of nanosized materials. Nat Nanotechnol. 2012;7(12):779-786.

74. Salvati A. The biomolecular corona of nanomedicines: effects on nanomedicine outcomes and emerging opportunities. Curr Opin Biotechnol. 2024;87:103101.

75. Ritz S, Schottler S, Kotman N, Baier G, Musyanovych A, Kuharev J, Landfester K, Schild H, Jahn O, Tenzer S, Mailander V. Protein corona of nanoparticles: distinct proteins regulate the cellular uptake. Biomacromolecules. 2015;16(4):1311-1321.

76. Merkel OM, Urbanics R, Bedocs P, Rozsnyay Z, Rosivall L, Toth M, Kissel T, Szebeni J. In vitro and in vivo complement activation and related anaphylactic effects associated with polyethylenimine and polyethylenimine-graft-poly(ethylene glycol) block copolymers. Biomaterials. 2011;32(21):4936-4942.

77. Cai R, Ren J, Ji Y, Wang Y, Liu Y, Chen Z, Farhadi Sabet Z, Wu X, Lynch I, Chen C. Corona of Thorns: The Surface Chemistry-Mediated Protein Corona Perturbs the Recognition and Immune Response of Macrophages. ACS Appl Mater Interfaces. 2020;12(2):1997-2008.

78. Cai R, Chen C. The Crown and the Scepter: Roles of the Protein Corona in Nanomedicine. Adv Mater. 2019;31(45):e1805740.

79. Suk JS, Xu Q, Kim N, Hanes J, Ensign LM. PEGylation as a strategy for improving nanoparticle-based drug and gene delivery. Adv Drug Deliv Rev. 2016;99(Pt A):28-51.

80. Suzuki Y, Ishihara H. Difference in the lipid nanoparticle technology employed in three approved siRNA (Patisiran) and mRNA (COVID-19 vaccine) drugs. Drug Metab Pharmacokinet. 2021;41:100424.

81. Kumar V, Qin J, Jiang Y, Duncan RG, Brigham B, Fishman S, Nair JK, Akinc A, Barros SA, Kasperkovitz PV. Shielding of Lipid Nanoparticles for siRNA Delivery: Impact on Physicochemical Properties, Cytokine Induction, and Efficacy. Mol Ther Nucleic Acids. 2014;3(11):e210.

82. Ogris M, Brunner S, Schuller S, Kircheis R, Wagner E. PEGylated DNA/transferrin-PEI complexes: reduced interaction with blood components, extended circulation in blood and potential for systemic gene delivery. Gene Ther. 1999;6(4):595-605.

83. Senior J, Delgado C, Fisher D, Tilcock C, Gregoriadis G. Influence of surface hydrophilicity of liposomes on their interaction with plasma protein and clearance from the circulation: studies with poly(ethylene glycol)-coated vesicles. Biochim Biophys Acta. 1991;1062(1):77-82.

84. Weber C, Voigt M, Simon J, Danner AK, Frey H, Mailander V, Helm M, Morsbach S, Landfester K. Functionalization of Liposomes with Hydrophilic Polymers Results in Macrophage Uptake Independent of the Protein Corona. Biomacromolecules. 2019;20(8):2989-2999.

85. Fang JL, Beland FA, Tang Y, Roffler SR. Flow cytometry analysis of anti-polyethylene glycol antibodies in human plasma. Toxicol Rep. 2021;8:148-154.

86. Kozma GT, Meszaros T, Berenyi P, Facsko R, Patko Z, Olah CZ, Nagy A, Fulop TG, Glatter KA, Radovits T, Merkely B, Szebeni J. Role of anti-polyethylene glycol (PEG) antibodies in the allergic reactions to PEG-containing Covid-19 vaccines: Evidence for immunogenicity of PEG. Vaccine. 2023;41(31):4561-4570.

87. Shi D, Beasock D, Fessler A, Szebeni J, Ljubimova JY, Afonin KA, Dobrovolskaia MA. To PEGylate or not to PEGylate: Immunological properties of nanomedicine's most popular component, polyethylene glycol and its alternatives. Adv Drug Deliv Rev. 2022;180:114079.

88. Klein PM, Klinker K, Zhang W, Kern S, Kessel E, Wagner E, Barz M. Efficient Shielding of Polyplexes Using Heterotelechelic Polysarcosines. Polymers (Basel). 2018;10(6).

89. Kang DD, Hou X, Wang L, Xue Y, Li H, Zhong Y, Wang S, Deng B, McComb DW, Dong Y. Engineering LNPs with polysarcosine lipids for mRNA delivery. Bioact Mater. 2024;37:86-93.

90. Beckert L, Kostka L, Kessel E, Krhac Levacic A, Kostkova H, Etrych T, Lächelt U, Wagner E. Acid-labile pHPMA modification of four-arm oligoaminoamide pDNA polyplexes balances shielding and gene transfer activity in vitro and in vivo. Eur J Pharm Biopharm. 2016;105:85-96.

91. Yamaleyeva DN, Makita N, Hwang D, Haney MJ, Jordan R, Kabanov AV. Poly(2-oxazoline)-Based Polyplexes as a PEG-Free Plasmid DNA Delivery Platform. Macromol Biosci. 2023;23(11):e2300177.

92. van Zyl DG, Mendes LP, Semper RP, Rueckert C, Baumhof P. Poly(2-methyl-2-oxazoline) as a polyethylene glycol alternative for lipid nanoparticle formulation. Frontiers in Drug Delivery. 2024;4.

93. Wang Y, Xu Z, Zhang R, Li W, Yang L, Hu Q. A facile approach to construct hyaluronic acid shielding polyplexes with improved stability and reduced cytotoxicity. Colloids Surf B Biointerfaces. 2011;84(1):259-266.

94. Luo J, Schmaus J, Cui M, Horterer E, Wilk U, Hohn M, Dather M, Berger S, Benli-Hoppe T, Peng L, Wagner E. Hyaluronate siRNA nanoparticles with positive charge display rapid attachment to tumor endothelium and penetration into tumors. J Control Release. 2021;329:919-933.

95. Kang B, Okwieka P, Schottler S, Seifert O, Kontermann RE, Pfizenmaier K, Musyanovych A, Meyer R, Diken M, Sahin U, Mailander V, Wurm FR, Landfester K. Tailoring the stealth properties of biocompatible polysaccharide nanocontainers. Biomaterials. 2015;49:125-134.

96. Kang B, Okwieka P, Schottler S, Winzen S, Langhanki J, Mohr K, Opatz T, Mailander V, Landfester K, Wurm FR. Carbohydrate-Based Nanocarriers Exhibiting Specific Cell Targeting with Minimum Influence from the Protein Corona. Angew Chem Int Ed Engl. 2015;54(25):7436-7440.

97. Gjetting T, Arildsen NS, Christensen CL, Poulsen TT, Roth JA, Handlos VN, Poulsen HS. In vitro and in vivo effects of polyethylene glycol (PEG)-modified lipid in DOTAP/cholesterol-mediated gene transfection. Int J Nanomedicine. 2010;5:371-383.

98. Fella C, Walker GF, Ogris M, Wagner E. Amine-reactive pyridylhydrazone-based PEG reagents for pH-reversible PEI polyplex shielding. Eur J Pharm Sci. 2008;34(4-5):309-320.

99. Liu M, Chu Y, Liu H, Su Y, Zhang Q, Jiao J, Liu M, Ding J, Liu M, Hu Y, Dai Y, Zhang R, Liu X, Deng Y, Song Y. Accelerated Blood Clearance of Nanoemulsions Modified with PEG-Cholesterol and PEG-Phospholipid Derivatives in Rats: The Effect of PEG-Lipid Linkages and PEG Molecular Weights. Mol Pharm. 2020;17(4):1059-1070.

100. Steffens RC, Wagner E. Directing the Way-Receptor and Chemical Targeting Strategies for Nucleic Acid Delivery. Pharm Res. 2023;40(1):47-76.

101. Vetter VC, Wagner E. Targeting nucleic acid-based therapeutics to tumors: Challenges and strategies for polyplexes. J Control Release. 2022;346:110-135.

102. Dilliard SA, Siegwart DJ. Passive, active and endogenous organ-targeted lipid and polymer nanoparticles for delivery of genetic drugs. Nat Rev Mater. 2023;8(4):282-300.

103. Ogris M, Wagner E. To be targeted: is the magic bullet concept a viable option for synthetic nucleic acid therapeutics? Hum Gene Ther. 2011;22(7):799-807.

104. Dilliard SA, Cheng Q, Siegwart DJ. On the mechanism of tissue-specific mRNA delivery by selective organ targeting nanoparticles. Proc Natl Acad Sci U S A. 2021;118(52).

105. Zhang R, El-Mayta R, Murdoch TJ, Warzecha CC, Billingsley MM, Shepherd SJ, Gong N, Wang L, Wilson JM, Lee D, Mitchell MJ. Helper lipid structure influences protein adsorption and delivery of lipid nanoparticles to spleen and liver. Biomater Sci. 2021;9(4):1449-1463.

106. Saber N, Estape Senti M, Schiffelers RM. Lipid nanoparticles for nucleic acid delivery beyond the liver. Hum Gene Ther. 2024.

107. Haase F, Pohmerer J, Yazdi M, Grau M, Zeyn Y, Wilk U, Burghardt T, Hohn M, Hieber C, Bros M, Wagner E, Berger S. Lipoamino bundle LNPs for efficient mRNA transfection of dendritic cells and macrophages show high spleen selectivity. Eur J Pharm Biopharm. 2024;194:95-109.

108. Zhao Y, Wang ZM, Song D, Chen M, Xu Q. Rational design of lipid nanoparticles: overcoming physiological barriers for selective intracellular mRNA delivery. Curr Opin Chem Biol. 2024;81:102499.

109. Wijagkanalan W, Kawakami S, Hashida M. Glycosylated carriers for cell-selective and nuclear delivery of nucleic acids. Front Biosci (Landmark Ed). 2011;16(8):2970-2987.

110. Kumar V, Turnbull WB. Targeted delivery of oligonucleotides using multivalent protein-carbohydrate interactions. Chem Soc Rev. 2023;52(4):1273-1287.

111. Sakurai Y, Harashima H. Hyaluronan-modified nanoparticles for tumor-targeting. Expert Opin Drug Deliv. 2019;16(9):915-936.

112. Friedrich M, Aigner A. Therapeutic siRNA: State-of-the-Art and Future Perspectives. BioDrugs. 2022;36(5):549-571.

113. Coelho T, Marques W, Jr., Dasgupta NR, Chao CC, Parman Y, Franca MC, Jr., Guo YC, Wixner J, Ro LS, Calandra CR, Kowacs PA, Berk JL, Obici L, Barroso FA, Weiler M, Conceicao I, Jung SW, Buchele G, Brambatti M, Chen J, Hughes SG, Schneider E, Viney NJ, Masri A, Gertz MR, Ando Y, Gillmore JD, Khella S, Dyck PJB, Waddington Cruz M, Investigators NE-T. Eplontersen for Hereditary Transthyretin Amyloidosis With Polyneuropathy. JAMA. 2023;330(15):1448-1458.

114. Geijtenbeek TB, Torensma R, van Vliet SJ, van Duijnhoven GC, Adema GJ, van Kooyk Y, Figdor CG. Identification of DC-SIGN, a novel dendritic cell-specific ICAM-3 receptor that supports primary immune responses. Cell. 2000;100(5):575-585.

115. Nair JK, Willoughby JL, Chan A, Charisse K, Alam MR, Wang Q, Hoekstra M, Kandasamy P, Kel'in AV, Milstein S, Taneja N, O'Shea J, Shaikh S, Zhang L, van der Sluis RJ, Jung ME, Akinc A, Hutabarat R, Kuchimanchi S, Fitzgerald K, Zimmermann T, van Berkel TJ, Maier MA, Rajeev KG, Manoharan M. Multivalent N-acetylgalactosamine-conjugated siRNA localizes in hepatocytes and elicits robust RNAi-mediated gene silencing. J Am Chem Soc. 2014;136(49):16958-16961.

116. Baenziger JU, Fiete D. Galactose and N-acetylgalactosamine-specific endocytosis of glycopeptides by isolated rat hepatocytes. Cell. 1980;22(2 Pt 2):611-620.

117. Sharon N, Lis H. History of lectins: from hemagglutinins to biological recognition molecules. Glycobiology. 2004;14(11):53R-62R.

118. Mammen M, Choi SK, Whitesides GM. Polyvalent Interactions in Biological Systems: Implications for Design and Use of Multivalent Ligands and Inhibitors. Angew Chem Int Ed Engl. 1998;37(20):2754-2794.

119. Lee YC. Biochemistry of carbohydrate-protein interaction. FASEB J. 1992;6(13):3193-3200.

120. Lepenies B, Lee J, Sonkaria S. Targeting C-type lectin receptors with multivalent carbohydrate ligands. Adv Drug Deliv Rev. 2013;65(9):1271-1281.

121. Pieters RJ. Maximising multivalency effects in protein-carbohydrate interactions. Org Biomol Chem. 2009;7(10):2013-2025.

122. Muller C, Despras G, Lindhorst TK. Organizing multivalency in carbohydrate recognition. Chem Soc Rev. 2016;45(11):3275-3302.

123. Gomez-Garcia M, Benito JM, Gutierrez-Gallego R, Maestre A, Mellet CO, Fernandez JM, Blanco JL. Comparative studies on lectin-carbohydrate interactions in low and high density homo- and heteroglycoclusters. Org Biomol Chem. 2010;8(8):1849-1860.

124. Weber M, Bujotzek A, Haag R. Quantifying the rebinding effect in multivalent chemical ligand-receptor systems. J Chem Phys. 2012;137(5):054111.

125. Ashwell G, Morell AG. The role of surface carbohydrates in the hepatic recognition and transport of circulating glycoproteins. Adv Enzymol Relat Areas Mol Biol. 1974;41(0):99-128.

126. Springer AD, Dowdy SF. GalNAc-siRNA Conjugates: Leading the Way for Delivery of RNAi Therapeutics. Nucleic Acid Ther. 2018;28(3):109-118.

127. Prakash TP, Graham MJ, Yu J, Carty R, Low A, Chappell A, Schmidt K, Zhao C, Aghajan M, Murray HF, Riney S, Booten SL, Murray SF, Gaus H, Crosby J, Lima WF, Guo S, Monia BP, Swayze EE, Seth PP. Targeted delivery of antisense oligonucleotides to hepatocytes using triantennary N-acetyl galactosamine improves potency 10-fold in mice. Nucleic Acids Res. 2014;42(13):8796-8807.

128. Wagener K, Bros M, Krumb M, Langhanki J, Pektor S, Worm M, Schinnerer M, Montermann E, Miederer M, Frey H, Opatz T, Rösch F. Targeting of Immune Cells with Trimannosylated Liposomes. Advanced Therapeutics. 2020;3(6):1900185.

129. Gonzalez-Rios N, Artigues M, Guerra-Rebollo M, Planas A, Borros S, Faijes M, Fornaguera C. Novel alpha-mannose-functionalized poly(beta-amino ester) nanoparticles as mRNA vaccines with increased antigen presenting cell selectivity in the spleen. J Mater Chem B. 2023;11(27):6412-6427.

130. Paurević M, Šrajer Gajdošik M, Ribić R. Mannose Ligands for Mannose Receptor Targeting. International Journal of Molecular Sciences. 2024;25(3):1370.

131. Keler T, Ramakrishna V, Fanger MW. Mannose receptor-targeted vaccines. Expert Opin Biol Ther. 2004;4(12):1953-1962.

132. Irache JM, Salman HH, Gamazo C, Espuelas S. Mannose-targeted systems for the delivery of therapeutics. Expert Opin Drug Deliv. 2008;5(6):703-724.

133. Chen J, Fang H, Hu Y, Wu J, Zhang S, Feng Y, Lin L, Tian H, Chen X. Combining mannose receptor mediated nanovaccines and gene regulated PD-L1 blockade for boosting cancer immunotherapy. Bioact Mater. 2022;7:167-180.

134. Wi TI, Byeon Y, Won JE, Lee JM, Kang TH, Lee JW, Lee YJ, Sood AK, Han HD, Park YM. Selective Tumor-Specific Antigen Delivery to Dendritic Cells Using Mannose-Labeled Poly(d, l-lactide-co-glycolide) Nanoparticles for Cancer Immunotherapy. J Biomed Nanotechnol. 2020;16(2):201-211.

135. Moku G, Vangala S, Gulla SK, Yakati V. In vivo Targeting of DNA Vaccines to Dendritic Cells via the Mannose Receptor Induces Long-Lasting Immunity against Melanoma. ChemBioChem. 2021;22(3):523-531.

136. Goswami R, Chatzikleanthous D, Lou G, Giusti F, Bonci A, Taccone M, Brazzoli M, Gallorini S, Ferlenghi I, Berti F, O'Hagan DT, Pergola C, Baudner BC, Adamo R. Mannosylation of LNP Results in Improved Potency for Self-Amplifying RNA (SAM) Vaccines. ACS Infect Dis. 2019;5(9):1546-1558.

137. Goswami R, O'Hagan DT, Adamo R, Baudner BC. Conjugation of Mannans to Enhance the Potency of Liposome Nanoparticles for the Delivery of RNA Vaccines. Pharmaceutics. 2021;13(2).

138. Rennick JJ, Johnston APR, Parton RG. Key principles and methods for studying the endocytosis of biological and nanoparticle therapeutics. Nat Nanotechnol. 2021;16(3):266-276.

139. Rejman J, Oberle V, Zuhorn IS, Hoekstra D. Size-dependent internalization of particles via the pathways of clathrin- and caveolae-mediated endocytosis. Biochem J. 2004;377(Pt 1):159-169.

140. Grau M, Wagner E. Strategies and mechanisms for endosomal escape of therapeutic nucleic acids. Curr Opin Chem Biol. 2024;81:102506.

141. Wittrup A, Ai A, Liu X, Hamar P, Trifonova R, Charisse K, Manoharan M, Kirchhausen T, Lieberman J. Visualizing lipid-formulated siRNA release from endosomes and target gene knockdown. Nat Biotechnol. 2015;33(8):870-876.

142. Behr JP. The Proton Sponge: a Trick to Enter Cells the Viruses Did Not Exploit. CHIMIA. 1997;51(1-2):34.

143. ur Rehman Z, Hoekstra D, Zuhorn IS. Mechanism of polyplex- and lipoplex-mediated delivery of nucleic acids: real-time visualization of transient membrane destabilization without endosomal lysis. ACS Nano. 2013;7(5):3767-3777.

144. Akita H, Kudo A, Minoura A, Yamaguti M, Khalil IA, Moriguchi R, Masuda T, Danev R, Nagayama K, Kogure K, Harashima H. Multi-layered nanoparticles for penetrating the endosome and nuclear membrane via a step-wise membrane fusion process. Biomaterials. 2009;30(15):2940-2949.

145. Xu E, Saltzman WM, Piotrowski-Daspit AS. Escaping the endosome: assessing cellular trafficking mechanisms of non-viral vehicles. J Control Release. 2021;335:465-480.

146. Kichler A, Leborgne C, Coeytaux E, Danos O. Polyethylenimine-mediated gene delivery: a mechanistic study. J Gene Med. 2001;3(2):135-144.

147. Bus T, Traeger A, Schubert US. The great escape: how cationic polyplexes overcome the endosomal barrier. J Mater Chem B. 2018;6(43):6904-6918.

148. Akinc A, Thomas M, Klibanov AM, Langer R. Exploring polyethylenimine-mediated DNA transfection and the proton sponge hypothesis. J Gene Med. 2005;7(5):657-663.

149. Midoux P, Monsigny M. Efficient gene transfer by histidylated polylysine/pDNA complexes. Bioconjug Chem. 1999;10(3):406-411.

150. Erbacher P, Roche AC, Monsigny M, Midoux P. Putative role of chloroquine in gene transfer into a human hepatoma cell line by DNA/lactosylated polylysine complexes. Exp Cell Res. 1996;225(1):186-194.

151. Wagner E, Ogris M, Zauner W. Polylysine-based transfection systems utilizing receptor-mediated delivery. Adv Drug Deliv Rev. 1998;30(1-3):97-113.

152. Wagner E, Plank C, Zatloukal K, Cotten M, Birnstiel ML. Influenza virus hemagglutinin HA-2 N-terminal fusogenic peptides augment gene transfer by transferrin-polylysine-DNA complexes: toward a synthetic virus-like gene-transfer vehicle. Proc Natl Acad Sci U S A. 1992;89(17):7934-7938.

153. Boeckle S, Wagner E, Ogris M. C- versus N-terminally linked melittin-polyethylenimine conjugates: the site of linkage strongly influences activity of DNA polyplexes. J Gene Med. 2005;7(10):1335-1347.

154. Lyu M, Yazdi M, Lin Y, Hohn M, Lachelt U, Wagner E. Receptor-Targeted Dual pH-Triggered Intracellular Protein Transfer. ACS Biomater Sci Eng. 2024;10(1):99-114.

155. Nakamura Y, Kogure K, Futaki S, Harashima H. Octaarginine-modified multifunctional envelope-type nano device for siRNA. J Control Release. 2007;119(3):360-367.

156. McClorey G, Banerjee S. Cell-Penetrating Peptides to Enhance Delivery of Oligonucleotide-Based Therapeutics. Biomedicines. 2018;6(2).

157. Wyman TB, Nicol F, Zelphati O, Scaria PV, Plank C, Szoka FC, Jr. Design, synthesis, and characterization of a cationic peptide that binds to nucleic acids and permeabilizes bilayers. Biochemistry. 1997;36(10):3008-3017.

158. Rehman Z, Zuhorn IS, Hoekstra D. How cationic lipids transfer nucleic acids into cells and across cellular membranes: recent advances. J Control Release. 2013;166(1):46-56.

159. Hoekstra D, Rejman J, Wasungu L, Shi F, Zuhorn I. Gene delivery by cationic lipids: in and out of an endosome. Biochem Soc Trans. 2007;35(Pt 1):68-71.

160. Kono K, Torikoshi Y, Mitsutomi M, Itoh T, Emi N, Yanagie H, Takagishi T. Novel gene delivery systems: complexes of fusigenic polymer-modified liposomes and lipoplexes. Gene Ther. 2001;8(1):5-12.

161. Schlich M, Palomba R, Costabile G, Mizrahy S, Pannuzzo M, Peer D, Decuzzi P. Cytosolic delivery of nucleic acids: The case of ionizable lipid nanoparticles. Bioeng Transl Med. 2021;6(2):e10213.

162. Thalmayr S, Grau M, Peng L, Pohmerer J, Wilk U, Folda P, Yazdi M, Weidinger E, Burghardt T, Hohn M, Wagner E, Berger S. Molecular Chameleon Carriers for Nucleic Acid Delivery: The Sweet Spot between Lipoplexes and Polyplexes. Adv Mater. 2023:e2211105.

163. Gagliardi M. Novel biodegradable nanocarriers for enhanced drug delivery. Ther Deliv. 2016;7(12):809-826.

164. Singh RP, Ramarao P. Accumulated polymer degradation products as effector molecules in cytotoxicity of polymeric nanoparticles. Toxicol Sci. 2013;136(1):131-143.

165. Lv H, Zhang S, Wang B, Cui S, Yan J. Toxicity of cationic lipids and cationic polymers in gene delivery. J Control Release. 2006;114(1):100-109.

166. Grandinetti G, Ingle NP, Reineke TM. Interaction of poly(ethylenimine)-DNA polyplexes with mitochondria: implications for a mechanism of cytotoxicity. Mol Pharm. 2011;8(5):1709-1719.

167. Grandinetti G, Smith AE, Reineke TM. Membrane and nuclear permeabilization by polymeric pDNA vehicles: efficient method for gene delivery or mechanism of cytotoxicity? Mol Pharm. 2012;9(3):523-538.

168. Beyerle A, Irmler M, Beckers J, Kissel T, Stoeger T. Toxicity pathway focused gene expression profiling of PEI-based polymers for pulmonary applications. Mol Pharm. 2010;7(3):727-737.

169. Moghimi SM, Symonds P, Murray JC, Hunter AC, Debska G, Szewczyk A. A two-stage poly(ethylenimine)-mediated cytotoxicity: implications for gene transfer/therapy. Mol Ther. 2005;11(6):990-995.

170. Hong S, Leroueil PR, Janus EK, Peters JL, Kober MM, Islam MT, Orr BG, Baker JR, Jr., Banaszak Holl MM. Interaction of polycationic polymers with supported lipid bilayers and cells: nanoscale hole formation and enhanced membrane permeability. Bioconjug Chem. 2006;17(3):728-734.

171. Zhang P, Wagner E. History of Polymeric Gene Delivery Systems. Top Curr Chem (Cham). 2017;375(2):26.

172. Hall A, Bartek J, Wagner E, Lachelt U, Moghimi SM. High-resolution bioenergetics correlates the length of continuous protonatable diaminoethane motif of four-armed oligo(ethanamino)amide transfectants to cytotoxicity. J Control Release. 2023;361:115-129.

173. Fischer D, Li Y, Ahlemeyer B, Krieglstein J, Kissel T. In vitro cytotoxicity testing of polycations: influence of polymer structure on cell viability and hemolysis. Biomaterials. 2003;24(7):1121-1131.

174. Klein PM, Wagner E. Bioreducible polycations as shuttles for therapeutic nucleic acid and protein transfection. Antioxid Redox Signal. 2014;21(5):804-817.

175. Gene Therapy Clinical Trials Worldwide. 09.05.2022. Available from: https://a873679.fmphost.com/fmi/webd/GTCT.

176. Bulcha JT, Wang Y, Ma H, Tai PWL, Gao G. Viral vector platforms within the gene therapy landscape. Signal Transduct Target Ther. 2021;6(1):53.

177. Vaheri A, Pagano JS. Infectious poliovirus RNA: a sensitive method of assay 2. Virology. 1965;27(3):434-436.

178. McCutchan JH, Pagano JS. Enchancement of the infectivity of simian virus 40 deoxyribonucleic acid with diethylaminoethyl-dextran. J Natl Cancer Inst. 1968;41(2):351-357.

179. Lopata MA, Cleveland DW, Sollner Webb B. High level transient expression of a chloramphenicol acetyl transferase gene by DEAE-dextran mediated DNA transfection coupled with a dimethyl sulfoxide or glycerol shock treatment. Nucleic Acids Res. 1984;12(14):5707-5717.

180. Yamamoto A, Kormann M, Rosenecker J, Rudolph C. Current prospects for mRNA gene delivery. Eur J Pharm Biopharm. 2009;71(3):484-489.

181. Schoenmaker L, Witzigmann D, Kulkarni JA, Verbeke R, Kersten G, Jiskoot W, Crommelin DJA. mRNA-lipid nanoparticle COVID-19 vaccines: Structure and stability. Int J Pharm. 2021;601:120586.

182. Elbashir SM, Harborth J, Lendeckel W, Yalcin A, Weber K, Tuschl T. Duplexes of 21-nucleotide RNAs mediate RNA interference in cultured mammalian cells. Nature. 2001;411(6836):494-498.

183. Zhang B, Farwell MA. microRNAs: a new emerging class of players for disease diagnostics and gene therapy. J Cell Mol Med. 2008;12(1):3-21.

184. Bauman J, Jearawiriyapaisarn N, Kole R. Therapeutic potential of splice-switching oligonucleotides. Oligonucleotides. 2009;19(1):1-13.

185. Gillmore JD, Gane E, Taubel J, Kao J, Fontana M, Maitland ML, Seitzer J, O'Connell D, Walsh KR, Wood K, Phillips J, Xu Y, Amaral A, Boyd AP, Cehelsky JE, McKee MD, Schiermeier A, Harari O, Murphy A, Kyratsous CA, Zambrowicz B, Soltys R, Gutstein DE, Leonard J, Sepp-Lorenzino L, Lebwohl D. CRISPR-Cas9 In Vivo Gene Editing for Transthyretin Amyloidosis. N Engl J Med. 2021;385(6):493-502.

186. Zuber G, Dauty E, Nothisen M, Belguise P, Behr JP. Towards synthetic viruses. AdvDrug DelivRev. 2001;52(3):245-253.

187. Wagner E. Strategies to improve DNA polyplexes for in vivo gene transfer: will "artificial viruses" be the answer? PharmRes. 2004;21(1):8-14.

188. Wu GY, Wu CH. Receptor-mediated in vitro gene transformation by a soluble DNA carrier system. Journal of Biological Chemistry. 1987;262(10):4429-4432.

189. Wightman L, Kircheis R, Rossler V, Carotta S, Ruzicka R, Kursa M, Wagner E. Different behavior of branched and linear polyethylenimine for gene delivery in vitro and in vivo. J Gene Med. 2001;3(4):362-372.

190. Dufes C, Uchegbu IF, Schatzlein AG. Dendrimers in gene delivery. Adv Drug Deliv Rev. 2005;57(15):2177-2202.

191. Zhou J, Wu J, Hafdi N, Behr JP, Erbacher P, Peng L. PAMAM dendrimers for efficient siRNA delivery and potent gene silencing. Chem Commun (Camb). 2006(22):2362-2364.

192. Kulkarni JA, Witzigmann D, Chen S, Cullis PR, van der Meel R. Lipid Nanoparticle Technology for Clinical Translation of siRNA Therapeutics. Acc Chem Res. 2019;52(9):2435-2444.

193. Wu GY, Wu CH. Receptor-mediated gene delivery and expression in vivo. Journal of Biological Chemistry. 1988;263(29):14621-14624.

194. Vaughan HJ, Green JJ, Tzeng SY. Cancer-Targeting Nanoparticles for Combinatorial Nucleic Acid Delivery. Adv Mater. 2020;32(13):e1901081.

195. Xiao Y, Shi K, Qu Y, Chu B, Qian Z. Engineering Nanoparticles for Targeted Delivery of Nucleic Acid Therapeutics in Tumor. Mol Ther Methods Clin Dev. 2019;12:1-18.

196. Bareford LM, Swaan PW. Endocytic mechanisms for targeted drug delivery. Adv Drug Deliv Rev. 2007;59(8):748-758.

197. Kawaguchi Y, Takeuchi T, Kuwata K, Chiba J, Hatanaka Y, Nakase I, Futaki S. Syndecan-4 Is a Receptor for Clathrin-Mediated Endocytosis of Arginine-Rich Cell-Penetrating Peptides. Bioconjug Chem. 2016;27(4):1119-1130.

198. Bros M, Nuhn L, Simon J, Moll L, Mailander V, Landfester K, Grabbe S. The Protein Corona as a Confounding Variable of Nanoparticle-Mediated Targeted Vaccine Delivery. Front Immunol. 2018;9:1760.

199. Berger SB, M.; Bantz, C.; Maskos, M.; Wagner, E. Performance of nanoparticles for biomedical applications: The *in vitro/in vivo* discrepancy. Biophysics Reviews. 2022;3(1).

200. Francia V, Schiffelers RM, Cullis PR, Witzigmann D. The Biomolecular Corona of Lipid Nanoparticles for Gene Therapy. Bioconjug Chem. 2020;31(9):2046-2059.

201. Johnson RN, Chu DS, Shi J, Schellinger JG, Carlson PM, Pun SH. HPMA-oligolysine copolymers for gene delivery: optimization of peptide length and polymer molecular weight. J Control Release. 2011;155(2):303-311.

202. Manzenrieder F, Luxenhofer R, Retzlaff M, Jordan R, Finn MG. Stabilization of virus-like particles with poly(2-oxazoline)s. Angew Chem Int Ed Engl. 2011;50(11):2601-2605.

203. Noga M, Edinger D, Rodl W, Wagner E, Winter G, Besheer A. Controlled shielding and deshielding of gene delivery polyplexes using hydroxyethyl starch (HES) and alpha-amylase. J Control Release. 2012;159(1):92-103.

204. Sato T, Nakata M, Yang Z, Torizuka Y, Kishimoto S, Ishihara M. In vitro and in vivo gene delivery using chitosan/hyaluronic acid nanoparticles: Influences of molecular mass of hyaluronic acid and lyophilization on transfection efficiency. J Gene Med. 2017;19(8).

205. Hornof M, de la Fuente M, Hallikainen M, Tammi RH, Urtti A. Low molecular weight hyaluronan shielding of DNA/PEI polyplexes facilitates CD44 receptor mediated uptake in human corneal epithelial cells. J Gene Med. 2008;10(1):70-80.

206. Elfinger M, Geiger J, Hasenpusch G, Uzgun S, Sieverling N, Aneja MK, Maucksch C, Rudolph C. Targeting of the beta(2)-adrenoceptor increases nonviral gene delivery to pulmonary epithelial cells in vitro and lungs in vivo. J Control Release. 2009;135(3):234-241.

207. Luo Y, Zhai X, Ma C, Sun P, Fu Z, Liu W, Xu J. An inhalable beta(2)-adrenoceptor ligand-directed guanidinylated chitosan carrier for targeted delivery of siRNA to lung. J Control Release. 2012;162(1):28-36.

208. Geiger J, Aneja MK, Hasenpusch G, Yuksekdag G, Kummerlowe G, Luy B, Romer T, Rothbauer U, Rudolph C. Targeting of the prostacyclin specific IP1 receptor in lungs with molecular conjugates comprising prostaglandin I2 analogues. Biomaterials. 2010;31(10):2903-2911.

209. Lachelt U, Wittmann V, Muller K, Edinger D, Kos P, Hohn M, Wagner E. Synthetic polyglutamylation of dual-functional MTX ligands for enhanced combined cytotoxicity of poly(I:C) nanoplexes. Mol Pharm. 2014;11(8):2631-2639.

210. Jenkins RG, Herrick SE, Meng QH, Kinnon C, Laurent GJ, McAnulty RJ, Hart SL. An integrin-targeted non-viral vector for pulmonary gene therapy. Gene Ther. 2000;7(5):393-400.

211. Benli-Hoppe T, Gol Ozturk S, Ozturk O, Berger S, Wagner E, Yazdi M. Transferrin Receptor Targeted Polyplexes Completely Comprised of Sequence-Defined Components. Macromol Rapid Commun. 2021:e2100602.

212. Wagner E, Zenke M, Cotten M, Beug H, Birnstiel ML. Transferrin-polycation conjugates as carriers for DNA uptake into cells. Proc Natl Acad Sci U S A. 1990;87(9):3410-3414.

213. Zenke M, Steinlein P, Wagner E, Cotten M, Beug H, Birnstiel ML. Receptor-mediated endocytosis of transferrin-polycation conjugates: an efficient way to introduce DNA into hematopoietic cells. Proc Natl Acad Sci U S A. 1990;87(10):3655-3659.

214. Buschle M, Cotten M, Kirlappos H, Mechtler K, Schaffner G, Zauner W, Birnstiel ML, Wagner E. Receptor-mediated gene transfer into human T lymphocytes via binding of DNA/CD3 antibody particles to the CD3 T cell receptor complex. Hum Gene Ther. 1995;6(6):753-761.

215. Ramishetti S, Kedmi R, Goldsmith M, Leonard F, Sprague AG, Godin B, Gozin M, Cullis PR, Dykxhoorn DM, Peer D. Systemic Gene Silencing in Primary T Lymphocytes Using Targeted Lipid Nanoparticles. ACS Nano. 2015;9(7):6706-6716.

216. Plank C, Zatloukal K, Cotten M, Mechtler K, Wagner E. Gene transfer into hepatocytes using asialoglycoprotein receptor mediated endocytosis of DNA complexed with an artificial tetra-antennary galactose ligand. Bioconjug Chem. 1992;3(6):533-539.

217. Uehara K, Harumoto T, Makino A, Koda Y, Iwano J, Suzuki Y, Tanigawa M, Iwai H, Asano K, Kurihara K, Hamaguchi A, Kodaira H, Atsumi T, Yamada Y, Tomizuka K. Targeted delivery to macrophages and dendritic cells by chemically modified mannose ligand-conjugated siRNA. Nucleic Acids Res. 2022.

218. Anraku Y, Kuwahara H, Fukusato Y, Mizoguchi A, Ishii T, Nitta K, Matsumoto Y, Toh K, Miyata K, Uchida S, Nishina K, Osada K, Itaka K, Nishiyama N, Mizusawa H, Yamasoba T, Yokota T, Kataoka K. Glycaemic control boosts glucosylated nanocarrier crossing the BBB into the brain. Nat Commun. 2017;8(1):1001.

219. Dohmen C, Frohlich T, Lachelt U, Rohl I, Vornlocher HP, Hadwiger P, Wagner E. Defined Folate-PEG-siRNA Conjugates for Receptor-specific Gene Silencing. Mol Ther Nucleic Acids. 2012;1:e7.

220. Sato Y, Murase K, Kato J, Kobune M, Sato T, Kawano Y, Takimoto R, Takada K, Miyanishi K, Matsunaga T, Takayama T, Niitsu Y. Resolution of liver cirrhosis using vitamin A-coupled liposomes to deliver siRNA against a collagen-specific chaperone. Nat Biotechnol. 2008;26(4):431-442.

221. Hopkins CR, Miller K, Beardmore JM. Receptor-mediated endocytosis of transferrin and epidermal growth factor receptors: a comparison of constitutive and ligand-induced uptake. J Cell Sci Suppl. 1985;3:173-186.

222. Wall DA, Hubbard AL. Receptor-mediated endocytosis of asialoglycoproteins by rat liver hepatocytes: biochemical characterization of the endosomal compartments. J Cell Biol. 1985;101(6):2104-2112.

223. Goldstein JL, Anderson RG, Brown MS. Coated pits, coated vesicles, and receptor-mediated endocytosis. Nature. 1979;279(5715):679-685.

224. McMahon HT, Boucrot E. Molecular mechanism and physiological functions of clathrin-mediated endocytosis. Nat Rev Mol Cell Biol. 2011;12(8):517-533.

225. Dauty E, Remy JS, Zuber G, Behr JP. Intracellular delivery of nanometric DNA particles via the folate receptor. Bioconjug Chem. 2002;13(4):831-839.

226. Lamaze C, Dujeancourt A, Baba T, Lo CG, Benmerah A, Dautry-Varsat A. Interleukin 2 receptors and detergent-resistant membrane domains define a clathrin-independent endocytic pathway. Mol Cell. 2001;7(3):661-671.

227. Pelkmans L, Helenius A. Endocytosis via caveolae. Traffic. 2002;3(5):311-320.

228. Nichols BJ. A distinct class of endosome mediates clathrin-independent endocytosis to the Golgi complex. Nat Cell Biol. 2002;4(5):374-378.

229. Blessing T, Kursa M, Holzhauser R, Kircheis R, Wagner E. Different strategies for formation of pegylated EGF-conjugated PEI/DNA complexes for targeted gene delivery. Bioconjug Chem. 2001;12(4):529-537.

230. Gestwicki JE, Cairo CW, Strong LE, Oetjen KA, Kiessling LL. Influencing receptor-ligand binding mechanisms with multivalent ligand architecture. J Am Chem Soc. 2002;124(50):14922-14933.

231. Fasting C, Schalley CA, Weber M, Seitz O, Hecht S, Koksch B, Dernedde J, Graf C, Knapp EW, Haag R. Multivalency as a chemical organization and action principle. Angew Chem Int Ed Engl. 2012;51(42):10472-10498.

232. Wagner E, Cotten M, Foisner R, Birnstiel ML. Transferrin-polycation-DNA complexes: the effect of polycations on the structure of the complex and DNA delivery to cells. Proc Natl Acad Sci U S A. 1991;88(10):4255-4259.

233. Elfinger M, Maucksch C, Rudolph C. Characterization of lactoferrin as a targeting ligand for nonviral gene delivery to airway epithelial cells. Biomaterials. 2007;28(23):3448-3455.

234. Diebold SS, Kursa M, Wagner E, Cotten M, Zenke M. Mannose polyethylenimine conjugates for targeted DNA delivery into dendritic cells. J Biol Chem. 1999;274(27):19087-19094.

235. Jia Z, Gong Y, Pi Y, Liu X, Gao L, Kang L, Wang J, Yang F, Tang J, Lu W, Li Q, Zhang W, Yan Z, Yu L. pPB Peptide-Mediated siRNA-Loaded Stable Nucleic Acid Lipid Nanoparticles on Targeting Therapy of Hepatic Fibrosis. Mol Pharm. 2018;15(1):53-62.

236. Parhiz H, Shuvaev VV, Pardi N, Khoshnejad M, Kiseleva RY, Brenner JS, Uhler T, Tuyishime S, Mui BL, Tam YK, Madden TD, Hope MJ, Weissman D, Muzykantov VR. PECAM-1 directed re-targeting of exogenous mRNA providing two orders of magnitude enhancement of vascular delivery and expression in lungs independent of apolipoprotein E-mediated uptake. J Control Release. 2018;291:106-115.

237. Tonigold M, Simon J, Estupinan D, Kokkinopoulou M, Reinholz J, Kintzel U, Kaltbeitzel A, Renz P, Domogalla MP, Steinbrink K, Lieberwirth I, Crespy D, Landfester K, Mailander V. Pre-adsorption of antibodies enables targeting of nanocarriers despite a biomolecular corona. Nat Nanotechnol. 2018;13(9):862-869.

238. York AW, Zhang Y, Holley AC, Guo Y, Huang F, McCormick CL. Facile synthesis of multivalent folate-block copolymer conjugates via aqueous RAFT polymerization: targeted delivery of siRNA and subsequent gene suppression. Biomacromolecules. 2009;10(4):936-943.

239. Kakizawa Y, Kataoka K. Block copolymer micelles for delivery of gene and related compounds. Adv Drug Deliv Rev. 2002;54(2):203-222.

240. Klein PM, Wagner E. Click-Shielded and Targeted Lipopolyplexes. Methods Mol Biol. 2019;2036:141-164.

241. Klein PM, Kern S, Lee DJ, Schmaus J, Hohn M, Gorges J, Kazmaier U, Wagner E. Folate receptor-directed orthogonal click-functionalization of siRNA lipopolyplexes for tumor cell killing in vivo. Biomaterials. 2018;178:630-642.

242. Glass EB, Masjedi S, Dudzinski SO, Wilson AJ, Duvall CL, Yull FE, Giorgio TD. Optimizing Mannose "Click" Conjugation to Polymeric Nanoparticles for Targeted siRNA Delivery to Human and Murine Macrophages. ACS Omega. 2019;4(16):16756-16767.

243. Elfinger M, Pfeifer C, Uezguen S, Golas MM, Sander B, Maucksch C, Stark H, Aneja MK, Rudolph C. Self-assembly of ternary insulin-polyethylenimine (PEI)-DNA nanoparticles for enhanced gene delivery and expression in alveolar epithelial cells. Biomacromolecules. 2009;10(10):2912-2920.

244. Nie Y, Schaffert D, Rodl W, Ogris M, Wagner E, Gunther M. Dual-targeted polyplexes: one step towards a synthetic virus for cancer gene therapy. J Control Release. 2011;152(1):127-134.

245. Kos P, Lachelt U, He D, Nie Y, Gu Z, Wagner E. Dual-targeted polyplexes based on sequence-defined peptide-PEG-oligoamino amides. J Pharm Sci. 2015;104(2):464-475.

246. Urnauer S, Schmohl KA, Tutter M, Schug C, Schwenk N, Morys S, Ziegler S, Bartenstein P, Clevert DA, Wagner E, Spitzweg C. Dual-targeted NIS polyplexes-a theranostic strategy toward tumors with heterogeneous receptor expression. Gene Ther. 2019;26(3-4):93-108.

247. Wang S, Reinhard S, Li C, Qian M, Jiang H, Du Y, Lachelt U, Lu W, Wagner E, Huang R. Antitumoral Cascade-Targeting Ligand for IL-6 Receptor-Mediated Gene Delivery to Glioma. Mol Ther. 2017;25(7):1556-1566.

248. Zhang C, Gu Z, Shen L, Liu X, Lin H. A Dual Targeting Drug Delivery System for Penetrating Blood-Brain Barrier and Selectively Delivering siRNA to Neurons for Alzheimer's Disease Treatment. Curr Pharm Biotechnol. 2017;18(14):1124-1131.

249. Zhang C, Gu Z, Shen L, Liu X, Lin H. In vivo Evaluation and Alzheimer's Disease Treatment Outcome of siRNA Loaded Dual Targeting Drug Delivery System. Curr Pharm Biotechnol. 2019;20(1):56-62.

250. Kopatz I, Remy JS, Behr JP. A model for non-viral gene delivery: through syndecan adhesion molecules and powered by actin. J Gene Med. 2004;6(7):769-776.

251. Hafez IM, Maurer N, Cullis PR. On the mechanism whereby cationic lipids promote intracellular delivery of polynucleic acids. Gene Ther. 2001;8(15):1188-1196.

252. Bisgaier CL, Siebenkas MV, Williams KJ. Effects of Apolipoproteins A-IV and A-I on the Uptake of Phospholipid Liposomes by Hepatocytes. Journal of Biological Chemistry. 1989;264(2):862-866.

253. Cullis PR, Chonn A, Semple SC. Interactions of liposomes and lipid-based carrier systems with blood proteins: Relation to clearance behaviour in vivo. Adv Drug Deliv Rev. 1998;32(1-2):3-17.

254. Yan X, Kuipers F, Havekes LM, Havinga R, Dontje B, Poelstra K, Scherphof GL, Kamps JA. The role of apolipoprotein E in the elimination of liposomes from blood by hepatocytes in the mouse. Biochem Biophys Res Commun. 2005;328(1):57-62.

255. Akinc A, Querbes W, De S, Qin J, Frank-Kamenetsky M, Jayaprakash KN, Jayaraman M, Rajeev KG, Cantley WL, Dorkin JR, Butler JS, Qin L, Racie T, Sprague A, Fava E, Zeigerer A, Hope MJ, Zerial M, Sah DW, Fitzgerald K, Tracy MA, Manoharan M, Koteliansky V, Fougerolles A, Maier MA. Targeted delivery of RNAi therapeutics with endogenous and exogenous ligand-based mechanisms. Mol Ther. 2010;18(7):1357-1364.

256. Kowalski PS, Capasso Palmiero U, Huang Y, Rudra A, Langer R, Anderson DG. Ionizable Amino-Polyesters Synthesized via Ring Opening Polymerization of Tertiary Amino-Alcohols for Tissue Selective mRNA Delivery. Adv Mater. 2018:e1801151.

257. Dahlman JE, Kauffman KJ, Xing Y, Shaw TE, Mir FF, Dlott CC, Langer R, Anderson DG, Wang ET. Barcoded nanoparticles for high throughput in vivo discovery of targeted therapeutics. Proc Natl Acad Sci U S A. 2017;114(8):2060-2065.

258. Cheng Q, Wei T, Farbiak L, Johnson LT, Dilliard SA, Siegwart DJ. Selective organ targeting (SORT) nanoparticles for tissue-specific mRNA delivery and CRISPR-Cas gene editing. Nat Nanotechnol. 2020;15(4):313-320.

259. Liu S, Cheng Q, Wei T, Yu X, Johnson LT, Farbiak L, Siegwart DJ. Membrane-destabilizing ionizable phospholipids for organ-selective mRNA delivery and CRISPR-Cas gene editing. Nat Mater. 2021;20(5):701-710.

260. Lee K, Jang B, Lee YR, Suh EY, Yoo JS, Lee MJ, Lee JY, Lee H. The cutting-edge technologies of siRNA delivery and their application in clinical trials. Arch Pharm Res. 2018;41(9):867-874.

261. Witzigmann D, Kulkarni JA, Leung J, Chen S, Cullis PR, van der Meel R. Lipid nanoparticle technology for therapeutic gene regulation in the liver. Adv Drug Deliv Rev. 2020;159:344-363.

262. Nienhuis AW, Nathwani AC, Davidoff AM. Gene Therapy for Hemophilia. Hum Gene Ther. 2016;27(4):305-308.

263. Asrani SK, Devarbhavi H, Eaton J, Kamath PS. Burden of liver diseases in the world. J Hepatol. 2019;70(1):151-171.

264. Rozema DB, Lewis DL, Wakefield DH, Wong SC, Klein JJ, Roesch PL, Bertin SL, Reppen TW, Chu Q, Blokhin AV, Hagstrom JE, Wolff JA. Dynamic PolyConjugates for targeted in vivo delivery of siRNA to hepatocytes. Proc Natl Acad Sci U S A. 2007;104(32):12982-12987.

265. Goma-Garces E, Perez-Gomez MV, Ortiz A. Givosiran for Acute Intermittent Porphyria. N Engl J Med. 2020;383(20):1989.

266. Garrelfs SF, Frishberg Y, Hulton SA, Koren MJ, O'Riordan WD, Cochat P, Deschenes G, Shasha-Lavsky H, Saland JM, Van't Hoff WG, Fuster DG, Magen D, Moochhala SH, Schalk G, Simkova E, Groothoff JW, Sas DJ, Meliambro KA, Lu J, Sweetser MT, Garg PP, Vaishnaw AK, Gansner JM, McGregor TL, Lieske JC, Collaborators I-A. Lumasiran, an RNAi Therapeutic for Primary Hyperoxaluria Type 1. N Engl J Med. 2021;384(13):1216-1226.

267. Scott LJ, Keam SJ. Lumasiran: First Approval. Drugs. 2021;81(2):277-282.

268. Lamb YN. Inclisiran: First Approval. Drugs. 2021;81(3):389-395.

269. Crooke ST, Baker BF, Xia S, Yu RZ, Viney NJ, Wang Y, Tsimikas S, Geary RS. Integrated Assessment of the Clinical Performance of GalNAc3-Conjugated 2'-O-Methoxyethyl Chimeric Antisense Oligonucleotides: I. Human Volunteer Experience. Nucleic Acid Ther. 2019;29(1):16-32.

270. Zanardi TA, Korbmacher B, Boone L, Engelhardt JA, Wang Y, Burel S, Prill B, Aghajan M, Guo S, Henry SP. Safety, Pharmacokinetic, and Pharmacodynamic Evaluation of a 2'-(2-Methoxyethyl)-D-ribose Antisense Oligonucleotide-Triantenarry N-Acetyl-galactosamine Conjugate that Targets the Human Transmembrane Protease Serine 6. J Pharmacol Exp Ther. 2021;377(1):51-63.

271. Watanabe A, Nakajima M, Kasuya T, Onishi R, Kitade N, Mayumi K, Ikehara T, Kugimiya A. Comparative Characterization of Hepatic Distribution and mRNA Reduction of Antisense Oligonucleotides Conjugated with Triantennary N-Acetyl Galactosamine and Lipophilic Ligands Targeting Apolipoprotein B. J Pharmacol Exp Ther. 2016;357(2):320-330.

272. Yamamoto T, Mukai Y, Wada F, Terada C, Kayaba Y, Oh K, Yamayoshi A, Obika S, Harada-Shiba M. Highly Potent GalNAc-Conjugated Tiny LNA Anti-miRNA-122 Antisense Oligonucleotides. Pharmaceutics. 2021;13(6).

273. Rouet R, Thuma BA, Roy MD, Lintner NG, Rubitski DM, Finley JE, Wisniewska HM, Mendonsa R, Hirsh A, de Onate L, Compte Barron J, McLellan TJ, Bellenger J, Feng X, Varghese A, Chrunyk BA, Borzilleri K, Hesp KD, Zhou K, Ma N, Tu M, Dullea R, McClure KF, Wilson RC, Liras S, Mascitti V, Doudna JA. Receptor-Mediated Delivery of CRISPR-Cas9 Endonuclease for Cell-Type-Specific Gene Editing. J Am Chem Soc. 2018;140(21):6596-6603.

274. Soutschek J, Akinc A, Bramlage B, Charisse K, Constien R, Donoghue M, Elbashir S, Geick A, Hadwiger P, Harborth J, John M, Kesavan V, Lavine G, Pandey RK, Racie T, Rajeev KG, Rohl I, Toudjarska I, Wang G, Wuschko S, Bumcrot D, Koteliansky V, Limmer S, Manoharan M, Vornlocher HP. Therapeutic silencing of an endogenous gene by systemic administration of modified siRNAs. Nature. 2004;432(7014):173-178.

275. Sato Y, Yoneda A, Shimizu F, Nishimura M, Shimoyama R, Tashiro Y, Kurata W, Niitsu Y. Resolution of fibrosis by siRNA HSP47 in vitamin A-coupled liposomes induces regeneration of chronically injured livers. J Gastroenterol Hepatol. 2021;36(12):3418-3428.

276. Paunovska K, Gil CJ, Lokugamage MP, Sago CD, Sato M, Lando GN, Gamboa Castro M, Bryksin AV, Dahlman JE. Analyzing 2000 in Vivo Drug Delivery Data Points Reveals Cholesterol Structure Impacts Nanoparticle Delivery. ACS Nano. 2018;12(8):8341-8349.

277. Paunovska K, Da Silva Sanchez AJ, Sago CD, Gan Z, Lokugamage MP, Islam FZ, Kalathoor S, Krupczak BR, Dahlman JE. Nanoparticles Containing Oxidized Cholesterol Deliver mRNA to the Liver Microenvironment at Clinically Relevant Doses. Adv Mater. 2019;31(14):e1807748.

278. Sago CD, Krupczak BR, Lokugamage MP, Gan Z, Dahlman JE. Cell Subtypes Within the Liver Microenvironment Differentially Interact with Lipid Nanoparticles. Cell Mol Bioeng. 2019;12(5):389-397.

279. Gan Z, Lokugamage MP, Hatit MZC, Loughrey D, Paunovska K, Sato M, Cristian A, Dahlman JE. Nanoparticles containing constrained phospholipids deliver mRNA to liver immune cells in vivo without targeting ligands. Bioeng Transl Med. 2020;5(3):e10161.

280. Pattipeiluhu R, Arias-Alpizar G, Basha G, Chan KYT, Bussmann J, Sharp TH, Moradi MA, Sommerdijk N, Harris EN, Cullis PR, Kros A, Witzigmann D, Campbell F. Anionic Lipid Nanoparticles Preferentially Deliver mRNA to the Hepatic Reticuloendothelial System. Adv Mater. 2022;34(16):e2201095.

281. Lee RT, Lee YC. Affinity enhancement by multivalent lectin-carbohydrate interaction. Glycoconj J. 2000;17(7-9):543-551.

282. Pricer WE, Ashwell G. The Binding of Desialylated Glycoproteins by Plasma Membranes of Rat Liver. Journal of Biological Chemistry. 1971;246(15):4825-4833.

283. Huang X, Leroux JC, Castagner B. Well-Defined Multivalent Ligands for Hepatocytes Targeting via Asialoglycoprotein Receptor. Bioconjug Chem. 2017;28(2):283-295.

284. Balwani M, Sardh E, Ventura P, Peiro PA, Rees DC, Stolzel U, Bissell DM, Bonkovsky HL, Windyga J, Anderson KE, Parker C, Silver SM, Keel SB, Wang JD, Stein PE, Harper P, Vassiliou D, Wang B, Phillips J, Ivanova A, Langendonk JG, Kauppinen R, Minder E, Horie Y, Penz C, Chen J, Liu S, Ko JJ, Sweetser

MT, Garg P, Vaishnaw A, Kim JB, Simon AR, Gouya L, Investigators E. Phase 3 Trial of RNAi Therapeutic Givosiran for Acute Intermittent Porphyria. N Engl J Med. 2020;382(24):2289-2301.

285. Frank-Kamenetsky M, Grefhorst A, Anderson NN, Racie TS, Bramlage B, Akinc A, Butler D, Charisse K, Dorkin R, Fan Y, Gamba-Vitalo C, Hadwiger P, Jayaraman M, John M, Jayaprakash KN, Maier M, Nechev L, Rajeev KG, Read T, Rohl I, Soutschek J, Tan P, Wong J, Wang G, Zimmermann T, de Fougerolles A, Vornlocher HP, Langer R, Anderson DG, Manoharan M, Koteliansky V, Horton JD, Fitzgerald K. Therapeutic RNAi targeting PCSK9 acutely lowers plasma cholesterol in rodents and LDL cholesterol in nonhuman primates. Proc Natl Acad Sci U S A. 2008;105(33):11915-11920.

286. Fitzgerald K, White S, Borodovsky A, Bettencourt BR, Strahs A, Clausen V, Wijngaard P, Horton JD, Taubel J, Brooks A, Fernando C, Kauffman RS, Kallend D, Vaishnaw A, Simon A. A Highly Durable RNAi Therapeutic Inhibitor of PCSK9. N Engl J Med. 2017;376(1):41-51.

287. Zhang MM, Bahal R, Rasmussen TP, Manautou JE, Zhong XB. The growth of siRNA-based therapeutics: Updated clinical studies. Biochem Pharmacol. 2021;189:114432.

288. Coelho T, Adams D, Silva A, Lozeron P, Hawkins PN, Mant T, Perez J, Chiesa J, Warrington S, Tranter E, Munisamy M, Falzone R, Harrop J, Cehelsky J, Bettencourt BR, Geissler M, Butler JS, Sehgal A, Meyers RE, Chen Q, Borland T, Hutabarat RM, Clausen VA, Alvarez R, Fitzgerald K, Gamba-Vitalo C, Nochur SV, Vaishnaw AK, Sah DW, Gollob JA, Suhr OB. Safety and efficacy of RNAi therapy for transthyretin amyloidosis. N Engl J Med. 2013;369(9):819-829.

289. Chen SL, Zheng MH, Shi KQ, Yang T, Chen YP. A new strategy for treatment of liver fibrosis: letting MicroRNAs do the job. BioDrugs. 2013;27(1):25-34.

290. Omar R, Yang J, Liu H, Davies NM, Gong Y. Hepatic Stellate Cells in Liver Fibrosis and siRNA-Based Therapy. Rev Physiol Biochem Pharmacol. 2016;172:1-37.

291. Freeley M, Long A. Advances in siRNA delivery to T-cells: potential clinical applications for inflammatory disease, cancer and infection. Biochem J. 2013;455(2):133-147.

292. Granot-Matok Y, Kon E, Dammes N, Mechtinger G, Peer D. Therapeutic mRNA delivery to leukocytes. J Control Release. 2019;305:165-175.

293. Linehan SA, Martinez-Pomares L, Gordon S. Macrophage lectins in host defence. Microbes Infect. 2000;2(3):279-288.

294. Taylor ME, Bezouska K, Drickamer K. Contribution to ligand binding by multiple carbohydrate-recognition domains in the macrophage mannose receptor. J Biol Chem. 1992;267(3):1719-1726.

295. Erbacher P, Bousser MT, Raimond J, Monsigny M, Midoux P, Roche AC. Gene transfer by DNA/glycosylated polylysine complexes into human blood monocyte-derived macrophages. Hum Gene Ther. 1996;7(6):721-729.

296. Lopukhov AV, Yang Z, Haney MJ, Bronich TK, Sokolsky-Papkov M, Batrakova EV, Klyachko NL, Kabanov AV. Mannosylated Cationic Copolymers for Gene Delivery to Macrophages. Macromol Biosci. 2021;21(4):e2000371.

297. Leber N, Kaps L, Yang A, Aslam M, Giardino M, Klefenz A, Choteschovsky N, Rosigkeit S, Mostafa A, Nuhn L, Schuppan D, Zentel R. alpha-Mannosyl-Functionalized Cationic Nanohydrogel Particles for Targeted Gene Knockdown in Immunosuppressive Macrophages. Macromol Biosci. 2019;19(7):e1900162.

298. Kaps L, Leber N, Klefenz A, Choteschovsky N, Zentel R, Nuhn L, Schuppan D. In Vivo siRNA Delivery to Immunosuppressive Liver Macrophages by alpha-Mannosyl-Functionalized Cationic Nanohydrogel Particles. Cells. 2020;9(8).

299. Gao H, Goncalves C, Gallego T, Francois-Heude M, Malard V, Mateo V, Lemoine F, Cendret V, Djedaini-Pilard F, Moreau V, Pichon C, Midoux P. Comparative binding and uptake of liposomes decorated with mannose oligosaccharides by cells expressing the mannose receptor or DC-SIGN. Carbohydr Res. 2020;487:107877.

300. Wang F, Xiao W, Elbahnasawy MA, Bao X, Zheng Q, Gong L, Zhou Y, Yang S, Fang A, Farag MMS, Wu J, Song X. Optimization of the Linker Length of Mannose-Cholesterol Conjugates for Enhanced mRNA Delivery to Dendritic Cells by Liposomes. Front Pharmacol. 2018;9:980.

301. East L, Isacke CM. The mannose receptor family. Biochim Biophys Acta. 2002;1572(2-3):364-386.

302. Inaba K, Swiggard WJ, Inaba M, Meltzer J, Mirza A, Sasagawa T, Nussenzweig MC, Steinman RM. Tissue distribution of the DEC-205 protein that is detected by the monoclonal antibody NLDC-145. I. Expression on dendritic cells and other subsets of mouse leukocytes. Cell Immunol. 1995;163(1):148-156.

303. Katakowski JA, Mukherjee G, Wilner SE, Maier KE, Harrison MT, DiLorenzo TP, Levy M, Palliser D. Delivery of siRNAs to Dendritic Cells Using DEC205-Targeted Lipid Nanoparticles to Inhibit Immune Responses. Mol Ther. 2016;24(1):146-155.

304. Kranz LM, Diken M, Haas H, Kreiter S, Loquai C, Reuter KC, Meng M, Fritz D, Vascotto F, Hefesha H, Grunwitz C, Vormehr M, Husemann Y, Selmi A, Kuhn AN, Buck J, Derhovanessian E, Rae R, Attig S, Diekmann J, Jabulowsky RA, Heesch S, Hassel J, Langguth P, Grabbe S, Huber C, Tureci O, Sahin U.

Systemic RNA delivery to dendritic cells exploits antiviral defence for cancer immunotherapy. Nature. 2016;534(7607):396-401.

305. Fabbri M, Smart C, Pardi R. T lymphocytes. Int J Biochem Cell Biol. 2003;35(7):1004-1008.

306. Peer D. Induction of therapeutic gene silencing in leukocyte-implicated diseases by targeted and stabilized nanoparticles: a mini-review. J Control Release. 2010;148(1):63-68.

307. Veiga N, Goldsmith M, Granot Y, Rosenblum D, Dammes N, Kedmi R, Ramishetti S, Peer D. Cell specific delivery of modified mRNA expressing therapeutic proteins to leukocytes. Nat Commun. 2018;9(1):4493.

308. Kedmi R, Veiga N, Ramishetti S, Goldsmith M, Rosenblum D, Dammes N, Hazan-Halevy I, Nahary L, Leviatan-Ben-Arye S, Harlev M, Behlke M, Benhar I, Lieberman J, Peer D. A modular platform for targeted RNAi therapeutics. Nat Nanotechnol. 2018;13(3):214-219.

309. Lokugamage MP, Sago CD, Gan Z, Krupczak BR, Dahlman JE. Constrained Nanoparticles Deliver siRNA and sgRNA to T Cells In Vivo without Targeting Ligands. Adv Mater. 2019;31(41):e1902251.

310. Ramishetti S, Hazan-Halevy I, Palakuri R, Chatterjee S, Naidu Gonna S, Dammes N, Freilich I, Kolik Shmuel L, Danino D, Peer D. A Combinatorial Library of Lipid Nanoparticles for RNA Delivery to Leukocytes. Adv Mater. 2020;32(12):e1906128.

311. Merkel OM, Zheng M, Debus H, Kissel T. Pulmonary gene delivery using polymeric nonviral vectors. Bioconjug Chem. 2012;23(1):3-20.

312. Renigunta A, Krasteva G, Konig P, Rose F, Klepetko W, Grimminger F, Seeger W, Hanze J. DNA transfer into human lung cells is improved with Tat-RGD peptide by caveoli-mediated endocytosis. Bioconjug Chem. 2006;17(2):327-334.

313. Scott ES, Wiseman JW, Evans MJ, Colledge WH. Enhanced gene delivery to human airway epithelial cells using an integrin-targeting lipoplex. J Gene Med. 2001;3(2):125-134.

314. Ferkol T, Kaetzel CS, Davis PB. Gene transfer into respiratory epithelial cells by targeting the polymeric immunoglobulin receptor. J Clin Invest. 1993;92(5):2394-2400.

315. Li S, Tan Y, Viroonchatapan E, Pitt BR, Huang L. Targeted gene delivery to pulmonary endothelium by anti-PECAM antibody. Am J Physiol Lung Cell Mol Physiol. 2000;278(3):L504-511.

316. Xie Y, Kim NH, Nadithe V, Schalk D, Thakur A, Kilic A, Lum LG, Bassett DJP, Merkel OM. Targeted delivery of siRNA to activated T cells via transferrin-polyethylenimine (Tf-PEI) as a potential therapy of asthma. J Control Release. 2016;229:120-129.

317. Kandil R, Xie Y, Heermann R, Isert L, Jung K, Mehta A, Merkel OM. Coming in and Finding Out: Blending Receptor-Targeted Delivery and Efficient Endosomal Escape in a Novel Bio-Responsive siRNA Delivery System for Gene Knockdown in Pulmonary T Cells. Adv Ther (Weinh). 2019;2(7).

318. Kollen WJ, Midoux P, Erbacher P, Yip A, Roche AC, Monsigny M, Glick MC, Scanlin TF. Gluconoylated and glycosylated polylysines as vectors for gene transfer into cystic fibrosis airway epithelial cells. Hum Gene Ther. 1996;7(13):1577-1586.

319. Kollen W, Erbacher P, Midoux P, Roche AC, Monsigny M, Glick MC, Scanlin TF. Glycosylated polylysines. Nonviral vectors for gene transfer into cystic fibrosis airway epithelial cells. Chest. 1997;111(6 Suppl):95S-96S.

320. Kollen WJ, Mulberg AE, Wei X, Sugita M, Raghuram V, Wang J, Foskett JK, Glick MC, Scanlin TF. High-efficiency transfer of cystic fibrosis transmembrane conductance regulator cDNA into cystic fibrosis airway cells in culture using lactosylated polylysine as a vector. Hum Gene Ther. 1999;10(4):615-622.

321. Kollen WJ, Schembri FM, Gerwig GJ, Vliegenthart JF, Glick MC, Scanlin TF. Enhanced efficiency of lactosylated poly-L-lysine-mediated gene transfer into cystic fibrosis airway epithelial cells. Am J Respir Cell Mol Biol. 1999;20(5):1081-1086.

322. Chen J, Gao X, Hu K, Pang Z, Cai J, Li J, Wu H, Jiang X. Galactose-poly(ethylene glycol)-polyethylenimine for improved lung gene transfer. Biochem Biophys Res Commun. 2008;375(3):378-383.

323. McLean JW, Fox EA, Baluk P, Bolton PB, Haskell A, Pearlman R, Thurston G, Umemoto EY, McDonald DM. Organ-specific endothelial cell uptake of cationic liposome-DNA complexes in mice. Am J Physiol. 1997;273(1 Pt 2):H387-404.

324. Zou SM, Erbacher P, Remy JS, Behr JP. Systemic linear polyethylenimine (L-PEI)-mediated gene delivery in the mouse. JGene Med. 2000;2(2):128-134.

325. Goula D, Benoist C, Mantero S, Merlo G, Levi G, Demeneix BA. Polyethylenimine-based intravenous delivery of transgenes to mouse lung. Gene Ther. 1998;5(9):1291-1295.

326. Bragonzi A, Dina G, Villa A, Calori G, Biffi A, Bordignon C, Assael BM, Conese M. Biodistribution and transgene expression with nonviral cationic vector/DNA complexes in the lungs. Gene Ther. 2000;7(20):1753-1760.

327. Kaczmarek JC, Patel AK, Kauffman KJ, Fenton OS, Webber MJ, Heartlein MW, DeRosa F, Anderson DG. Polymer-Lipid Nanoparticles for Systemic Delivery of mRNA to the Lungs. Angew Chem Int Ed Engl. 2016;55(44):13808-13812.

328. Kaczmarek JC, Kauffman KJ, Fenton OS, Sadtler K, Patel AK, Heartlein MW, DeRosa F, Anderson DG. Optimization of a Degradable Polymer-Lipid Nanoparticle for Potent Systemic Delivery of mRNA to the Lung Endothelium and Immune Cells. Nano Lett. 2018;18(10):6449-6454.

329. Kaczmarek JC, Patel AK, Rhym LH, Palmiero UC, Bhat B, Heartlein MW, DeRosa F, Anderson DG. Systemic delivery of mRNA and DNA to the lung using polymer-lipid nanoparticles. Biomaterials. 2021;275:120966.

330. Cheng Y, Yumul RC, Pun SH. Virus-Inspired Polymer for Efficient In Vitro and In Vivo Gene Delivery. Angew Chem Int Ed Engl. 2016;55(39):12013-12017.

331. Feldmann DP, Cheng Y, Kandil R, Xie Y, Mohammadi M, Harz H, Sharma A, Peeler DJ, Moszczynska A, Leonhardt H, Pun SH, Merkel OM. In vitro and in vivo delivery of siRNA via VIPER polymer system to lung cells. J Control Release. 2018;276:50-58.

332. Baldassi D, Ambike S, Feuerherd M, Cheng CC, Peeler DJ, Feldmann DP, Porras-Gonzalez DL, Wei X, Keller LA, Kneidinger N, Stoleriu MG, Popp A, Burgstaller G, Pun SH, Michler T, Merkel OM. Inhibition of SARS-CoV-2 replication in the lung with siRNA/VIPER polyplexes. J Control Release. 2022;345:661-674.

333. Pardridge WM. Blood-brain barrier delivery. Drug Discov Today. 2007;12(1-2):54-61.

334. Cardoso AL, Simoes S, de Almeida LP, Plesnila N, Pedroso de Lima MC, Wagner E, Culmsee C. Tf-lipoplexes for neuronal siRNA delivery: a promising system to mediate gene silencing in the CNS. J Control Release. 2008;132(2):113-123.

335. Huang RQ, Qu YH, Ke WL, Zhu JH, Pei YY, Jiang C. Efficient gene delivery targeted to the brain using a transferrin-conjugated polyethyleneglycol-modified polyamidoamine dendrimer. FASEB J. 2007;21(4):1117-1125.

336. Somani S, Blatchford DR, Millington O, Stevenson ML, Dufes C. Transferrin-bearing polypropylenimine dendrimer for targeted gene delivery to the brain. J Control Release. 2014;188:78-86.

337. Zhang Y, Boado RJ, Pardridge WM. In vivo knockdown of gene expression in brain cancer with intravenous RNAi in adult rats. J Gene Med. 2003;5(12):1039-1045.

338. Huang R, Ke W, Liu Y, Jiang C, Pei Y. The use of lactoferrin as a ligand for targeting the polyamidoamine-based gene delivery system to the brain. Biomaterials. 2008;29(2):238-246.

339. Somani S, Robb G, Pickard BS, Dufes C. Enhanced gene expression in the brain following intravenous administration of lactoferrin-bearing polypropylenimine dendriplex. J Control Release. 2015;217:235-242.

340. Ke W, Shao K, Huang R, Han L, Liu Y, Li J, Kuang Y, Ye L, Lou J, Jiang C. Gene delivery targeted to the brain using an Angiopep-conjugated polyethyleneglycol-modified polyamidoamine dendrimer. Biomaterials. 2009;30(36):6976-6985.

341. Bruun J, Larsen TB, Jolck RI, Eliasen R, Holm R, Gjetting T, Andresen TL. Investigation of enzyme-sensitive lipid nanoparticles for delivery of siRNA to blood-brain barrier and glioma cells. Int J Nanomedicine. 2015;10:5995-6008.

342. Kumar P, Wu H, McBride JL, Jung KE, Kim MH, Davidson BL, Lee SK, Shankar P, Manjunath N. Transvascular delivery of small interfering RNA to the central nervous system. Nature. 2007;448(7149):39-43.

343. Liu Y, Huang R, Han L, Ke W, Shao K, Ye L, Lou J, Jiang C. Brain-targeting gene delivery and cellular internalization mechanisms for modified rabies virus glycoprotein RVG29 nanoparticles. Biomaterials. 2009;30(25):4195-4202.

344. Hwang DW, Son S, Jang J, Youn H, Lee S, Lee D, Lee YS, Jeong JM, Kim WJ, Lee DS. A brain-targeted rabies virus glycoprotein-disulfide linked PEI nanocarrier for delivery of neurogenic microRNA. Biomaterials. 2011;32(21):4968-4975.

345. Gao Y, Wang ZY, Zhang J, Zhang Y, Huo H, Wang T, Jiang T, Wang S. RVG-peptide-linked trimethylated chitosan for delivery of siRNA to the brain. Biomacromolecules. 2014;15(3):1010-1018.

346. Park TE, Singh B, Li H, Lee JY, Kang SK, Choi YJ, Cho CS. Enhanced BBB permeability of osmotically active poly(mannitol-co-PEI) modified with rabies virus glycoprotein via selective stimulation of caveolar endocytosis for RNAi therapeutics in Alzheimer's disease. Biomaterials. 2015;38:61-71.

347. Alvarez-Erviti L, Seow Y, Yin H, Betts C, Lakhal S, Wood MJ. Delivery of siRNA to the mouse brain by systemic injection of targeted exosomes. Nat Biotechnol. 2011;29(4):341-345.

348. Conceicao M, Mendonca L, Nobrega C, Gomes C, Costa P, Hirai H, Moreira JN, Lima MC, Manjunath N, Pereira de Almeida L. Intravenous administration of brain-targeted stable nucleic acid lipid particles alleviates Machado-Joseph disease neurological phenotype. Biomaterials. 2016;82:124-137.

349. Liu Y, He X, Kuang Y, An S, Wang C, Guo Y, Ma H, Lou J, Jiang C. A bacteria deriving peptide modified dendrigraft poly-l-lysines (DGL) self-assembling nanoplatform for targeted gene delivery. Mol Pharm. 2014;11(10):3330-3341.

350. Liu Y, Li J, Shao K, Huang R, Ye L, Lou J, Jiang C. A leptin derived 30-amino-acid peptide modified pegylated poly-L-lysine dendrigraft for brain targeted gene delivery. Biomaterials. 2010;31(19):5246-5257.

351. Marcos-Contreras OA, Greineder CF, Kiseleva RY, Parhiz H, Walsh LR, Zuluaga-Ramirez V, Myerson JW, Hood ED, Villa CH, Tombacz I, Pardi N, Seliga A, Mui BL, Tam YK, Glassman PM, Shuvaev VV, Nong J, Brenner JS, Khoshnejad M, Madden T, Weissmann D, Persidsky Y, Muzykantov VR. Selective targeting of nanomedicine to inflamed cerebral vasculature to enhance the blood-brain barrier. Proc Natl Acad Sci U S A. 2020;117(7):3405-3414.

352. Min HS, Kim HJ, Naito M, Ogura S, Toh K, Hayashi K, Kim BS, Fukushima S, Anraku Y, Miyata K, Kataoka K. Systemic Brain Delivery of Antisense Oligonucleotides across the Blood-Brain Barrier with a Glucose-Coated Polymeric Nanocarrier. Angew Chem Int Ed Engl. 2020;59(21):8173-8180.

353. Descamps L, Dehouck MP, Torpier G, Cecchelli R. Receptor-mediated transcytosis of transferrin through blood-brain barrier endothelial cells. Am J Physiol. 1996;270(4 Pt 2):H1149-1158.

354. Mills E, Dong XP, Wang F, Xu H. Mechanisms of brain iron transport: insight into neurodegeneration and CNS disorders. Future Med Chem. 2010;2(1):51-64.

355. Prades R, Oller-Salvia B, Schwarzmaier SM, Selva J, Moros M, Balbi M, Grazu V, de La Fuente JM, Egea G, Plesnila N, Teixido M, Giralt E. Applying the retro-enantio approach to obtain a peptide capable of overcoming the blood-brain barrier. Angew Chem Int Ed Engl. 2015;54(13):3967-3972.

356. Huang RQ, Ke WL, Qu YH, Zhu JH, Pei YY, Jiang C. Characterization of lactoferrin receptor in brain endothelial capillary cells and mouse brain. J Biomed Sci. 2007;14(1):121-128.

357. Singh CSB, Eyford BA, Abraham T, Munro L, Choi KB, Okon M, Vitalis TZ, Gabathuler R, Lu CJ, Pfeifer CG, Tian MM, Jefferies WA. Discovery of a Highly Conserved Peptide in the Iron Transporter Melanotransferrin that Traverses an Intact Blood Brain Barrier and Localizes in Neural Cells. Front Neurosci. 2021;15:596976.

358. Eyford BA, Singh CSB, Abraham T, Munro L, Choi KB, Hill T, Hildebrandt R, Welch I, Vitalis TZ, Gabathuler R, Gordon JA, Adomat H, Guns EST, Lu CJ, Pfeifer CG, Tian MM, Jefferies WA. A Nanomule Peptide Carrier Delivers siRNA Across the Intact Blood-Brain Barrier to Attenuate Ischemic Stroke. Front Mol Biosci. 2021;8:611367.

359. Demeule M, Regina A, Che C, Poirier J, Nguyen T, Gabathuler R, Castaigne JP, Beliveau R. Identification and design of peptides as a new drug delivery system for the brain. J Pharmacol Exp Ther. 2008;324(3):1064-1072.

360. Demeule M, Currie JC, Bertrand Y, Che C, Nguyen T, Regina A, Gabathuler R, Castaigne JP, Beliveau R. Involvement of the low-density lipoprotein receptor-related protein in the transcytosis of the brain delivery vector angiopep-2. J Neurochem. 2008;106(4):1534-1544.

361. Sakamoto K, Shinohara T, Adachi Y, Asami T, Ohtaki T. A novel LRP1-binding peptide L57 that crosses the blood brain barrier. Biochem Biophys Rep. 2017;12:135-139.

362. Rodrigues JP, Prajapati N, DeCoster MA, Poh S, Murray TA. Efficient LRP1-Mediated Uptake and Low Cytotoxicity of Peptide L57 In Vitro Shows Its Promise as CNS Drug Delivery Vector. J Pharm Sci. 2021;110(2):824-832.

363. Golden PL, Maccagnan TJ, Pardridge WM. Human blood-brain barrier leptin receptor. Binding and endocytosis in isolated human brain microvessels. J Clin Invest. 1997;99(1):14-18.

364. Huey R, Hawthorne S, McCarron P. The potential use of rabies virus glycoprotein-derived peptides to facilitate drug delivery into the central nervous system: a mini review. J Drug Target. 2017;25(5):379-385.

365. Shabanpoor F, Hammond SM, Abendroth F, Hazell G, Wood MJA, Gait MJ. Identification of a Peptide for Systemic Brain Delivery of a Morpholino Oligonucleotide in Mouse Models of Spinal Muscular Atrophy. Nucleic Acid Ther. 2017;27(3):130-143.

366. Maher F, Vannucci SJ, Simpson IA. Glucose transporter proteins in brain. FASEB J. 1994;8(13):1003-1011.

367. Suzuki K, Miura Y, Mochida Y, Miyazaki T, Toh K, Anraku Y, Melo V, Liu X, Ishii T, Nagano O, Saya H, Cabral H, Kataoka K. Glucose transporter 1-mediated vascular translocation of nanomedicines enhances accumulation and efficacy in solid tumors. J Control Release. 2019;301:28-41.

368. Costantino L, Gandolfi F, Tosi G, Rivasi F, Vandelli MA, Forni F. Peptide-derivatized biodegradable nanoparticles able to cross the blood-brain barrier. J Control Release. 2005;108(1):84-96.

369. Tosi G, Fano RA, Bondioli L, Badiali L, Benassi R, Rivasi F, Ruozi B, Forni F, Vandelli MA. Investigation on mechanisms of glycopeptide nanoparticles for drug delivery across the blood-brain barrier. Nanomedicine (Lond). 2011;6(3):423-436.

370. Tosi G, Vergoni AV, Ruozi B, Bondioli L, Badiali L, Rivasi F, Costantino L, Forni F, Vandelli MA. Sialic acid and glycopeptides conjugated PLGA nanoparticles for central nervous system targeting: In vivo pharmacological evidence and biodistribution. J Control Release. 2010;145(1):49-57.

371. Rigon L, Salvalaio M, Pederzoli F, Legnini E, Duskey JT, D'Avanzo F, De Filippis C, Ruozi B, Marin O, Vandelli MA, Ottonelli I, Scarpa M, Tosi G, Tomanin R. Targeting Brain Disease in MPSII: Preclinical Evaluation of IDS-Loaded PLGA Nanoparticles. Int J Mol Sci. 2019;20(8).

372. Koirala A, Makkia RS, Conley SM, Cooper MJ, Naash MI. S/MAR-containing DNA nanoparticles promote persistent RPE gene expression and improvement in RPE65-associated LCA. Hum Mol Genet. 2013;22(8):1632-1642.

373. Koirala A, Conley SM, Makkia R, Liu Z, Cooper MJ, Sparrow JR, Naash MI. Persistence of non-viral vector mediated RPE65 expression: case for viability as a gene transfer therapy for RPE-based diseases. J Control Release. 2013;172(3):745-752.

374. Han Z, Koirala A, Makkia R, Cooper MJ, Naash MI. Direct gene transfer with compacted DNA nanoparticles in retinal pigment epithelial cells: expression, repeat delivery and lack of toxicity. Nanomedicine (Lond). 2012;7(4):521-539.

375. Sun D, Schur RM, Lu ZR. A novel nonviral gene delivery system for treating Leber's congenital amaurosis. Ther Deliv. 2017;8(10):823-826.

376. Malamas AS, Gujrati M, Kummitha CM, Xu R, Lu ZR. Design and evaluation of new pH-sensitive amphiphilic cationic lipids for siRNA delivery. J Control Release. 2013;171(3):296-307.

377. Wang XL, Ramusovic S, Nguyen T, Lu ZR. Novel polymerizable surfactants with pH-sensitive amphiphilicity and cell membrane disruption for efficient siRNA delivery. Bioconjug Chem. 2007;18(6):2169-2177.

378. Gujrati M, Malamas A, Shin T, Jin E, Sun Y, Lu ZR. Multifunctional cationic lipid-based nanoparticles facilitate endosomal escape and reduction-triggered cytosolic siRNA release. Mol Pharm. 2014;11(8):2734-2744.

379. Sun D, Maeno H, Gujrati M, Schur R, Maeda A, Maeda T, Palczewski K, Lu ZR. Self-Assembly of a Multifunctional Lipid With Core-Shell Dendrimer DNA Nanoparticles Enhanced Efficient Gene Delivery at Low Charge Ratios into RPE Cells. Macromol Biosci. 2015;15(12):1663-1672.

380. Sun D, Schur RM, Sears AE, Gao SQ, Vaidya A, Sun W, Maeda A, Kern T, Palczewski K, Lu ZR. Non-viral Gene Therapy for Stargardt Disease with ECO/pRHO-ABCA4 Self-Assembled Nanoparticles. Mol Ther. 2020;28(1):293-303.

381. Gonzalez-Fernandez F, Ghosh D. Focus on Molecules: interphotoreceptor retinoid-binding protein (IRBP). Exp Eye Res. 2008;86(2):169-170.

382. Sun D, Sahu B, Gao S, Schur RM, Vaidya AM, Maeda A, Palczewski K, Lu ZR. Targeted Multifunctional Lipid ECO Plasmid DNA Nanoparticles as Efficient Non-viral Gene Therapy for Leber's Congenital Amaurosis. Mol Ther Nucleic Acids. 2017;7:42-52.

383. Sun D, Schur RM, Sears AE, Gao SQ, Sun W, Naderi A, Kern T, Palczewski K, Lu ZR. Stable Retinoid Analogue Targeted Dual pH-Sensitive Smart Lipid ECO/pDNA Nanoparticles for Specific Gene Delivery in the Retinal Pigment Epithelium. ACS Appl Bio Mater. 2020;3(5):3078-3086.

384. Rajala A, Wang Y, Zhu Y, Ranjo-Bishop M, Ma JX, Mao C, Rajala RV. Nanoparticle-assisted targeted delivery of eye-specific genes to eyes significantly improves the vision of blind mice in vivo. Nano Lett. 2014;14(9):5257-5263.

385. Takahashi Y, Chen Q, Rajala RVS, Ma JX. MicroRNA-184 modulates canonical Wnt signaling through the regulation of frizzled-7 expression in the retina with ischemia-induced neovascularization. FEBS Lett. 2015;589(10):1143-1149.

386. Liu HA, Liu YL, Ma ZZ, Wang JC, Zhang Q. A lipid nanoparticle system improves siRNA efficacy in RPE cells and a laser-induced murine CNV model. Invest Ophthalmol Vis Sci. 2011;52(7):4789-4794.

387. Patel S, Ryals RC, Weller KK, Pennesi ME, Sahay G. Lipid nanoparticles for delivery of messenger RNA to the back of the eye. J Control Release. 2019;303:91-100.

388. Huang X, Chau Y. Investigating impacts of surface charge on intraocular distribution of intravitreal lipid nanoparticles. Exp Eye Res. 2019;186:107711.

389. Zhu SN, Nolle B, Duncker G. Expression of adhesion molecule CD44 on human corneas. Br J Ophthalmol. 1997;81(1):80-84.

390. Lerner LE, Schwartz DM, Hwang DG, Howes EL, Stern R. Hyaluronan and CD44 in the human cornea and limbal conjunctiva. Exp Eye Res. 1998;67(4):481-484.

391. Culty M, Nguyen HA, Underhill CB. The hyaluronan receptor (CD44) participates in the uptake and degradation of hyaluronan. J Cell Biol. 1992;116(4):1055-1062.

392. de la Fuente M, Seijo B, Alonso MJ. Bioadhesive hyaluronan-chitosan nanoparticles can transport genes across the ocular mucosa and transfect ocular tissue. Gene Ther. 2008;15(9):668-676.

393. de la Fuente M, Seijo B, Alonso MJ. Novel hyaluronic acid-chitosan nanoparticles for ocular gene therapy. Invest Ophthalmol Vis Sci. 2008;49(5):2016-2024.

394. Contreras-Ruiz L, de la Fuente M, Parraga JE, Lopez-Garcia A, Fernandez I, Seijo B, Sanchez A, Calonge M, Diebold Y. Intracellular trafficking of hyaluronic acid-chitosan oligomer-based nanoparticles in cultured human ocular surface cells. Mol Vis. 2011;17:279-290.

395. Prakash TP, Mullick AE, Lee RG, Yu J, Yeh ST, Low A, Chappell AE, Ostergaard ME, Murray S, Gaus HJ, Swayze EE, Seth PP. Fatty acid conjugation enhances potency of antisense oligonucleotides in muscle. Nucleic Acids Res. 2019;47(12):6029-6044.

396. Chappell AE, Gaus HJ, Berdeja A, Gupta R, Jo M, Prakash TP, Oestergaard M, Swayze EE, Seth PP. Mechanisms of palmitic acid-conjugated antisense oligonucleotide distribution in mice. Nucleic Acids Res. 2020;48(8):4382-4395.

397. Ostergaard ME, Jackson M, Low A, A EC, R GL, Peralta RQ, Yu J, Kinberger GA, Dan A, Carty R, Tanowitz M, Anderson P, Kim TW, Fradkin L, Mullick AE, Murray S, Rigo F, Prakash TP, Bennett CF, Swayze EE, Gaus HJ, Seth PP. Conjugation of hydrophobic moieties enhances potency of antisense oligonucleotides in the muscle of rodents and non-human primates. Nucleic Acids Res. 2019;47(12):6045-6058.

398. Biscans A, Coles A, Haraszti R, Echeverria D, Hassler M, Osborn M, Khvorova A. Diverse lipid conjugates for functional extra-hepatic siRNA delivery in vivo. Nucleic Acids Res. 2019;47(3):1082-1096.

399. Biscans A, Caiazzi J, McHugh N, Hariharan V, Muhuri M, Khvorova A. Docosanoic acid conjugation to siRNA enables functional and safe delivery to skeletal and cardiac muscles. Mol Ther. 2021;29(4):1382-1394.

400. Hendricks WP, Yang J, Sur S, Zhou S. Formulating the magic bullet: barriers to clinical translation of nanoparticle cancer gene therapy. Nanomedicine (Lond). 2014;9(8):1121-1124.

401. Dowdy SF. Overcoming cellular barriers for RNA therapeutics. Nat Biotechnol. 2017;35(3):222-229.

402. Tieu TW, Y.; Cifuentes-Rius, A.; Voelcker, N.H. Overcoming Barriers: Clinical Translation of siRNA Nanomedicines. Advanced Therapeutics. 2021;4(9).

403. Salvati A, Pitek AS, Monopoli MP, Prapainop K, Bombelli FB, Hristov DR, Kelly PM, Aberg C, Mahon E, Dawson KA. Transferrin-functionalized nanoparticles lose their targeting capabilities when a biomolecule corona adsorbs on the surface. Nat Nanotechnol. 2013;8(2):137-143.

404. Zhang H, Wu T, Yu W, Ruan S, He Q, Gao H. Ligand Size and Conformation Affect the Behavior of Nanoparticles Coated with in Vitro and in Vivo Protein Corona. ACS Appl Mater Interfaces. 2018;10(10):9094-9103.

405. Xiao W, Wang Y, Zhang H, Liu Y, Xie R, He X, Zhou Y, Liang L, Gao H. The protein corona hampers the transcytosis of transferrin-modified nanoparticles through blood-brain barrier and attenuates their targeting ability to brain tumor. Biomaterials. 2021;274:120888.

406. Wang Y, Zhang H, Xiao W, Liu Y, Zhou Y, He X, Xia X, Gong T, Wang L, Gao H. Unmasking CSF protein corona: Effect on targeting capacity of nanoparticles. J Control Release. 2021;333:352-361.

407. Dai Q, Walkey C, Chan WC. Polyethylene glycol backfilling mitigates the negative impact of the protein corona on nanoparticle cell targeting. Angew Chem Int Ed Engl. 2014;53(20):5093-5096.

408. Saunders NRM, Paolini MS, Fenton OS, Poul L, Devalliere J, Mpambani F, Darmon A, Bergere M, Jibault O, Germain M, Langer R. A Nanoprimer To Improve the Systemic Delivery of siRNA and mRNA. Nano Lett. 2020;20(6):4264-4269.

409. Caracciolo G, Cardarelli F, Pozzi D, Salomone F, Maccari G, Bardi G, Capriotti AL, Cavaliere C, Papi M, Lagana A. Selective targeting capability acquired with a protein corona adsorbed on the surface of 1,2-dioleoyl-3-trimethylammonium propane/DNA nanoparticles. ACS Appl Mater Interfaces. 2013;5(24):13171-13179.

410. Steffens RC, Folda P, Fendler NL, Hohn M, Bucher-Schossau K, Kempter S, Snyder NL, Hartmann L, Wagner E, Berger S. GalNAc- or Mannose-PEG-Functionalized Polyplexes Enable Effective Lectin-Mediated DNA Delivery. Bioconjug Chem. 2024;35(3):351-370.

411. ASGCT Gene, Cell, & RNA Therapy Landscape Report. 2023 15.11. Available from: https://asgct.org/publications/landscape-report.

412. Ginn SL, Amaya AK, Alexander IE, Edelstein M, Abedi MR. Gene therapy clinical trials worldwide to 2017: An update. J Gene Med. 2018:e3015.

413. Wagner E. Polymers for siRNA Delivery: Inspired by Viruses to be Targeted, Dynamic, and Precise. Acc Chem Res. 2012;45(7):1005-1013.

414. Van Bruggen C, Hexum JK, Tan Z, Dalal RJ, Reineke TM. Nonviral Gene Delivery with Cationic Glycopolymers. Accounts of Chemical Research. 2019;52(5):1347-1358.

415. Grandinetti G, Reineke TM. Exploring the mechanism of plasmid DNA nuclear internalization with polymer-based vehicles. Mol Pharm. 2012;9(8):2256-2267.

416. Pozzi D, Colapicchioni V, Caracciolo G, Piovesana S, Capriotti AL, Palchetti S, De Grossi S, Riccioli A, Amenitsch H, Laganà A. Effect of polyethyleneglycol (PEG) chain length on the bio-nano-interactions between PEGylated lipid nanoparticles and biological fluids: from nanostructure to uptake in cancer cells. Nanoscale. 2014;6(5):2782-2792.

417. Schöttler S, Landfester K, Mailänder V. Controlling the Stealth Effect of Nanocarriers through Understanding the Protein Corona. Angew Chem, Int Ed Engl. 2016;55(31):8806-8815.

418. Kos P, Lachelt U, Herrmann A, Mickler FM, Doblinger M, He D, Krhac Levacic A, Morys S, Brauchle C, Wagner E. Histidine-rich stabilized polyplexes for cMet-directed tumor-targeted gene transfer. Nanoscale. 2015;7(12):5350-5362.

419. Morys S, Krhac Levacic A, Urnauer S, Kempter S, Kern S, O. Rädler J, Spitzweg C, Lächelt U, Wagner E. Influence of Defined Hydrophilic Blocks within Oligoaminoamide Copolymers: Compaction versus Shielding of pDNA Nanoparticles; 2017.

420. Salcher EE, Kos P, Fröhlich T, Badgujar N, Scheible M, Wagner E. Sequence-defined four-arm oligo(ethanamino)amides for pDNA and siRNA delivery: Impact of building blocks on efficacy. J Controlled Release. 2012;164(3):380-386.

421. He D. Combinatorial optimization of nucleic acid carriers for folate-targeted delivery. In.Faculty of Chemistry and Pharmacy. Munich: Ludwig-Maximilians-Universität Munich; 2016.

422. Müller K, Kessel E, Klein PM, Höhn M, Wagner E. Post-PEGylation of siRNA Lipo-oligoamino Amide Polyplexes Using Tetra-glutamylated Folic Acid as Ligand for Receptor-Targeted Delivery. Molecular Pharmaceutics. 2016;13(7):2332-2345.

423. Morys S, Urnauer S, Spitzweg C, Wagner E. EGFR Targeting and Shielding of pDNA Lipopolyplexes via Bivalent Attachment of a Sequence-Defined PEG Agent. Macromol Biosci. 2018;18(1):1700203.

424. Zhang W, Müller K, Kessel E, Reinhard S, He D, Klein PM, Höhn M, Rödl W, Kempter S, Wagner E. Targeted siRNA Delivery Using a Lipo-Oligoaminoamide Nanocore with an Influenza Peptide and Transferrin Shell. Adv Healthcare Mater. 2016;5(12):1493-1504.

425. Loy D, Klein P, Krzysztoń R, Lächelt U, Rädler J, Wagner E. A microfluidic approach for sequential assembly of siRNA polyplexes with a defined structure-activity relationship. PeerJ Materials Science. 2019;1.

426. He J, Xu S, Mixson AJ. The Multifaceted Histidine-Based Carriers for Nucleic Acid Delivery: Advances and Challenges. Pharmaceutics. 2020;12(8).

427. Midoux P, Pichon C, Yaouanc J-J, Jaffrès P-A. Chemical vectors for gene delivery: a current review on polymers, peptides and lipids containing histidine or imidazole as nucleic acids carriers. Br J Pharmacol 2009;157(2):166-178.

428. Pichon C, Gonçalves C, Midoux P. Histidine-rich peptides and polymers for nucleic acids delivery. Adv Drug Delivery Rev. 2001;53(1):75-94.

429. McKenzie DL, Kwok KY, Rice KG. A Potent New Class of Reductively Activated Peptide Gene Delivery Agents. J Biol Chem. 2000;275:9970-9977.

430. Aldawsari H, Raj BS, Edrada-Ebel R, Blatchford DR, Tate RJ, Tetley L, Dufès C. Enhanced gene expression in tumors after intravenous administration of arginine-, lysine- and leucine-bearing polyethylenimine polyplex. Nanomedicine. 2011;7(5):615-623.

431. Yu QY, Zhan YR, Zhang J, Luan CR, Wang B, Yu XQ. Aromatic Modification of Low Molecular Weight PEI for Enhanced Gene Delivery. Polymers (Basel). 2017;9(8).

432. Creusat G, Rinaldi A-S, Weiss E, Elbaghdadi R, Remy J-S, Mulherkar R, Zuber G. Proton Sponge Trick for pH-Sensitive Disassembly of Polyethylenimine-Based siRNA Delivery Systems. Bioconjugate Chem. 2010;21(5):994-1002.

433. Wang F, Hu K, Cheng Y. Structure–activity relationship of dendrimers engineered with twenty common amino acids in gene delivery. Acta Biomater. 2016;29:94-102.

434. Richter F, Martin L, Leer K, Moek E, Hausig F, Brendel JC, Traeger A. Tuning of endosomal escape and gene expression by functional groups, molecular weight and transfection medium: a structure–activity relationship study. Journal of Materials Chemistry B. 2020;8(23):5026-5041.

435. He D, Muller K, Krhac Levacic A, Kos P, Lachelt U, Wagner E. Combinatorial Optimization of Sequence-Defined Oligo(ethanamino)amides for Folate Receptor-Targeted pDNA and siRNA Delivery. Bioconjug Chem. 2016;27(3):647-659.

436. Plank C, Tang MX, Wolfe AR, Szoka FC, Jr. Branched cationic peptides for gene delivery: role of type and number of cationic residues in formation and in vitro activity of DNA polyplexes. Hum Gene Ther. 1999;10(2):319-332.

437. Hunter CA, Sanders JKM. The nature of .pi.-.pi. interactions. J Am Chem Soc. 1990;112(14):5525-5534.

438. Tan Z, Dhande YK, Reineke TM. Cell Penetrating Polymers Containing Guanidinium Trigger Apoptosis in Human Hepatocellular Carcinoma Cells unless Conjugated to a Targeting N-Acetyl-Galactosamine Block. Bioconjug Chem. 2017;28(12):2985-2997.

439. Taori VP, Lu H, Reineke TM. Structure–Activity Examination of Poly(glycoamidoguanidine)s: Glycopolycations Containing Guanidine Units for Nucleic Acid Delivery. Biomacromolecules. 2011;12(6):2055-2063.

440. Nair JK, Attarwala H, Sehgal A, Wang Q, Aluri K, Zhang X, Gao M, Liu J, Indrakanti R, Schofield S, Kretschmer P, Brown CR, Gupta S, Willoughby JLS, Boshar JA, Jadhav V, Charisse K, Zimmermann T, Fitzgerald K, Manoharan M, Rajeev KG, Akinc A, Hutabarat R, Maier MA. Impact of enhanced metabolic

stability on pharmacokinetics and pharmacodynamics of GalNAc-siRNA conjugates. Nucleic Acids Res. 2017;45(19):10969-10977.

441. Foster DJ, Brown CR, Shaikh S, Trapp C, Schlegel MK, Qian K, Sehgal A, Rajeev KG, Jadhav V, Manoharan M, Kuchimanchi S, Maier MA, Milstein S. Advanced siRNA Designs Further Improve In Vivo Performance of GalNAc-siRNA Conjugates. Mol Ther. 2018;26(3):708-717.

442. Sato Y, Matsui H, Yamamoto N, Sato R, Munakata T, Kohara M, Harashima H. Highly specific delivery of siRNA to hepatocytes circumvents endothelial cell-mediated lipid nanoparticle-associated toxicity leading to the safe and efficacious decrease in the hepatitis B virus. J Control Release. 2017;266:216-225.

443. Hashiba K, Sato Y, Harashima H. pH-labile PEGylation of siRNA-loaded lipid nanoparticle improves active targeting and gene silencing activity in hepatocytes. J Control Release. 2017;262:239-246.

444. Dhande YK, Wagh BS, Hall BC, Sprouse D, Hackett PB, Reineke TM. N-Acetylgalactosamine Block-co-Polycations Form Stable Polyplexes with Plasmids and Promote Liver-Targeted Delivery. Biomacromolecules. 2016;17(3):830-840.

445. Lee CC, Grandinetti G, McLendon PM, Reineke TM. A polycation scaffold presenting tunable "click" sites: conjugation to carbohydrate ligands and examination of hepatocyte-targeted pDNA delivery. Macromol Biosci. 2010;10(6):585-598.

446. Egli M, Manoharan M. Chemistry, structure and function of approved oligonucleotide therapeutics. Nucleic Acids Research. 2023;51(6):2529-2573.

447. Delehedde C, Ciganek I, Rameix N, Laroui N, Gonçalves C, Even L, Midoux P, Pichon C. Impact of net charge, targeting ligand amount and mRNA modification on the uptake, intracellular routing and the transfection efficiency of mRNA lipopolyplexes in dendritic cells. Int J Pharm. 2023;647:123531.

448. Lv S, Song K, Yen A, Peeler DJ, Nguyen DC, Olshefsky A, Sylvestre M, Srinivasan S, Stayton PS, Pun SH. Well-Defined Mannosylated Polymer for Peptide Vaccine Delivery with Enhanced Antitumor Immunity. Adv Healthcare Mater. 2022;11(9):e2101651.

449. Sun B, Zhao X, Wu Y, Cao P, Movahedi F, Liu J, Wang J, Xu ZP, Gu W. Mannose-Functionalized Biodegradable Nanoparticles Efficiently Deliver DNA Vaccine and Promote Anti-tumor Immunity. ACS Appl Mater Interfaces. 2021;13(12):14015-14027.

450. Le Moignic A, Malard V, Benvegnu T, Lemiègre L, Berchel M, Jaffrès PA, Baillou C, Delost M, Macedo R, Rochefort J, Lescaille G, Pichon C, Lemoine FM, Midoux P, Mateo V. Preclinical evaluation of mRNA trimannosylated lipopolyplexes as therapeutic cancer vaccines targeting dendritic cells. J Controlled Release. 2018;278:110-121.

451. Van der Jeught K, De Koker S, Bialkowski L, Heirman C, Tjok Joe P, Perche F, Maenhout S, Bevers S, Broos K, Deswarte K, Malard V, Hammad H, Baril P, Benvegnu T, Jaffrès PA, Kooijmans SAA, Schiffelers R, Lienenklaus S, Midoux P, Pichon C, Breckpot K, Thielemans K. Dendritic Cell Targeting mRNA Lipopolyplexes Combine Strong Antitumor T-Cell Immunity with Improved Inflammatory Safety. ACS Nano. 2018;12(10):9815-9829.

452. Perche F, Gosset D, Mével M, Miramon M-L, Yaouanc J-J, Pichon C, Benvegnu T, Jaffrès P-A, Midoux P. Selective gene delivery in dendritic cells with mannosylated and histidylated lipopolyplexes. J Drug Targeting. 2011;19(5):315-325.

453. White KL, Rades T, Furneaux RH, Tyler PC, Hook S. Mannosylated liposomes as antigen delivery vehicles for targeting to dendritic cells. J Pharm Pharmacol. 2006;58(6):729-737.

454. Macri C, Jenika D, Ouslinis C, Mintern JD. Targeting dendritic cells to advance cross-presentation and vaccination outcomes. Seminars in immunology. 2023;68:101762.

455. Hager S, Fittler FJ, Wagner E, Bros M. Nucleic Acid-Based Approaches for Tumor Therapy. Cells. 2020;9(9):2061.

456. Zeyn Y, Hobernik D, Wilk U, Pöhmerer J, Hieber C, Medina-Montano C, Röhrig N, Strähle CF, Thoma-Kress AK, Wagner E, Bros M, Berger S. Transcriptional Targeting of Dendritic Cells Using an Optimized Human Fascin1 Gene Promoter. In.Int J Mol Sci; 2023.

457. Schaffert D, Kiss M, Rödl W, Shir A, Levitzki A, Ogris M, Wagner E. Poly(I:C)-mediated tumor growth suppression in EGF-receptor overexpressing tumors using EGF-polyethylene glycol-linear polyethylenimine as carrier. Pharm Res. 2011;28(4):731-741.

458. Rodl W, Taschauer A, Schaffert D, Wagner E, Ogris M. Synthesis of Polyethylenimine-Based Nanocarriers for Systemic Tumor Targeting of Nucleic Acids. Methods Mol Biol. 2019;1943:83-99.

459. Ponader D, Wojcik F, Beceren-Braun F, Dernedde J, Hartmann L. Sequence-defined glycopolymer segments presenting mannose: synthesis and lectin binding affinity. Biomacromolecules. 2012;13(6):1845-1852.

460. Soria-Martinez L, Bauer S, Giesler M, Schelhaas S, Materlik J, Janus K, Pierzyna P, Becker M, Snyder NL, Hartmann L, Schelhaas M. Prophylactic Antiviral Activity of Sulfated Glycomimetic Oligomers and Polymers. J Am Chem Soc. 2020;142(11):5252-5265.

461. Bernardes GJ, Kikkeri R, Maglinao M, Laurino P, Collot M, Hong SY, Lepenies B, Seeberger PH. Design, synthesis and biological evaluation of carbohydrate-functionalized cyclodextrins and liposomes for hepatocyte-specific targeting. Org Biomol Chem. 2010;8(21):4987-4996.

462. Lindhorst TK, Kötter S, Krallmann-Wenzel U, Ehlers S. Trivalent α-D-mannoside clusters as inhibitors of type-1 fimbriae-mediated adhesion of Escherichia coli: structural variation and biotinylation. J Chem Soc, Perkin Trans 1. 2001(8):823-831.

463. Andre S, O'Sullivan S, Koller C, Murphy PV, Gabius HJ. Bi- to tetravalent glycoclusters presenting GlcNAc/GalNAc as inhibitors: from plant agglutinins to human macrophage galactose-type lectin (CD301) and galectins. Org Biomol Chem. 2015;13(14):4190-4203.

464. Ebbesen MF, Itskalov D, Baier M, Hartmann L. Cu Elimination from Cu-Coordinating Macromolecules. ACS Macro Lett. 2017;6(4):399-403.

465. Skirtenko N, Richman M, Nitzan Y, Gedanken A, Rahimipour S. A facile one-pot sonochemical synthesis of surface-coated mannosyl protein microspheres for detection and killing of bacteria. Chem Commun (Camb). 2011;47(45):12277-12279.

466. Salvador LAE, M.; Kihlberg, J. Preparation of building blocks for glycopeptide synthesis by glycosylation of Fmoc amino acids having unprotected carboxyl groups. Tetrahedron. 1995;51(19):5643-5656.

467. Russ V, Elfberg H, Thoma C, Kloeckner J, Ogris M, Wagner E. Novel degradable oligoethylenimine acrylate ester-based pseudodendrimers for in vitro and in vivo gene transfer. Gene Ther. 2008;15(1):18-29.

468. Kramer S, Langhanki J, Krumb M, Opatz T, Bros M, Zentel R. HPMA-Based Nanocarriers for Effective Immune System Stimulation. Macromol Biosci. 2019;19(6):e1800481.

469. Zhang M, June SM, Long TE. 5.02 - Principles of Step-Growth Polymerization (Polycondensation and Polyaddition). In: Matyjaszewski K, Möller M, editors. Polymer Science: A Comprehensive Reference. Amsterdam: Elsevier; 2012. p. 7-47.

470. Fantoni NZ, El-Sagheer AH, Brown T. A Hitchhiker's Guide to Click-Chemistry with Nucleic Acids. Chemical Reviews. 2021;121(12):7122-7154.

471. Morris VB, Labhasetwar V. Arginine-rich polyplexes for gene delivery to neuronal cells. Biomaterials. 2015;60:151-160.

472. Agrawal A, Leng Q, Imtiyaz Z, Mixson AJ. Exploring the outer limits of polyplexes. Biochemical and Biophysical Research Communications. 2023;678:33-38.

473. Wang X, Gobbo P, Suchy M, Workentin MS, Hudson RHE. Peptide-decorated gold nanoparticles via strain-promoted azide–alkyne cycloaddition and post assembly deprotection. RSC Advances. 2014;4(81):43087-43091.

474. Baldwin JE. Rules for ring closure. Journal of the Chemical Society, Chemical Communications. 1976(18):734-736.

475. Thapa B, Kumar P, Zeng H, Narain R. Asialoglycoprotein Receptor-Mediated Gene Delivery to Hepatocytes Using Galactosylated Polymers. Biomacromolecules. 2015;16(9):3008-3020.

476. Popielarski SR, Hu-Lieskovan S, French SW, Triche TJ, Davis ME. A nanoparticle-based model delivery system to guide the rational design of gene delivery to the liver. 2. In vitro and in vivo uptake results. Bioconjug Chem. 2005;16(5):1071-1080.

477. Behzadi S, Serpooshan V, Tao W, Hamaly MA, Alkawareek MY, Dreaden EC, Brown D, Alkilany AM, Farokhzad OC, Mahmoudi M. Cellular uptake of nanoparticles: journey inside the cell. Chem Soc Rev. 2017;46(14):4218-4244.

478. Li J, Chen L, Zhang X, Zhang Y, Liu H, Sun B, Zhao L, Ge N, Qian H, Yang Y, Wu M, Yin Z. Detection of Circulating Tumor Cells in Hepatocellular Carcinoma Using Antibodies against Asialoglycoprotein Receptor, Carbamoyl Phosphate Synthetase 1 and Pan-Cytokeratin. PLOS ONE. 2014;9(4):e96185.

479. Park J-H, Kim KL, Cho E-W. Detection of surface asialoglycoprotein receptor expression in hepatic and extra-hepatic cells using a novel monoclonal antibody. Biotechnology Letters. 2006;28(14):1061-1069.

480. Liu J, Hu B, Yang Y, Ma Z, Yu Y, Liu S, Wang B, Zhao X, Lu M, Yang D. A new splice variant of the major subunit of human asialoglycoprotein receptor encodes a secreted form in hepatocytes. PLoS One. 2010;5(9):e12934.

481. Spiess M, Schwartz AL, Lodish HF. Sequence of human asialoglycoprotein receptor cDNA. An internal signal sequence for membrane insertion. Journal of Biological Chemistry. 1985;260(4):1979-1982.

482. Fernandez-Marino I, Anfray C, Crecente-Campo J, Maeda A, Ummarino A, Teijeiro-Valino C, Blanco-Martinez D, Mpambani F, Poul L, Devalliere J, Germain M, Correa J, Fernandez-Villamarin M, Allavena P, Fernandez-Megia E, Alonso MJ, Andon FT. Mannose-modified hyaluronic acid nanocapsules for the targeting of tumor-associated macrophages. Drug Deliv Transl Res. 2023;13(7):1896-1911.

483. Zhu S, Niu M, O'Mary H, Cui Z. Targeting of tumor-associated macrophages made possible by PEG-sheddable, mannose-modified nanoparticles. Mol Pharm. 2013;10(9):3525-3530.

484. Conniot J, Scomparin A, Peres C, Yeini E, Pozzi S, Matos AI, Kleiner R, Moura LIF, Zupančič E, Viana AS, Doron H, Gois PMP, Erez N, Jung S, Satchi-Fainaro R, Florindo HF. Immunization with mannosylated nanovaccines and inhibition of the immune-suppressing microenvironment sensitizes melanoma to immune checkpoint modulators. Nat Nanotechnol. 2019;14(9):891-901.

485. Diebold SS, Plank C, Cotten M, Wagner E, Zenke M. Mannose receptor-mediated gene delivery into antigen presenting dendritic cells. Somatic Cell Mol Genet. 2002;27(1-6):65-74.

486. Irache JM, Salman HH, Gamazo C, Espuelas S. Mannose-targeted systems for the delivery of therapeutics. Expert Opin Drug Delivery. 2008;5(6):703-724.

487. Mitchell DA, Fadden AJ, Drickamer K. A novel mechanism of carbohydrate recognition by the C-type lectins DC-SIGN and DC-SIGNR. Subunit organization and binding to multivalent ligands. J Biol Chem. 2001;276(31):28939-28945.

488. Feinberg H, Castelli R, Drickamer K, Seeberger PH, Weis WI. Multiple modes of binding enhance the affinity of DC-SIGN for high mannose N-linked glycans found on viral glycoproteins. J Biol Chem. 2007;282(6):4202-4209.

489. Feinberg H, Mitchell DA, Drickamer K, Weis WI. Structural basis for selective recognition of oligosaccharides by DC-SIGN and DC-SIGNR. Science. 2001;294(5549):2163-2166.

490. Copland MJ, Baird MA, Rades T, McKenzie JL, Becker B, Reck F, Tyler PC, Davies NM. Liposomal delivery of antigen to human dendritic cells. Vaccine. 2003;21(9-10):883-890.

491. Astarie-Dequeker C, N'Diaye EN, Le Cabec V, Rittig MG, Prandi J, Maridonneau-Parini I. The mannose receptor mediates uptake of pathogenic and nonpathogenic mycobacteria and bypasses bactericidal responses in human macrophages. Infect Immun. 1999;67(2):469-477.

492. Soilleux EJ, Morris LS, Leslie G, Chehimi J, Luo Q, Levroney E, Trowsdale J, Montaner LJ, Doms RW, Weissman D, Coleman N, Lee B. Constitutive and induced expression of DC-SIGN on dendritic cell and macrophage subpopulations in situ and in vitro. J Leukocyte Biol. 2002;71(3):445-457.

493. Nguyen DN, Green JJ, Chan JM, Longer R, Anderson DG. Polymeric Materials for Gene Delivery and DNA Vaccination. Adv Mater. 2009;21(8):847-867.

494. Xiang SD, Scholzen A, Minigo G, David C, Apostolopoulos V, Mottram PL, Plebanski M. Pathogen recognition and development of particulate vaccines: does size matter? Methods. 2006;40(1):1-9.

495. Jilek S, Merkle HP, Walter E. DNA-loaded biodegradable microparticles as vaccine delivery systems and their interaction with dendritic cells. Adv Drug Delivery Rev. 2005;57(3):377-390.

496. Sedaghat B, Stephenson R, Toth I. Targeting the Mannose Receptor with Mannosylated Subunit Vaccines. Curr Med Chem. 2014;21(30):3405-3418.

497. Reddy ST, Swartz MA, Hubbell JA. Targeting dendritic cells with biomaterials: developing the next generation of vaccines. Trends Immunol. 2006;27(12):573-579.

498. Liu Y, Reineke TM. Degradation of Poly(glycoamidoamine) DNA Delivery Vehicles: Polyamide Hydrolysis at Physiological Conditions Promotes DNA Release. Biomacromolecules. 2010;11(2):316-325.

499. Smith AE, Sizovs A, Grandinetti G, Xue L, Reineke TM. Diblock glycopolymers promote colloidal stability of polyplexes and effective pDNA and siRNA delivery under physiological salt and serum conditions. Biomacromolecules. 2011;12(8):3015-3022.

500. Buckwalter DJ, Sizovs A, Ingle NP, Reineke TM. MAG versus PEG: Incorporating a Poly(MAG) Layer to Promote Colloidal Stability of Nucleic Acid/“Click Cluster” Complexes. ACS Macro Letters. 2012;1(5):609-613.

501. Phillips HR, Tolstyka ZP, Hall BC, Hexum JK, Hackett PB, Reineke TM. Glycopolycation–DNA Polyplex Formulation N/P Ratio Affects Stability, Hemocompatibility, and in Vivo Biodistribution. Biomacromolecules. 2019;20(4):1530-1544.

502. Dillinger AE, Guter M, Froemel F, Weber GR, Perkumas K, Stamer WD, Ohlmann A, Fuchshofer R, Breunig M. Intracameral Delivery of Layer-by-Layer Coated siRNA Nanoparticles for Glaucoma Therapy. Small. 2018;14(50):e1803239.

503. Dreaden EC, Morton SW, Shopsowitz KE, Choi J-H, Deng ZJ, Cho N-J, Hammond PT. Bimodal Tumor-Targeting from Microenvironment Responsive Hyaluronan Layer-by-Layer (LbL) Nanoparticles. ACS Nano. 2014;8(8):8374-8382.

504. Griffioen AW, Coenen MJH, Damen CA, Hellwig SMM, van Weering DHJ, Vooys W, Blijham GH, Groenewegen G. CD44 Is Involved in Tumor Angiogenesis; an Activation Antigen on Human Endothelial Cells. Blood. 1997;90(3):1150-1159.

505. Steffens RC, Thalmayr S, Weidinger E, Seidl J, Folda P, Hohn M, Wagner E. Modulating efficacy and cytotoxicity of lipoamino fatty acid nucleic acid carriers using disulfide or hydrophobic spacers. Nanoscale. 2024;16(29):13988-14005.

506. Witten J, Hu Y, Langer R, Anderson DG. Recent advances in nanoparticulate RNA delivery systems. Proc Natl Acad Sci U S A. 2024;121(11):e2307798120.

507. Tsuchida CA, Wasko KM, Hamilton JR, Doudna JA. Targeted nonviral delivery of genome editors in vivo. Proc Natl Acad Sci U S A. 2024;121(11):e2307796121.

508. Berger S, Lachelt U, Wagner E. Dynamic carriers for therapeutic RNA delivery. Proc Natl Acad Sci U S A. 2024;121(11):e2307799120.

509. Pack DW, Hoffman AS, Pun S, Stayton PS. Design and development of polymers for gene delivery. Nat Rev Drug Discov. 2005;4(7):581-593.

510. Miyata K, Oba M, Nakanishi M, Fukushima S, Yamasaki Y, Koyama H, Nishiyama N, Kataoka K. Polyplexes from poly(aspartamide) bearing 1,2-diaminoethane side chains induce pH-selective, endosomal membrane destabilization with amplified transfection and negligible cytotoxicity. J Am Chem Soc. 2008;130(48):16287-16294.

511. Kumar R, Santa Chalarca CF, Bockman MR, Bruggen CV, Grimme CJ, Dalal RJ, Hanson MG, Hexum JK, Reineke TM. Polymeric Delivery of Therapeutic Nucleic Acids. Chem Rev. 2021;121(18):11527-11652.

512. Neuberg P, Kichler A. Recent developments in nucleic acid delivery with polyethylenimines. Adv Genet. 2014;88:263-288.

513. Gosselin MA, Guo W, Lee RJ. Efficient gene transfer using reversibly cross-linked low molecular weight polyethylenimine. Bioconjug Chem. 2001;12(6):989-994.

514. Thomas M, Ge Q, Lu JJ, Chen J, Klibanov AM. Cross-linked small polyethylenimines: while still nontoxic, deliver DNA efficiently to mammalian cells in vitro and in vivo. Pharm Res. 2005;22(3):373-380.

515. Kloeckner J, Bruzzano S, Ogris M, Wagner E. Gene carriers based on hexanediol diacrylate linked oligoethylenimine: effect of chemical structure of polymer on biological properties. Bioconjug Chem. 2006;17(5):1339-1345.

516. Breunig M, Lungwitz U, Liebl R, Goepferich A. Breaking up the correlation between efficacy and toxicity for nonviral gene delivery. Proc Natl Acad Sci U S A. 2007;104(36):14454-14459.

517. Zintchenko A, Philipp A, Dehshahri A, Wagner E. Simple modifications of branched PEI lead to highly efficient siRNA carriers with low toxicity. Bioconjug Chem. 2008;19(7):1448-1455.

518. Knorr V, Russ V, Allmendinger L, Ogris M, Wagner E. Acetal linked oligoethylenimines for use as pH-sensitive gene carriers. Bioconjug Chem. 2008;19(8):1625-1634.

519. Yu H, Russ V, Wagner E. Influence of the molecular weight of bioreducible oligoethylenimine conjugates on the polyplex transfection properties. AAPS J. 2009;11(3):445-455.

520. Chiper M, Tounsi N, Kole R, Kichler A, Zuber G. Self-aggregating 1.8kDa polyethylenimines with dissolution switch at endosomal acidic pH are delivery carriers for plasmid DNA, mRNA, siRNA and exon-skipping oligonucleotides. J Control Release. 2017;246:60-70.

521. Scholz C, Kos P, Leclercq L, Jin X, Cottet H, Wagner E. Correlation of length of linear oligo(ethanamino) amides with gene transfer and cytotoxicity. ChemMedChem. 2014;9(9):2104-2110.

522. Coll JL, Chollet P, Brambilla E, Desplanques D, Behr JP, Favrot M. In vivo delivery to tumors of DNA complexed with linear polyethylenimine. Hum Gene Ther. 1999;10(10):1659-1666.

523. Uchida H, Itaka K, Nomoto T, Ishii T, Suma T, Ikegami M, Miyata K, Oba M, Nishiyama N, Kataoka K. Modulated protonation of side chain aminoethylene repeats in N-substituted polyaspartamides promotes mRNA transfection. J Am Chem Soc. 2014;136(35):12396-12405.

524. Forrest ML, Koerber JT, Pack DW. A degradable polyethylenimine derivative with low toxicity for highly efficient gene delivery. Bioconjug Chem. 2003;14(5):934-940.

525. Knorr V, Ogris M, Wagner E. An acid sensitive ketal-based polyethylene glycol-oligoethylenimine copolymer mediates improved transfection efficiency at reduced toxicity. Pharm Res. 2008;25(12):2937-2945.

526. Liu J, Chang J, Jiang Y, Meng X, Sun T, Mao L, Xu Q, Wang M. Fast and Efficient CRISPR/Cas9 Genome Editing In Vivo Enabled by Bioreducible Lipid and Messenger RNA Nanoparticles. Adv Mater. 2019;31(33):e1902575.

527. Shen Z, Liu C, Wang Z, Xie F, Liu X, Dong L, Pan X, Zeng C, Wang PG. Development of a Library of Disulfide Bond-Containing Cationic Lipids for mRNA Delivery. Pharmaceutics. 2023;15(2).

528. Chen X, Yang J, Liang H, Jiang Q, Ke B, Nie Y. Disulfide modified self-assembly of lipopeptides with arginine-rich periphery achieve excellent gene transfection efficiency at relatively low nitrogen to phosphorus ratios. J Mater Chem B. 2017;5(7):1482-1497.

529. Liang H, Hu A, Chen X, Jin R, Wang K, Ke B, Nie Y. Structure optimization of dendritic lipopeptide based gene vectors with the assistance from molecular dynamic simulation. J Mater Chem B. 2019;7(6):915-926.

530. Guo J, Wan T, Li B, Pan Q, Xin H, Qiu Y, Ping Y. Rational Design of Poly(disulfide)s as a Universal Platform for Delivery of CRISPR-Cas9 Machineries toward Therapeutic Genome Editing. ACS Cent Sci. 2021;7(6):990-1000.

531. Wang Y, Ma B, Abdeen AA, Chen G, Xie R, Saha K, Gong S. Versatile Redox-Responsive Polyplexes for the Delivery of Plasmid DNA, Messenger RNA, and CRISPR-Cas9 Genome-Editing Machinery. ACS Appl Mater Interfaces. 2018;10(38):31915-31927.

532. Chen G, Ma B, Wang Y, Gong S. A Universal GSH-Responsive Nanoplatform for the Delivery of DNA, mRNA, and Cas9/sgRNA Ribonucleoprotein. ACS Appl Mater Interfaces. 2018;10(22):18515-18523.

533. Chen Z, Tian Y, Yang J, Wu F, Liu S, Cao W, Xu W, Hu T, Siegwart DJ, Xiong H. Modular Design of Biodegradable Ionizable Lipids for Improved mRNA Delivery and Precise Cancer Metastasis Delineation In Vivo. J Am Chem Soc. 2023;145(44):24302-24314.

534. Lin Y, Wilk U, Pohmerer J, Horterer E, Hohn M, Luo X, Mai H, Wagner E, Lachelt U. Folate Receptor-Mediated Delivery of Cas9 RNP for Enhanced Immune Checkpoint Disruption in Cancer Cells. Small. 2023;19(2):e2205318.

535. Rui Y, Wilson DR, Tzeng SY, Yamagata HM, Sudhakar D, Conge M, Berlinicke CA, Zack DJ, Tuesca A, Green JJ. High-throughput and high-content bioassay enables tuning of polyester nanoparticles for cellular uptake, endosomal escape, and systemic in vivo delivery of mRNA. Sci Adv. 2022;8(1):eabk2855.

536. Vecsey-Semjen B, Becker KF, Sinski A, Blennow E, Vietor I, Zatloukal K, Beug H, Wagner E, Huber LA. Novel colon cancer cell lines leading to better understanding of the diversity of respective primary cancers. Oncogene. 2002;21(30):4646-4662.

537. Hartmann L, Häfele S, Peschka-Süss R, Antonietti M, Börner HG. Sequence Positioning of Disulfide Linkages to Program the Degradation of Monodisperse Poly(amidoamines). Macromolecules. 2007;40(22):7771-7776.

538. Meister A. Glutathione metabolism and its selective modification. J Biol Chem. 1988;263(33):17205-17208.

539. Schafer FQ, Buettner GR. Redox environment of the cell as viewed through the redox state of the glutathione disulfide/glutathione couple. Free Radic Biol Med. 2001;30(11):1191-1212.

540. Plank C, Oberhauser B, Mechtler K, Koch C, Wagner E. The influence of endosome-disruptive peptides on gene transfer using synthetic virus-like gene transfer systems. J Biol Chem. 1994;269(17):12918-12924.

541. Ogris M, Carlisle RC, Bettinger T, Seymour LW. Melittin enables efficient vesicular escape and enhanced nuclear access of nonviral gene delivery vectors. J Biol Chem. 2001;276(50):47550-47555.

542. Pelisek J, Gaedtke L, DeRouchey J, Walker GF, Nikol S, Wagner E. Optimized lipopolyplex formulations for gene transfer to human colon carcinoma cells under in vitro conditions. J Gene Med. 2006;8(2):186-197.

8 Publications

Review

Steffens RC, Wagner E, *Directing the Way—Receptor and Chemical Targeting Strategies for Nucleic Acid Delivery,* Pharm Res. 2023; 40(1): 47–76.
https://doi.org/10.1007%2Fs11095-022-03385-w

Research Articles

Steffens RC, Folda P, Fendler NL, Höhn M, Bücher-Schossau K, Kempter S, Snyder NL, Hartmann L, Wagner E, Berger S, *GalNAc- or mannose-PEG functionalized polyplexes enable effective lectin-mediated DNA delivery,* Bioconjugate Chem. (2024) 35, 351-370,
https://doi.org/10.1021/acs.bioconjchem.3c00546

Steffens RC, Thalmayr S, Weidinger E, Höhn M, Seidl J, Folda P, Wagner E, *Modulating efficacy and cytotoxicity of lipamino fatty acid nucleic acid carriers using disulfide or hydrophobic spacers,* Nanoscale (2024) 16, 13988-14005,
https://doi.org/10.1039/d4nr01357c

Patent

Wagner E, Peng L, Berger S, Thalmayr S, Folda P, Haase F, Grau M, Germer J, Yazdi M, Weidinger E, Burghardt T, **Steffens R**, Seidl J, *Novel carriers for nucleic acid and/or protein delivery,* PCT/EP2023/082604.

9 Acknowledgements

First of all, I would like to express my sincere gratitude to Prof. Dr. Ernst Wagner for giving me the opportunity to research in his working group. I am deeply grateful for his guidance and support, as well as for introducing me to the fascinating world of nanoparticles and nucleic acid delivery, in my belief the most cutting-edge and promising technology in pharmaceutical sciences. It was a great chance to learn from your expertise.

I would like to thank the members of the examination committee for their time, interest, and consideration, especially Prof. Dr. Olivia Merkel for agreeing to take on the second review of my thesis.

I would also like to thank the scientific and technical staff who have supported this work by analytical measurements. Special thanks to the mass spectrometry department, led by Dr. Spahl, as well as Dr. Allmendinger and Mrs. Glas for NMR analyses. Furthermore, I thank Susanne Kempter for performing TEM measurements.

I thank my collaboration partners from Heinrich-Heine-University Düsseldorf and Davidson College in Davidson, North Carolina: Nika Fendler, Dr. Katharina Bücher-Schossau, Prof. Dr. Nicole L. Snyder and Prof. Dr. Laura Hartmann for the fruitful cooperation on glyco-functionalized polyplexes. My special thanks go to Nicole and Laura, who have been a great inspiration to me since the beginning of my scientific career, and I appreciate their passion for science and research. Thank you for your encouragement and how you opened the world of research to young scientists.

Many thanks to Prof. Dr. Ulrich Lächelt, who initiated the collaboration with Laura Hartmann and Nicole Snyder. I'm very thankful for always providing scientific support and numerous discussions.

Great thanks to our technicians, especially Wolfgang Rödl, Miriam Höhn, Melinda Kiss and Lorina Bawej for keeping the lab running and your support. Wolfgang – I cannot imagine a lab without you! Thanks for your technical support, for taking care of materials ordering, technical instruments and so much more. Miriam and Melinda for your expertise and help in cell culture, for your patience when teaching a chemist how to work with cells.

A special thanks to all members of AK Wagner who have accompanied me during my PhD. You always created a great working atmosphere in the lab, and we worked greatly together as a team. Thanks for all scientific discussions, where everyone found his or her niche, shared their experiences and provided support, when needed. I really enjoyed working with you. Besides that, I will never forget our team events, starting with a ski trip to Kühtai in

2020, Christmas parties, visits at the Wiesn, birthday and housewarming parties, evenings in the Biergarten, our Wandertag at Tegernsee and so many more.

Dr. Simone Berger, thank you for supporting me from day one, for a quick familiarization with the processes in the lab, many fruitful discussions on research projects and for being a great collaboration partner.

Thanks to Sophie M. Thalmayr, Eric Weidinger, Paul Folda, Johanna Seidl for great collaboration on several research projects. Melina Grau and Tobias Burghardt for many discussions on sometimes tedious syntheses and for MALDI measurements.

To those of you, with whom I not directly collaborated with, you lighted up long days at work, especially my office-partners Mina Yazdi, Victoria Vetter and Bianca Köhler, as well as Dr. Franziska Haase, Dr. Janin Germer, Dr. Anna-Lina Lessl and Dr. Jana Pöhmerer. Many of you have become more than colleagues and I'm grateful for our friendships.

Last, but not least, I would like to thank my parents, Manuela and Olaf, and my brother Markus for your endless support and continuous encouragement, even though I break family traditions. Finally, I thank Max, for being by my side for almost half of my life, for your patience, emotional support and endless love. You always find a way to cheer me up after a failed experiment and celebrated every success.